Ministry of Higher Education and Scientific Research
University of Babylon / College of Science
Department of Chemistry

Synthesis, Identification and Evaluation of Antibacterial Activity of MO(M: Mg, Fe, V) based Silica nano composites

A thesis Submitted to the College of Science, University of Babylon in Partial Fulfillment of Requirement of the Degree of Doctorate of Philosophy in Chemistry Science

By

Marwa Mohammed Ali Obaid Hassan Al-Hasnawi

B.Sc. Chemistry Science - University of Babylon College of Science women 2013

M. Sc. Chemistry Science - University of Babylon 2016

Supervisors

Prof. Abbas A-Ali Drea Al-Salhi

2023 A.D.

1444 A.H.

بسم الله الرحمن الرحيم

اللَّهُ لَا إله إِلَّا هُوَ الْحَيُّ الْقَيُّومُ لَا تَأْخُذُهُ سِنَةٌ وَلَا نَوْمٌ لَهُ مَا فِي السَّمَوَاتِ وَمَا فِي الْأَرْضِ مَنْ ذَا الَّذِي يَشْفَعُ عِنْدَهُ إِلَّا بِإِذْنِهِ يَعْلَمُ مَا بَيْنَ أَيْدِيهِمْ وَمَا خَلْفَهُمْ ۖ وَلَا يُحِيطُونَ بِشَيْءٍ مِنْ عِلْمِهِ إِلَّا بِمَا شَاءَ وَسِعَ كُرْسِيُّهُ السَّمَوَاتِ وَالْأَرْضَ ۖ وَلَا يَئُودُهُ حِفْظُهُمَا وَهُوَ الْعَلِيُّ الْعَظِيمُ.

صدق الله العظيم

سورة البقرة-اية 255

وزارة التعليم العالي والبحث العلمي

جامـــعة بابـــل/كلية العلوم

قسم الكيمياء

تخليق وتوصيف وتقييم الفعالية المضادة للبكتيريا للمواد النانوية المحملة على السليكاMO (V, Fe, Mg :M)

اطروحة مقدمة الى كلية العلوم- جامعة بابل

وهي جزء من متطلبات نيل درجة دكتوراه فلسفة في العلوم /الكيمياء

من قبل

مروة محمد علي عبيد حسان الحسناوي

بكالوريوس علوم كيمياء - جامعة بابل كلية العلوم للبنات 2013

ماجستير علوم كيمياء - جامعة بابل 2016

بإشراف

أ.د عباس عبد علي دريع الصالحي

1444 هـ

2023 م

الخلاصة

يتألف هذا العمل من خمسة مراحل مختلفة لتحضير وتشخيص مواد كيميائية جديدة واجراء اختبارات مختلفة لبيان فاعليتها الاحيائية وتأثيرها على الخلايا السرطانية للجلد وذلك بالاعتماد مخلفات قشور الشلب.

المرحلة الأولى: -

استخلاص مادة السليكا بالاعتماد على استعمال قشور الشلب كمادة خام. حيث تم غسل القشور جيدا بالماء المقطر و معاملتها بحامض الخليك، ثم حرق القشور بدرجة 700 درجة سيلزية, كذلك تم تنقية اوكسيد السليكا الناتج المستخلص بطريقة التصعيد عند درجة حرارة 100درجة سيلزية للحصول على ناتج أوكسيد سليكا عالي النقاوة. شخصت الخصائص التركيبية لبلورات السليكا بوساطة قياسات الأجهزة الطيفية مثل تقنية حيود الاشعة السينية ومجهر الماسح الالكتروني عالي الدقة ومطيافية تشتت الطاقة بالأشعة السينية وقياس المساحة السطحية ومعدل حجم الفجوات ومطيافية الاشعة تحت الحمراء.

المرحلة الثانية: -

تحضير متراكبات اكاسيد نانوية ثنائية من مادة السيلكا, حيث تم تحضير متراكبي خامس أوكسيد الفناديوم أوكسيد السليكا واوكسيد الحديد أوكسيد السليكا(SiO_2/V_2O_5, Fe_xO_y/SiO_2)بطريقة المحلول الجيلاتيني (sol-gel) اما متراكب أوكسيد المغنيسيوم أوكسيد السليكا(SiO_2/MgO) فحضر بالطريقة الرطبة. تم احتساب كل من المساحة السطحية والحجم المسامي ومعدل نصف القطر، حيث وجد تباين ملحوظ في المساحة السطحية لمتراكبات الاكاسيد الثنائية النانوية المحضرة التي كانت تتصف بزيادة كبيرة في المساحة السطحية مقارنة مع اوكسيد السليكا. اختبر تأثير درجة حرارة التحميص على مادة السليكا والمتراكبات المحضرة بنسب تركيبية مختلفة ضمن المدى الحراري ما بين 300 و 700 درجة مئوية. وجد ان حجوم البلورات النانوية المحضرة تتراوح ما بين 16 و 60 نانوميتر.

المرحلة الثالثة:-

تضمنت دراسة الفعالية الحيوية لاوكسيد السليكا و المتراكبات الاوكسيدية النانوية ضد انواع من البكتريا الموجبة مثل *staphylococcus aurrus* والبكتريا السالبة *Eschreca .coli ,Pseudomonas* المعزولة من الجروح والحروق التي تصيب الانسان حيث تم تقدير الفعالية البيولوجية من خلال استعمال مطيافية الاشعة المرئية والتي تسمى الطريقة الغير مباشرة حيث اظهرت النتائج ان MgO/SiO_2 يمتلك اعلى فعالية لتثبيط بكتريا الجروح والحروق مقارنة مع بقية الاكاسيد الثنائية النانوية

المحضرة كذلك تم الحصول على تثبيط بكتيري عالي الكفاءة لل SiO_2/V_2O_5 عند درجة حرارة حرق 300^0C , من خلال نتائج الدراسة وجد ان الاوكسيد الثنائي النانو Fe_xO_y/SiO_2 يحتاج الى تركيز عالي يتم تحضيره لإعطاء فعالية تثبط ضد بكتريا الجروح والحروق المدروسة حيث بالرغم من المساحة السطحية العالية الا ان الفعالية لم تكن بنفس الكفاءة.

كذلك اشتملت الدراسة الحالية معرفة فعالية التثبيط للأكاسيد النانوية المحضرة $SiO_2,SiO_2/V_2O_5,SiO_2/MgO$ و Fe_xO_y/SiO_2 ضد الانواع البكتريا المختلفة من خلال تطبيق الاكاسيد النانوية ومعاملتها كمضادات حيوية موضعية وتطبيقها على مادة الشاش الطبي بعد اجراء التعقيم للشاش الطبي المستخدم واستخدام طريقة زرع الاطباق لمعرفة فعالية التثبيط البكتيري من خلال قياس منطقة التثبيط البكتيري وذلك باستعمال جرعات مختلفة من المضادات الحيوية ($SiO_2,Fe_xO_y/SiO_2$, $SiO_2/V_2O_5,SiO_2/MgO$) حيث لوحظ من خلال النتائج ان MgO/SiO_2 (E4-MG-50) يمتلك فعالية تثبيط بكفاءة عالية حتى في الجرعات او التراكيز الواطئة ضد البكتريا (لبكتريا الغرام السالبة والغرام الموجبة) عند تحضير النموذج في درجة حرارة حرق 300 درجة سيلزية , كذلك تم تقدير نسبة(MIC) التي تمثل الحد الأدنى من تركيز المثبط اي أقل تركيز للمضادات الحيوية التي تعمل على تثبيط الجراثيم (يمنع نمو البكتريا) حيث تم تقديرها من اجل تقييم الفعالية البالوجية للمضادات النانوية المحضرة من خلال قياس تراكيزها على البكتريا السالبة *E.Coli*. كذلك تقدير (MBC) للمواد المحضرة التي تمثل أقل تركيز للمضادات النانوية المحضرة($SiO_2,Fe_xO_y/SiO_2$,$SiO_2/V_2O_5,SiO_2/MgO$) الازم لقتل البكتيريا خلال فترة زمنية من 18-24 ساعة حضن عند درجة $37\ ^0C$ حيث وجد نسبة (MIC) للأكاسيد المحضرة($SiO_2,Fe_xO_y/SiO_2,SiO_2/V_2O_5,SiO_2/MgO$,) (156.2, 312.5, 937 , 1250) µg/mlعلى التوالي.

المرحلة الرابعة: -

تم تحضير تراكيب علاجية مقترحة (مستحضرات طبية) من المتراكبات الاوكسيدية النانوية ذات الكفاءة الأعلى في مكافحة البكتيريا (MgO/SiO_2 [E4-MG-50]و SiO_2/V_2O_5). تم اختبار هذه المواد من خلال التعرف على تأثير هذه المستحضرات على البكتريا المؤثرة في حالات الجروح والحروق(*S.aureas*). وجد ان التراكيب العلاجية المحضرة ذات فعالية علاجية كبيرة في الحد من تأثير البكتيريا والقضاء عليها لدى المصابين بالجروح والحروق وبفعالية متكافئة لكل من المتراكبات الاوكسيدة النانوية المستعملة في المراهم العلاجية المقترحة.

المرحلة الخامسة: -

تم اختبار الفعالية السمية البيولوجية للمتراكبات النانوية المحضرة ومدى تأثير هذه المواد على معالجة خط خلايا الجلد السرطانية A-134,حيث اظهرت الفحوصات نتائج واعدة لتأثير المواد النانوية المحضرة على قتل الخلايا السرطانية. وجد ان المتراكبات الاوكسيدية (متراكب أوكسيد المغنيسيوم أوكسيد السليكا[E4-MG-50] ومتراكب خامس أوكسيد الفناديوم أوكسيد السليكا) تتميز بكفاءة عالية في قتل الخلايا السرطانية وبتراكيز قليلة وذلك عند مقارنتها مع الخلايا الطبيعية وهذا ما يجعلها تتميز بانتقائية وكفاءة لاستعمالها كمادة دوائية طبية لمعالجة الخلايا السرطانية دون إظهار سمية عالية تجاه خط الخلايا الطبيعية-101.

Declaration

I, Marwa Mohammed Ali Obaid who conducted this study entitle

"Synthesis, Identification and evaluation of antibacterial activity of Nano materials based on Silicon dioxide" and submitted it as a partial fulfillment of the requirement for a doctoral degree in Science of Chemistry. The research was carried out at the Departments of Chemistry and Biology, college of science Babylon University. The study was carried out under the supervision Prof. Dr. Abbas Abid Ali Drea department of Chemistry, college of Science, Babylon University.

I, confirm that the work presented in this thesis has not been previously submitted for a M.Sc., doctorate, or diploma at any higher education institution. I also declare that all information in this document has been and presented in accordance with the academic rules and ethical conducts. I also declare that, as required by these rules and conducts. I have fully cited and documented all methods, figures and results that are not original to this work, or any information that is not derived from this work. I confirm that this has been indicated in this thesis.

Dedication

To my family father, mother and my sister, Doaa Mohammed Ali whose Support me all time

To my best friend

Marwa-Ali

Acknowledgments

First of all, I would like to express my great appreciation to the Almighty, God for his support and enabling me to complete this work.

I wish to express my sincere appreciation to my supervisor Prof. Dr.Abbas Abaid Drea for his suggestions scientific research. My gratitude to the University of Babylon, College of Science. I would like to express my thanks and gratitude to Prof. Dr. Saadon Abdullah Aowda. I wish to express my gratitude to Prof. Dr. Abbas Jasim Atiyah , Assist Prof. Dr. Saba, Assist Prof. Dr. Noor Salman Biological Department, Assist. Prof. Dr. Kaiser N. Madlum College of Medicine, the University of Babylon, Assist. Prof. Dr Masoud Khazaei (Drug, Delivery Disposition and Dynamics) Monash Institute of Pharmaceutical Sciences (MIPS) Australia and Assist Prof. Dr. Ahmed Khudair College of Women Science. I wish to express my gratitude to miss Maryam. I wish also thank to my respected father, mother, my sister Duaa and also thank for all friends. I wish also to show gratefulness for all source researches.

Summary

This work is consisted of five different stages to prepare and investigate of chemical materials, conducting various tests to show their biological effectiveness and their effect on cancer cells of the skin, by relying on the remnants of rice husks.

Stage one:

Extraction of silica oxide from rice husks as a raw material. Where the remnants of rice husks are washed well with distilled water and treated with acetic acid, then the husks are burned at 700 °C, and the extracted silica oxide is also purified by reflux method at a temperature of 100 °C to obtain a high purity of silica oxide product.

The structural properties of silica oxide are characterized by employing spectroscopic measurements such as the infrared spectroscopy ,X-ray diffraction technique, high-resolution scanning electron microscope (FESEM), X-ray energy dispersal spectroscopy(EDX), as well as the measurement of the surface area, and average pore size (BET).

Stage two:

Preparation of nano binary oxides from silica, where the compounds of vanadium pentoxide silica oxide and iron oxide silica (SiO_2/V_2O_5, Fe_xO_y/SiO_2) are prepared by the Sol-Gel method. While the nano binary oxide of magnesium oxide (SiO_2/MgO) is prepared by silica oxide through the wet method. The surface area, pore volume and average radius were calculated. A noticeable variation is found in the surface area of the prepared nanocomposite oxide is characterized significant increment in the surface area compared to silica oxide. Estimation effect of the calcination temperature on the silica material and the prepared composites at different ratios have been done within the thermal range

between 300 and 700 °C. It was found that the sizes of the prepared nanocrystals ranged between (16 - 60) nm.

Stage three:

Included a study of the biological activity of nano silica oxide and binary oxide nanoparticles against types of Gram-positive bacteria such as staphylococcus aureus, Gram-negative bacteria *Pseudomonas* and *Escherichia coli* that are isolated from human wounds and burns. The biological activity is estimated by using visible-ray spectroscopy (indirect method). The results showed that MgO/SiO_2 has the highest activity of inhibiting the bacteria of wounds and burns compared to the rest of the prepared nano binary oxides. Also, a highly efficient bacterial inhibition of SiO_2/V_2O_5 was obtained at a burning temperature of 300˚C, through the results of the study. It was found the nano binary oxide Fe_xO_y/SiO_2 needs to be prepared in a higher concentration than the rest of the prepared oxides to give an inhibiting effect against the bacteria of wounds and burns. Where, despite the high surface area, the effectiveness is not the same.

The inhibition effect of the prepared silica oxide and nano binary oxides SiO_2/V_2O_5, SiO_2/MgO, and Fe_xO_y/SiO_2 against different bacterial species has been done through the application of nano-oxides. The prepared composites are treated as topical antibiotics by applying them to the medical gauze material after performing the sterilization of the used medical gauze and using the method of culture dishes. The bacterial inhibition activity estimation is done by measuring the bacterial inhibition area (zone inhibition) through different doses are the test antibiotics. Nano binary oxide (E4-MG-50) is noted at low concentrations, the inhibition activity is found high against bacterial Gram-negative and Gram-positive when the sample was prepared at a burning temperature of 300 ˚C. The lowest concentration of antibiotics that inhibit microbially

(prevents bacterial growth) was estimated to evaluate the biological effectiveness of the prepared nano-antibiotics by measuring the effect of different concentrations of the prepared nano-antibiotics on Gram-negative bacteria *E.Coli*. Also, the lowest concentration is estimated for the prepared nanoparticles (SiO_2, SiO_2/V_2O_5, SiO_2/MgO, and Fe_xO_y/SiO_2) that are needed to kill bacteria during 18-24 hours incubated at a temperature of 37˚C. The MIC ratio of the prepared oxides is found (SiO_2, SiO_2/V_2O_5, SiO_2/MgO, and Fe_xO_y/SiO_2) (1250, 312.5, 156.2, and 937,) µg/ml respectively.

Stage four:

Proposed therapeutic compositions (medicinal ointments) have been prepared from nanocomposites with higher antibacterial efficiency SiO_2/MgO[E4-MG-50] and SiO_2/V_2O_5. These nanocomposites have been tested by identifying the effect of these preparations on bacteria affecting wounds and burns (*S.aureas*). The prepared therapeutic structures are found to be highly effective in reducing and eliminating the effect of bacteria in people with wounds and burns and with equal effectiveness for each of the nanocomposites used in the proposed therapeutic ointments.

Stage five:

The biotoxicity of the prepared nanocomposites and the extent to which these substances affect the treatment of the cancer skin-A431 cell line are tested. The tests showed promising results of the effect of the prepared nanomaterials on the killing of cancer cells. It was found that oxide composites (SiO_2/MgO[E4-MG-50] and SiO_2/V_2O_5) are characterized by high efficiency in killing cancer cells and in low concentrations when compared with normal cells and this makes them characterized by selectivity and efficiency to be used as a medicinal drug to treat cancer cells without showing high toxicity towards the normal cell line-101.

Table of contents

Lists of Tables

Lists of Figures

List of Symbols And Abbreviations

Symbol	Description
A^0	Angstrom
α	alpha
AK	Actinic keratosis
Ag NPs	Silver Nanoparticles
NMs	Nanomaterials
BET	Branure-Emeet-Teller
B16F10	Murine melanoma cell line
BC	Breast Cancer
BJH	Barrett-Joyner-Halenda
C	Centigrade
CVD	Chemical Vapor Deposition
CB	Conduction band
DDW	Deuterium-depleted water
DSC	Differential scanning calorimetry
DNA	Deoxyribonucleic acid
E. Coli	Escherichia coli
Eq	Equation
eV	Electron volt
EDX	Energy dispersive X-ray
FsaR	Fibrosarcoma cells
IUPAC	International union of pure and applied chemistry
g	Gram
HCC	Hepatocellular carcinoma
K	Kelvin
kCal	Kilocalorie
LEDs	Light Emitting Diodes
NSCLC	Non-small cell lung cancer
NMs	nanomaterials
µ	Microliter
MBC	Minimum Bactericidal concentration
MDA-MB-231	human breast cancer cell line
MIC	Minimum Inhibitory concentration
MNPs	Magnetic nanoparticles
MDBK	Madin-Darby Canine kidney cells

min	minute
ml	milliliter
PLAL	Pulse Laser Ablation in Liquid
PTP	Protein Tyrosine Phosphatases
PBS	Phosphate Buffer Solution
Vp	Pore volume
ROS	Reactive Oxidation Species
RPMI-164	Roswell Park Memorial Institute Medium
RHA	Rice Husk Ash
RNA	Ribonucleic acid
SC	Skin cancer
S.aureus	Staphylococcus aureus
SFETB	French Society for Burn Injuries
SCCVII	squamous carcinoma cells
SSA	specific surface area
TEM	Transmission electron microscopy
θ	Theta
UV-Vis	Ultra violet-visible
V79	hamster lung fibroblast cell line
VB	Valance band
λ	wavelength

1-1General Introduction

Richard Feynman introduced the first concept of nanotechnology in 1959. Norio Taniguchi, a Japanese scientist expressed the term nanotechnology in 1974[1]. Nanotechnology processing of specific atoms, molecules, or substances into individual atoms is structured for the production of products and devices with specific properties of nanoparticles [2]. Nanomaterials deal with the scale of materials between 1 to 100 nm. Research has been a concern in the last decades upon the development of nanoparticles and their applications in various scopes such as therapeutics, physiological and biological fields [3-5].

The human body found many physiological inorganic metals like zinc, iron, magnesium, copper and Vanadium, that have wide importance to physiological activity. This element is necessary for the regulation of the vital activity of the body and deficiencies may cause disease [6].

Traditional chemical and physical ways of nanomaterial synthesis consider one reason for nanomaterial toxicity in the human body. Natural product as raw as a precursor material for synthesis is preferred to overcome this problem [7,1]. There are a two-synthesis approach to producing nanomaterial, there are the top-down approach and the bottom-up approach. The first one is decreasing the size from bulk structures to the smallest structure since the irregularity of the surface structure is the main issue with the top-down approach . The second one involves the synthesis of nanomaterial from the atomic level which is more frequently used to prepare nano-scale components with uniform size, shape and distribution [8,9].

Nanotechnology appears to be able to greatly increase production rates with reduced costs, solve significant health issues and be interesting in medical fields. Nanoparticles are used to transmit drugs, light, heat, or other materials to specific cells such as cancer cells since nanoparticles interact with diseased cells. Also, nanoparticles can use as an antimicrobial against many different microorganisms [10,11]. Nanotechnology is considered the most imminent technology of the twenty-first century and is viewed as a significant benefit for the cosmetics business. Cosmeceuticals are the fastest expanding segment of the personal care market, with usage increasing significantly over time. [12]. The morphology, size, shape, composition, homogeneity, and aggregation of nanoparticles are all used to classify the nanoparticles depending on the preparation methods used considered one of the most important aspects of this field [13]. These are further divided into inorganic, organic, and carbon-based NPs based on their chemical structures [14]. There are several methods for various forms of nanoparticle preparations such as the following in figure 1-1. [15].

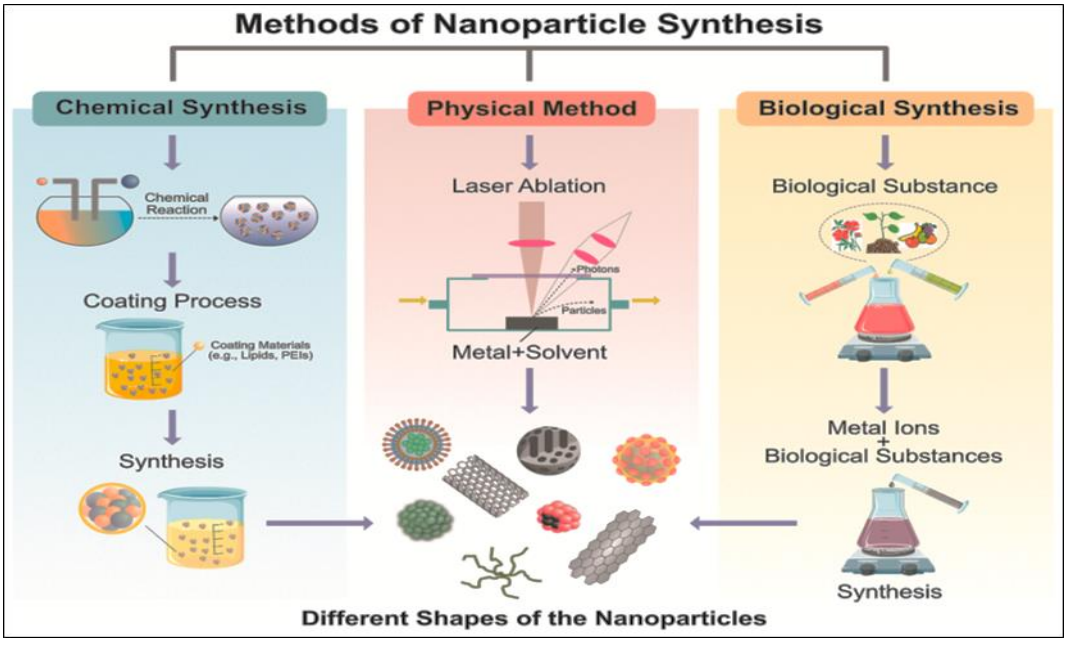

Figure 1-1. Majors synthesis methods of nanoparticles of different shapes [15].

Plant extracts are commonly employed in the production of nanoparticle materials. The mechanism of nanoparticle synthesis, on the other hand, is not well understood. As a result, research is required to fully comprehend the production of nanoparticles employing particular pure compounds [16,17]. Various metal nanoparticles have been widely exploited for a wide range of medical applications. Among them, gold nanoparticles (AuNPs) are widely reported to guide an impressive resurgence and are highly remarkable. AuNPs, with their multiple, unique functional properties, and ease of synthesis, have attracted extensive attention. The unique properties of AuNPs suggest their broad applications, including drug and gene delivery, photothermal therapy, diagnosis, and imaging. Moreover, further applications, arise from their antimicrobial (antibacterial and antifungal), antioxidant, and anticancer activities [18].

Gold when at the nanoscale it reflects the red colour and several other colours, so the coloured is seen as gold in especially nano medicines promise new therapeutic methodology. Researchers also benefited from this phenomenon in designing therapeutic systems that are used to kill cancer cells in normal light without harming healthy cells. [18,19] Nanotechnology represents an advance in the medical field with the ability to deliver drugs to specific cells using nanoparticles [20].

Nanomaterials have the ability to combat human diseases such as viruses, bacteria and can be used to heal a variety of wounds [21]. Nanomaterials have become more popular recently as a result of advances in nanotechnology. Nanoparticles have piqued the curiosity of scientists due to their specific properties, to be used in wound healing properties antimicrobial [22, 23].

The use of nanomaterial increases the degradation of microorganism's membrane structures such as Ag-NPs and their complexes, in particular, are commonly used for objectives of antibacterial and wound healing [24,25]. Traditional wound dressings can't keep up with the demands of wound care. Because of their unique qualities, nanofiber mats, and nanocomposites, as the next generation of wound dressings, expedite healing and prevent bacterial infections. [26]

1-2. Preparation Methods of Nanomaterial

The preparation processes are carried out by controlling the precise selection of the degree of acidity, the concentration of the reactants and the temperature of the mixing method, where the shape and characteristics of the prepared nanomaterial depend on the control of the conditions of the experiment [27]. There are several physical and chemical methods of preparation [28]. The latter has been interested in using the method that relies on the use of natural materials instead of chemicals that are more toxic and expensive [29,30], while biological methods that depend on natural materials that involve the production and development of ways to synthesis new nanomaterial that be environmentally friendly [31], cheaper and have better properties with preventing pollution environment. Also, the physical techniques method has been especially advantageous for a chemical method that uses toxic materials but is considerably more expensive if compare with other methods therefore green chemistry method used in this search is more appropriate [32,33].

Various methods are available to synthesis nanomaterial such as shown in figure 1-2.

1. Mechanical grinding/milling is a top-down approach that involves employing grinders to decompose large structural particles into coarse particles.

2. Laser ablation is a technique for removing layers of solid metal using a high-powered laser.

3. Electro-explosion is a top-down approach in which a high-power pulsed current is passed through a thin metal wire, causing metal ions in the wire to explode

4. CVD is a bottom-up process in which a solid metal is deposited on another hot metal surface using a separate chemical reaction in the vapour or gas phase

5. The sol-gel method is a bottom-up approach to colloidal nanoparticle synthesis.

6. Green synthesis of the environment emerging nanoparticle production systems should be cost-effective, easy to synthesis, and environmentally friendly as a result, biosynthesis and green synthesis is preferable approaches for their manufacturing [34].

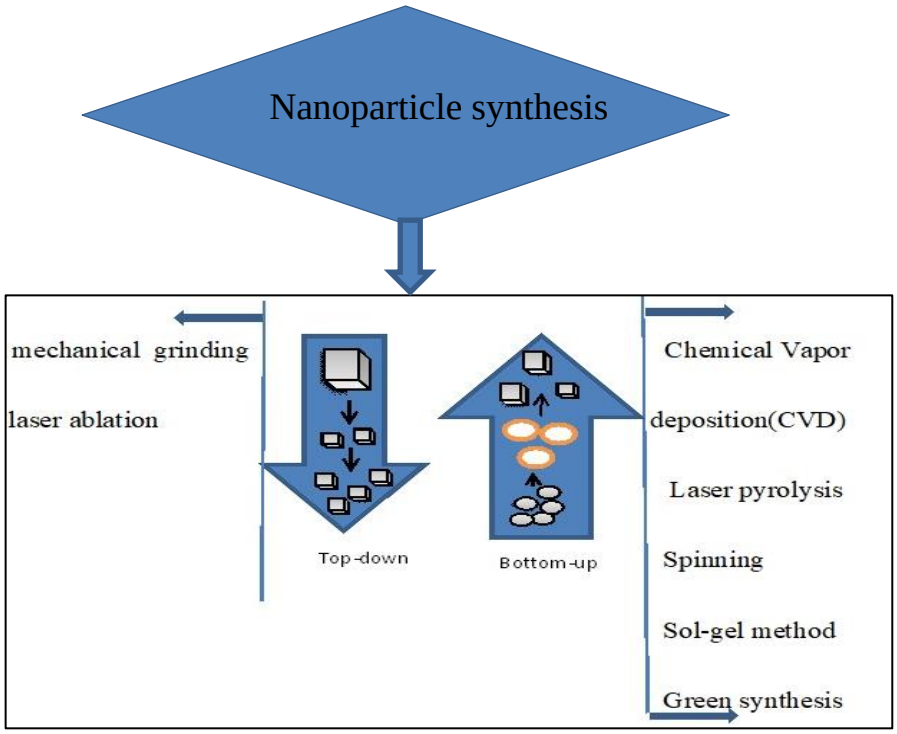

Figure 1-2. Two approaches of nanoparticles synthesis, Top-down and bottom-up.

1-3. Green chemistry

Green chemistry is the creation of chemical products and processes that minimize or eliminate the use of hazardous substances [35, 36].

Green synthesis is a new field of bio-nanotechnology that offers economic and environmental advantages over traditional chemical and physical methods [37]. Nanomaterials produced using a green synthesis method have a lot of potential for industrial use. Since it is less expensive, safer, and pollutes the atmosphere less than other methods [38-41].

For the processing of nanomaterials, conditions such as acidity, reactant concentration, and mixing temperature may be regulated [42,43]. The structural properties of nanocrystal materials are determined by the method used to prepare those [44].

Several physical-chemical and green chemistry methods of preparation have been used since the latter one has been much more interesting due to relies on the use of natural raw materials instead of chemicals that are more toxic and expensive [45].

Green chemists are interested in finding new ways to make chemicals [46]. Many products can be made from renewable feedstocks (corn, and biomass), fuels (ethanol and biodiesel), plastics, and other materials [47]. The role of green chemistry in the environment is many chemicals end up in the atmosphere as a result of deliberate release during use (e.g pesticides), accidental releases (e.g manufacturing emissions), or disposal [48]. Green chemicals are either degraded into harmless goods or recycled for reuse [49].

Rice husk is of natural product that can be used as raw material for green chemistry to synthesis nanomaterials. By using ash (that's yielded by burring raw plant materials), which is an agricultural product that represents 20% of the world's annual rice production of 649.7 million tons [50]. These wastes may convert into nanomaterials that have important medical applications such as the production of silica and its use as antibiotics that are used as effective topical dressings in the treatment of bacteria and microbes that afflict patients with wounds and burns, which cause delays in healing [51].

1-4. Structural Classification of Nanomaterial

Nanomaterials have unique chemical and physical properties such as surface area, distribution of size, stability, morphology, melting temperature, charge capacity, and magnetic properties. Nanomaterials play important role in the chemical activity, that's based on their size and bulk structure [52-55].

Such as solid nanocrystals, clusters, nanotubes, nanowires, and colloid material [56]. Colloid material that has dimensions rang 1-1000 nm [57].

1-5. Role of NPs in antimicrobial activity and mechanism

Nano particals used in the antimicrobial activity are one of the important widely interest during the last years in the nanotechnology field, it's shown significant advancements in many applications in physical, chemical biological sciences, medical, and health care fields [58].

Nanomaterials can work as an antibiotic against various bacteria such as Ag NPs [59]. Silver is being employed in a growing number of medical items, the most common contemporary application is as a biocide for preventing infections in long-term problem areas such as burns, traumatic wounds, and diabetic ulcers [60]. Burns are still a severe clinical issue.

However, infections, not burns, are the leading cause of death among burn victims today [61]. Also Au, ZnO, and SiO_2 nanoparticles have a biological activity to use as antibiotics for treatment of burns, wounds, and in medication of many infectious diseases [62], nanomaterial used as biomedical by work on inhibition of functions of enzymes and essential proteins which results in breaking up the replication of nucleic acids of bacteria like *E. coli, Pesedomonou, S.auruse* and other, [63]. The concentration of nanomaterial plays an essential role in the inhibition of the growth of microbial or bacteria the mechanism of nanoparticles to work as an antibacterial is still disputed by researchers, but there are supposed three mechanism steps that involve the first generation of reactive oxidative species (ROS) essential to their antibacterial efficacy figure 1-3. [64,65]. ROS comprise strong reactive oxidants that cause damage to cell membranes and peptidoglycan such as hydroxyl radicals (OH^{-1}) superoxide radicals ($O^{\cdot -}_2$) and oxygen (O_2) [66, 67].

Two mechanisms release nanomaterials ions and attach to the cell membrane after attaching occurs a change in the cell membrane of bacteria prevents transport channels and then causes cell death [68,69]. The efficiency of this process builds on particle size, morphology, the concentration of ions and the surface area of nanoparticles [65]. Finally interaction of metal atoms to the thiol group of enzymes and then deactivation of function enzymes [70].

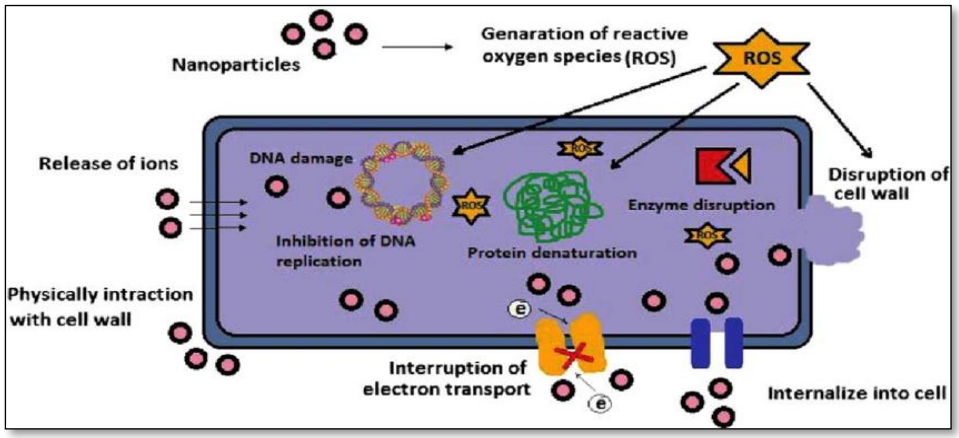

Figure 1-3. Different mechanisms of antimicrobial activity of the nanoparticles [64].

1-6. Antibacterial detection method

Antimicrobial functionalization of textiles is significant for a variety of purposes, including preventing the breakdown of textile materials, creating more effective wound dressings, and preventing infections or odours caused by bacterial growth [71]. Bacterial classification in two major types such as shown in figure 1-4 gram-positive and gram-negative depend on membrane structure, bacterial that has peptidoglycan thickens layer be more resistant to agents of antibiotic while bacterial with thin peptidoglycan layer be lower resistant to attachment of antibiotic nanoparticles, gram-positive content of teichoic acid while the gram-negative absence of teichoic acid [72-74]. Microbial growth can be measured using a variety of direct and indirect approaches. In the direct

method, the bacterial growth effects are measured using a suitable technique such as serial dilution, plate count, and disk diffusion method [75]. Also, can be evaluated antibacterial activity by used to assess indirect methods depending on turbidity analysis by utilizing a spectrophotometer [76,77].

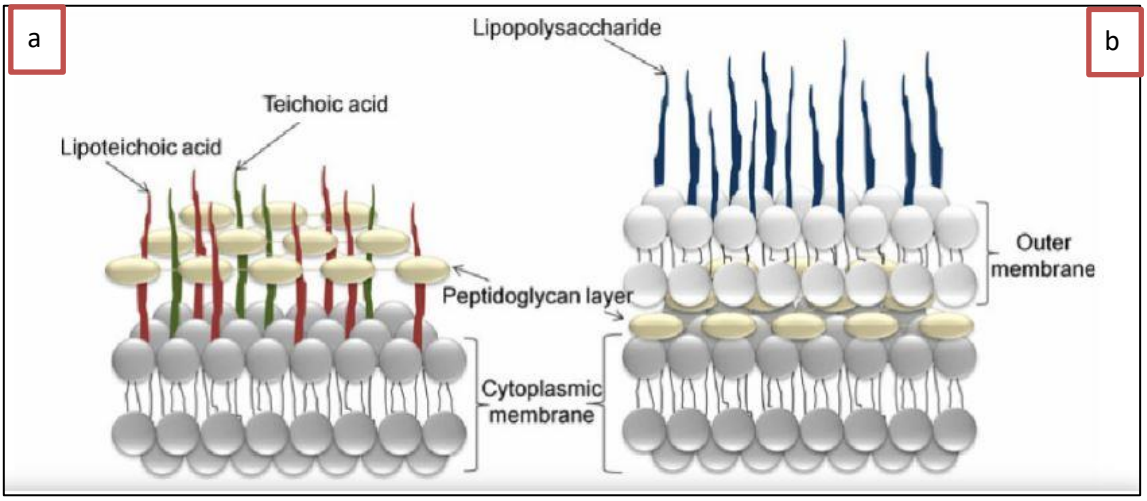

Figure 1-4. The membrane structure of a. G. Positive and b. G. Negative bacterial [78].

1-6-1.Plate count method

Petri dishes are used for each reading in plate counting techniques. Agar plate is prepared, and with the use of a sterile spreader, one plate of inoculums and other plates with inoculum and nanoparticle solutions are spread on it; this plate is incubated for 24 hours at 37°C and the colonies on each plate were then counted. The percentage of inhibition that grows with each step is then calculated [78,79].

1-6-2.Disk diffusion method

To make liquid culture, the bacteria culture is combined with nutrient broth. The sterile nutrient agar solution is then prepared and placed in dishes to solidify. With the aid of a cork borer, holes are then made. A sterile cotton bud is used to disperse the bacterial culture on the agar. After

stabilizing the holes with a solution of metallic NPs, the plates are incubated for 24 hours at 37°C. The inhibition zones are detected the next day [80].

1-7. Antibiotics for treating infected burn wounds

Antibiotics may be used to cure underlying diseases, lower morbidity and avoid death. Antibiotics should be administered after an infection has been diagnosed, according to the recommendations of the French Society for Burn Injuries (FSBI) [81]. Antimicrobial topical therapy is often used to prevent or treat infections, or as a supplement to other treatments [82].

Wound treatments should be matched to the bacteria that are causing the infection, and they should not promote medication resistance. Antibiotics taken orally have not been routinely used in these instances due to indications that they are ineffective [83].

Antibiotics are more difficult to use in persons with infected burn wounds than in other disorders. This is since in a burned person, the pharmacokinetic properties of antibiotics (absorption, distribution, metabolism, and excretion) are altered, and there are considerable differences across individuals [84].

Antibiotics such as ciprofloxacin and Penicillins immune to the enzyme Penicillinase have lost their effectiveness against Staphylococcus aureus, the most common pathogen found in wound infection sites, therefore many searches are interested in preparing alternatives to antibacterial drugs that have more efficacy and available [85]. Hemostasis, inflammation, proliferation, and reconstruction are the steps of the wound healing process [86]. Wound healing is a very complex process that takes time to complete [87], as the remodelling phase required to establish the correct environment can range from 2-3 weeks [88]. Wound management is an ongoing process

that includes the full range of comprehensive clinical evaluations, procedures and interventions used to care for patients with wounds [89].

Adequate wound care treatment is a major clinical concern, and the field of wound care is becoming increasingly important [88]. Chronic wound care is a research sector focused on producing better and more efficient materials for wound dressings [90]. Physicians should ensure that an assessment of patient pain and wound etiology is made when making judgments about dressing product selection [91].

Conventional wound dressing materials may cause the wound to dry out. Conventional wound dressings can adhere mechanically to the wound surface, making changing a wound dressing difficult and even painful. Thus, wound healing therapy based on the use of nanomaterials (NMs) has opened up new avenues and benefits in this sector [92]. Currently, two distinct types of NMs can be explored for wound healing. Specifically, nanoparticles are capable of healing as a result of the inherent qualities of nanomaterials, as well as nanomaterials as carriers of therapeutic chemicals [93]. The effects of different nanomaterials on wound healing are variable, as they depend on their physical and chemical properties. On the mechanism of production of reactive oxidized species (ROS) by metallic NPs nanoparticles that play a large role in their production, as ROS can cause peptidoglycan damage. Reactive oxygen species can also inhibit transcription, translation, and enzymatic activity, thus causing bacterial killing [64,65].

Because of their high surface area of nanomaterials to volume ratio and unique chemical and physical properties, nanoscale materials have recently appeared as novel antimicrobial agents such as AgO, MgO, CuO, Au, ZnO, Fe_2O_3 and SiO_2 nanoparticles with low toxicity and have high antimicrobial effectiveness[94].

Stationary phase Bacterial growth slows dramatically because of a lack of basic nutrients, a change in the pH of the medium, a lack of oxygen in the water and the accumulation of their poisonous metabolic wastes. Death phase cells die in this phase the bacterial population decreases, death phase begins as a result of the consumption of nutrients and the accumulation of toxic products [95].

1-8 Rice Husk Ash and Silica oxide product

Silica oxide is a highly versatile inorganic chemical molecule. It can take the form of a gel, a crystalline structure, or an amorphous structure. It is found on the earth's crust. However, producing pure silica is an energy-intensive process. Numerous industrial processes employing conventional raw materials necessitate a high level of precision and temperatures in a furnace of more than 700 ˚C. A straightforward chemical reaction that uses a non-traditional source material for silica extraction: rice husk ash. Rice husk ash is one of the most common types of ash among the family of other raw materials, silica-rich raw materials comprise approximately 90-98 %silica after complete combustion of agro-wastes [96].

Rice husk is a common boiler fuel, and the ash produced frequently causes disposal issues, the chemical procedure presented here not only eliminates waste but also recovers a precious silica product, as well as several beneficial associate recoveries. The amorphous and white silica recovered from the rice plant's hull and straw may have an extremely high specific surface area, SSA. [97, 98]. The acid treatment of the rice husk before burning is an essential step in the synthesis of a high specific surface area of silica. Indeed, acid treatment is the optimal method for obtaining high-purity silica. This search demonstrates how to obtain the high specific surface area of silica with effective combustion temperatures on purity.

Additionally, the rice husk may be pretreated with hot water to remove impurities. This approach enables the simultaneous recovery of biomass energy and synthesis of high-quality silica at thermoelectric facilities, without the possibility of corrosive compounds being used during the combustion process. Acid treatments may also be appropriate, provided that organic acids like as acetic are employed, as they break down in the burning process into water and carbon dioxide. Utilizing rice husk as the raw material, two million tons of pure high-grade silica may be produced annually to meet the enormous demand of a variety of industries businesses that utilize it [99].

1-9.Chemical composition of RHA

There are various ways to preparation of silica nanoparticles such as the Sol-gel method and precipitation method, in our work depends on the extraction of silica oxide by using rice husks ash as precursor material that contains 80-90% of silica with other metallic impurities like Alumina Al_2O_3 and Potassium oxide [100]. Table 1-1 explained it

Table 1-1. Chemical constituent percentage of RHA [100].

Component	Percentage %
Silica (SiO_2)	91.1
Alumina (Al_2O_3)	0.4
(Ferric oxide (Fe_2O_3	0.4
Calcium oxide (CaO)	0.4
Sodium (Na_2O)	0.1
Magnesium oxide (MgO)	0.5
Potassium oxide (KaO)	2.2

Rice husk can be obtained from agricultural waste material, around 80 million tons of RHA are produced annual. It has lightweight according to reports, nearly 0.23 tons of husk is produced for every ton of rice produced. Rice husk is abundantly grown in Malaysia after each paddy gathering

season, with over 400,000 metric tons of rice husk produced annually. Rice husk is large, bulky, and only a small portion of it is used for fuel which causes a disposal challenge. Because rice ash is available and free of cost that makes the material valuable for researchers, especially which is the continent's many compositions as shown in table1-1. Mesoporous silica is a porous substance that has been employed as an absorbent because of its unusual surface and pore features, including a large surface area and a large pore volume [101-104].

1-10. Structure and Crystal Morphology of Silica oxide

The silicon atom is bound to four oxygen atoms in a tetrahedral structure. The majority of oxygen atoms would be bound to two silicon atoms, resulting in two silicon atoms as shown in figure 1-5. Silica is also known as silica oxide or silicic acid. Silica oxide surface is a common descriptor such as hydrophobic and hydrophilic. A hydrophobic surface does not absorb the interaction water. If a surface adsorbs water it is known as hydrophilic. The silicon is hydrophobic has a nearly 90-degree angle. Oxides with a thickness greater than $30A^0$ are hydrophilic [105].

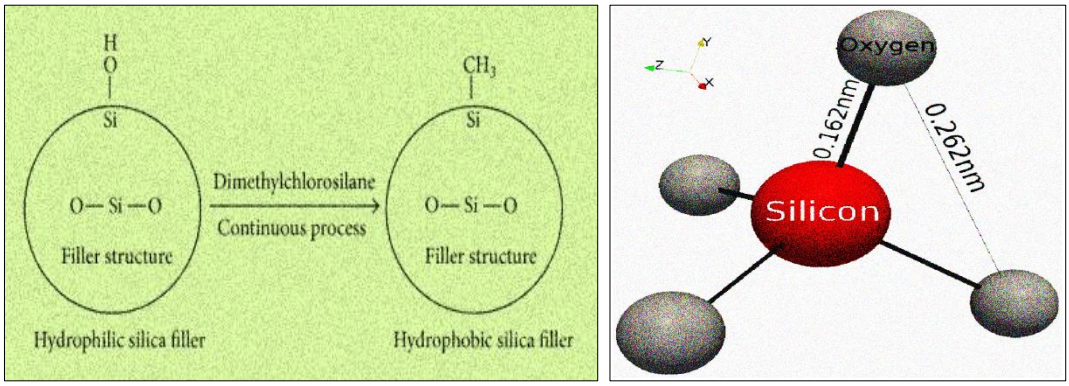

Figure 1-5. Descriptors crystal structure of silica oxide [105]

Silicon dioxide can extraction from many natural sources such as quartz, sand, charcoal, bamboo leaves and rice husks that all minerals which can be found in abundance in nature. Silica is used in a variety of

applications that demand high purity. Silica is a raw material utilized in a wide variety of sectors, including semiconductors, ceramics, polymers, and materials. This silica is typically synthesized by fusing quartz at high temperatures, yielding ultrapure polycrystalline silicon and silicon hydride. Along with environmental and economic benefits, low-energy, simpler techniques of obtaining pure silica open up new industrial possibilities for RHA. [106,107]. One of the most widely applied substrates in DNA biosensors is silica nanoparticles, also known as silicon dioxide nanoparticles or silica nanoparticles. They have garnered considerable attention in recent years because of their low toxicity, stability and ability to be functionalized with a wide variety of compounds and polymers .

Due to the unique geometric features of nanostructured silica, it may be used to create enhanced biomaterial conjugates with a variety of hybrid nanomaterials. Thus, dye-doped fluorescent silica nanoparticles enhance DNA sensing signal amplification. The porous structure, adsorption properties and high surface activity of silicon dioxide nanoparticles make them suitable for utilization as an antimicrobial agent [108]. The physical properties of silica are mentioned in Table 1-2.

Silicon's magnetic and optical properties suggest the possibility of simultaneously producing new modified magnetic-luminescent materials based on the Si-SiO_2 combination in powder or thin-film form, in amorphous, crystalline, or mixed amorphous-nanocrystalline states with better parameters. These composite materials can be used to create cutting-edge optical (lasers, LEDs, etc.) and spintronic devices [109].

Table1-2. Physical properties of silicon dioxide nanoparticles[110]

Melting point	Molecular weight	Color	Density	Morphology	Bandgap energy
1700 ˚C	60.08.518 g/mol	White powder	2.5 g/cm^3	Amorphose	1.12 ev

1-11. Vanadium pentoxide (V_2O_5)

Depending on the oxidation state of the vanadium metal, it may form a variety of different compounds with oxygen Vanadium pentoxide V_2O_5, is now the most solid nanoparticle available stable and hence the most common form of vanadium oxide[111]. It has some properties such as dispersed, high purity, and spherical surface morphology, Vanadium pentoxide (V_2O_5) can be used extensively in industrial and chemical reactions filed such as optical files by the manufacturer of laser crystals, Nanofibers and nanowires. it is an n-type semiconductor substance and the most stable oxide[112]. Vanadium pentoxide nanoparticles have improved magnetic properties, antibacterial and antifungal activity, and photocatalytic degradation activity. Various properties of Vanadium pentoxide catalysts depend on their particle size and morphology[113,114].

Vanadium pentoxide is used as an antibacterial. Engineered nanoparticles with increasing antibacterial effectiveness have been employed as effective coating agents on surgical tools and implants in recent years to reduce the incidence of implant-associated infections[115].

Vanadium pentoxide is coupled with silicon dioxide by sol-gel method but the study used tetraethyl orthosilicate as a precursor and application in dehydration of n-butane [116]. In last years many researchers intriguing by Vanadium pentoxide material, due to several uses in photocatalysts

degradation, lithium-ion batteries, sensors, and electrochromic instruments[117]. Table 1-3 mention of some physical properties of it.

Table 1-3 Physical properties of Vanadium pentoxide (V_2O_5) nanoparticles[118]

Melting point	Molecular weight	Colour	Density	Bandgap energy
690 ˚C	181.88 g/mol	Yellow powder	3.356 g/cm^3	2.4 ev

1-12 Magnesium oxide

Magnesium is an alkaline earth metal, it has an atomic weight of 12. Magnesium considers a necessary component of the healthy human body[119]. Magnesium (Mg) element inter in all metabolic pathways. Magnesium element in the regulation of biochemical reaction of more than 200 enzymes, blood pressure and blood glucose regulation human body takes it from a natural source as food or by takes as a dietary supplement[120]. Magnesium oxide white solid powder consider a source of magnesium elements. it is utilized as an antacid to treat heartburn and dyspepsia. Magnesium oxide (MgO) is a unique material simple oxide and it has a wide range of utilization, Magnesium oxide MgO with a high surface area when being in nanoscale show up promises advantage in many applications such as degradation of the toxic chemical by adsorbent it, also magnesium oxide has unique optical, electronic, catalytic and magnetic properties[121]. MgO is a significant inorganic compound with a broad bandgap as shown in table 1-4[122]. It has been used in a variety of applications, including, catalyst supports, catalysis, toxic waste remediation, refractory materials and adsorbents, additives in heavy fuel oils, reflective and anti-reflective coatings, superconducting and ferroelectric thin films as substrates, superconductors, and lithium-ion

batteries, among others[123]. MgO is used in medicine to treat heartburn, stomach ulcers, and to regenerate bone[124]. MgO nanoparticles have recently demonstrated promise in the treatment of tumours. Additionally, MgO nanoparticles exhibit significant antibacterial potential. [125]

Magnesium oxide (MgO) has been extensively explored due to its unusual properties as a solid with a strong ionic character, a simple stoichiometry and crystal structure, as well as surface structural flaws, and new uses in a variety of fields, including electronics, adsorption, catalysis, ceramics, and petrochemical products reflective and anti-reflective coatings, and numerous other fields[126].

Table 1-4.Physical properties of Magnesium oxide (MgO) nanoparticles [126]

Melting point	Molecular weight	Colour	Density	Bandgap energy
2858 ˚C	40.30 g/mol	White powder	3. 58 g/cm^3	5.7 ev

Magnesium oxide is an inorganic oxide that is biocompatible and non-toxic[127]. Cancer cells are destroyed by Magnesium oxide (MgO) nanoparticles. It has also been discovered that it produces reactive oxygen species (ROS), which causes apoptosis, the death of cells that occurs in the normal and controlled part of an organism,s growth or development(128). Magnesium oxide (MgO) nanoparticles inorganic hygroscopic material that connects by an ionic bond, oxygen atom give pairs of electrons whereas the magnesium atom takes electron such as shown in figure 1-6 [129].

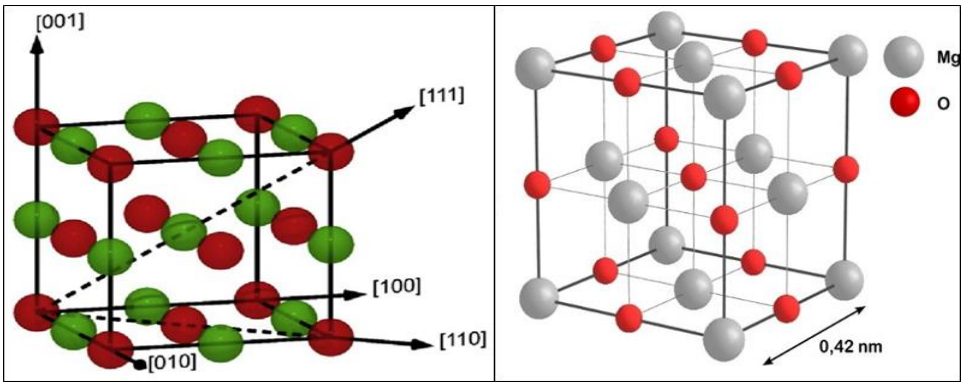

Figure 1-6. Crystal structure of Magnesium oxide (MgO)[129]

The aim objective of this present work is the modification of the surface of MgO nanoparticles and explain it is its function as an antibacterial agent by application to the wound dressing.

1-13.Iron oxide (Fe_xO_y)

Magnetic materials have in interesting to many researchers because iron has unique chemical and physical properties which differ significantly from bulk material. Nanostructured magnetic material has a wide range of applications such as hyperthermia [130], gas sensors, information storage media, magnetic refrigeration, bioabsorption, ceramic matrixes, drug delivery, antibiotics activity for microbial treatment and catalyst applications [131]. Different elements are magnetic nanostructured such as Fe, Co, Ni, metal oxide Fe_3O_4 and nanocomposites like iron oxide nanoparticles supported on silica materials[132]. Iron has a biological function in our bodies, it is an essential element for haemoglobin production, that majer protine for transfer oxygen from the lungs to tissues, and also complete of enzymes to the synthesis of collagen and it is important in immunesysteme[133].

Nowadays magnetic nanoparticle materials composites with several different compositions of catalyst heterogeneous with high efficiency, this magnetic nanoparticle solid can be easily separated[134].

Due to the heterogeneous particle size distribution, controlled phase synthesis, and morphology, we have used the sol-gel technique in this work to ensure that iron oxide has better physical and chemical properties.

1-14 Nano binary oxide of Semiconductors

This method depended on the bandgap energy between the valence band and conductance band in the piratical of semiconductors, increasing the responsiveness of a semiconductor with a high bandgap in ultraviolet light by connecting it to another semiconductor with a tiny bandgap in visible light. That means if the bandgap for the partial semiconductor is large than the energy lamp used in the radiation process therefore the electrons cannot exit from the valence band to the conductance band and the energy of radiation lose as heat, to solve this problem used piratical semiconductor has a bandgap smaller to make a couple with other piratical semiconductors that possess a large bandgap and therefore excited electrons transfer from the conductance band for practice that has a smaller bandgap and injection to the conductance band for practice that has a large bandgap and thus the excited state is quenching figure 1-8 explain this process [135-137].

1-15.Microbial E.coli ,S.aureose and Pseudomonas

The scientific name *Escherichia coli* is a type of gram-negative bacteria, the most important bacterium that lives in the intestines of mammals. *Escherichia coli* discover in 1885 by German doctor Theodor Escherich [138]. It lives naturally in the intestines of humans and animals, and at the same time, it is an opportunistic bacteria that causes many diseases such as sepsis and bacteremia, the optimum temperature for its growth is 36-37 ˚C[139]. *E.coli* bacteria are recognized to be resistant to many antibiotics such as lactams-β, aminoglycosides and quinolones [140,-

142] because of the high virulence of this bacteria and its resistance to many antibiotics, as mentioned above, to solve this problem, the study included the preparation of nanomaterials that act as antibiotics against microbes and a study of their efficacy. *S.aureose* Gram-positive bacteria, their name appears in the form of yellow-coloured colonies, when grown in blood agar, *Staphylococcus* can live in absence of oxygen. Staphylococcus aureus usually lives naturally on the skin of humans. It causes a range of diseases epidermis inflammation, meningitis and septicemia [143].

Penicillin, upon its discovery, showed high efficacy against Staphylococcus aureus, as Penicillin works to inhibit the formation of peptidoglycan bonds that protect the bacterial cell wall, Penicillin antibiotics affect the formation of the cell wall, leading to its death, but the problem of penicillin resistance has become common and has increased in recent times to become close to 100% in most countries of the world [144].

Not only do the skin and intestine host millions of commensal bacteria, but they also must rely on a variety of protective mechanisms to prevent pathogen entrance. As a result, the skin and intestine have established site-specific physical, chemical, microbiological, and immunologic barriers to protect against harmful microorganisms and sustain health[145]. Skin considers the first line of work as a physical barrier by protecting against external microbial contamination, when occurring damage to human skin by burin or wound that causes penetrating of microbial inside skin and causes inflammation of it. Human skin also acts as a chemical barrier, producing antimicrobial peptides[146]. *Pseudomonas* Gram-negative bacterial resistance of certain antibiotics, identified by Walter Migula Antipseudomonal to Pinciline. *Pseudomonas* bacteria are genera important bacteria because they are widespread due to their pathogenicity for humans, animals and plants, these bacteria can live

in diverse environments, they are free to live in soil and river water these bacteria inhabit damp areas, such as sinks, toilets, and insufficiently chlorinated swimming pools, and expired ineffective disinfecting solutions[147]. This bacteria can be found in the armpits and genital area of healthy people, Pesudomonose bacterial infection can be a simple external infection and be a serious, life-threatening disorder for people with diabetes and for patients who take medications that suppress the immune system, such as those used to treat cancer, or to prevent rejection of transplanted organs. These bacteria can cause infections in the blood, skin, bones, ears, eyes, urinary tract, heart valves, and lungs, as well as in wounds (such as burns, injuries, or surgical incisions). The widespread use of antibiotics in treating this bacterium, that it led to the development of resistance to antibiotics[148,149].

1-16.Cell culture

Cell culture is the process of removing cells from an organism and placing them in a fluid media. Under the right conditions, the cells can survive, develop, and proliferate. Cell division (mitosis) or other processes, such as apoptosis, can be used to identify and describe growth differentiation, the process by which cells can transform into specific types that are capable of performing duties similar to tissues or organs as a whole organism [150]. It is a technique used to allow cells to grow in physiologically desired settings. It is first used to examine tissue growth and maturation, virus biology, and vaccine evolution genes in sickness and health, as well as the utilization of hybrid cells to produce biopharmaceutics. Cell culture is most typically used in clinical settings connected to the evolution of model systems for studying basic cell biology replicating disease pathways or investigating the toxicity of novel drugs are

two examples of research compounds. The primary benefits of adopting this cell culture technology are as follows genes and molecular pathways can be manipulated. The purpose and benefit of cell culture are to train the researcher and familiarize him or her with the technique of undergoing cell setup and effectively propagating cells in vitro, as well as to ensure the safety of the cells researcher and aseptic settings that are free of contamination [151].

1-17. Cell's viability

Cell viability and proliferation rates are utilized as measures of cell health. Physical and chemical agents can both have an impact on cell health and metabolism. Various techniques can bring harm or even death to a person such as cell membrane breakdown and protein inhibition in cultured cell synthesis, enzymatic processes, and irreversible receptor binding. To determine the cell death caused by these mechanisms, there is a need for reliable and reproducible short-term cytotoxicity and cell viability assays[152].

1-18. Vero cells

Vero cells are generated from the kidney of the African green monkey (Cercopithecus aethiops). Vero cells are a widely used mammalian continuous cell line, particularly in virology research and medical research, but it is also employed in a variety of other purposes, such as bacterial propagation and intracellular bacteria research parasites, as well as the effects of different chemicals and toxins on mammalian systems aspects [153].

1-19. Nanoparticles and Skin Cancer

The skin is the body's biggest organ and acts as the first line of defence against bacteria, ultraviolet radiation, and toxins. Additionally, the skin's strong barrier qualities limit salt and moisture loss while regulating the body's temperature. Skin diseases have opened up new opportunities for treatment by using nanoparticles [154]. The skin's barrier function makes it difficult for nanoparticles to penetrate the tissue, but when the barrier is partially disrupted by damage or inflammation, as is the situation with skin cancer this may promote nanoparticle penetration. Skin cancer can be roughly categorized into two types: (a) melanomas, which begin from melanocytes, such as shown in fiuger 1-7 and (b) non-melanoma skin cancers, which develop from epidermal cells [155] . Nanoparticles that penetrate the epidermis gain access to live and immunologically active cells and have the potential to travel to the lymph nodes[154].

The nanoparticles' have a challenge in the topical treatment of skin cancer, AK (Actinic Keratosis) and NMSCs (non-melanoma skin cancer) typically manifest clinically as hyperkeratotic or SC-thickened plaques, nodules, or

lesions. The scaly, thicker SC may prevent topically delivered nanoparticles from penetrating the lesion, hence limiting therapy efficacy [154]. While the physicochemical features of NPs play a role in beginning the interactions required to penetrate the SC barrier, the payload's biological or clinical effects occur at the cellular level following their exposure to the milieu of the skin malignancy. Apart from that, there are distinctions in the skin and tumour permeability varies according to anatomical location the SC is thick on the palmar regions of hair follicle density, skin moisture, and pH [156].

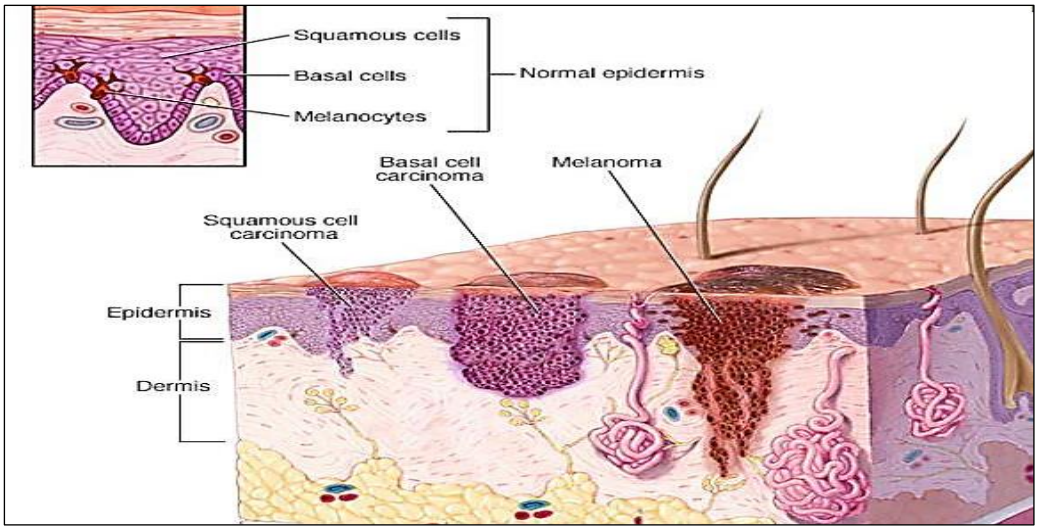

Figure 1-7. Skin cancer development site[157].

1-20.Literature survey

In 2013 Huaxu Gong *et al*. SiO_2/C nanocomposites have been prepared by coating with aniline onto the surface of SiO_2 nanospheres via a diazotization reaction and carbonizing treatment. The XRD pattern and High resolution transmission electron microscope show that the amorphous SiO_2 nanoparticles are coated with carbon [158].

In 2014 Zhou Mao *et al*. A series of nanocomposites consisting of zero-valent iron nanoparticles (ZVI NPs) encapsulated in SiO_2 microspheres were successfully synthesized through a successive two-step method. The catalytic performance of SiO_2-encapsulated nanocomposites for the degradation of organic dyes was investigated using methylene blue (MB) as the model dye in the presence of H_2O_2[159].

1n 2015 Charu Bharti *et al* . Demonstrate a previous search for the term "synthesis." By employing the sol-gel process, which entails two steps: hydrolysis and condensation, a mesoporous silica nanopowder is created. In an aqueous solution, hydrolysis produces colloidal particles; at neutral pH, condensation occurs, resulting in the formation of a gel-like three-

dimensional network structure via siloxane cross-linking. This technique results in the creation of mesoporous silica with a diameter of between 60 - 1000 nm[160].

In 2015 Xueliang Liu *et al* . The preparation of a nano Fe/Ni alloy on a silica substrate and its application to the viscosity reduction of heavy oil, the preparation of nano zero-valent iron and nickel particles in a silica composite (SiO_2/Fe/Ni) is accomplished by sodium borohydride reduction of a ferric chloride and nickel chloride mixed solution in the presence of surface-modified silica. The results indicate that the SiO_2/Fe/Ni catalyst exhibits activity in the aquathermolysis of heavy oils [161].

In 2016 Van Thi Thanh Ho . The sol-gel and chemical reduction strategies for generating Fe/SiO_2 NPs composites are studied in this work. They discovered that the Fe/SiO_2 nanocomposite behaves differently depending on the Fe/SiO_2 ratio. Discovered that when the Fe nanoparticles are uniformly dispersed over the SiO_2 support, the surface area of Fe on SiO_2 increases and the stability of Fe on SiO_2 increases when compared to pure Fe. Fe/SiO_2 has a surface area of approximately 50.108 m^2/g, which is significantly greater than the surface area of pure Fe (26 m^2/g). The results of this work reveal that a sol-gel and a chemical reduction procedure can be employed to create a very uniform distribution and surface area of Fe/SiO_2 nanocomposite[162].

In 2016 Usama Zulfiqar *et al* .They are investigating the synthesis of silica nanoparticles from tetraethyl orthosilicate, as well as the synthesis of silica nanoparticles from sodium silicate solution in an alkaline media[163].

In 2017 S.V. Lazareva *et al.* The colloidal silica (silica sol) nanoparticles are produced through ammonia and hydrochloric acid-catalyzed

tetraethoxysilane hydrolysis, followed by condensation and polymerization [164].

In 2017 Jahanbakhsh, Ali *et al* .The current work fabricates novel magnetic nanocomposites from Fe_3O_4-Hydrogel and Fe_3O_4@SiO_2-Hydrogel. Poly(styrene-alt-maleic anhydride) is used as a hydrogel component. The hydrogel is extremely efficient at removing some organic and inorganic pollutants from water samples, including methylene blue. Magnetic Fe_3O_4 nanoparticles may help in the separation of hydrogen from the water following magnet removal [165].

In 2018 Euiseob Yang *et al*. The synthesis of innovative SiO_2@V_2O_5@Al_2O_3 catalysts demonstrates the highest catalytic activity when used in the conversion of methane to formaldehyde with a selectivity of 57.8 % [166].

In 2018 William E. Taifan *et al* . The electrical structure and reactivity of Cu- and Zn-promoted wet-kneaded MgO/SiO_2 catalysts were determined during the ethanol to 1,3-Butadiene conversion[167].

In 2018Lee, Dae-Won *et al* . This article method for producing silica-coated Fe_3O_4 nanoparticles that may be used to bioseparate fetuin from fetal bovine serum and albumin from eggs. In this study, uniform Fe_3O_4 particles are prepared using a single iron precursor and then coated with SiO_2 to form silica-coated Fe_3O_4 NPs via hydrolysis and condensation of tetraethyl orthosilicate in ethanol and H_2O medium [168].

In 2019 VirendraKumar Yadava et al. The production and characterisation of amorphous silica nanoparticles from fly ash using the sol-gel process; the resulting silica nanoparticles exhibit a variety of properties[169].

In 2019 Krisztian Nemeth *et al* .The present publication describes the successful fabrication of multi-walled carbon nanotubes (MWCNT) coated with SiO_2–MgO nanoparticles via the sol-gel method to facilitate their incorporation into polymer matrices. Magnesium acetate tetrahydrate and tetraethyl orthosilicate were used as precursors [170].

In 2020 Abdulrazzaq, H. T *et al.* This work involved the development of a model MgO–SiO_2 catalyst and the analysis of the reaction kinetics of ethanol dehydrogenation to acetaldehyde using this material [171].

In 2020J.Sastre-Hernandez et al. In this work silicon dioxide (SiO_2) is synthesized from rice husk as raw material. The sodium peroxide (Na_2O_2) influence as a precursor on the catalytic activity of the final product was investigated[172].

In 2021 Leshan Usgodaarachchi *et al*. Surface-controlled amine functionalization of mesoporous silica nanoparticles produced from rice husk for effective adsorption of methylene blue from aqueous solution. The amorphous silica nanoparticles have a surface area of 150 m^2 /g and a diameter of 50–60 nm[173].

In2021 Jun Gyeong Lee *et al*. studied the role of a vanadium oxide supported by mesoporous silica (VOx/m-SiO_2) catalysts in the oxidation of methane to formaldehyde is being investigated[174].

In 2021 Mohammadi, Somaye *et al*. The work developed a hollow MgO/SiO_2 nanocatalyst with excellent base characteristics. This heterogeneous catalyst was synthesized from TEOS [175].

In 2021 Jingdong Shi *et at* . Studying cytotoxic properties of silica (SiO_2) particles against cancer remains debatable. The purchased submicron silica particles (SM-SiO_2) are identified by SEM and EDX. They demonstrated

potent cytotoxicities on hepatocellular carcinoma (HCC), non-small cell lung cancer (NSCLC), and breast cancer (BC), which ranked first in incidence among the tumour types[176].

In 2022 PratibhaSharma *et al*. Green synthesis of nanomaterials is a sustainable, biologically safe, reliable, and eco-friendly approach. This review deals with the green synthesis of silica nanoparticles (SiO_2 NPs) with emphasis on the engineering surface properties for enhanced adsorption capability and their applications as novel nano-adsorbents for water pollutants removal [177].

1-21 Aims of present Project

The main aims of the present work are to synthesis, characterized and investigate biological activity for some new composite oxides as a reagent for medical skin treatments, as follows

1. Preparation of nano-silica oxide powder by using green synthesis based on a natural product of rice husk as starting raw material for new composite oxides.

2. Preparation of nanocomposite (SiO_2/V_2O_5/, MgO/ SiO_2, and Fe_xO_y/SiO_2) by using modified sol-gel method, wet method and sol-gel method respectively.

3. Estimation of the optimum condition for the prepared nanocomposite such as percent ratio of preparing and temperature of calcination.

4. Characterization of the chemical and physical structures of the prepared nanocomposite by using a different instrumental technique such as X-ray diffraction, energy-dispersive x-ray spectroscopy (EDX), field emission scanning electron microscopy (FE-SEM), FT-IR techniques and BET.

5. Investigation of the antibacterial activity for the prepared nanocomposite toward some bacterial *E.Coli*, *S.aureas* and *Pseudomonas* by indirect method.

6. Investigation of the antibiotic activity assay by using a wound dressing

7. Determination of Minimum Inhibitory concentration (MIC) and Minimum Bactericidal Concentration (MBC) of an antimicrobial agent for the prepared nanocomposite required to kill a certain bacterium.

8. Preparation of some ointment medical cream base on nano binary oxide SiO_2/V_2O_5 and MgO/SiO_2.

9. Estimation of the effect of nano preparative materials on skin cancer cell lineA431.

10. Estimation cytotoxicity of nano preparative materials on Vero cell line101.

2. Experimental

2-1. Chemical Materials

Chemicals that have been used are described in table 2-1.

Table 2-1. Chemicals according to purities and were manufactured.

No	Chemical Materials	Manufacture	Purity %
1	Vanadium oxide	S.D. Fine-chem. Ltd., India	99%
2	Sodium hydroxide (NaOH)	Barcelona-Spain	99%
3	Magnesium oxide MgO	Alfa, Aesar, USA	99%
4	Oxalic acid	Alfa, Aesar, USA	99.93%
5	Tetra ethyl ortho silicate (TEOS)	Emirates industrial gases	99%
6	$Fe(NO_3)3.9H_2O$	Emirates industrial gases	99.9%
7	Ammonium hydroxide (NH_4OH)	Alfa, Aesar, USA	99.6%
8	Sulfuric acid H_2SO_4	Alfa, Aesar, USA	97%
9	Ethanol	Alfa, Aesar, USA	99.93%
10	Hydrochloric acid HCl	Aldrich, German	36%
13	Mueller-Hinton agar	Aldrich, Germany	97%
14	Nutrient broth	BDH, England.	99%
15	Sodium chloride NaCl	Sigma, Aldrich, Germany	99%
16	RPMI Medium 1640	Gibco-TM	97%
17	Bees wax white	Cera Alba	99%
18	Borax decahydrate	BDH	99%

19	MTT(3-(4,5- Dimethylthiazole-2-yl)- 2,5-diphenyl-2H tetrazolium bromide) dye powder	Sigma-Aldrich-M12128	95%
20	Fetal bovine serum (FBS)	Europe –Euro lone	99%
21	Trypsin Ethylene diamine tetra acetic acid (EDTA) powder	US biological	95%
22	Phosphate buffer saline packets	BioPLUS chemicals	95%
23	Sodium bicarbonate powder	ANTACID	97%
24	Skin cancer cell line A431 and Vero cells 101 line	National Institute of Genetic Engineering and Biotechnology in Tehran, Iran,	-

2.2 Instruments Analysis

Instruments that have been used are described in table. 2-2.

Table 2-2. Instruments according to their manufacturers' companies and location.

No	Apparatus	Company	location
1	X-Ray Diffraction	2700 AB HAO YUAN, Shimadzu,Japan	Sharif University of Technology, Iran, Tehran,
2	Filed Emission Scanning electron microscopy (FE-SEM)	MAG 400 Kx Germany	Sharif University of Technology, Iran, Tehran,
3	Energy-Dispersive X-ray Spectroscopy (EDX)	MAG 400 Kx Germany	Sharif University of Technology, Iran, Tehran,
4	Brunauer-Emmett-Teller (BET) Surface Area	Horiba SA-9600	Sharif University of Technology, Iran, Tehran,
5	Electrical Magnetic stirrer	Heidolph- Mr Hei-Standard-Germany.	College of Science, University of Babylon

6	Spectrophotometer visible-1650	shimadzu	College of Science, University of Babylon
7	Fourier Transform Infrared spectrophotometer.	8400S, Shimadzu-Japan.	College of Science, University of Babylon
8	furnaces	XIN YOO electronic components co. Ltd.	College of Science, University of Babylon
9	pH meter	Hanna-Romana.	College of Pharmacy, University of Babylon
10	Sonication bath	FALC-Italy	College of Science, University of Babylon
11	Oven	Memmert-Germany.	College of Science, University of Babylon
12	Inverted Microscopy	Germany	College of Science, University of Babylon
13	Incubator	Memmert-Germany.	College of Science, University of Babylon
14	Autoclave	(HIRAYAMA)	College of women science, University of Babylon
15	ELISA Reader (Microplate reader)	800-TS-Germany	College of women science, University of Babylon

2-3.Extraction of silica oxide from rice husk ash

The rice husks (RH) are cleaned from the soil. RH treated with acetic acid then washed with hot distilled water and dried at 100 °C for 3 hours. Then it is burned at 700°C for 3 hours, the product is white ash. About 10 g of burning sample is treatment with 80 ml of sodium hydroxide (NaOH) solution 2.5 N concentration under a magnetic stirrer, at 100 °C for 4 hours dissolve the silica existing in RHA by using a 250 Erlenmeyer flask. The resulting are filtered and washed with warm

distilled water, the product is transparent viscous and colourless, it is a sodium silica solution such as the following reaction

SiO_2 (RHA) + 2NaOH → Na_2SiO_3+ H_2O…2-1

Using titration method to extraction of pure silica oxide. By preparing 5N of sulfuric acid solution H_2SO_4 and gradually adding to sodium silica solution with a magnetic stirrer under 100-90˚C in this step complete precipitation of silica and form of sodium sulphate as the following reaction

Na_2SiO_3+ H_2SO_4 → SiO_2 + Na_2SO_4 + H_2O ... 2-2

The gel product washing many times with warm distilled water to remove the sodium sulphate impurities. To extract of pure nano-silica dioxide by using the refluxing method with 100 ml of Hydrochloric acid (6 N) HCl solution for 6 hours under 80-90 ˚C. Addition of boiling stone for uniform temperature distribution [178,179]. The purpose of the reflexing process is to heat the solution for the longest period without losing volume, as a complete melting of the sample is achieved, which is thermodynamically preferred, as it increases the speed of the reaction, regulates the crystals, and obtains nanoparticles [180]. After the reflexing process finishes the product solution is filtrated and participation washed with warm distilled water to remove impurity, then dried in the oven at 100 ˚C for 24 hours. Characterization of nano powder silica oxide by X-ray diffraction (2700 AB HAO YUAN), energy-dispersive x-ray spectroscopy (EDX), field emission scanning electron microscopy (FE-SEM), and FT-IR techniques.

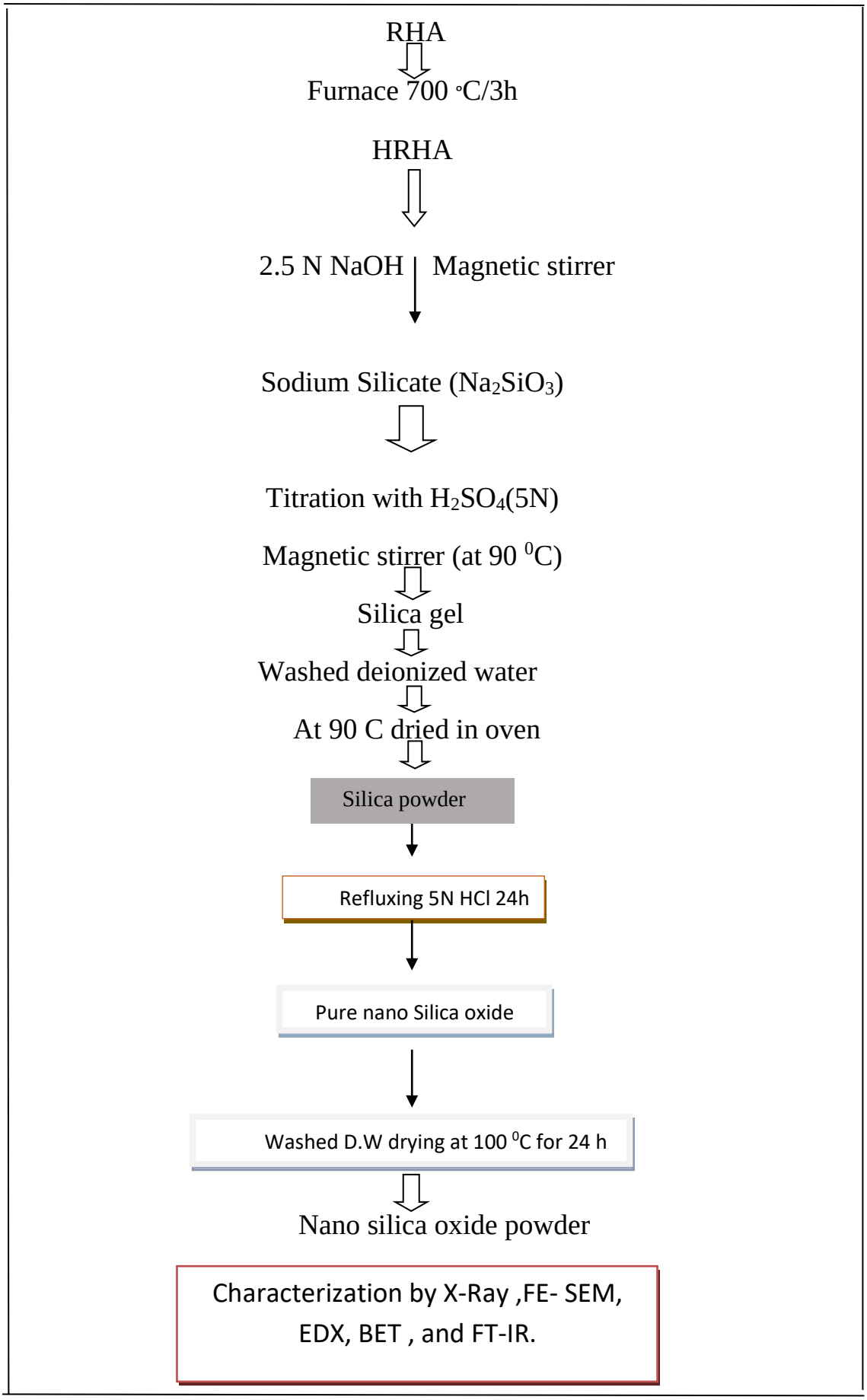

Schema2-1. Schematic diagram of Nano silica powder preparation.

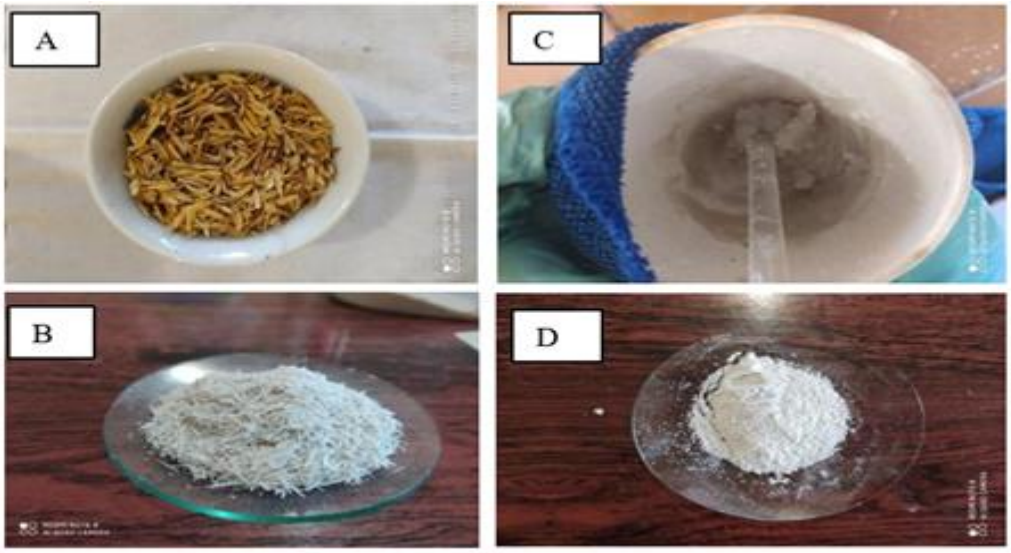

Figure2-2 .Images of preparation steps of Nano silica oxide. A. Rice husk, B. Rice husk ash at 700 ˚C, C. silica gel, and D. Nano silica oxide powder.

Figure 2- 3. Image reflexing process of silica oxide to form nanoparticles of silica oxide without impurity.

2-4 Effect of burn temperature on the colour of rice husk ash

Rice husk is calcination to produce RHA. The ash form can either be white, black or grey depending on the calcination temperature. Silica with high purity can be obtained from rice husk ash when calcination with high temperature and gat on white ash (181).

Table 2-3. Effect of combustion temperature on the ash from rice husk.

Combustions	Time/Hour	Colour of ash
200	3	**Without change**
300	3	**Black**
400	3	**Dark brown**
500	3	**Light brown**
600	3	**Whitish**
700	3	**White**

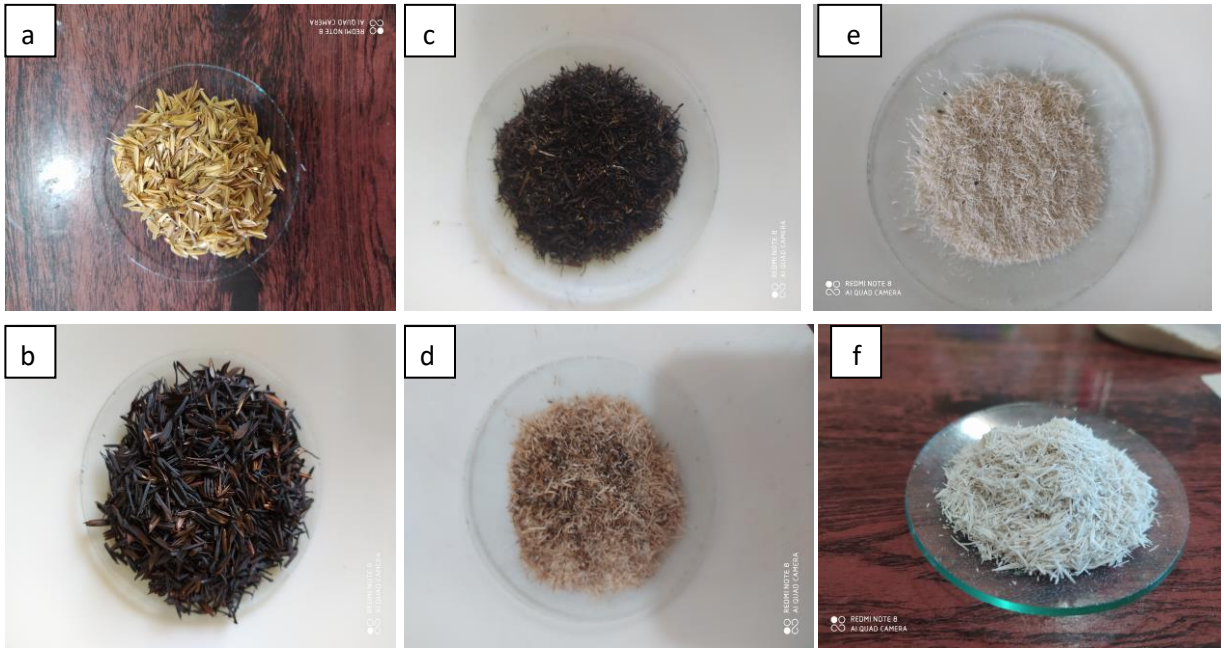

Figure 2-4. Effect combustion temperature on rice husk at a. 200˚C, b.300 ˚C, c.400˚C ,d.500 ˚C, e.600˚C, and f.700˚C.

2-5. Effect of calcination temperatures on Nano silicon oxide

Nano silica oxide that is prepared by green synthesis method study affected of calcination temperatures on it. By taking the difference range from calcination temperatures (300, 400, 500,600, and 700) ˚C and studying the effect of it on average particle size and activity of surface for nano-silica oxide extracted from rice ash.

2-6. Synthesis of nano binary oxide SiO_2/V_2O_5

Synthesis of Nano binary oxide SiO_2/V_2O_5 by using a modified sol-gel method that involves preparation of three steps the first involve preparation of silica gel from RHA such as shown in previous pages.

Second step preparation of solution by adding 15 mL of deionized water, 35 ml ethanol and 7 ml ammonia are added into 250 Erlenmeyer flask. Then stirring at room temperature. Three-step involve dissolving 0.5 g of Vanadium pentaoxide [V_2O_5] in 15 ml of deionized water and mixing it with the silica powder and adding it to the second solution. After that ultrasonic treatment for 15 minutes. The colloidal dispersion is stirred for 12 hours. Nanocomposites are separated by centrifuge and washed with deionized water three times, and then dried in an oven at 60°C [182].

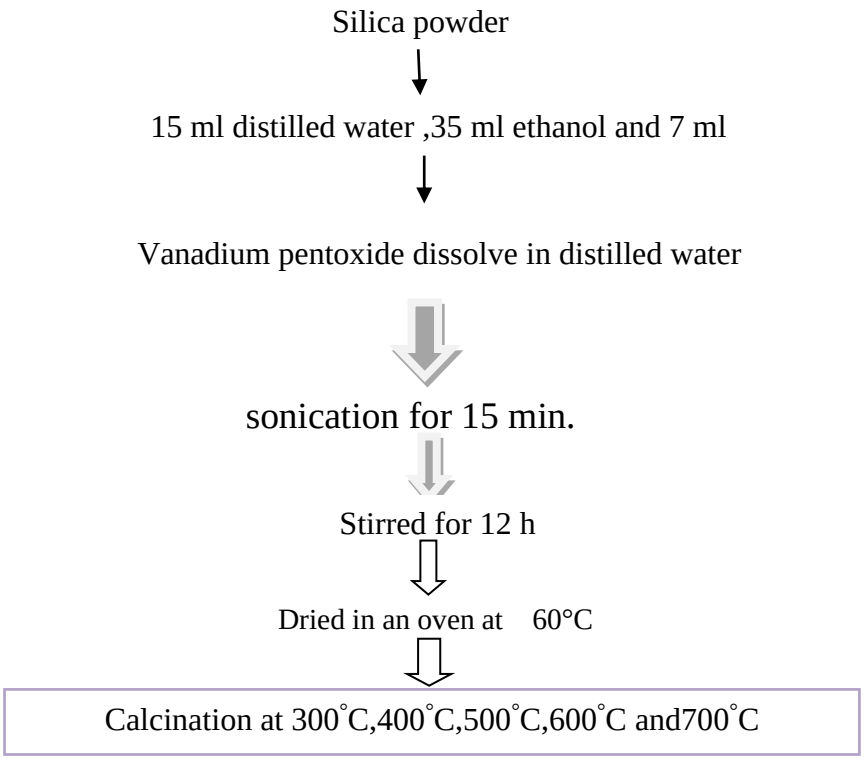

Schema 2-5. The schematic diagram for preparation of nano binary oxide SiO_2/V_2O_5 powder.

Figure 2-6. Steps of reaction to gate on Nano binary oxide SiO_2/V_2O_5 a.at first of mix b. after 12 h of the stirrer, c. when dried in an oven at 60 ˚C, and d. after calcination at 300 ˚C for 3 hours.

2-7 .Effect of calcination temperatures on Nano binary oxide SiO_2/V_2O_5

Nano binary oxide SiO_2/V_2O_5 product that is prepared by a sol-gel method depends on RHA as raw material. Study the affected calcination temperatures on a product by taking the difference range of calcinations temperatures (300,400,500,600 and 700) ˚C. Measure FE-SEM, EDX, FT-IR and BET for Nano binary oxide SiO_2/V_2O_5 with different calculations temperatures.

2-8.Synthesis Nano binary oxide Fe_xO_y/SiO_2 by Sol-gel method

By using the Sol-gel method to preparation of Fe_xO_y/SiO_2 nanoparticles by preparing two solutions [183]. The first solution consists of tetra ethyl orthosilicate (TEOS) 1ml dissolved in 10ml of ethanol. Solution two is prepared by mixing iron nitrate $Fe(NO_3)3.9H_2O$ (0.6) g with oxalic acid ($H_2C_2O_4.2H_2O$) 1g dissolved in 10 ml of ethanol and adding the mixture to the first solution. The two solutions are stirred for 4 hours then the solution ageing for two days. Gel formation washing many time by deionized water, and then dry at 60 ˚C. Then calcination at difference calcination temperatures (300-700)˚C.

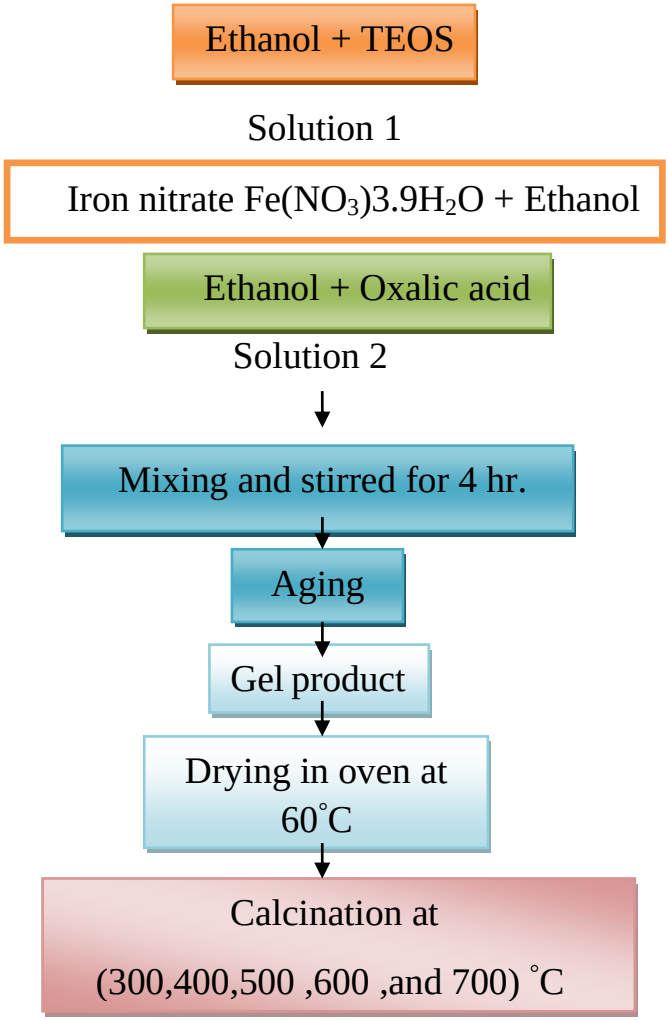

Figure 2-7. Scheme diagram for the synthesis of nano binary oxide Fe_xO_y/SiO_2.

Figure 2-8. Image for nano binary oxide Fe_xO_y/SiO_2 a. before calcination b. after calcination at 300˚C, and c. calcination at 700 ˚C

2-9 Study the effect of calcination temperatures on magnetic nano binary oxide Fe_xO_y/SiO_2

Nano binary oxide Fe_xO_y/SiO_2 product prepared by sol-gel method the studies of the affected calcination temperatures on practical size, surface area and the concentration of elements found in sample product. by taking 1g from product milling by mortar and calcination it at a different range of calcinations temperatures (300,400,500,600, and700) ˚C for three hours. Then measure X-ray diffraction FE-SEM, EDX, FT-IR and BET for Nano binary oxide Fe_xO_y/SiO_2.

2-10 Synthesis of Nano binary oxide MgO/SiO_2

Nano binary antibiotic oxide MgO/SiO_2 synthesis by using the wet method, the process involves taking difference percentage weight from nano silica that prepared at first stage from RHA and difference percentage weight from magnesium oxide such as following table 2-4. Each of the different percentages dissolve in 10 ml ethanol and 10 ml deionized water is added to the beaker 100 ml. After that ultrasonic treatment for 15 minutes, the mixture solution is permanently stirred at 50 ˚C until dry then washed for much time with deionized water, and then dried in an oven at 100 ˚C.

Table 2-4. Preparation of antibiotics with different ratios at calcination temperatures of 300˚C.

Antibiotic	Percentage MgO/SiO_2	Calcination temperature ˚C
E1-MG-75	0.75/0.25	300
E2-MG-25	0.25/0.75	300
E3-MG-90	0.9/0.1	300
E4-MG-50	0.5/0.5	300

2-11. Effect of calcination temperatures on the synthesis of Nano antibiotic MgO/SiO_2

Many of the experiments we are made to study the synthesis many of antibiotics of Nano binary oxide MgO/SiO_2 by using the wet method and study the effect of calcination temperatures on each percentage (0.75/0.25, 0.25/0.75,0.9/0.1, and 0.5/0.5) such as shown in table 2-5.

Table 2-5. The preparation of antibiotics with different ratios and each ration combustion at different calcination temperatures.

Calcination temperatures ˚C	Antibiotic 1 MgO/SiO_2	Antibiotic2 MgO/SiO_2	Antibiotic 3 MgO/SiO_2	Antibiotic 4 MgO/SiO_2
300	0.75/0.25	0.25/0.75	0.9/0.1	0.5/0.5
400	0.75/0.25	0.25/0.75	0.9/0.1	0.5/0.5
500	0.75/0.25	0.25/0.75	0.9/0.1	0.5/0.5
600	0.75/0.25	0.25/0.75	0.9/0.1	0.5/0.5
700	0.75/0.25	0.25/0.75	0.9/0.1	0.5/0.5

2-12. Study the effect of antibiotic of Nano binary oxide MgO/SiO_2 on a different type of bacterial

Preparing many antibiotic stock solutions from nano binary oxide MgO/SiO_2 by taking a different concentration of each antibiotic with different calcination temperatures. Studying antibiotic activity for each sample with different types of microbes Gram-positive such as *S.aureas* and Gram-negative such as *E.Coli* and *Pseudomonas*.

Table 2-6. The preparation of antibiotics with different ratios and each ration combustion at different calcination temperatures.

Calcination temperatures ˚C	Antibiotic1 MgO/SiO_2	Antibiotic2 MgO/SiO_2	Antibiotic 3 MgO/SiO_2	Antibiotic 4 MgO/SiO_2
300	E1-MG-75	E2-MG-25	E3-MG-90	E4- MG-50
400	D1-MG-75	D2-MG-25	D3-MG-90	D4- MG-50
500	C1-MG-75	C2-MG-25	C3-MG-90	C4- MG-50
600	B1-MG-75	B2-MG-25	B3-MG-90	B4 -MG-50
700	A1-MG-75	A2-MG-25	A3-MG-90	A4-MG-50

2-13. Antibacterial test by an indirect method

Antibiotic activity measure of pure Nano silica oxide extracted from RHA, and Nano composited SiO_2/ V_2O_5, Fe_xO_y/SiO_2 and SiO_2/MgO. Antibacterial is tested against different types of bacterial gram-positive *Staphylococcus aureus* and gram-negative *E.Coli* and *Pseudomonas* by using the spectrophotometric (indirect method). The spectrophotometric method involves the preparation of solutions of nutrient broth powder by dissolving 13 g in 1000 ml of distilled water and sterilizing in the autoclave at 121 ˚C for 15 min. Sodium chloride solution was prepared by dissolving 1 gram of NaCl in 100 ml distilled

water and then sterilized in an autoclave for 15 min. A study of the effect of antimicrobial activity with different concentrations of synthesis nano binary oxide stock solution was prepared for each synthesis nano binary oxide (SiO_2, SiO_2/ V_2O_5, Fe_xO_y/SiO_2, and SiO_2/MgO,).By weighing 0.05 g of binary oxide dissolved in 20 ml of 10% DMSO. Stock solution with a concentration of 2500 µg/ml was sterilized in an autoclave for 15 min at 121 ˚C and treated with ultrasonic for 24 h. Then preparations of different concentrations of synthesis nano binary oxide from stock solutions (SiO_2, SiO_2/ V_2O_5, Fe_xO_y/SiO_2 and SiO_2/MgO). Added 1 ml of bacterial (*E.Coli, Staphylococcus aureus* and *Pseudomonas*) for each concentration then incubate at 37 ˚C for 24 h [64]. The antibacterial activity percentage of each type of bacterial (*E.Coli, Staphylococcus aureus* and *Pseudomonas*) with different concentrations was calculated by using the following equation

Antibacterial activity percentage = (Growth of control – growth of treatment) *100
Growth of control
…(2-5)

Study the effect of inhibition growth of Gram-positive and Gram-negative bacterial such as (*Escherichia coli*, *Staphylococcus aureus* and *Pseudomonas*) by using nano binary oxide (SiO_2, SiO_2/ V_2O_5, Fe_xO_y/SiO_2 and SiO_2/MgO) with difference calcination temperatures for each sample and take difference concentration from stock solutions for each sample with difference calcination temperatures.

2-14. Antibiotic assay by using a wound dressing

This method depends on the preparation of the culture of bacteria with a concentration of $1.5*10^{8}$ CFU/ml. Preparation of Muller Hinton agar solution by weighting 38 g in 1000 ml distilled water and sterilizing in an autoclave for 15 min at 121 ˚C and 1 atom, after cooling to 35 ˚C pour in Petri dishes and waited to be solidified. Then preparation stock

solution of nan binary oxide (SiO_2, SiO_2/ V_2O_5, $Fe_xO_y/SiO_2$and SiO_2/MgO) was also sterilized in an autoclave for 20 min at 121 ˚C. Stock solutions sonication for four hours. After that take bandage (gauze) is cut in a circle shape with a diameter between (2.5-3) cm. After that gauze pieces are sterilized in the oven at a temperature of 80 ˚C. The gauze pieces were immersed in nano oxide solutions that were prepared in different doses (high, medium, and low) dose. Petri dishes are incubated for 24 h at 37 ˚C. On the next day observed inhibition percentage growth (zone inhibition) measures for samples.

2-15. Determination of MIC and MBC

The MBC and MIC tests are measures for nano binary oxide (SiO_2, SiO_2/V_2O_5, $Fe_xO_y/SiO_2$and SiO_2/MgO) MBC the minimum concentration of an antimicrobial agent required to kill a certain bacterium. The MBC is calculated in a sequence of steps following the completion of a Minimum Inhibitory Concentration (MIC) test. A pure culture of Nutrient Broth preparation the sterile in an autoclave, take series concentration for silica oxide (1500, 1250, 625, 156.2 and 31.25) µg/ml and added 1 ml of G-negative bacterial (*E.Coli*) for all tubes, then all tubes test incubation period 24 h at 37˚C. All previous steps are repeated for the rest of the nano composition concentration (312.5, 156,31.25,and 15.625) µg/ml for SiO_2/MgO (1000,937,625,312,156.2,31.23) µg/ml for Fe_xO_y/SiO_2 ,and (625, 312.5, 156.2, and 31.25) µg/ml**.** for SiO_2/ V_2O_5 respectively.

2-16. Preparation of some medical ointment

Composition of medical ointments from the prepared active ingredient and applying them to medical gauze the preparation method includes several steps preparation of an ointment base. Which consists of

two phases, the first is an oil phase including emulsifier materials and the second is an aqueous phase. The oil phase includes weight of 12.5 g of beeswax white and 70 ml of paraffin oil, and it is placed in a ceramic jar inside a water bath at 60˚C. Then added the mineral oil (paraffin) and mix well. An aqueous phase preparation by weight of 1g of borax and 1g of water dissolves the borax into the water in a water bath at 60 ˚C (both liquid phase and oil phase at the same temperature). After completing the melting process for the oil phase, the water phase is gradually added to the oil phase with continuous stirring. Benzoic acid (0.1%) a preservative is added to its antibacterial. [184]. Benzoic acid itself has low toxicity [185].

Figure 2-9. Medical ointment cream preparation from nano binary oxide SiO_2/MgO E4-MG-50 (left) and SiO_2/V_2O_5 (right).

2-16-1 Study activity of medical ointment on *S.aureas*

After preparation ointment base takes 1g from emulsions and mixes with different weights of (0.04, 0.06, 0. 08 and 0.1) gram of nano active powder (SiO_2/V_2O_5 and SiO_2/MgO). Each weight of nano-active powder is mixed well to ensure the homogeneity of the active substance with the emulsion (ointment base) to obtain an effective medicinal ointment.

After that, a prepared culture of bacteria, sterile nutrient agar solution is prepared and put into dishes and waited to be solidified. After that holes are generated with the help of a cork borer. Bacterial culture is spread on the agar with a sterile cotton bud. Holes are filled nano effective medicinal ointment. After that, the plates are incubated for 24 h at 37˚C. The zones of inhibition are observed the next day and calculated.

2-17. Preparation of stoke solutions

Preparation of stoke solutions from synthesis silica oxide and nano binary oxide (SiO_2/ V_2O_5, Fe_xO_y/SiO_2 and SiO_2/MgO) nanoparticles with a concentration of 20000 µg/ml by dissolving 0.05 g in 2.5ml of DMSO, the prepared solutions are sterilized in the autoclave (HIRAYAMA) for 30 minutes.

2-17.1 Preparation of Tissue Culture Medium

Liquid RPMI-1640 medium is prepared according to US Biologics from RPMI-1640 medium powder as the following: Weighting RPMI-1640 powder to obtain 16.353 grams and dissolved in 900ml of distilling water without heating, 2 g of sodium bicarbonate can be added if required with gentle stirring to adjust pH additional water was added to obtain 1 litre then filtered using 0.22-micron membrane. Penicillin-Streptomycin at 1% was added and 10% fetal bovine serum was also added, then filter-sterilized using a 0.22-micron membrane filter. The mixture contains heat-labile compounds that can be damaged with autoclaving. The prepared media should be kept at 4°C and used within a short period.

2-17.2 Preparation of cell line

2-17.2.1Thawing of Vero cells 101 lines, and skin cancer cell-A431 lines

The frozen cells (skin cancer cell-A341 and vireo cell) line vial is removed from a liquid nitrogen container with caution and directly placed into a beaker containing pre-warmed (37°C) sterile DDW. The vial is removed from the water before the ice floccule dissolved completely, and then it is wiped with 70% ethanol. Without delay, the cell suspension content of the vial is pipetted under a laminar flow cabinet into a 15 ml sterile plastic centrifuge tube containing 10 ml of pre-warmed serum-free medium. Centrifugation was done at 1000 rpm for 5 minutes and the supernatant is aspirated and decanted. The cells pellet was re-suspended into a 5ml warm (37˚C) serum medium and transferred into a 75 ml size cell culture flask, incubated at 37˚C and the serum medium was replaced on the next day [186].

2-17.2.2Sub-culturing of cell culture

The cells (skin cancer cell-A341 and vireo cell) lines are checked and examined using the inverted microscope with phase contrast capabilities to ensure that the cells are healthy and sub confluent and free of contamination. The laminar flow is sanitized by wiping off the surface of the working area with 70% ethanol. The growth medium is removed from the flask using a pipette and wash the monolayer with a sufficient volume of PBS (Phosphate Buffer Solution) to ensure the removal of all media from the flask. an appropriate volume of the trypsin/EDTA solution is added to the flask and incubated at 37 °C to allow the cells to detach from the inside surface of the flask (within 2-10 min). - The cells (skin cancer cell-A341 and vireo cell) are examined using an inverted

microscope to ensure that all the cells are detached and in suspension. Gently tap the flask with the palm a couple of times to release any remaining detached cells. The trypsin is inactivated by adding an equal volume of serum-containing media to the flask. Then the cell suspension is divided into two flasks and labelled each flask with a cell line name, passage number, and date. The cell line is incubated at 37°C for 24 h [187].

2-17.2.3Maintenance of cell culture

Cells (skin cancer cell-A341 and Vero cell) are routinely checked under an inverted microscope for any contamination and the cells are given a new medium (RPMI) every 2 to 3 days based on colour changes. The cells are maintained in supplemented medium with 10 % serum and kept at 37 ºC in an incubator. After the cells have achieved more than 80 % confluence, they were subculture [188].

2-17-2-4. Harvesting of cell culture

Harvesting is a technique that uses proteolytic enzymes to detach adherent cells from the surface of a cell culture flask. First, the growth medium in the vessel is aspirated and discarded. PBS (Phosphate Buffer Solution) is used to wash the cells twice. Afterwards, the enzymatic harvesting solution is added to the vessel. After 10 minutes, the proteolytic reaction is neutralized by adding the serum-containing culture medium. The cells in the tissue culture flasks are harvested by using different enzymatic solutions composed of different concentrations of trypsin and Ethylenediaminetetraacetic acid (EDTA) [189].

2-18. Vitro Method to Measure Cytotoxicity of prepared nano powders agents skin cancer-A431cells and Vero cells-101 line.

Cell lines including Vero cells-101 line and skin cancer-A431cells lines are seeded and labelled in 96 tissue culture plates. All cells (skin cancer-A431cells and Vero cells) are treated with different concentrations of synthesis nano-silica oxide powder and nano binary oxide (SiO_2/ V_2O_5, Fe_xO_y /SiO_2 and SiO_2/MgO) nanoparticles. Studying the effect of these nanoparticles with different concentrations (2000, 1000,500,250,125, and 62.5) µg/ml for nano-silica oxide and nanomagnetic binary oxide (Fe_xO_y /SiO_2). But at the same time, the preparation of the following concentrations from stock solution (2000,1000,500,250,125,62.5,31.25, 15.26 and 7.81) µg/ml for nano binary oxide (SiO_2/ V_2O_5 and SiO_2/MgO) where they are prepared, where sterile test tubes were prepared, take1 ml of the complete medium mentioned above was added into test tubes, except for tube number one was added 1.8 ml and 200µl from the stock solutions for nano-silica oxide and nano binary oxide (SiO_2/ V_2O_5, Fe_xO_y/SiO_2 and SiO_2/MgO) with a concentration of 20000µg/ml. First tube the concentration of it 2000 µg/ml, then is make a series of dilutions to prepare the following concentrations (1000, 500,250,125, and 62.5) µg/ml. After the preparation of the concentrations is completed, 200 µl is taken from each concentration and added to all cells (skin cancer-A431cells and Vero cells) that were seeded into a 96-well cell culture microtiter plate. Each concentration is replicated four times as a control group for each cell type. Then the plate was covered with a self-plastic lid and incubated at 37˚C for 24 hours, at the end of the exposure period, the cell lines growth was assessed by cytotoxicity assay by MTT assay. After the incubation

period add 200 µl of the MTT labelling reagent to each well, and incubate the 96-well cell culture microtiter plate for 4 h in a humidified environment, such as 37°C, 5–6.5% CO_2. The optical density (OD) measurement of each well is determined using a microplate (ELISA) reader at once, using a micro-plate reader set the wavelength at 570 nm. The user should open the micro-plate reader in advance, preheat the instrument, and set the testing parameter [190].

2-19. Identification of prepared nano powders

X-ray diffraction (2700 AB HAO YUAN), energy-dispersive x-ray spectroscopy (EDX), field emission scanning electron microscopy (FE-SEM), Spectrophotometer Visible-1650 Shimadzu and FT-IR techniques are used to characterize the effects of magnesium oxide, vanadium oxide and iron on modifying structural parameters and surface qualities of silica amorphous. Identification of chemical bonds formed by the strong interaction between nano binary oxide and silica oxide this interaction is suggested to be essential for the balanced surface acid: base sites.

2-19- 1 X-Ray diffraction and crystal size

Characterization and identification of pure nano-silica oxide powder extracted from rice husk ash, and nano binary oxide SiO_2/V_2O_5, Fe_xO_y/SiO_2 and SiO_2/MgO, and measure of average crystal size by utilization of X-Ray diffraction technology instrument model 2700 AB HAO YUAN Shimadzu, Japan is employed with Cu-kα as a radiation source wavelength 1.540 Å, and scanning started from (10-80) 2^{θ} X-ray diffraction technology used the sample attended as homogenous powder put on a slice slide and put in an x-ray path. spectra obtained contain diffraction angles, and interlayer distance between the surface in the crystal (d). This information is gate by Bragg's equation:-

$n\lambda=2d \sin^{\theta}$… (2-6)

Average crystal size can measure from x-ray diffraction technology data by the Scherrer equation [191].

$L = k\lambda/\beta \cos^{o} \ldots$ (2-7)

L= thickness of crystallite (mean crystal size), K= Scherrer s constant depends on crystal shape (0.94 is spherical, 0.90 tube or rode and 0.89 or 0.85 wire or other shapes), λ= is the wavelength (0.1540 nm), β= FWHM * Π/180 and$^{\theta}$ = is Bragg angle.

2-19-2Brunauer-Emmett-Teller (BET) Surface Area and pore-size distribution

The most extensively used approach for determining the surface area and pore size distribution of nitrogen adsorption is 77 K. The Brunauer–Emmett–Teller (BET) and Barrett–Joyner–Halenda (BJH) models are often used as analytical techniques for determining the adsorption/desorption isotherms. As all porous structures adsorb tiny gas molecules, the specific surface area calculated by BET is proportional to the overall surface area reactive surface (192). The specific surface area (m^2/g.) of synthesized samples is determined. The samples are dried using nitrogen purging or at extreme temperatures in a vacuum. At the boiling point of nitrogen (-196°C), the volume of gas adsorbed on the surface of the particles is determined. The amount of gas adsorbed is proportional to the overall surface of the particles, including any pores.

2-19-3. Field Emission Scanning Electron Microscope (FE-SEM)

SEM visual study of a surface assists in the identification of contaminates or unknown particles . FESEM analysis is used for particle characterization, such as wear debris created during mechanical wear testing, in addition to surface evaluation. FESEM analysis' high magnification, high-resolution imaging assists in the measurement of the

number, size, and shape of tiny particles, helping clients to better understand their material's wear qualities. The size and morphology of the nanostructures are determined for nano-silica oxide and nano binary oxide SiO_2/ V_2O_5, SiO_2/Fe_xO_y and SiO_2/MgO, at different calcination temperatures (300, 400, 500,600 and 700) ˚C using (FE-SEM MAG 400 Kx Germany). The solutions are either cast onto glass slides, dried, and then mounted to a sample holder using a little amount of dry powder deposited on a carbon paste-coated surface. To increase conductivity, the samples are subsequently coated with gold in argon gas. The secondary electron mode enables the presentation of a picture and thus the observation of particles.

2-19-4.Energy-dispersive x-ray spectroscopy (EDX)

Energy-dispersive x-ray spectroscopy is a qualitative analysis to find what elements are present in an unknown specimen by identifying the lines in the X-ray spectrum using tables of energies or wavelengths. Because a complete spectrum may be produced fast, the EDX spectrometer is very valuable for qualitative investigation. EDX spectrometer is used to identify nano binary oxide SiO_2/V_2O_5, Fe_xO_y /SiO_2 and SiO_2/MgO, at different calcination temperatures (300, 400, 500, 600 and 700) ˚C.

2-19-5. Fourier Transform Infrared Spectroscopy (FTIR)

FTIR spectra provide information about the chemical composition of solids, liquids, and gases. The most frequently encountered application is in the identification of unfamiliar materials. In most cases, the information content is quite particular, allowing for precise differentiation across similar elements. The rapidity with which FTIR analysis is performed makes it particularly suitable for screening applications.

Fourier Transform Infrared spectrum modal FTIR-8400S SHIMADZU, Japan of used for measuring silica oxide powder and nano binary oxide SiO_2/ V_2O_5, SiO_2/FexOy and SiO_2/MgO, at different calcination temperatures (300, 400, 500,600 and 700) ˚C. With a scanning range of 4000-400 cm^{-1}. Fourier Transform Infrared Spectroscopy study functions group and type bond in samples structure of nano-silica oxide and nano coupled SiO_2/ V_2O_5, SiO_2/FexOy and SiO_2/MgO, at different calcination temperatures.

2-19-6. Spectrophotometer

Visible -1650 Shimadzu spectrophotometer, Japan, is used to study the effect of inhibition growth of microbial that carried out on many types of (Gram-positive *Staphylococcus aureus* and Gram-negative *Escherichia coli* and *pseudomonas*) according to the indirect method that recommended by Clinical Lab. By taking various concentrations of antibiotic silica oxide. It is prepared from raw materials rice husk ash, and antibiotics of nanocomposites such as SiO_2/V_2O_5, MgO/SiO_2 and Fe_xO_y/SiO_2 with different calcination temperatures.

2-19-7. ELISA- Micro-plate Readers

Using absorbance, micro-plate readers-800-TS- Germany detect and process biological and chemical data. The optical density (OD value) of each well (96-well plate) is determined at once, using a micro-plate reader set to 570 nm after the mixed plate sample. The user should open the micro-plate reader in advance, preheat the instrument, and set the testing parameters.

3-1 Characterization of silica oxide and their nano composites

Extraction of silica oxide is being from washed rice husks by distilled water several times to remove impurities and soil particles. At last acid, treatment is used to remove alkaline elements before burning the rice husk. This is a necessary step in the production of high-purity silica and surface area. Rice Husk Ash (RHA) is an agricultural waste that contains several significant extraneous components. Therefore, thermal and acid treatments are effective, yielding a material with a high reduction in alkaline element content.[100] . To get on silica oxide with high purity using reflexing method and calcination at 700 $^{\circ}$C to get on RHA with white colour such as shown in figure 2-2. The purpose of the reflexing process is to heat the solution for the longest period without losing volume, as a complete melting of the sample is achieved, which is thermodynamically preferred, as it increases the speed of the reaction, regulates the crystals, and obtains nanoparticles [180].

3-1-1.X-Ray Diffraction Patterns and crystal size of nano-silica oxide powder

The pattern of the nano-silica oxide powder is characterized and detected after extraction from (RHA) by the X-ray diffraction technique, Cu Kα (λ = 1.54 A^0). Figure (3-1) shows the pattern of nano-silica oxide is orthorhombic amorphous. The diffraction peak of nano-silica oxide appears at 2θ [Theta] (24.149) show a single broad peak which is characteristic of amorphas silica . The average crystal size of silica oxide powder calculates from the Deby-Scherrer equation as shown in table3-1. The formation of amorphous nano silica oxide, with maximum intensity and particle size in the nanoscale [1] is shown in table 1-3.

Table 3-1. The crystal size of nano Silica oxide powder.

NO.	2θ [Theta]	Crystallite size (nm)
1	19.8980	42.862
2	21.8158	28.624
3	24.149	28.733
4	26.4091	47.740
5	28.0972	43.457
6	30.109	38.208
7	32.3190	58.477

Intensity

Figure 3-1. X-ray diffraction spectra of nano silica oxide powder at calcination temperature 300 ˚C.

3-1-2. X-Ray Diffraction Patterns and crystal size of nano binary oxide SiO_2/V_2O_5.

The modified sol-gel method counts on to synthesis of nano binary oxide SiO_2/V_2O_5. RHA is used as a precursor material instead of tetraethyl orthosilicate (TEOS). Nanocomposites SiO_2/V_2O_5 powder result is characterized by X-ray diffraction technique. Figure (3-3) explained a comparison between the x-ray pattern of vanadium pentoxide V_2O_5 pattern and nano binary oxide SiO_2/V_2O_5. Whereas

occurrence of new peaks with high intensity in pattern nano binary oxide SiO_2/V_2O_5 powder at 2^{θ} that's equal to 18.290, 23.812 and 28.406 with shift other peaks. When compared to the vanadium pentoxide V_2O_5 pattern in figure 3-2 the shift of peaks induced the overlap of small ion Si^{+4} with the lattice of pentoxide V_2O_5 crystal by the interaction between large ionic radiusV^{+5} 0.068nm [193] compare with a small ionic radius of Si^{+4} 0.040 nm. [194]. Also, results of X-ray diffraction show the average crystal size of binary oxide SiO_2/V_2O_5 powder in the nanoscale is smaller than the vanadium pentoxide V_2O_5 pattern as shown in table 3-2. The Scherrer equation is used to determine the average size of the crystallites qualitatively. X-ray diffraction of pure initial materials vanadium pentoxide V_2O_5 to explain the natural crystalline structure as shown in figure3-2.

$$L=k\lambda/\beta Cos\theta \quad \text{.....3-1[191].}$$

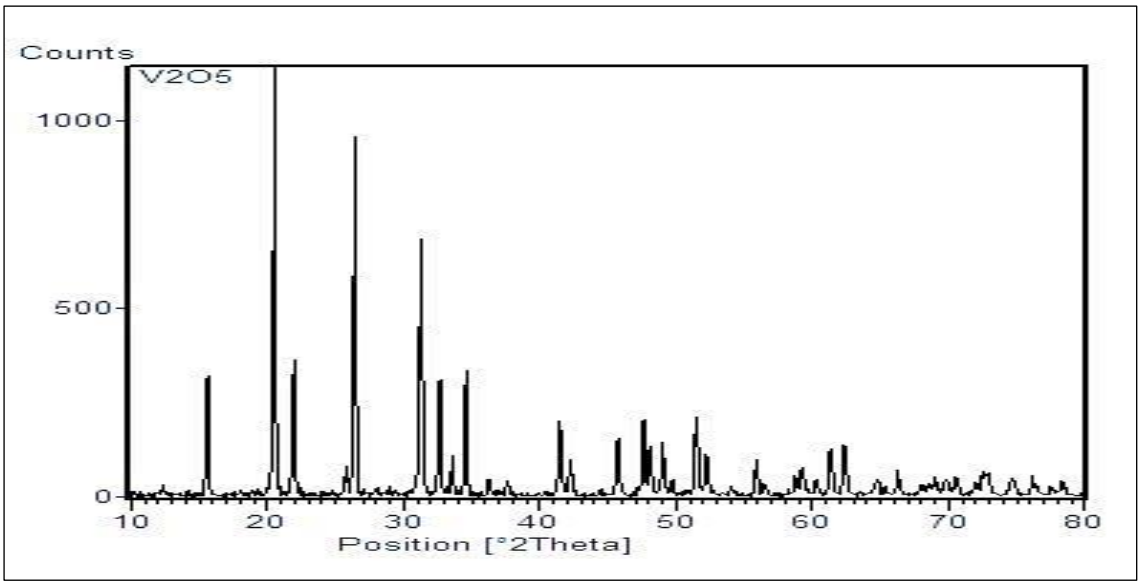

Figure 3-2. X-ray diffraction spectra of vanadium pentoxide at calcination temperature 300 ˚C.

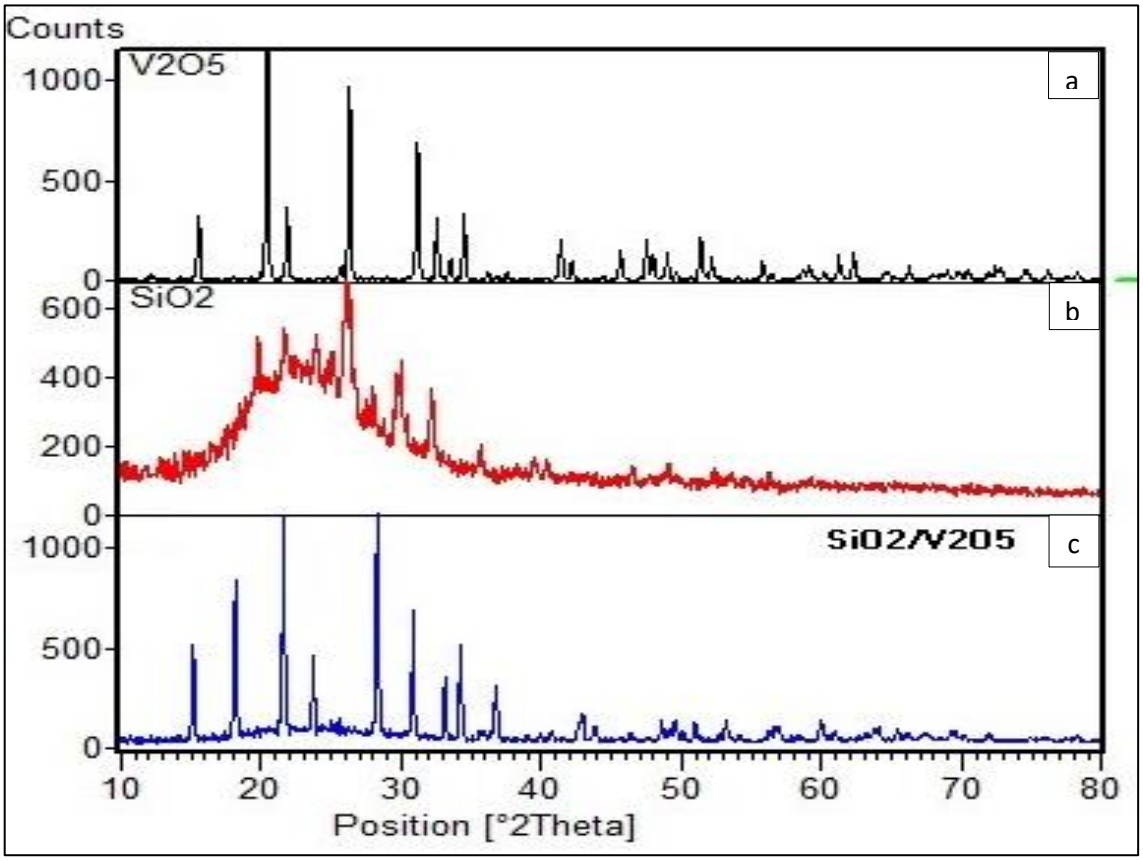

Figure 3-3. X-ray diffraction spectra of patterns a. Vanadium pentoxide V_2O_5, b. silica oxide and c. Nano binary oxide SiO_2/V_2O_5

Table 3-2. The crystal size of nano binary oxide SiO_2/V_2O_5 and vanadium oxide powders.

No	2^0[Th]	Crystal size nm SiO_2/V_2O_5	2^0[Th]	Crystal size nm V_2O_5
1	15.2739	42.450	15.6523	56.790
2	18.2904	36.779	20.5511	54.667
3	21.6912	37.019	22.0030	54.735
4	23.8126	27.193	26.4254	63.407
5	28.4068	47.623	31.2893	48.253
6	30.9426	43.421	32.6402	58.750
7	33.2276	43.622	34.5876	44.269
8	34.3261	43.724	41.4943	60.116
9	35.9159	17.551	47.5958	46.101

3-1-3. X-ray diffraction and crystal size of Nano binary oxide MgO/SiO_2

Characterization of nano binary oxide MgO/SiO_2 **(E4-MG-50)** which were prepared from composited magnesium oxide and silica oxide by using the wet method. Compression is marked between pure primary material and product of nano binary oxide MgO/SiO_2 **(E4-MG-50)** as shown in figure (3-4). That appears distribution of peaks at a range of 2θ (10-80) deg . X-ray diffraction techniques can be used to understand the crystalline. Figure 3-4 shows the diffraction peak of nano binary oxide MgO/SiO_2 **(E4-MG-50)** appeared at 2theta values indexing the structure is orthorhombic. From figure 3-4 of nano binary oxide, MgO/SiO_2 **(E4-MG-50)** observe at 2theta 20-30 broad peak index to silica oxide present in the crystal structure of nano binary oxide MgO/SiO_2 **(E4-MG-50)**. Also, observe shift peak at 2 theta 42.689 and 62.096 which indicates an overlap between silica oxide and magnesium oxide. produce nano binary oxide with new physicochemical properties. The shift conforms to the overlap of Si^{+4} with MgO. The shift of peaks difference is due to the ionic radius of Si^{+4}(0.040nm) being smaller compared to that of Mg^{+}(0.072nm) [195]. The average size crystal of (E4-MG-50) powder calculates from the Deby-Scherrer equation as shown in table3-3.

Table 3-3. The crystal size of nano binary oxide SiO_2/MgO

No	2 Theta	Crystal size(nm) SiO_2/MgO	2 Theta	Crystal size(nm)/MgO
1	29.235	62.855	38.5811	42.832
2	42.689	16.997	42.4623	42.934
3	62.096	16.138	62.1788	33.291
4	78.326	21.484	75.4137	38.542

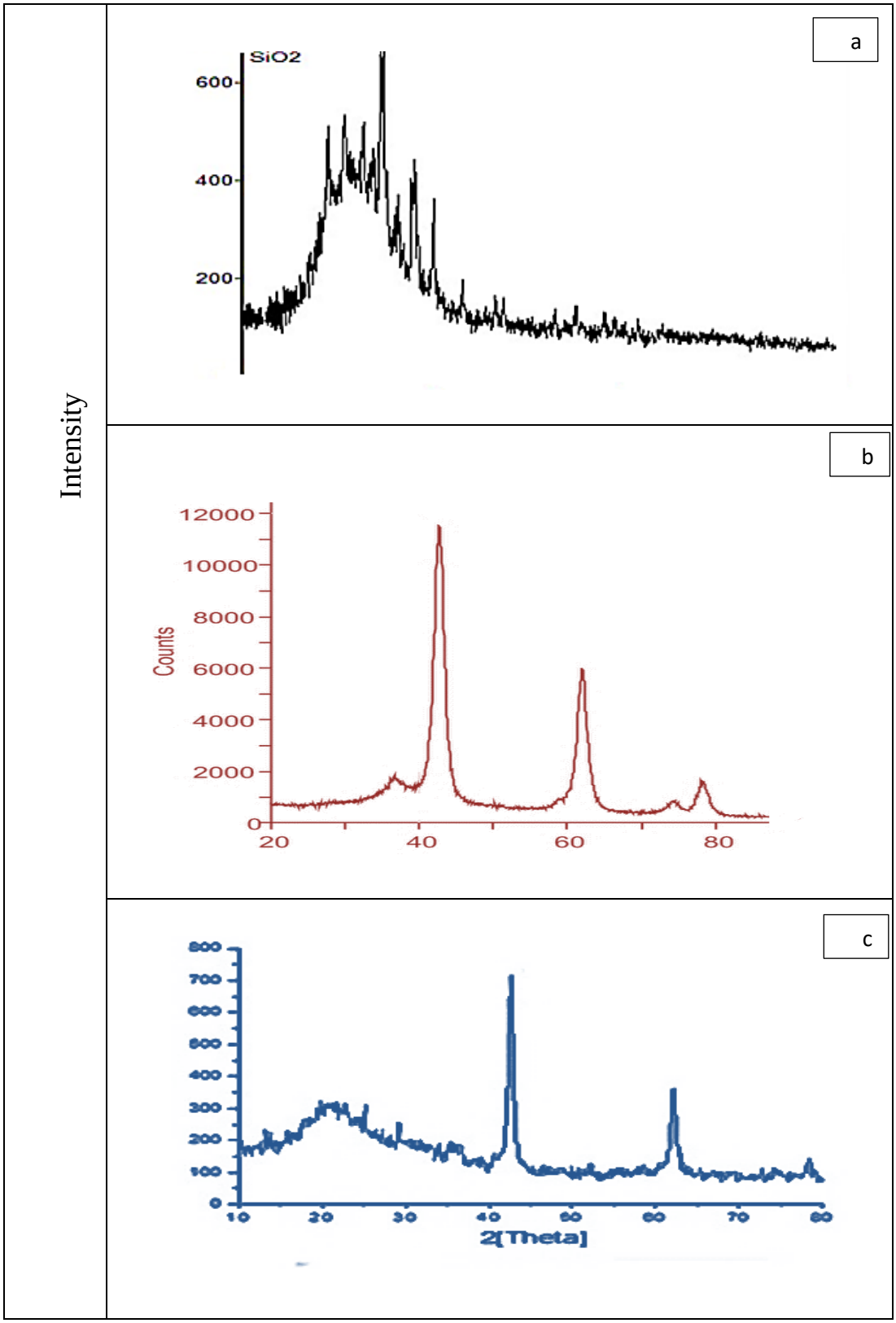

Figure 3-4. X-ray diffraction of patterns a. nano silica oxide b. magnesium oxide MgO, and c. Nano binary oxide SiO_2/MgO (E4-MG-50).

3-1-4. X-ray diffraction and crystal size of Nano binary oxide Fe_xO_y/SiO_2

Nano silica oxide is depicted at low diffraction angles before any treatment, as shown in figure (3-5 a). It exhibits a broad peak in figure (3-5b) that shows the XRD pattern of the nano binary oxide powder Fe_xO_y/SiO_2. At low angles, the broad peak is identical to silica oxide as seen in figure (3-5 a) every other peak in compared to hematite (Fe_xO_y), to gate details about the particles size of nano binary oxide Fe_xO_y/SiO_2 by using Deby-Scherrer equation that depends on XRD peaks of pattern nano binary oxide Fe_xO_y/SiO_2 are calculated from the strong broad peak intense line at 2theta such as shown in table (3-4).

Table 3-4. The crystal size of nano binary oxide Fe_xO_y/SiO_2 powder.

No	2 [Theta]	crystal size(nm)
1	20.0	22.912
2	22.4	37.009
3	23.4	31.942
4	24.3	35.105
5	32.02	43.966

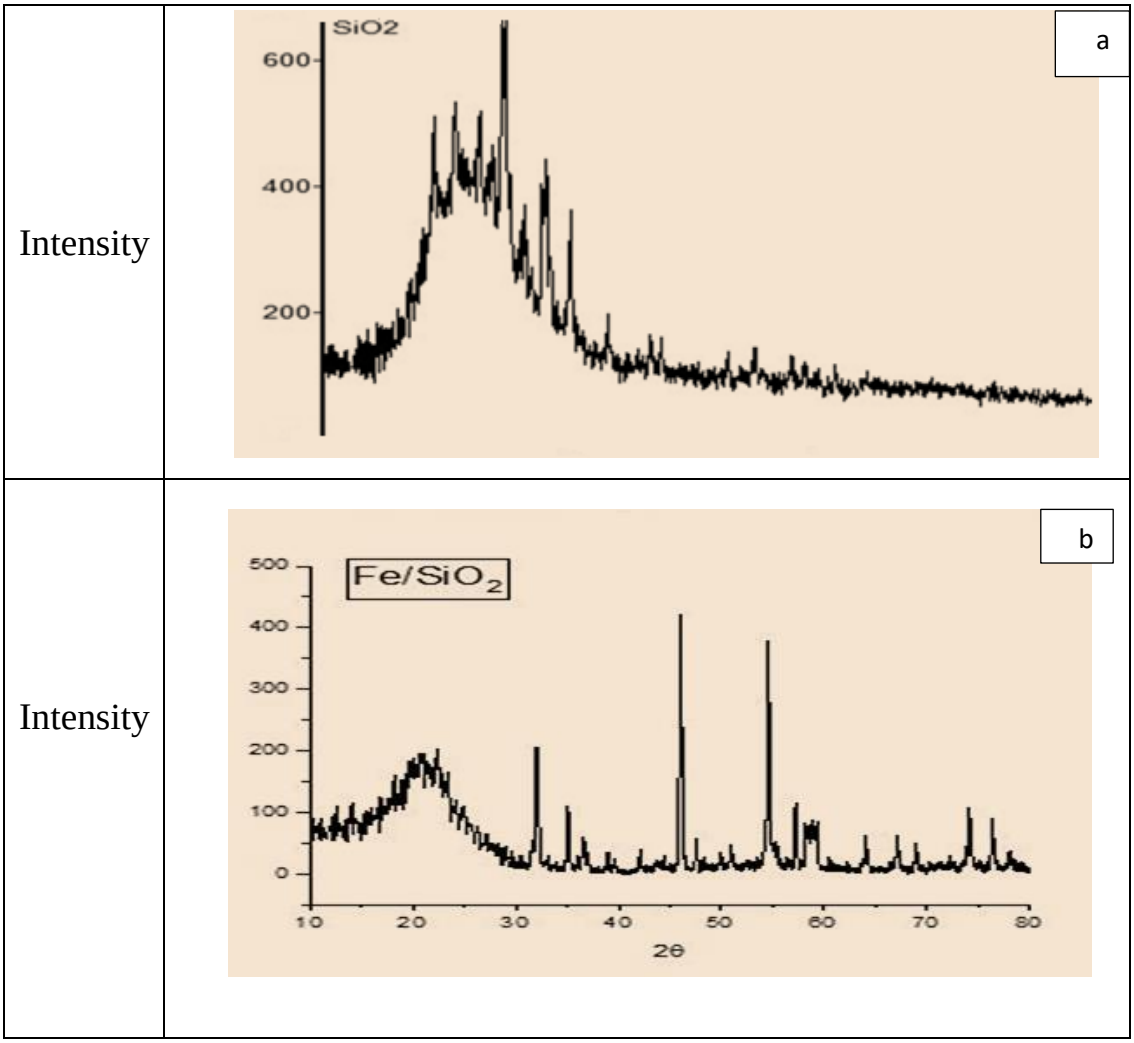

Figure3-5 .X-ray patterns of a. silica oxide, and b. the nano binary oxide Fe_xO_y/SiO_2

3-2.Field Emission Scanning Electron Microscopy (FE-SEM)

Green synthesis of nano silica oxide powder is studied morphology. shape, particle size, and surface of nano silica The surface structure of the oxide and nano binary oxide (SiO_2/V_2O_5, MgO/SiO_2, and Fe_xO_y/SiO_2) at different calcination temperatures (300˚C,400˚C,500˚C, 600˚C, and 700˚C), characterization by using Field Emission Scanning Electron Microscopy.

3-2-1. Field Emission Scanning Electron Microscopy of nano silica oxide

Emission of Fields microscopy is utilized to investigate the morphology of silica oxide nanoparticles after being extracted from RHA. This approach is three-dimensional, has a high resolution, and is unambiguous images [196]. The surface images of the samples at different temperatures of calcination were obtained from FESEM analyses. The micrographs presented in figures (3-6 to 3-10) show a significant effect of heating on the size and distribution of the particles on the surface. As shown in figures (3-6 to 3-10), the surface morphologies of the samples are marked by the existence of particles with different grain sizes and distributions. As a consequence of this investigation, it is determined that nano silica oxide powder exhibit a semispherical structure [197]. Average particle sizes are between 35.953 -48.543 nm as shown in table (3-5). The study affected calcination temperatures with differences ranging from (300-700) ˚C on the morphology of surface structure, and distribution of partial and crystal size. The results of FESEM for nano-silica oxide have an average crystal size smaller at calcination temperature of 500˚C, when increasing calcination temperatures the size of semispherical particle for nano silica oxide increase from 35.953 nm to 48.543 nm at calcination temperatures (500 and 700) ˚C, respectively as illustrated in figures from (3-6 to 3-10).

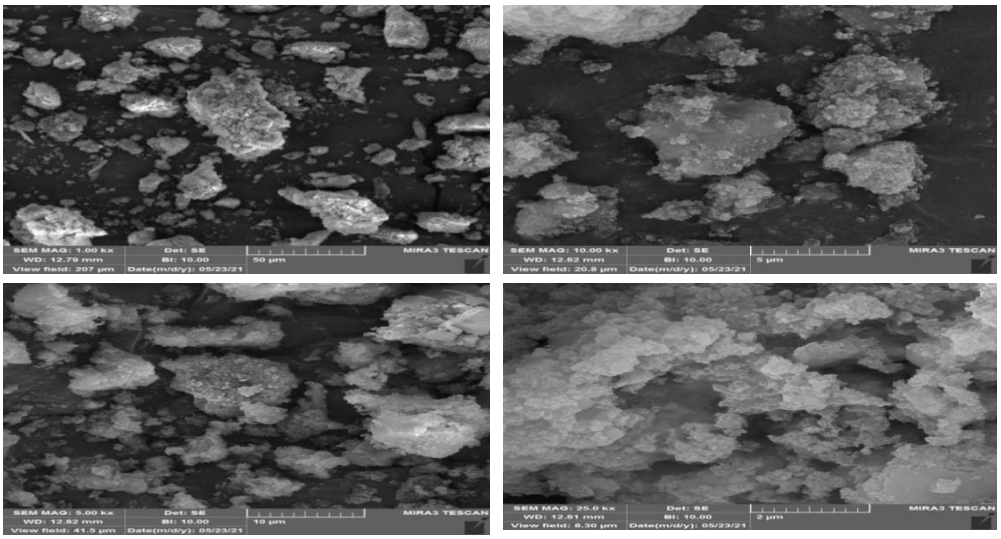

Figure 3-6 FE- SEM images of nano silica oxide powder at a calcination temperature of 300 ˚C.

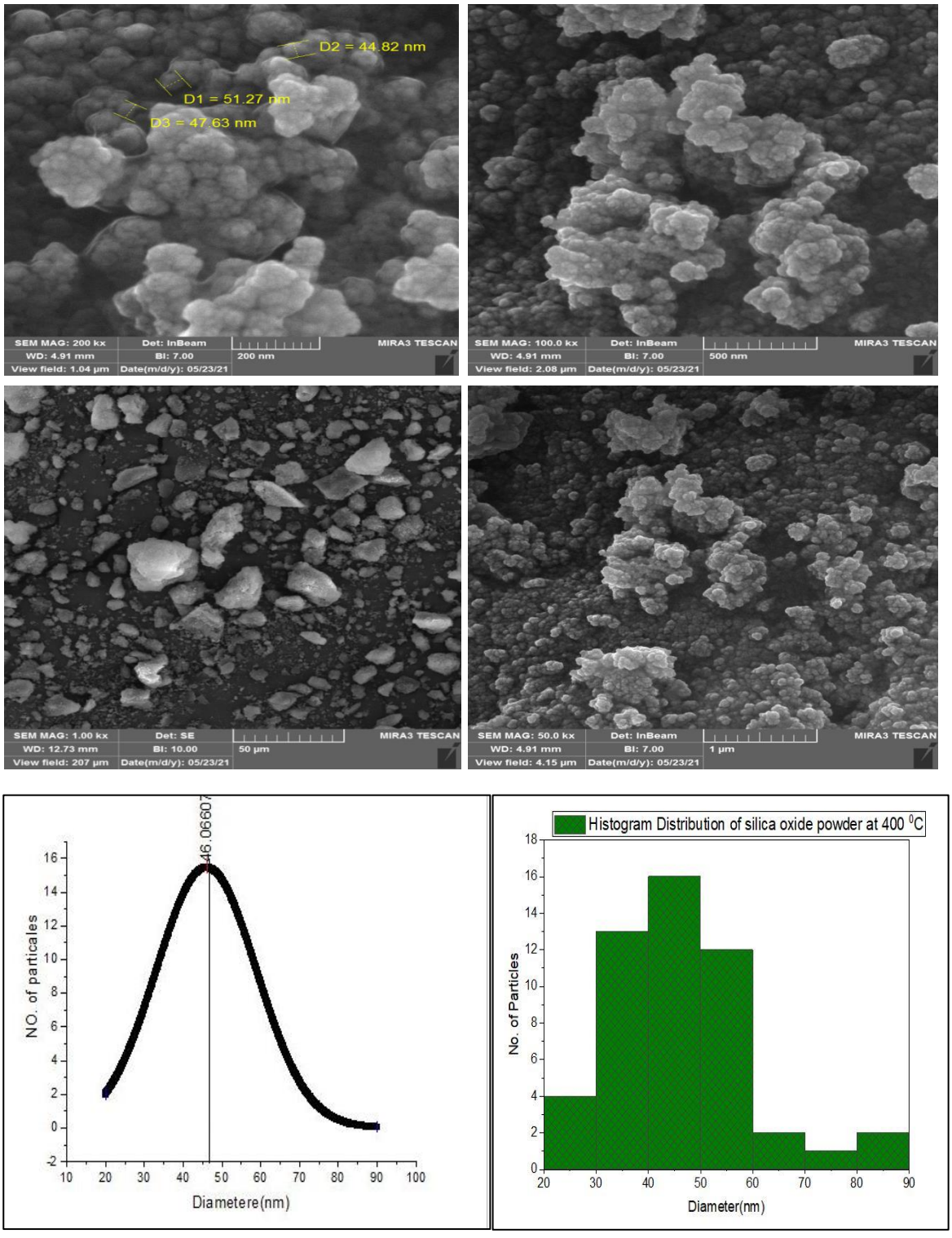

Figure 3-7:-FE- SEM images of silica oxide powder with different scales and average particle grain size at a calcination temperature of 400˚C

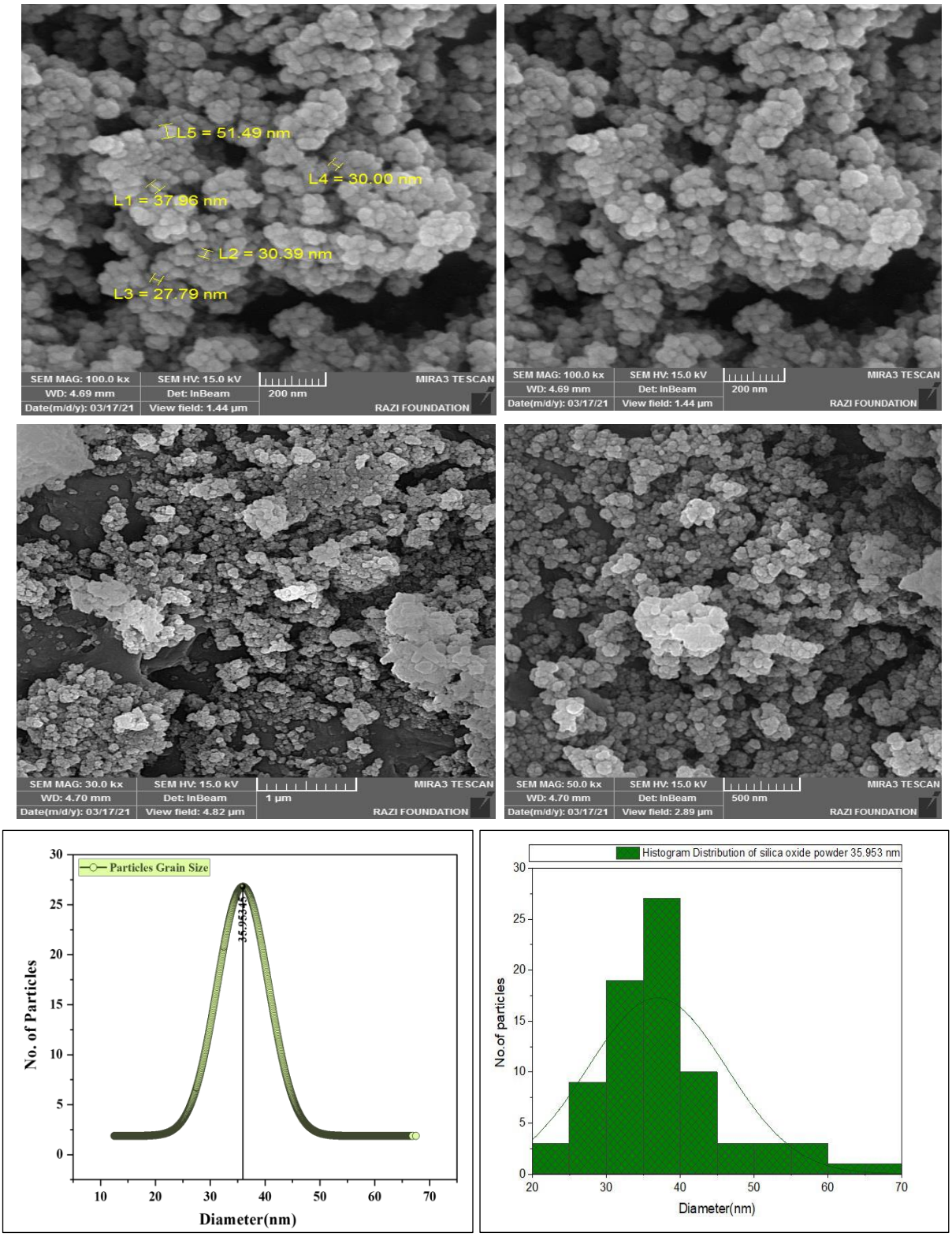

Figure 3-8:-FE- SEM images of silica oxide powder with different scales and average particle grain size at a calcination temperature of 500 ˚C.

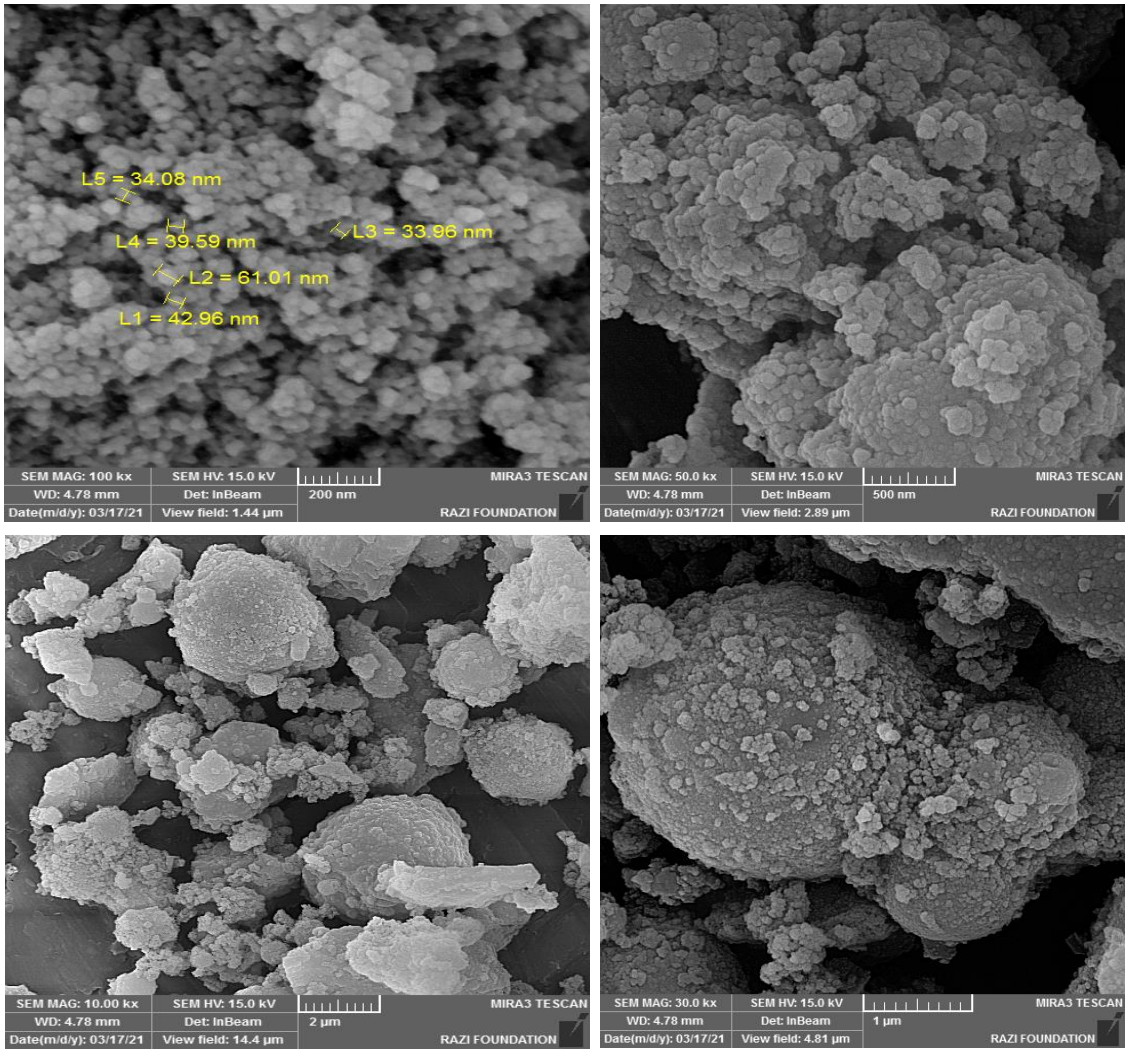

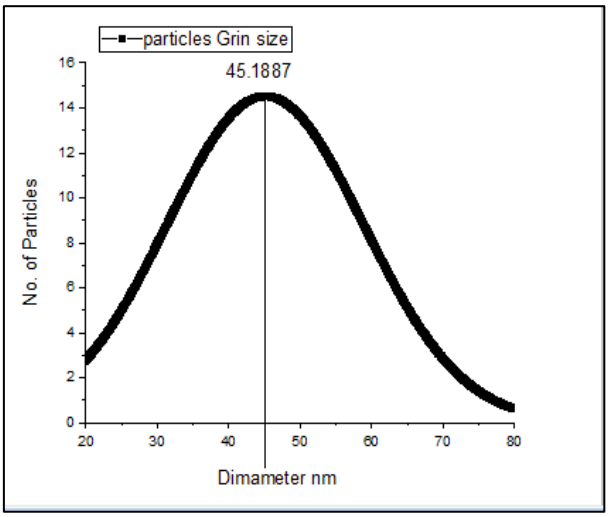

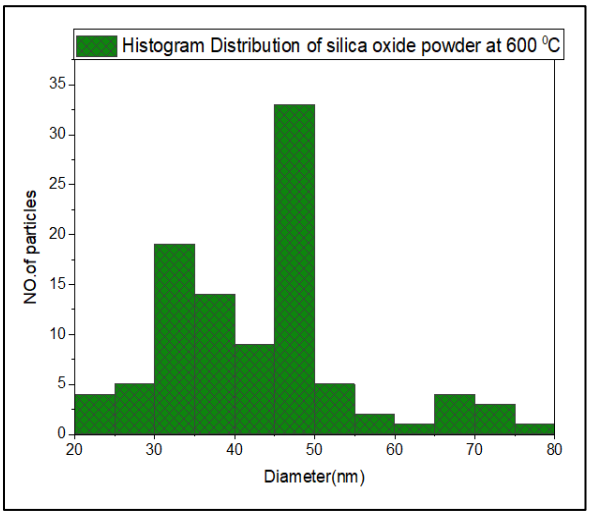

Figure 3-9:-FE- SEM images of silica oxide powder with different scales and average particle grain size at a calcination temperature of 600 ˚C.

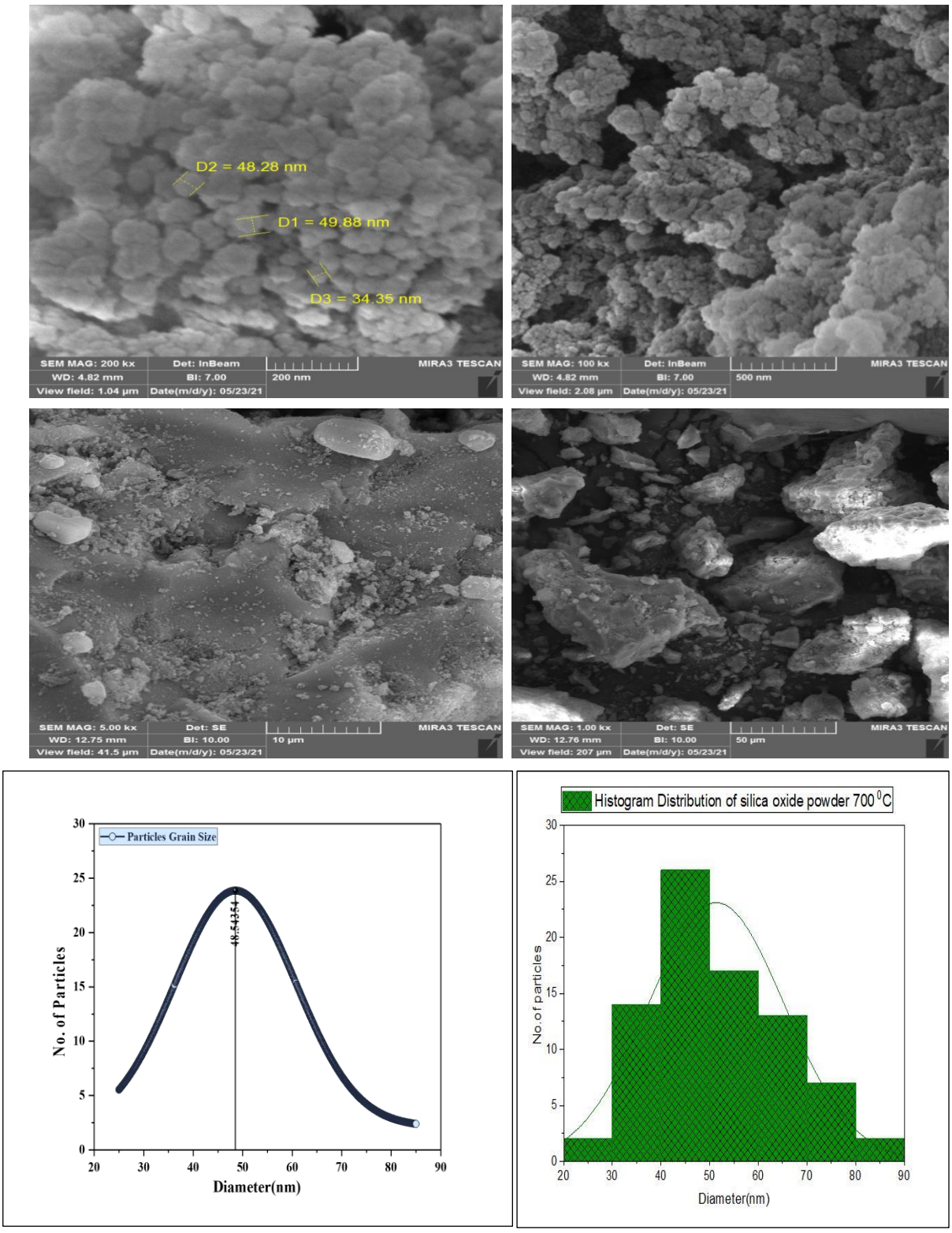

Figure 3-10:-FE- SEM images of silica oxide powder with different scales and average particle grain size at a calcination temperature of 700 ˚C.

Table 3-5. The average grain size of nano silica oxide and particle diameter at different burning temperatures

Temperature(˚C)	Diameter(nm)	Average Grain Size(nm)
400	20 - 90	46.066
500	20 - 70	35.953
600	20 - 80	45.188
700	20 - 90	48.543

3-2-2.Field Emission Scanning Electron Microscopy of nano binary oxide SiO_2/V_2O_5

Field-emission scanning electron microscopy (FESEM) is used to study the morphology of nano binary oxide **SiO_2/V_2O_5** nanoparticles after. The microscope provides accurate three-dimensional images of the crystallographic method. The morphology of the thin films prepared using this technique was studied from 3D images within (200 and 500) nm, (50 and 10) µm scale range.

Study the effect of calcination temperatures with a different range from 300 to 700 ˚C on the morphology of surface structure, distribution of particle and particle size. Those tests show that nano binary oxide **SiO_2/V_2O_5** NPs is a semispherical shape with average particles diameters degrees that went between (29.95 to 41.63) nm depending on the different ranges of burning from (300 to 700) °C respectively, as shown in table (3-7) and figures (3-11 to 3-15) respectively. The increase in temperature affected the crystal grain size and crystal grain size distribution. It is noted that the smallest crystal size appeared at calcination temperature of (300°C) and its amount was (29.95nm), then that crystal size increased according to the increase in calcination temperature until the crystal size is equal to (41.63nm) at 700°C.

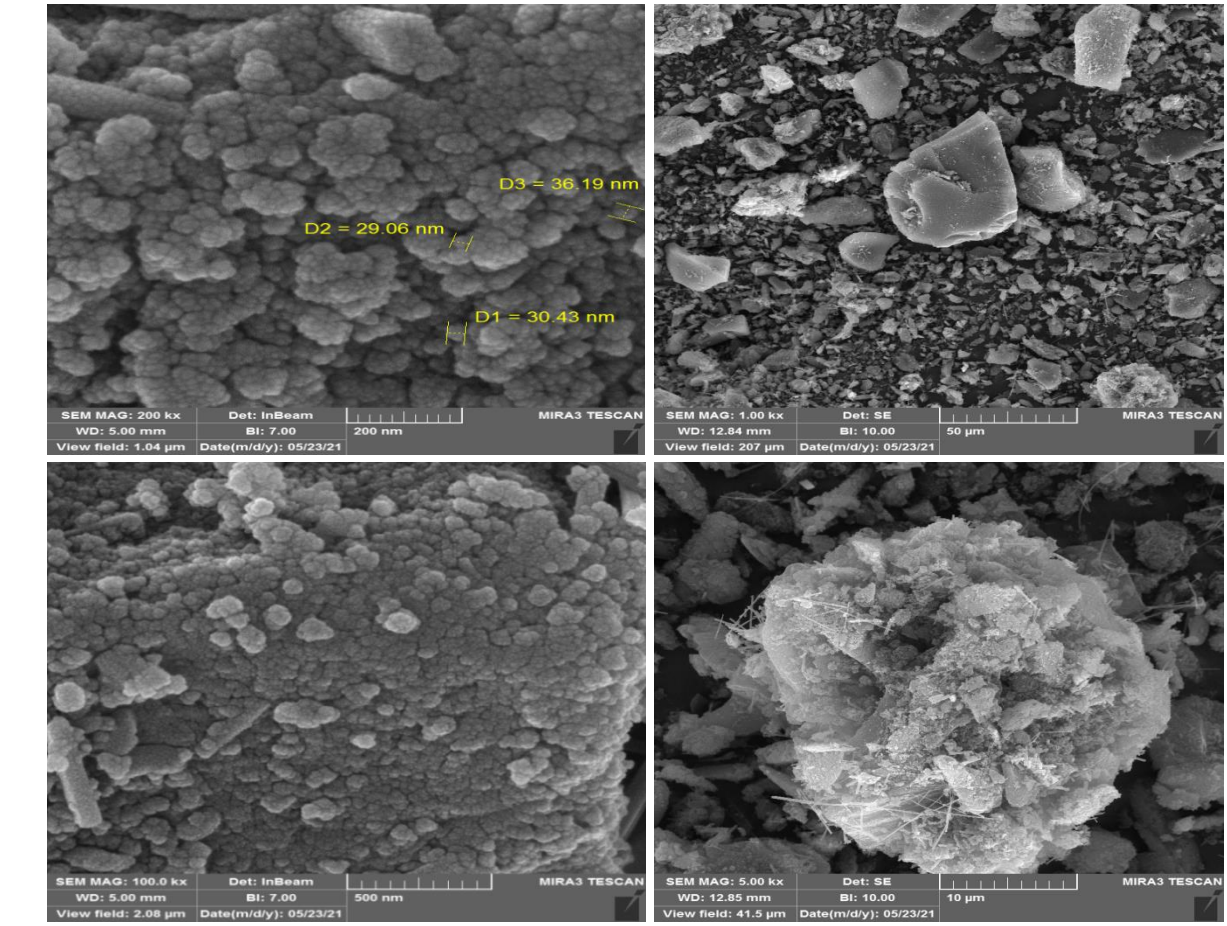

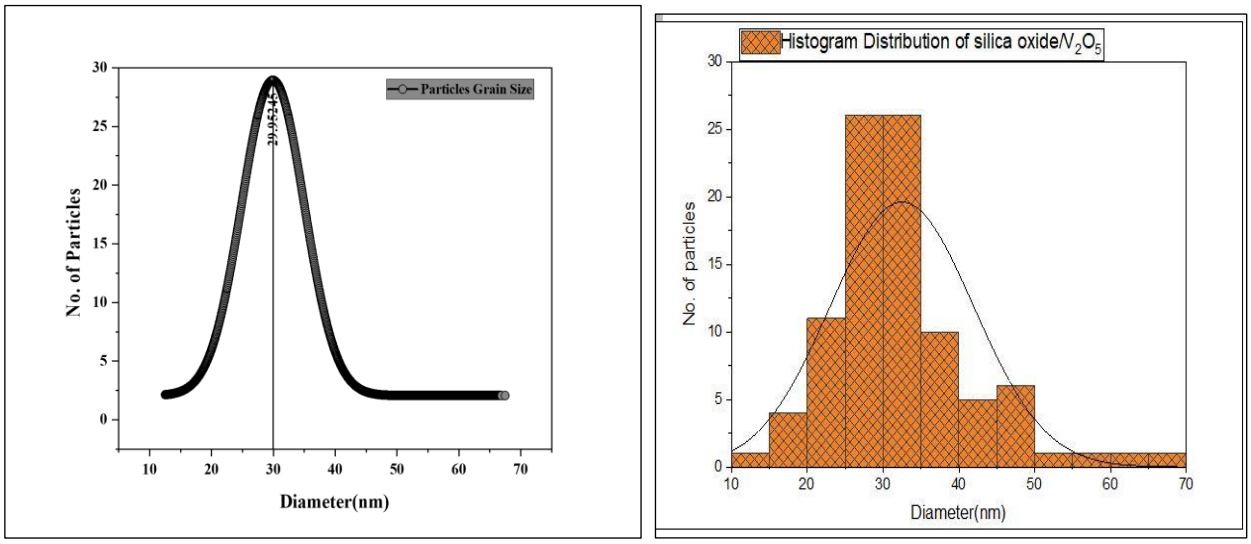

Figure3-11:-FE- SEM images of nano binary oxide SiO_2/V_2O_5 powder with average particle grain size at a calcination temperature of 300 ˚C.

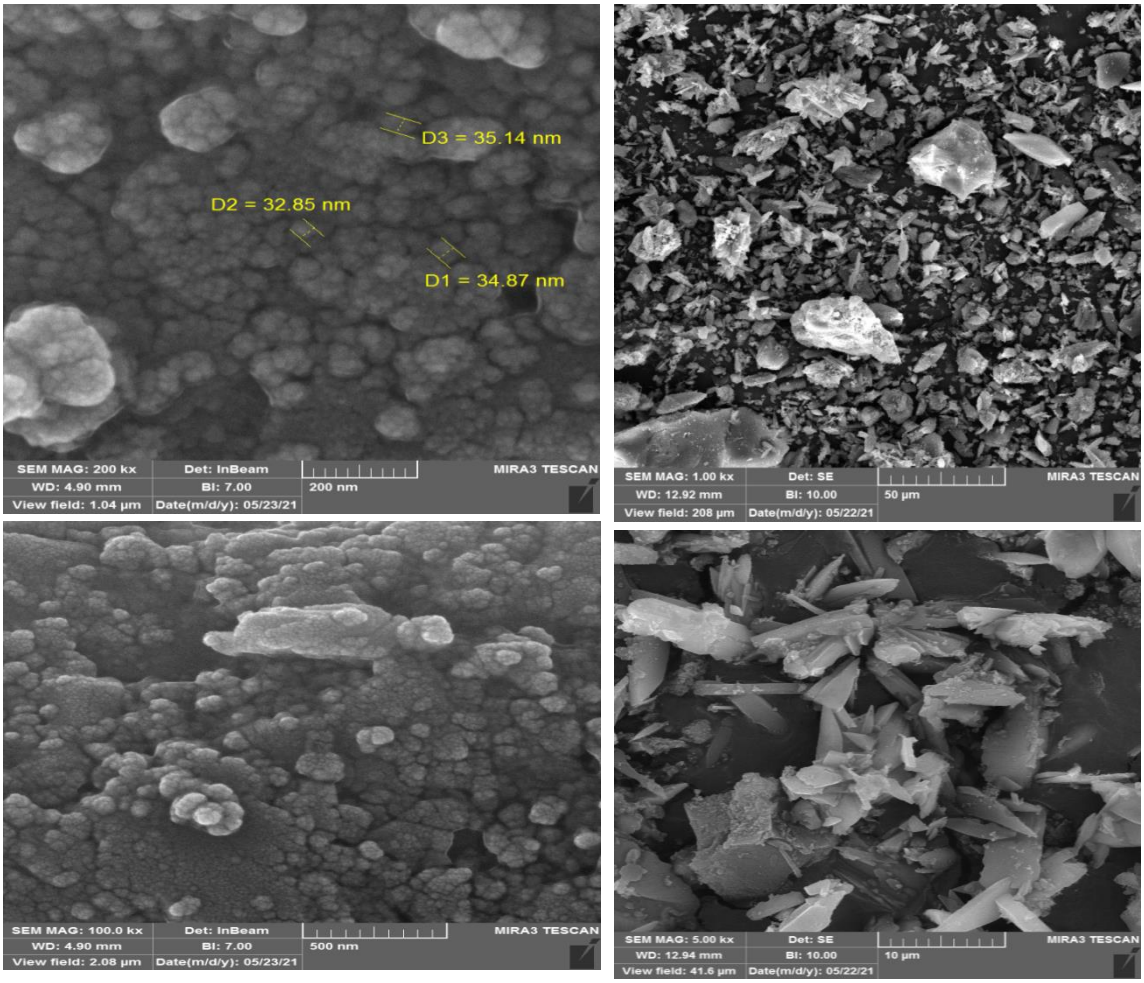

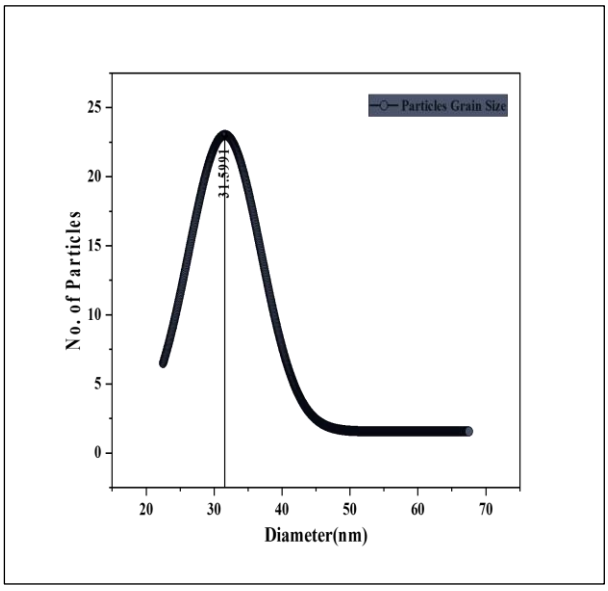

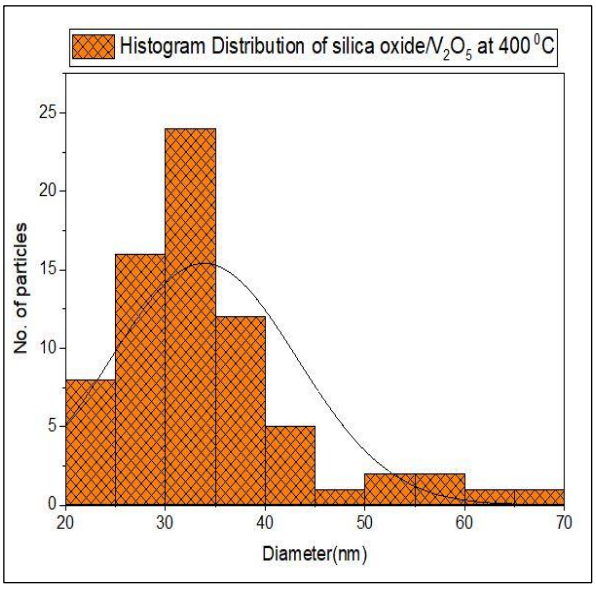

Figure3-12:-FE-SEM images of nano binary oxide SiO_2/V_2O_5 powder with average particle grain size at a calcination temperature of 400 ˚C.

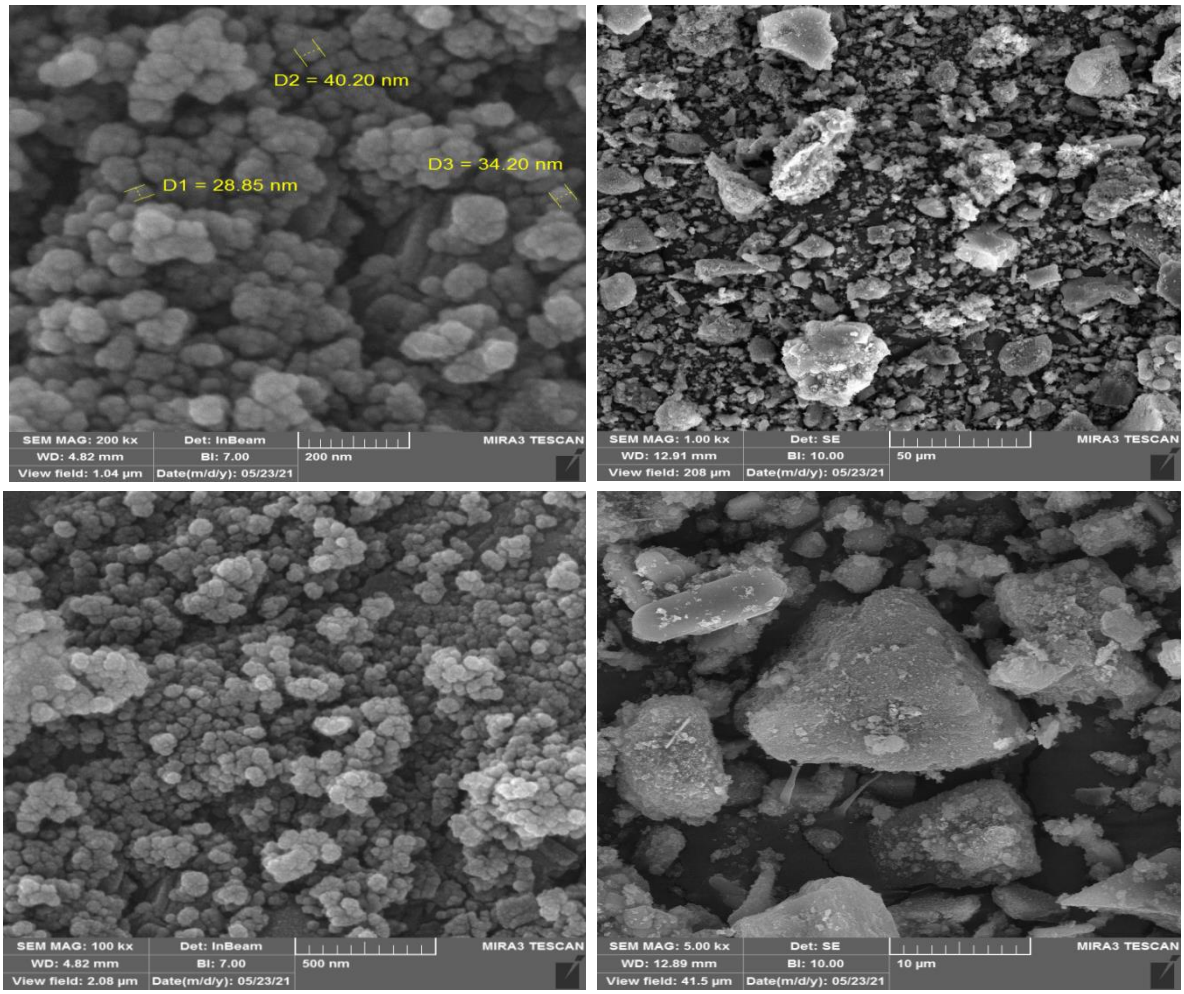

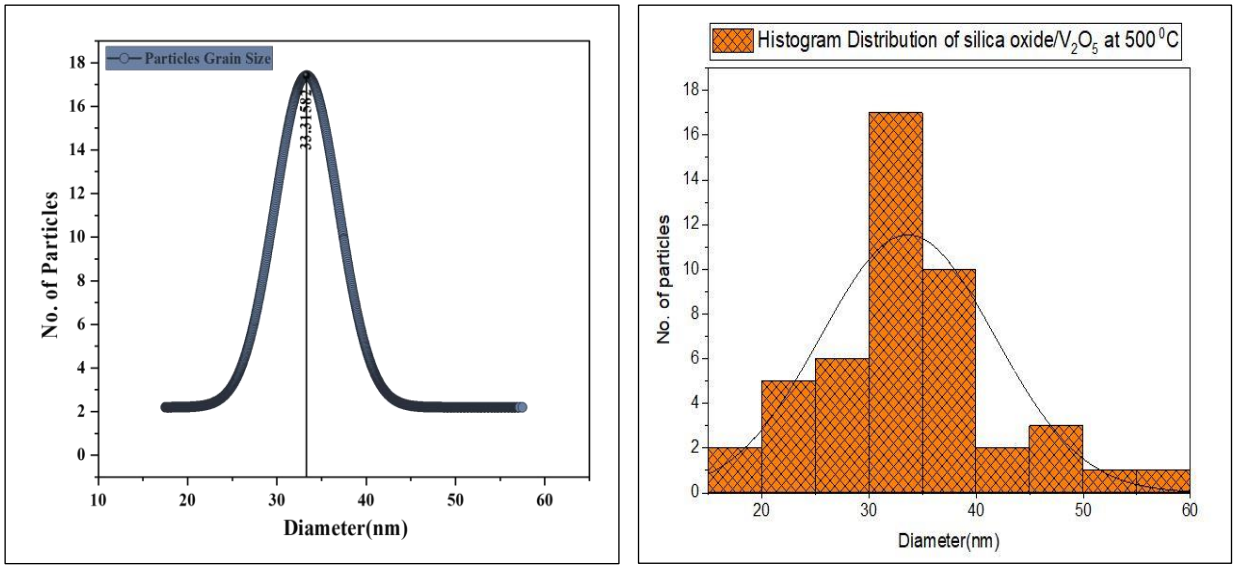

Figure3-13:-FE-SEM images of nano binary oxide SiO_2/V_2O_5 powder with average particle grain size at calcination temperature 500 ˚C.

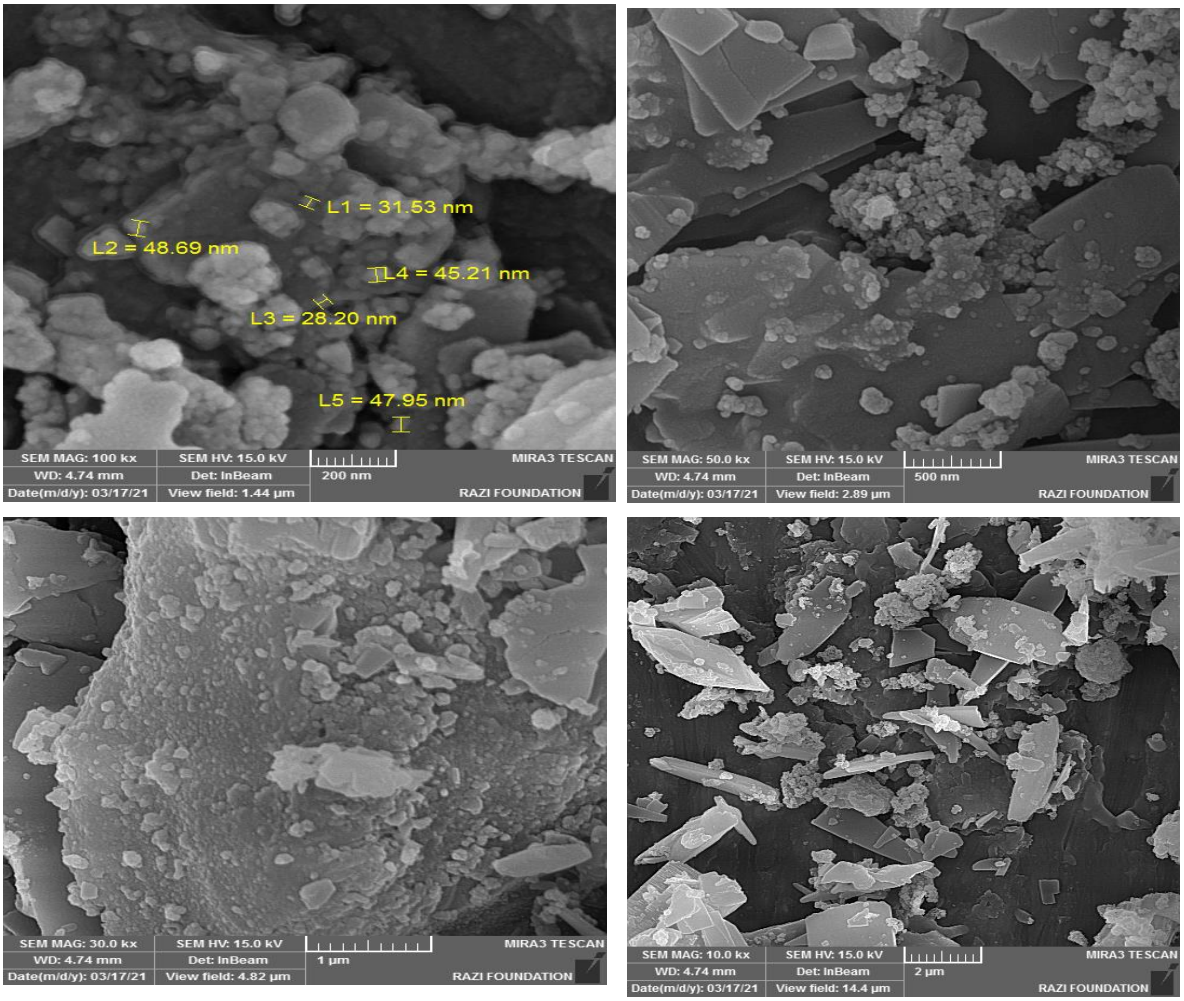

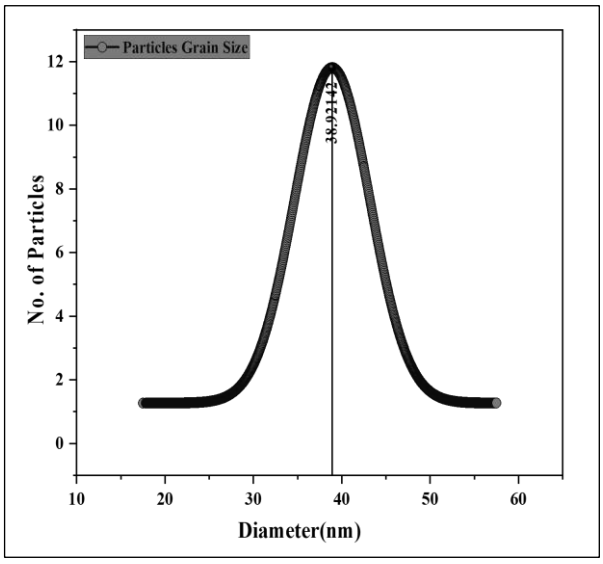

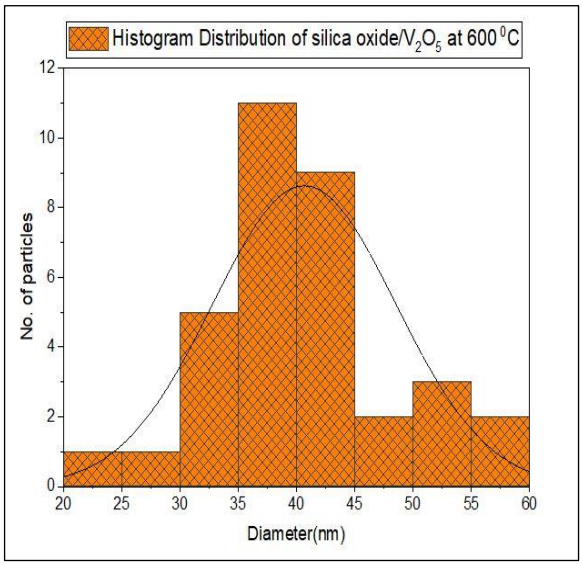

Figure3-14:-FE- SEM images of nano binary oxide SiO_2/V_2O_5 powder with average particle grain size at a calcination temperature of 600 ˚C.

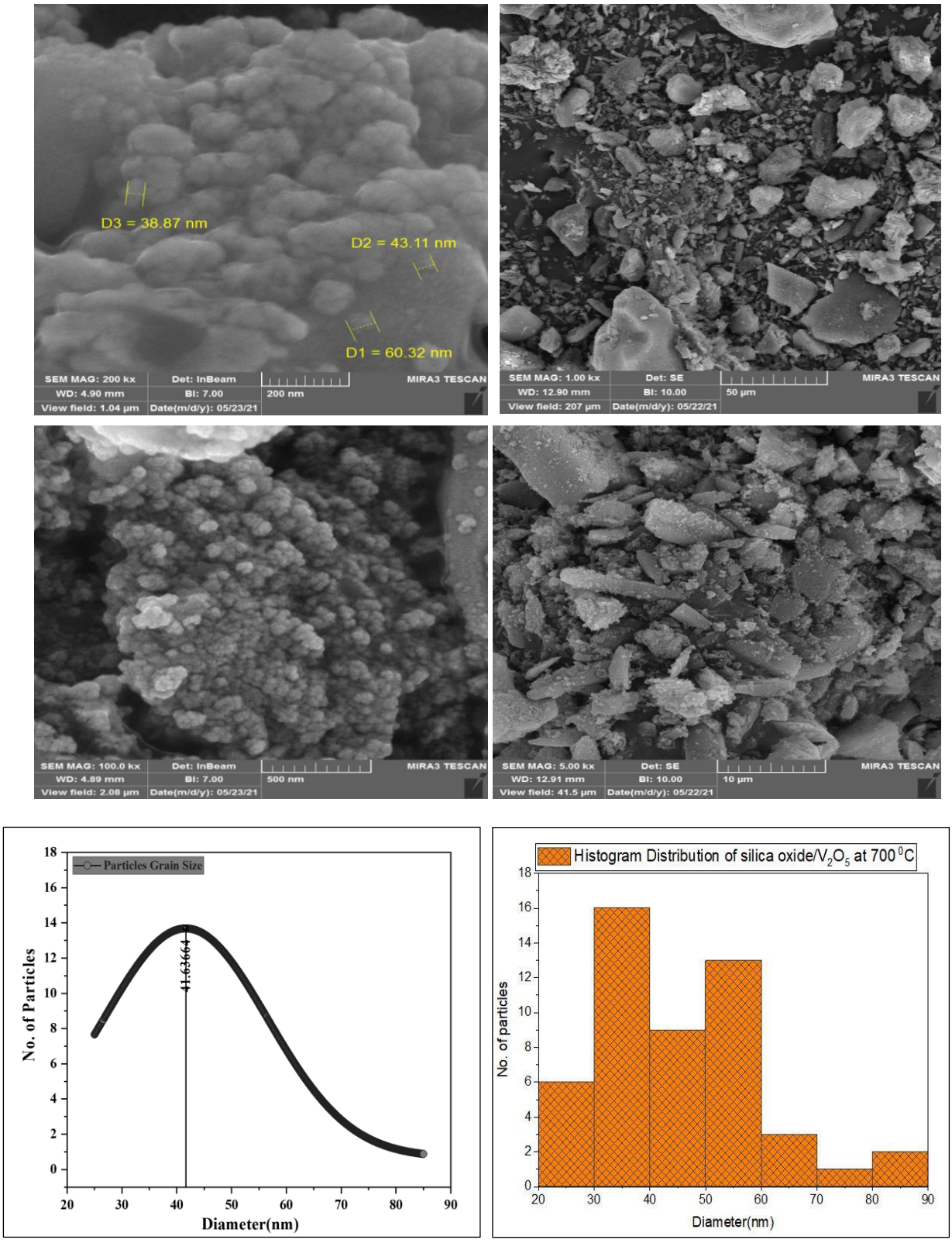

Figure3-15:-FE- SEM images of nano binary oxide SiO_2/V_2O_5 powder with average particle grain size at a calcination temperature of 700 ˚C.

Table 3-6. The average grain size of nanoparticle and particle diameter at different burning temperatures for nano binary oxide V_2O_5/SiO_2.

Temperature(°C)	Diameter(nm)	Average Grain Size(nm)
300	10 - 70	29.95
400	20-70	31.59
500	15 - 60	33.31
600	20 - 60	38.92
700	20 - 90	41.63

3-2-3. Field Emission Scanning Electron Microscopy of nano binary oxide MgO/SiO_2

The morphology of nano binary oxide MgO/SiO_2 nanoparticles are studied using field-emission scanning electron microscopy (FESEM). This microscope captures three-dimensional images of the crystallographic process in high resolution. The morphology of thin films generated with this approach is investigated using three-dimensional pictures on the 200 nm scale.

To examine the morphology and particle size of MgO/SiO_2 nanoparticles, FESEM images of nanoparticles are shown in figures (3-16 – 3-20). The results indicate that nano binary oxide MgO/SiO_2 **(A4-MG-50)** nanoparticles with an average size of 28.5nm are produced at calcination temperature 700˚C. FESEM images of MgO/SiO_2 NPs generated using a wet method that shown in figure (3-16 – 3-20), with differences in scale of 10µm, 50µm,200 nm, and 500 nm the shape of nano composited is spherical. According to figure (3-17), the average crystal size of nano composited MgO/SiO_2 **(B4-MG-50)** NPs is 27.71nm at 600 ˚C as shown in table (3-8).

The scanning electron microscopy (FESEM) revealed good surface properties, energy-dispersive X-ray analysis (EDX) confirmed the presence of Mg, Si in the sample, and X-ray diffractometry (XRD) confirmed the formation of the particle size of nano binary oxide MgO/SiO_2 in nanoscale. Noted from the results the average particle size of nano composited MgO/SiO_2 NPs increased with increased calcination temperatures as shown in table (3-8).

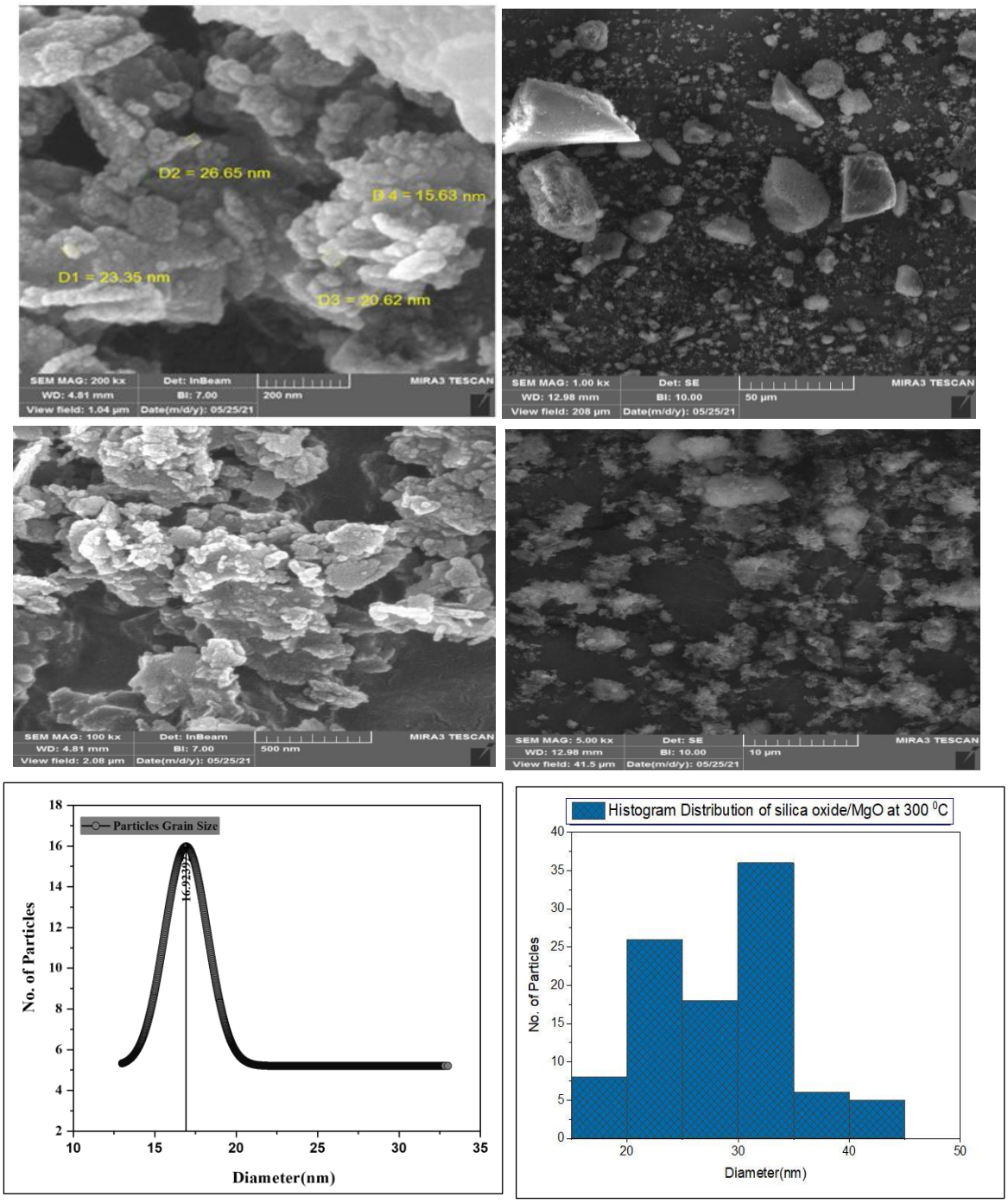

Figure .3-16:-FE- SEM images of Nano binary oxide silica oxide /MgO (E4-MG-50) powder with different scales and average particle grain size.

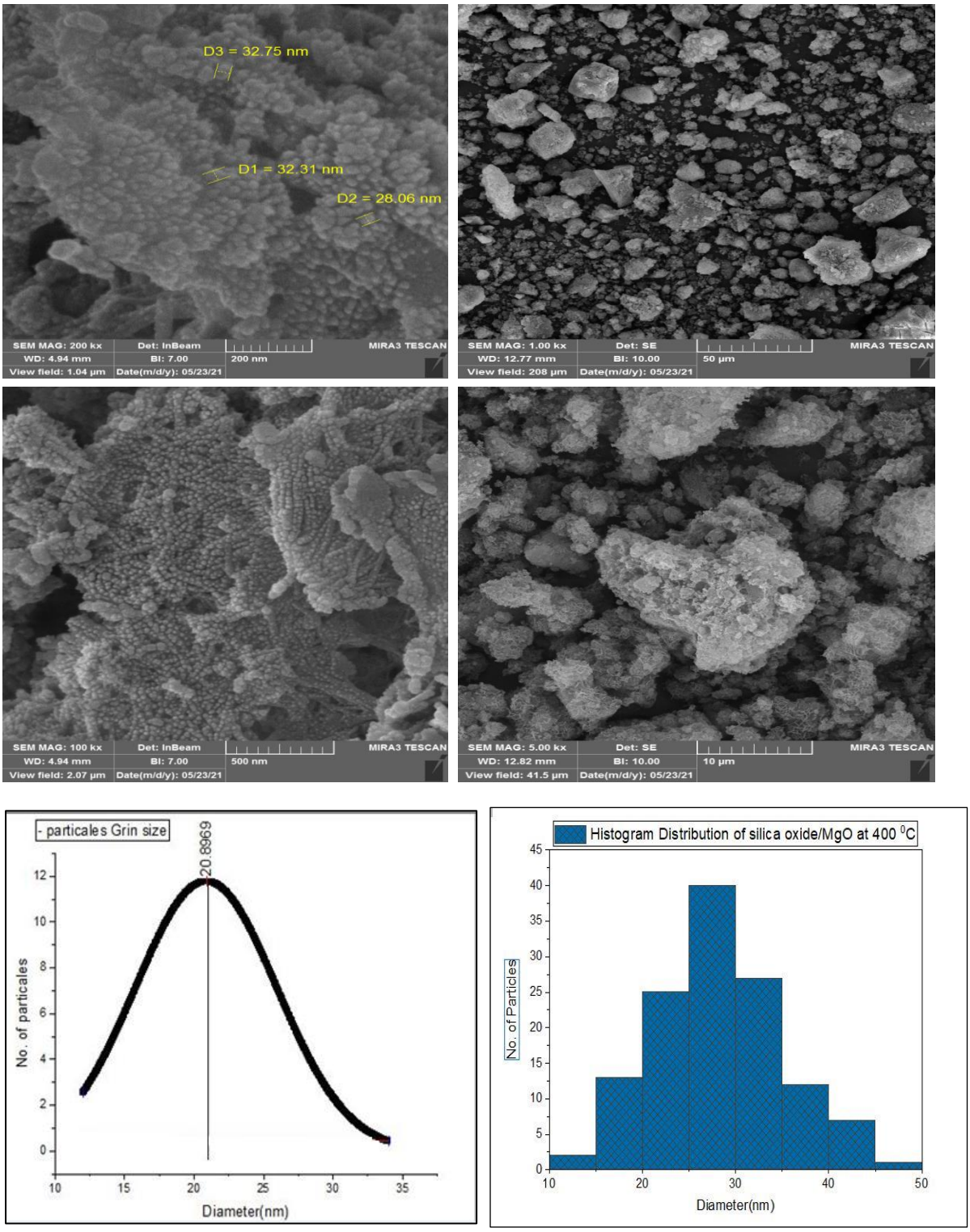

Figure .3-17:-FE- SEM images of Nano binary oxide silica oxide /MgO(D4-MG-50) powder with different scales and an average particle grain size.

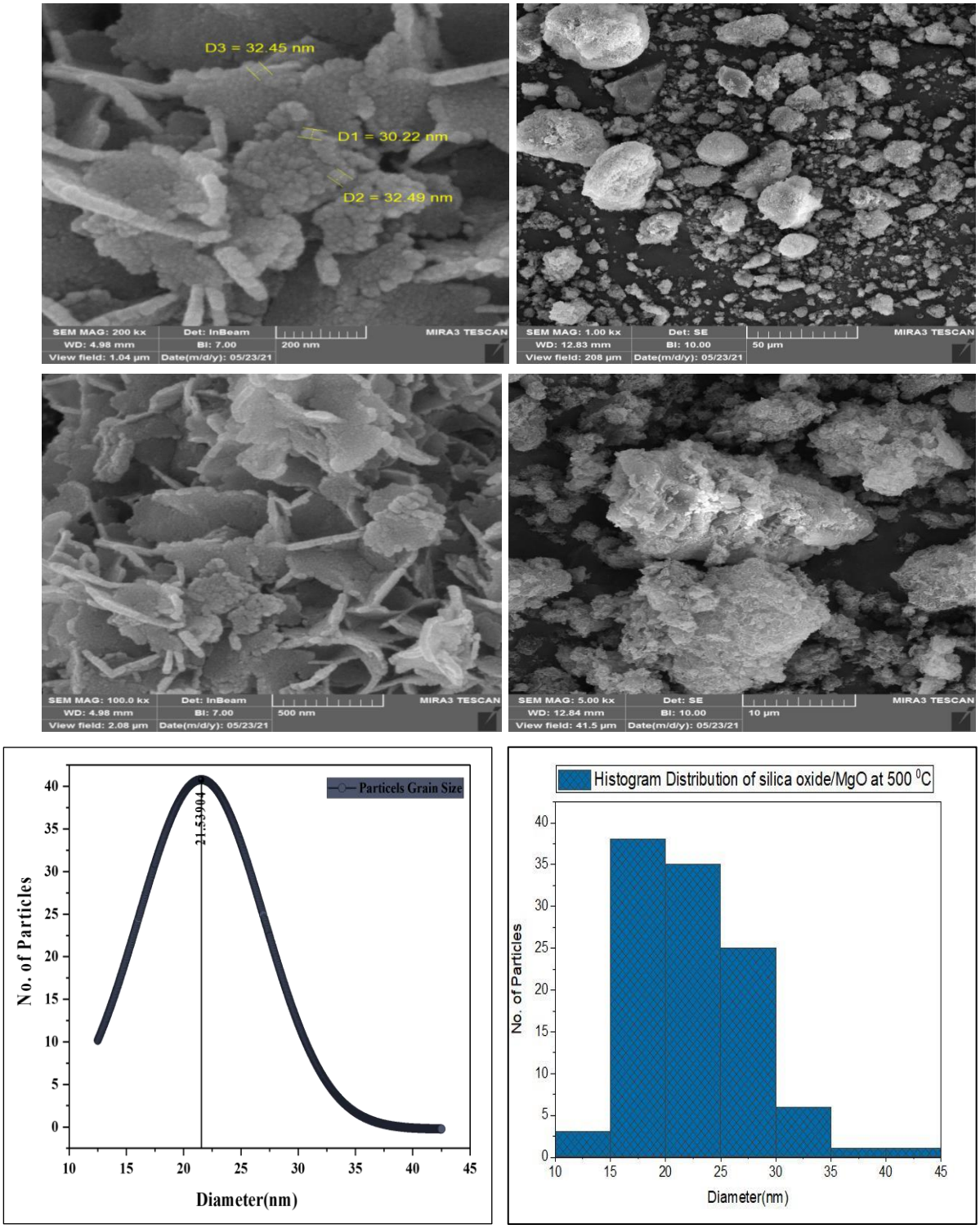

Figure .3-18:-FE- SEM images of Nano binary oxide silica oxide /MgO(C4-MG-50) powder with different scales and an average particle grain size.

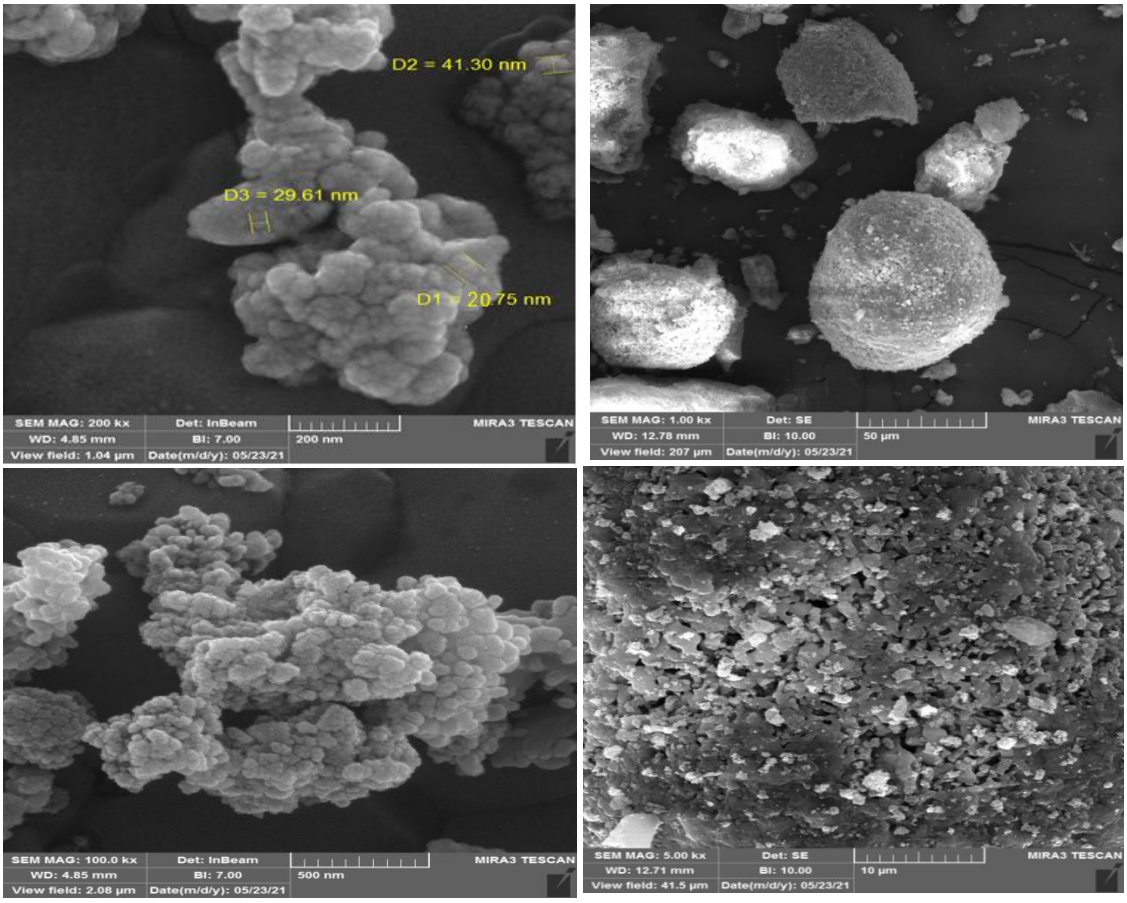

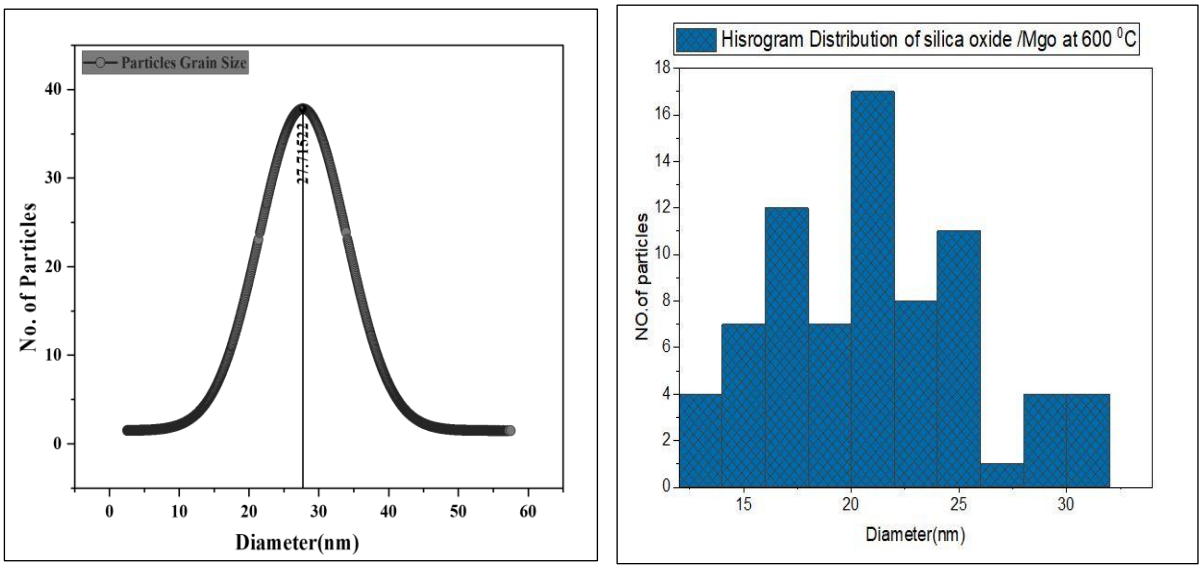

Figure 3-19:-FE- SEM images of Nano binary oxide silica oxide /MgO (B4-MG-50) powder with different scales and the average particle grain size.

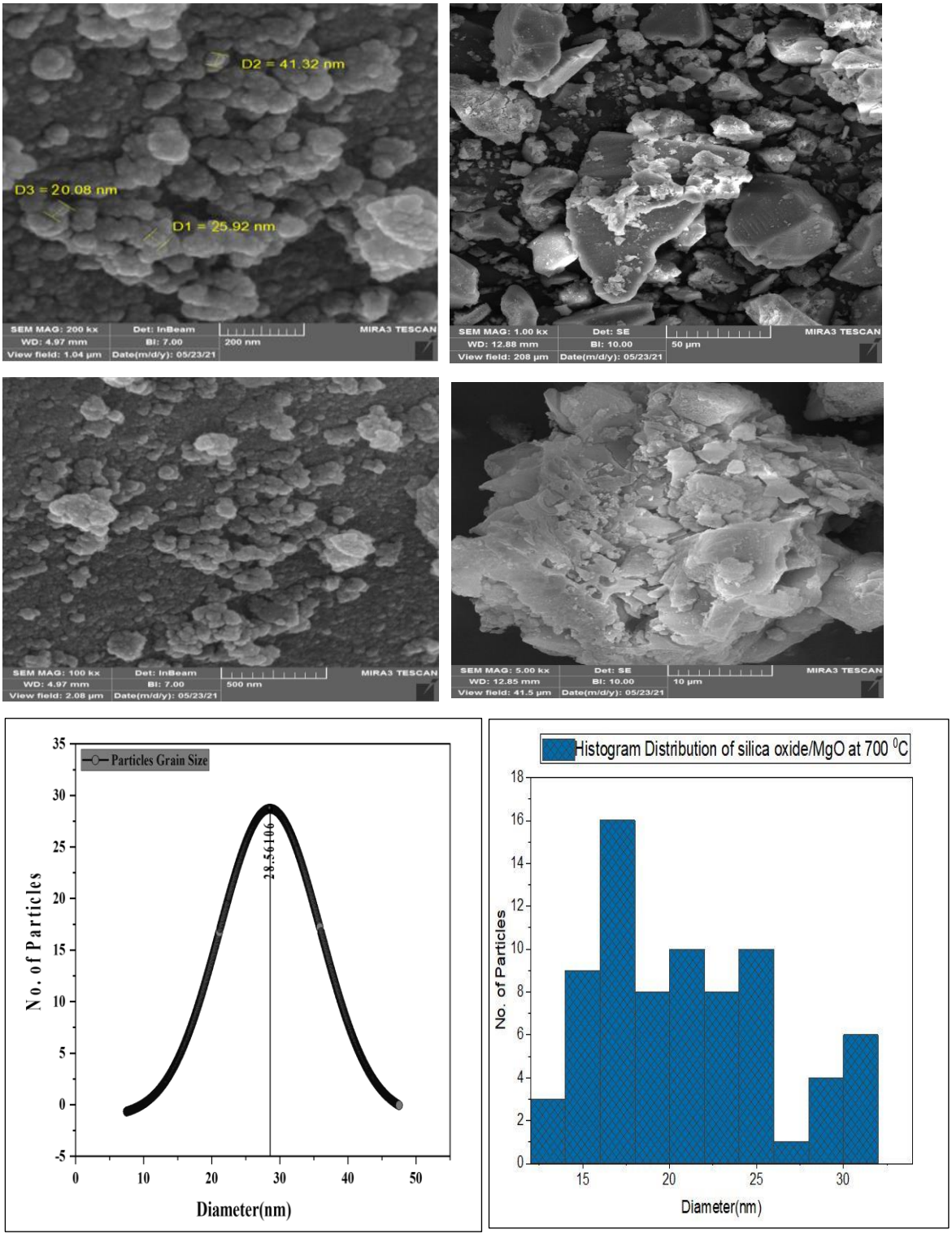

Figure .3-20:-FE- SEM images of Nano binary oxide silica oxide /MgO (A4-MG-50) powder with different scales and the average particle grain size.

Table 3-7. Average grain size nanoparticle and particle diameter at different burning temperatures for nano binary oxide MgO/SiO_2.

Antibiotic: (°C)	Diameter (nm)	Average Grain Size(nm)
(A4-MG-50):700	15-45	28.56
(B4-MG-50):600	10 - 50	27.71
(C4-MG-50):500	10 - 45	21.53
(D4-MG-50):400	10 - 35	20.89
(E4-MG-50):300	12 - 35	16.92

3-2-4Field Emission Scanning Electron Microscopy (FE-SEM)of nanomagnetic binary oxide Fe_xO_y/SiO_2

After preparation of nano binary oxide Fe_xO_y/siO_2 by sol-gel method study effect calcination temperatures on nanomagnetic binary oxide $\mathbf{Fe_xO_y/SiO_2}$ at difference range (300 to 700) ^{0}C. Field emission scanning electron microscopy (FESEM) (MAG 400 Kx Germany) is used to examine the surface morphology of nano binary oxide $\mathbf{Fe_xO_y/SiO_2}$ and energy dispersive X-ray spectroscopy (EDX) is utilized to determine the elemental composition. FESEM confirmed the morphology of nano binary oxide $\mathbf{Fe_xO_y/SiO_2}$ particles is semispherical [198], for all samples such as shown in figures (3-21-3-25) the results of field emission scanning electron microscopy at different calcination temperatures show the average particles size decrease with the increase of calcination temperatures at 400 °C, then the average of particles size increase (growth of nano composited particles) with increase burning more than 400°C such as shown in table (3-9). [199] FESEM illustrates the micrographs of silica oxide-doped with iron oxide NPs generated through the sol-gel method. It demonstrates that the particles of nano binary oxide $\mathbf{Fe_xO_y/SiO_2}$ at calcination temperate 400 °C are perfectly spherical and distributed on the abrasive surface more homogenous as shown in figure (3-22).

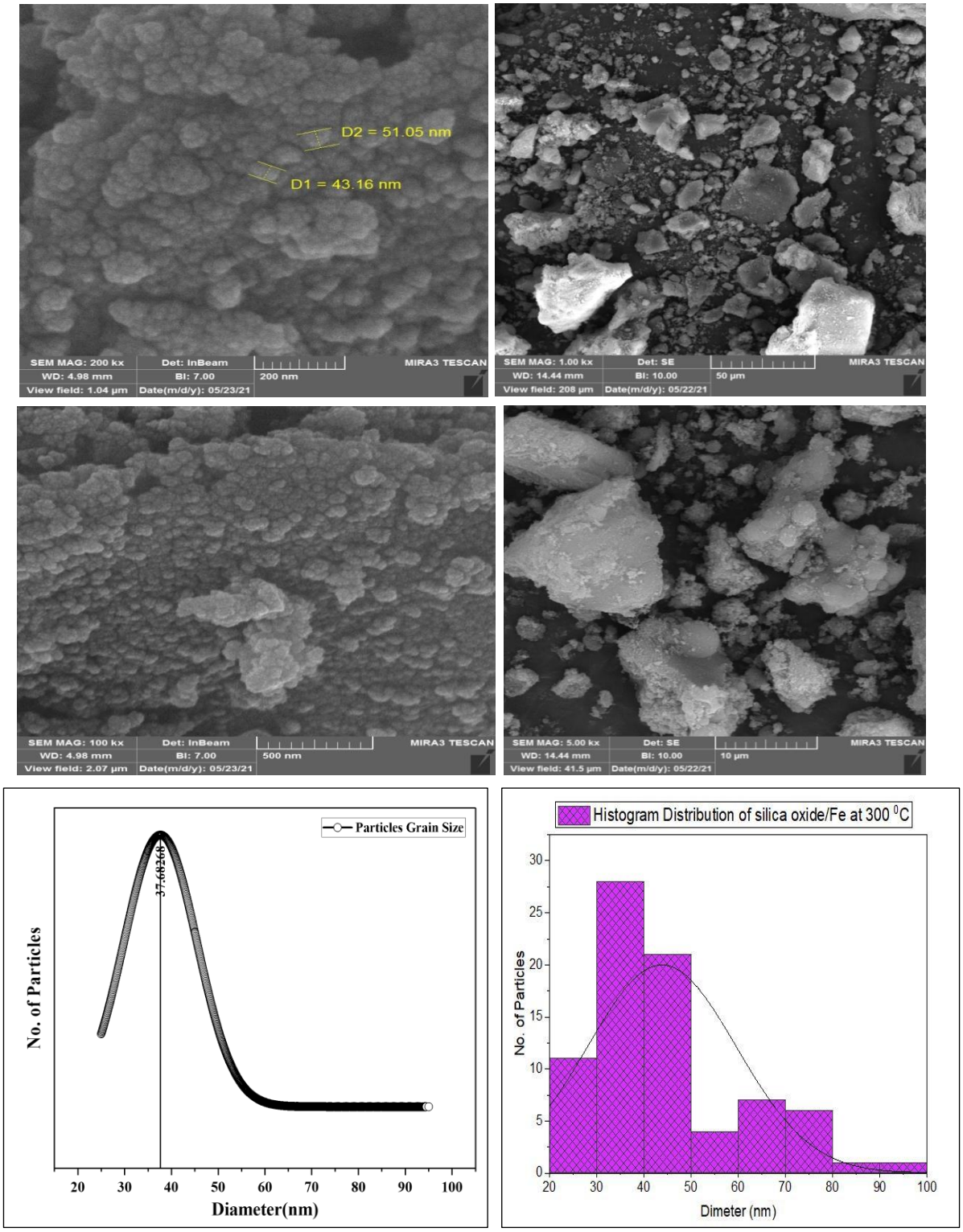

Figure3-21:-FE-SEM images of Nano binary oxide Fe_xO_y/SiO_2 powder at various scales with average particle grain size at a calcination temperature of 300 ˚C.

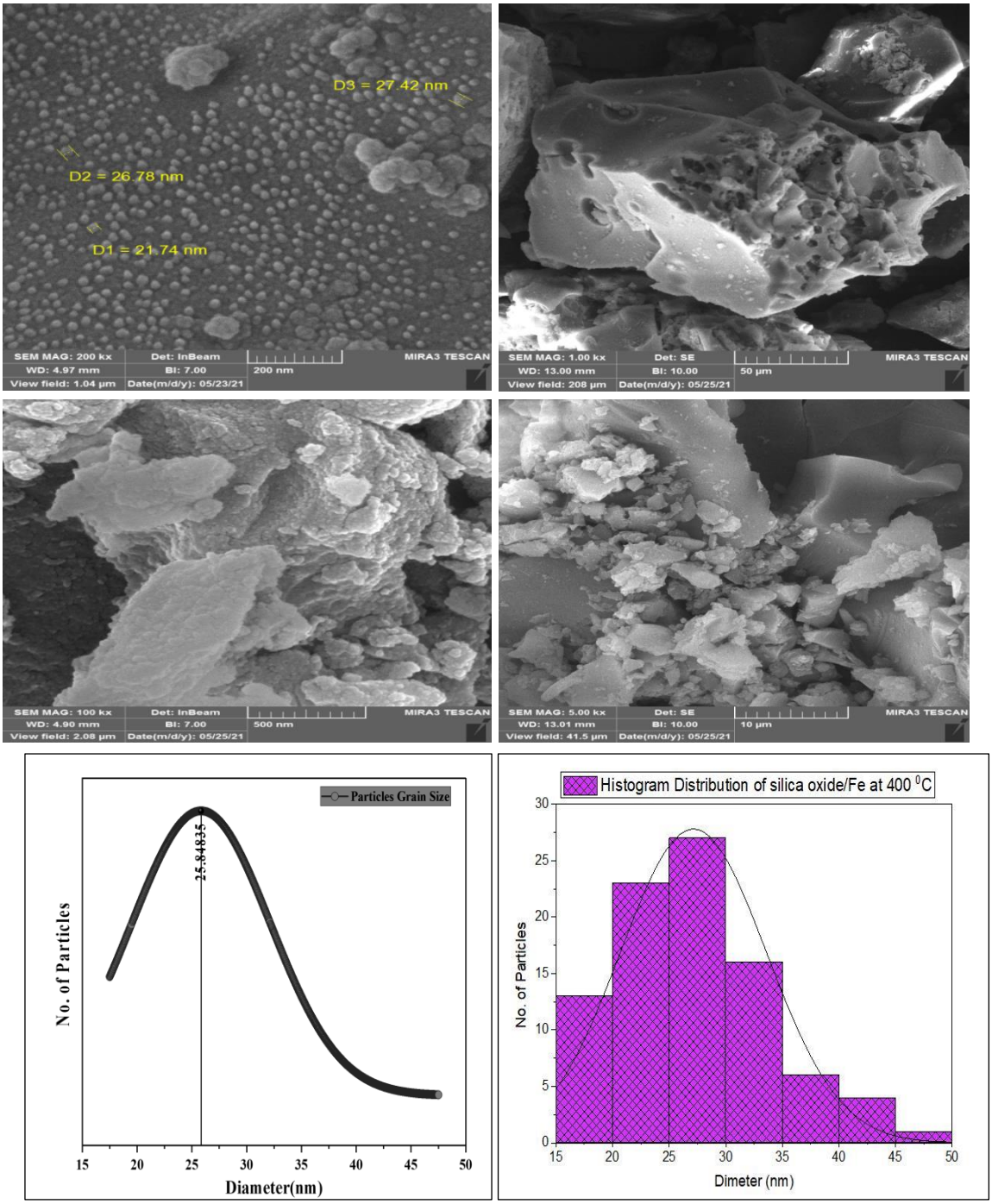

Figure3-22:-FE-SEM images of Nano binary oxide Fe_xO_y/SiO_2 powder at various scales with average particle grain size at a calcination temperature of 400 ˚C.

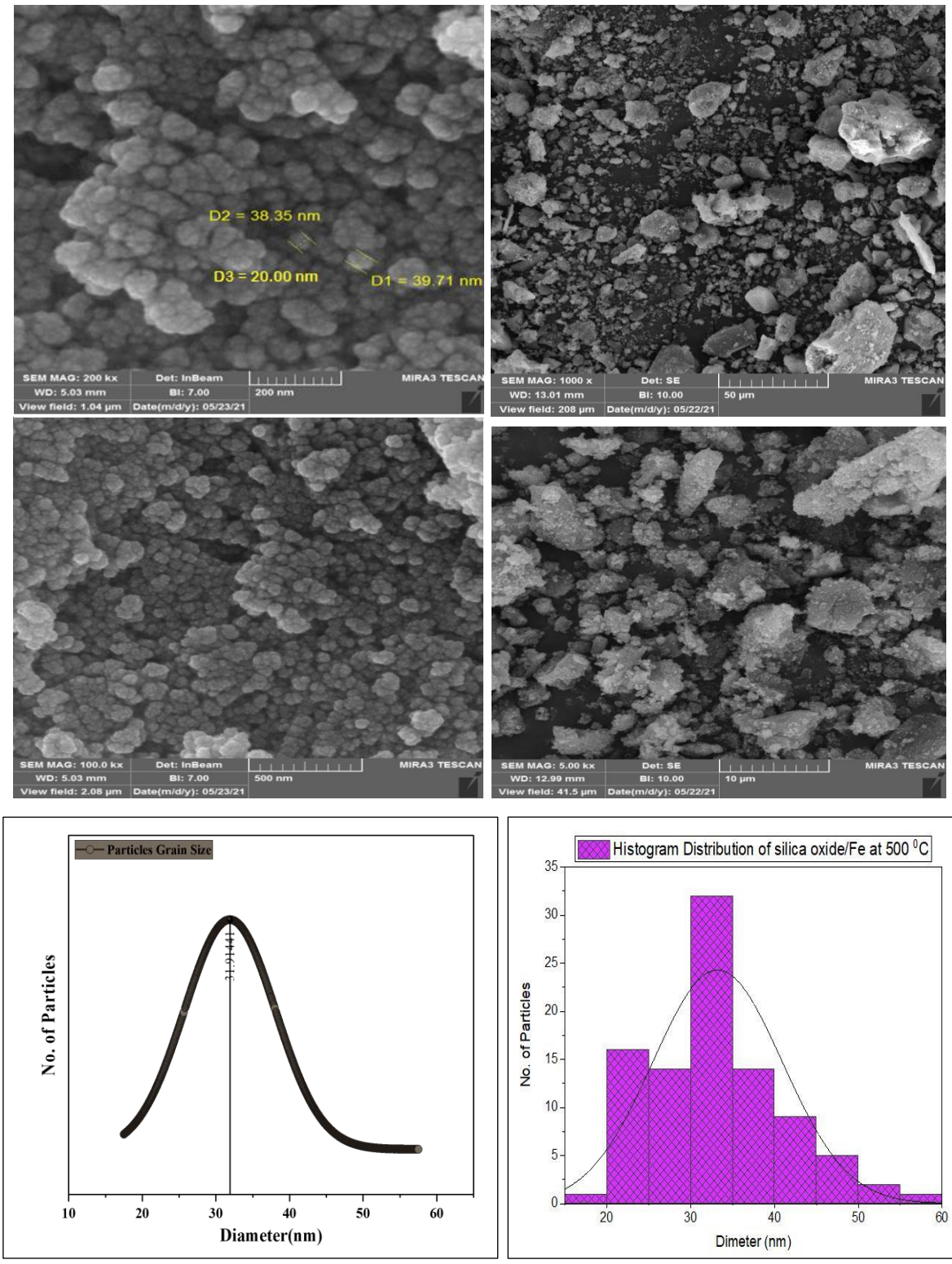

Figure3-23:-FE-SEM images of Nano binary oxide Fe_xO_y/SiO_2 powder at various scales with average particle grain size at a calcination temperature of 500 ˚C.

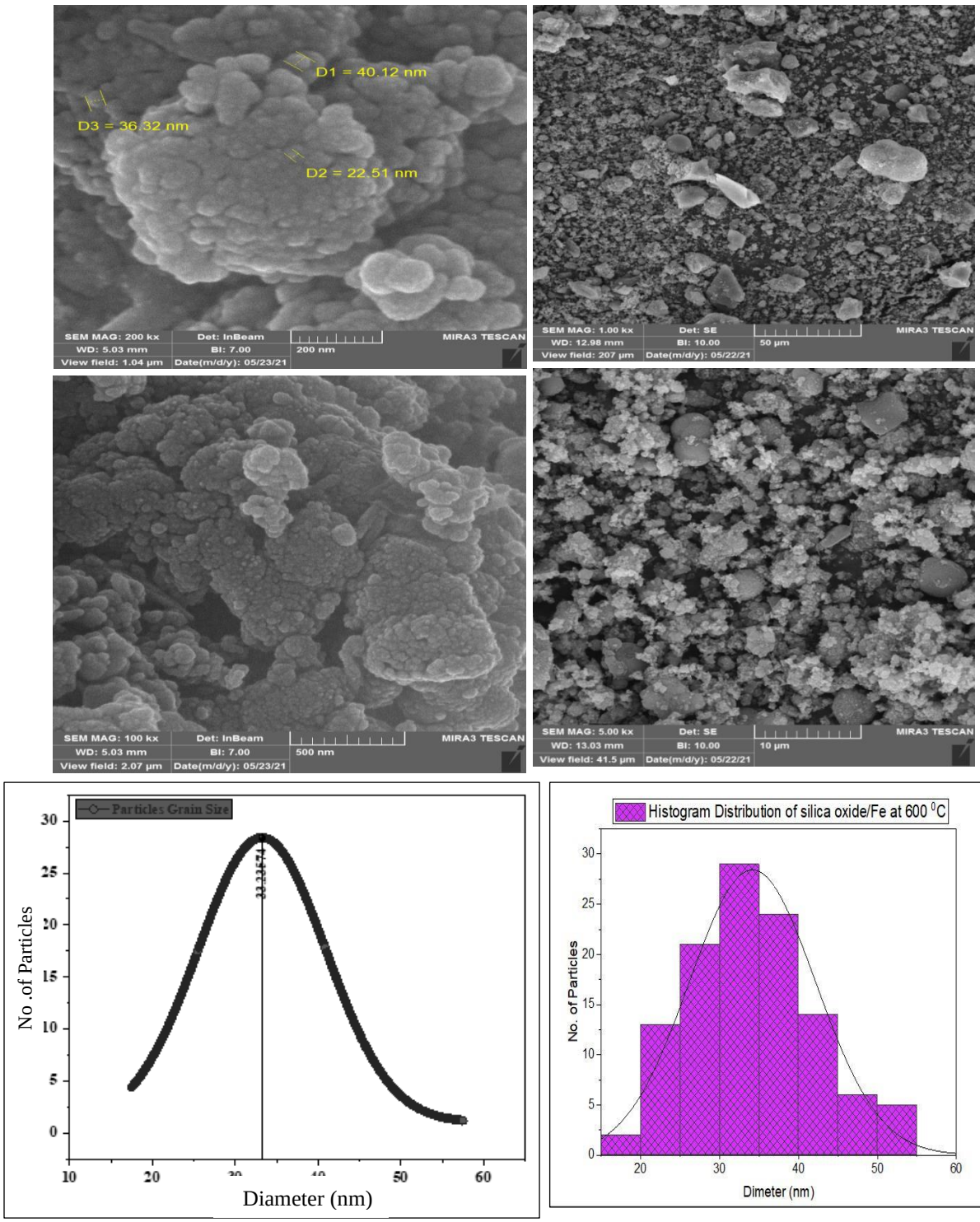

Figure3-24:-FE-SEM images of Nano binary oxide Fe_xO_y/SiO_2 powder at various scales with average particle grain size at a calcination temperature of 600 ˚C.

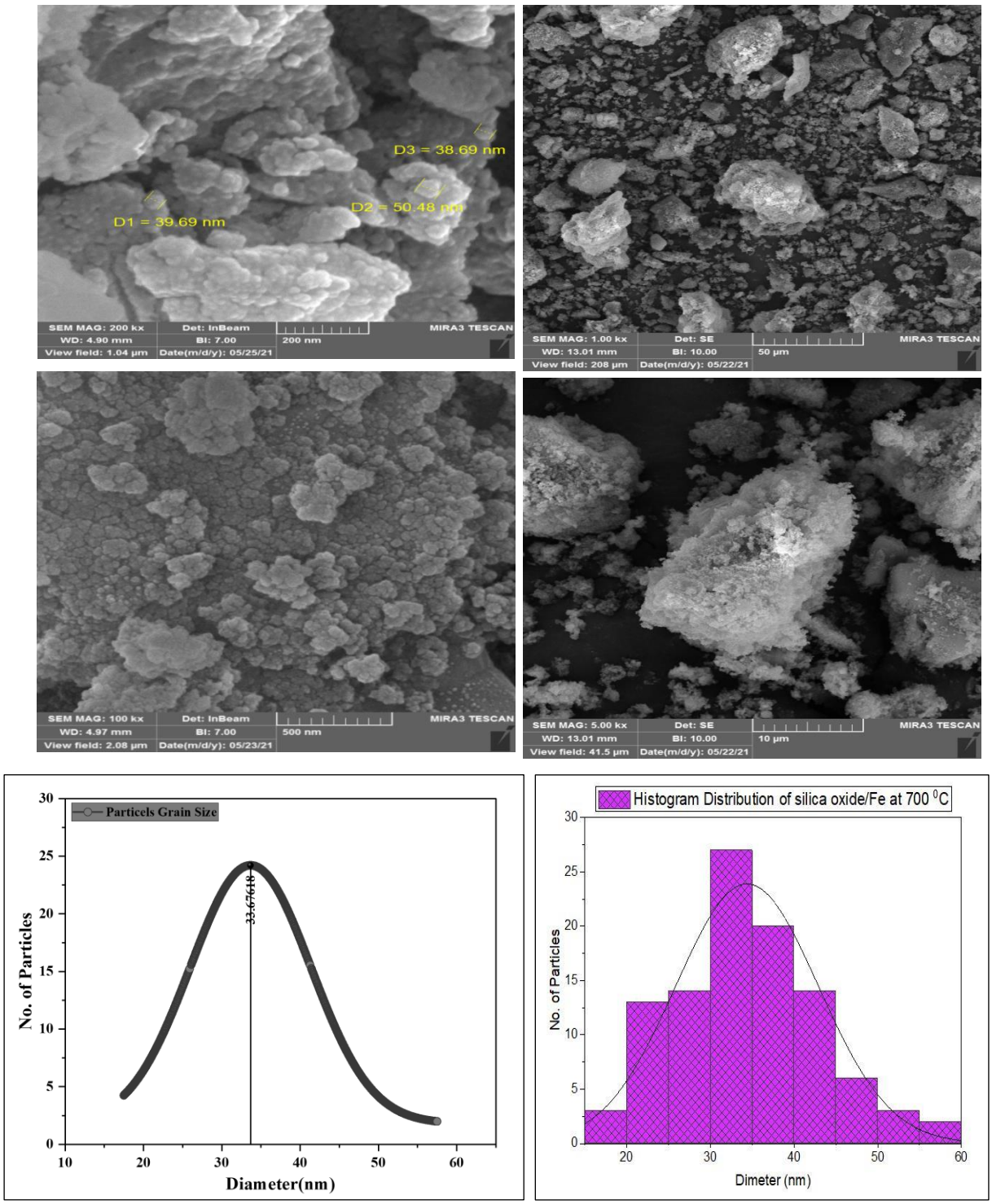

Figure3-25:-FE-SEM images of Nano binary oxide Fe_xO_y/SiO_2 powder at various scales with average particle grain size at a calcination temperature of 700 ˚C.

Table 3-8. The average grain size of nanoparticle and particle diameter at different burning temperatures for nanomagnetic binary oxide Fe_xO_y/SiO_2.

Temperature(°C)	Diameter(nm)	Average Grain Size(nm)
300	20 - 90	37.68
400	15 - 50	25.84
500	15 - 60	31.91
600	15 - 55	33.23
700	15 - 60	33.67

3-3. Brunauer-Emmett-Teller (BET) Surface Area and Pore-Size Distribution

BET instruments can benefit in various measurements. BET based on N_2 adsorption temperature of (-196 ^{0}C) is used to determine the specific surface area (SBET), pore-volume, and average diameter (BJH) of silica oxide NPs and nano binary oxides (SiO_2/V_2O_5, MgO/SiO_2, and Fe_xO_y/SiO_2) samples. Characterization of silica oxide NPs and nano binary oxides (SiO_2/V_2O_5, MgO/SiO_2, and Fe_xO_y/SiO_2) samples by BET with a different range of calcination temperatures between (300 -700) ˚C.

All of the figures of nano binary oxides (SiO_2/V_2O_5, MgO/SiO_2, and Fe_xO_y/SiO_2) show adsorption isotherms that according to the IUPAC. The results of (BJH) measurement pore volume and average diameter can know if these nanoparticles are mesoporous (200).

The results of average crystal size comparison with the results of another instrument, like FE-SEM and the average size crystal that calculated from the Debye Scherrer equation to show if the surface area is inversely proportional to, the surface area increases as the size of the crystal decreases, and vice versa as shown in table (3-10).

3-3-1. Brunauer-Emmett-Teller (BET) Surface Area and Pore-Size Distribution of nano silica oxide

BET measurements can typically use to determine the relationship between the particle size and the surface area. Additionally, this metric enables us to classify the pore size, as the form of the adsorption isotherm enables us to catalogue. The porous structure of the materials, which might be micro,meso, and macroporous if pores diameters (≥1, 1-100, ≤ 100) nm respectively from results of BET for nano-silica oxide show the average BJH pore diameter ranging between (4.99-10.18) nm such as shown in table (3-9). This demonstrates that these nanoparticles have mesoporous nature as per the IUPAC definition [201]. observe from results of specific surface area (S_{BET}) for silica oxide powder extracted from RHA with different ranges of calcination temperatures (300,400,500,600, and 700)˚C, the surface area of silica oxide equal to 91.108 m^2/g at calcination temperature 300 ˚C, with crystal size 47.832 nm, when to increase calcination temperature the surface area increase equal to 95.1437 m^2/g at 400 ˚C, with average crystal size 47.0187 nm the optimum surface area was173.786 mg/cm^3 at 500 ˚C with small crystal size 34.5251nm. These results may be due to the nature of silica oxide being more extensive at higher calcination temperatures, [202]. But when to increase calcination temperature more than 500˚C noted surface area decrease 100 .431 m^2/g, and 88.913 m^2/g at 600 ˚C and 700 ˚C respectively with an increased crystal size. Figure (3-26) displays the N_2 adsorption isotherms and pore diameter of these samples. All Figures display a type VI isotherm given by the IUPAC classification.

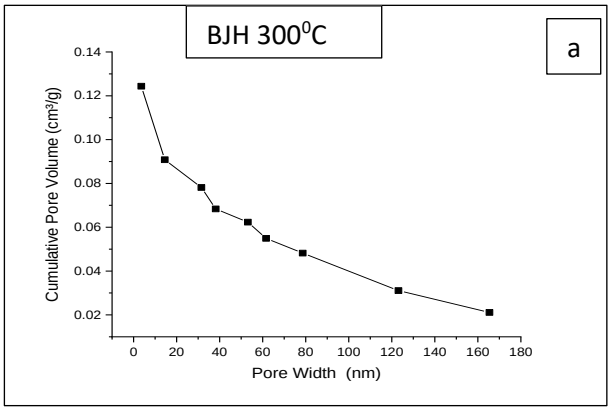
BJH 300^{0}C
a
Cumulative Pore Volume (cm³/g)
Pore Width (nm)

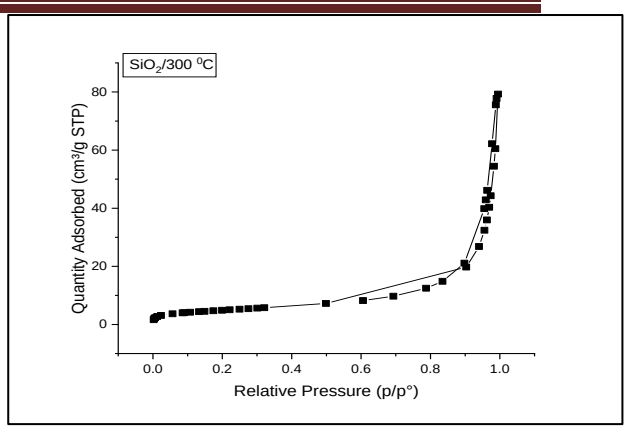
SiO$_2$/300 ^{0}C
Quantity Adsorbed (cm³/g STP)
Relative Pressure (p/p°)

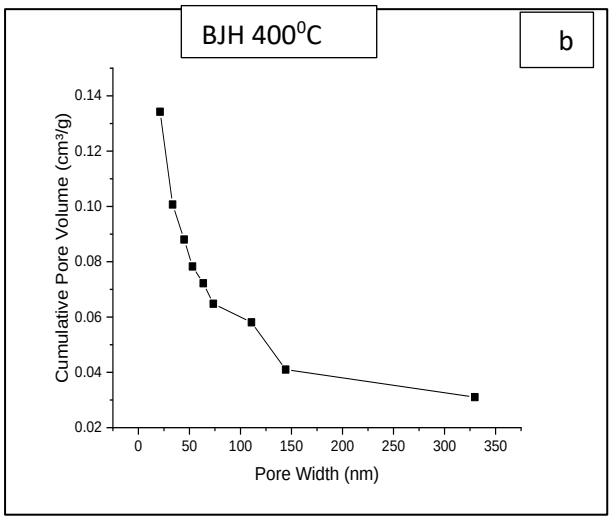
BJH 400^{0}C
b
Cumulative Pore Volume (cm³/g)
Pore Width (nm)

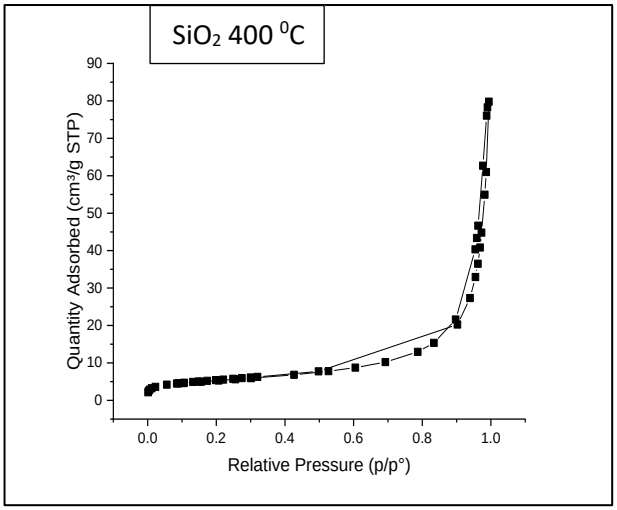
SiO$_2$ 400 ^{0}C
Quantity Adsorbed (cm³/g STP)
Relative Pressure (p/p°)

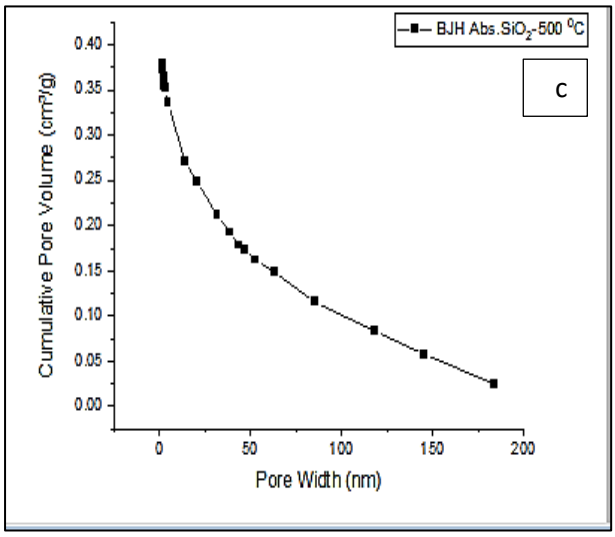
BJH Abs.SiO$_2$-500 ^{0}C
c
Cumulative Pore Volume (cm³/g)
Pore Width (nm)

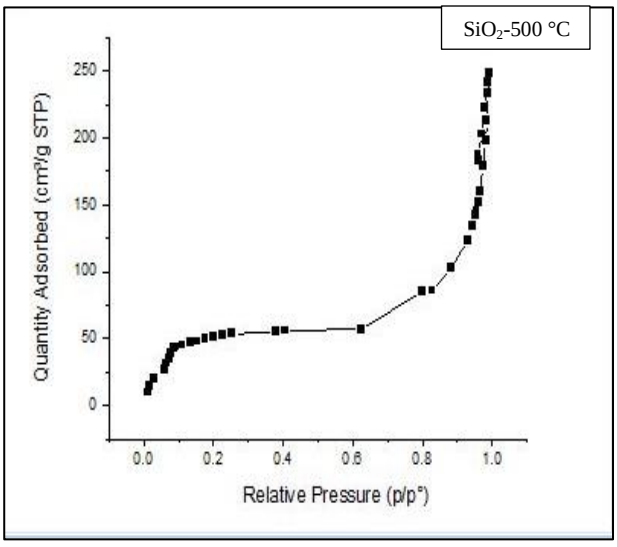
SiO$_2$-500 °C
Quantity Adsorbed (cm³/g STP)
Relative Pressure (p/p°)

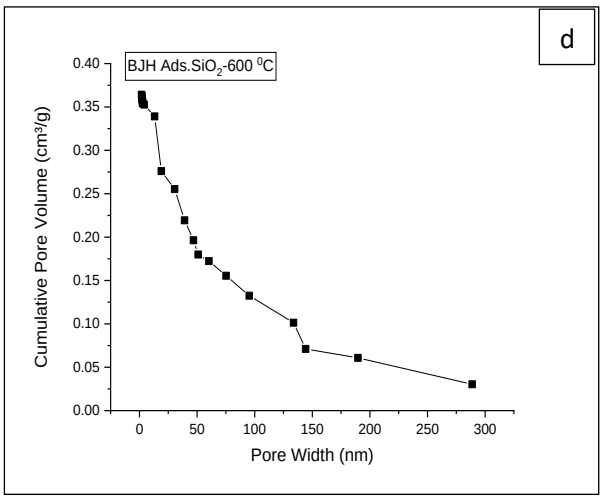
d
BJH Ads.SiO$_2$-600 ^{0}C
Cumulative Pore Volume (cm³/g)
Pore Width (nm)

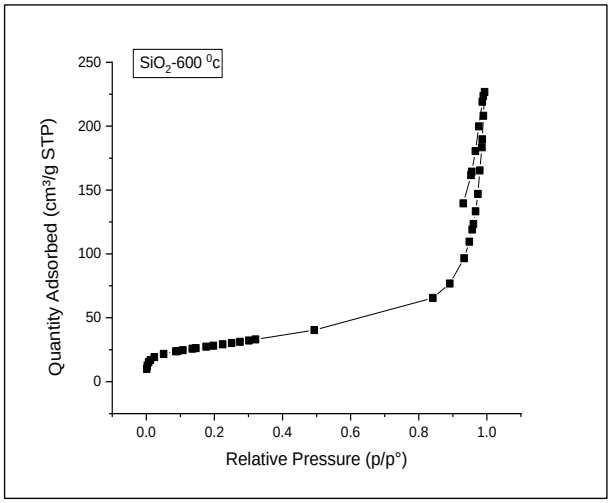
SiO$_2$-600 ^{0}c
Quantity Adsorbed (cm³/g STP)
Relative Pressure (p/p°)

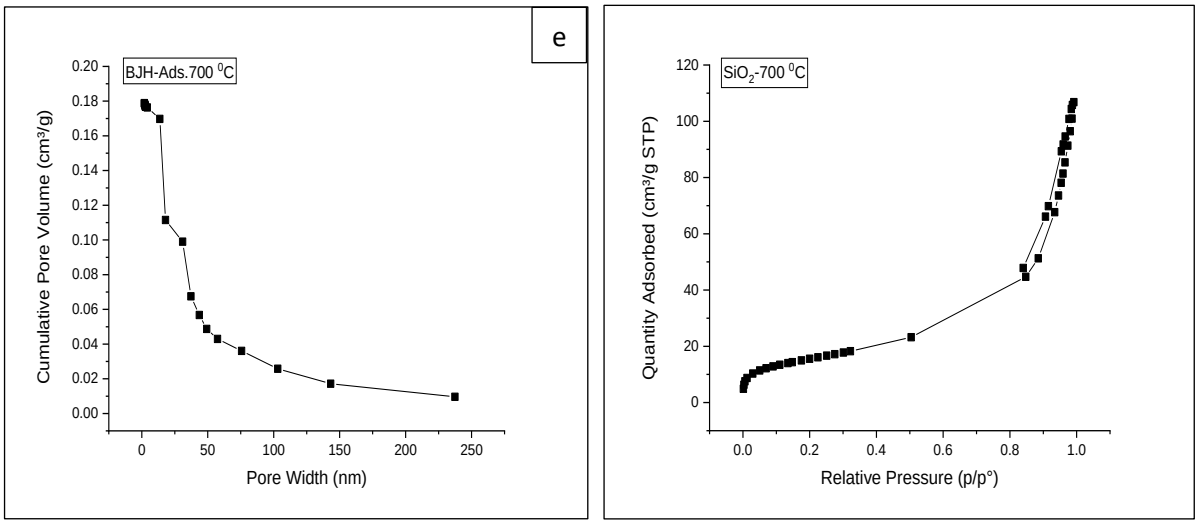

Figure3-26.Nitrogen adsorption isotherms and pore size distribution for nano silica oxide at (a. 300, b.400, c.500, and, d. 600, and e.700) ˚C.

Table3-9. Surface area BET(m^2/g) with average size crystal of nano silica oxide at different calcination temperatures.

SiO_2	Calcination temperature ^{0}C	Surface area BET(m^2/g)	Average Pore Volume(cm^3/g)	Average Pore diameter(nm)	Average size crystal (nm)
300		91.134	0.111275	9.1831	47.832
400		95.143	0.117897	10.007	47.018
500		173.786	0.216952	4.993	34.525
600		100.459	0.172330	6.861	46.943
700		88.913	0.100767	8.424	48.309

3-3-2. Brunauer-Emmett-Teller (BET) Surface Area and Pore-Size Distribution of nano binary oxide SiO_2/V_2O_5

Nano binary oxide **SiO_2/V_2O_5** has a surface area and pore volume significantly larger than silica oxide. The results show the surface area of nano binary oxide **SiO_2/V_2O_5** 195.4760 m^2/g at 300 ˚C with a particle size of 29.845 nm as shown in figures (3-27). The results showed that the surface area is inversely proportional to the average size crystal calculated from the Debye Scherrer equation when the crystal size decreases surface area increases, and vice versa as shown in table (3-10). Thus, the calcination of nano binary oxide **SiO_2/V_2O_5** results in a decrease in the specific surface area of all samples examined, which is proportional to the calcination temperature. Noted that an increase in calcination temperature of more than 300 ˚C results in a significant decrease in surface areas with an increase in the particle size. [203]

All figures (3-27) depict an isotherm classified as type IV by the International Union of Pure and Applied Chemistry [200]. The average diameter of the BJH pores is between (4and 10) nm, indicating that these nanoparticles are mesoporous as shown in table (3-11).

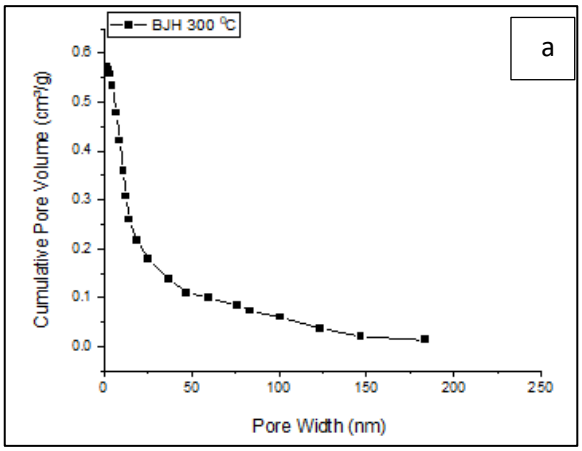
BJH 300 °C
a
Cumulative Pore Volume (cm³/g)
Pore Width (nm)

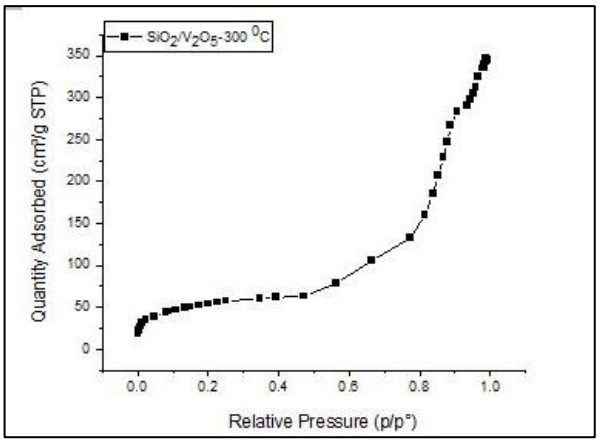
SiO2/V2O5-300 °C
Quantity Adsorbed (cm³/g STP)
Relative Pressure (p/p°)

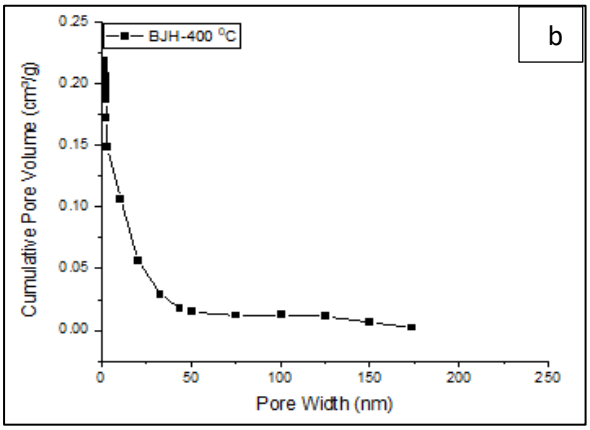
BJH-400 °C
b
Cumulative Pore Volume (cm³/g)
Pore Width (nm)

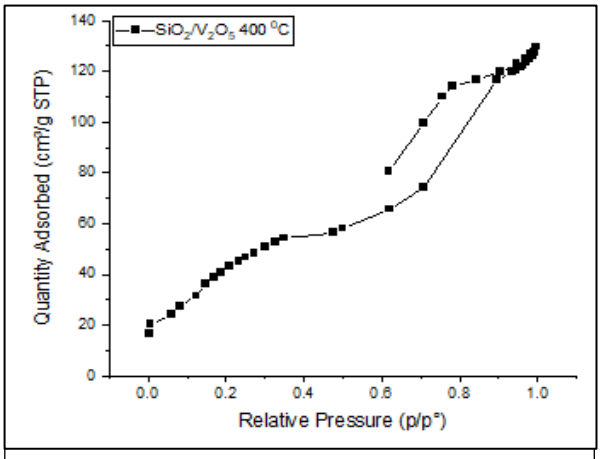
SiO2/V2O5 400 °C
Quantity Adsorbed (cm³/g STP)
Relative Pressure (p/p°)

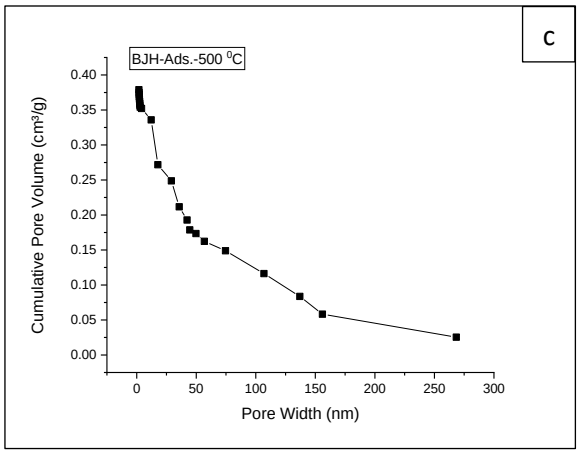
BJH-Ads.-500 °C
c
Cumulative Pore Volume (cm³/g)
Pore Width (nm)

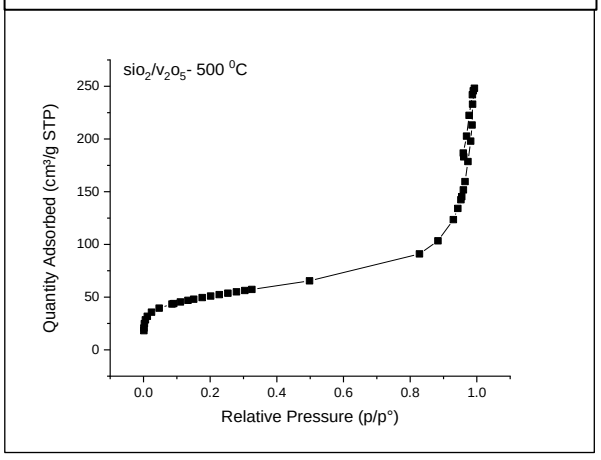
sio2/v2o5- 500 °C
Quantity Adsorbed (cm³/g STP)
Relative Pressure (p/p°)

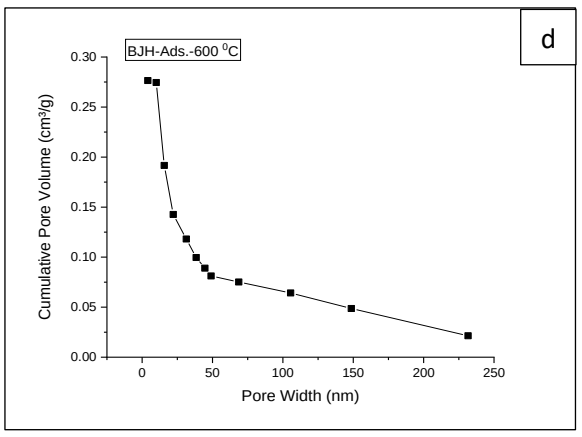
BJH-Ads.-600 °C
d
Cumulative Pore Volume (cm³/g)
Pore Width (nm)

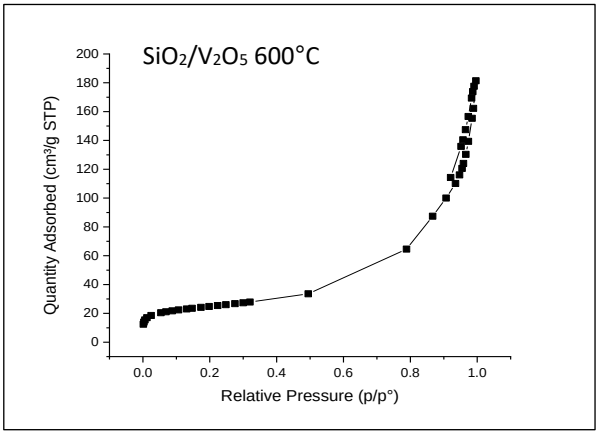
SiO2/V2O5 600°C
Quantity Adsorbed (cm³/g STP)
Relative Pressure (p/p°)

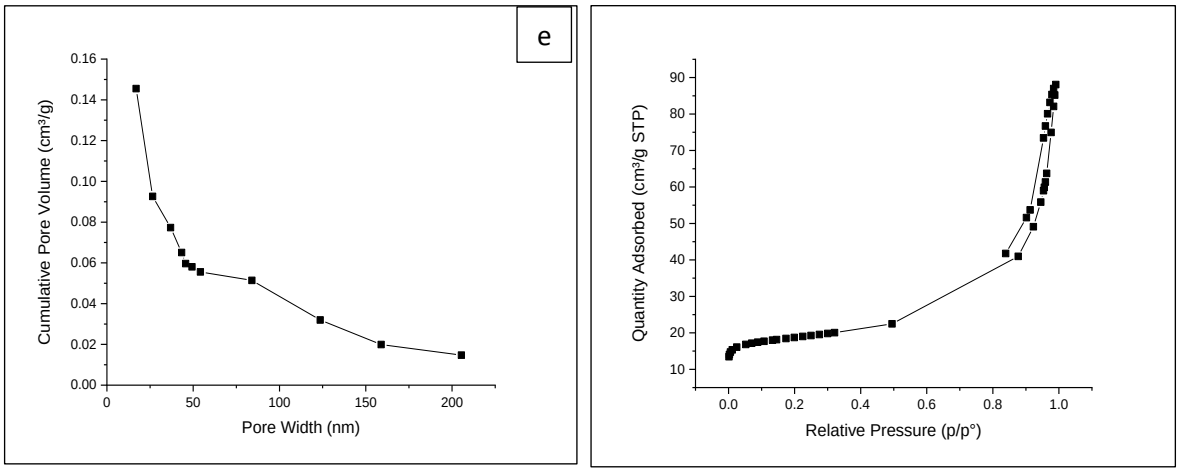

Figure3-27.Nitrogen adsorption isotherms and pore size distribution for nano silica oxide/V_2O_5 at (a. 300,b.400,c.500, d.600 and e.700)˚C.

Table 3-10. Surface area BET(m^2/g) with average size crystal of nano binary oxide SiO_2/V_2O_5 at different calcination temperatures.

SiO_2 /V_2O_5	Calcination temperature ˚C	Surface area BET(m^2/g)	Average Pore Volume(cm^3/g)	Average Pore diameter nm	Average size crystal (nm)
	300	195.476	0.308801	7.909	29.845
	400	187.591	0.277486	4.082	32.421
	500	178.831	0.228306	4.540	34.159
	600	166.405	0.221013	10.415	40.863
	700	127.673	0.202326	10.454	43.249

3-3-3. Brunauer-Emmett-Teller (BET) Surface Area and Pore-Size Distribution of nano binary oxide MgO /SiO_2 at difference percentage.

The adsorption isotherms for the binary mixed oxides synthesized by the wet method with different percentages. Table (3- 11) summarizes the Brunauer-Emmett-Teller (BET) for MgO /SiO_2 (E1-MG-75, E2-MG-25, E3-MG-90, and E4-MG-50)from the adsorption isotherms. The specific pore volume Vp is determined using the molar volumes of gaseous and liquid nitrogen and the adsorbed amount of nitrogen. While the nano binary oxide MgO /SiO_2 (E1-MG-75, E2-MG-25, E3-MG-90, and E4-MG-50) are comparable, the specific surface area (SBET) and pore volume (Vp) of mixed oxides are highly dependent on the MgO and silica oxide content. So nano binary oxide MgO/SiO_2 give the greatest value for surface areas (BET) for E4-MG-50 equal to 457.380 m^2/g. The mixed oxides with a weight percentage of magnesium oxide (E4-MG-50) have much larger surface areas than pure silica oxide. But at the same time noted with a high weight percentage of magnesium oxide contents E3-MG-90, the surface area is smaller as shown in table (3-11) at the same calcination temperature. [204]. The International Union of Pure and Applied Chemistry classifies all figures (3-28) as Type IV isotherms. The BJH pores have an average diameter of between (4 -6) nm, indicating that they are mesoporous.

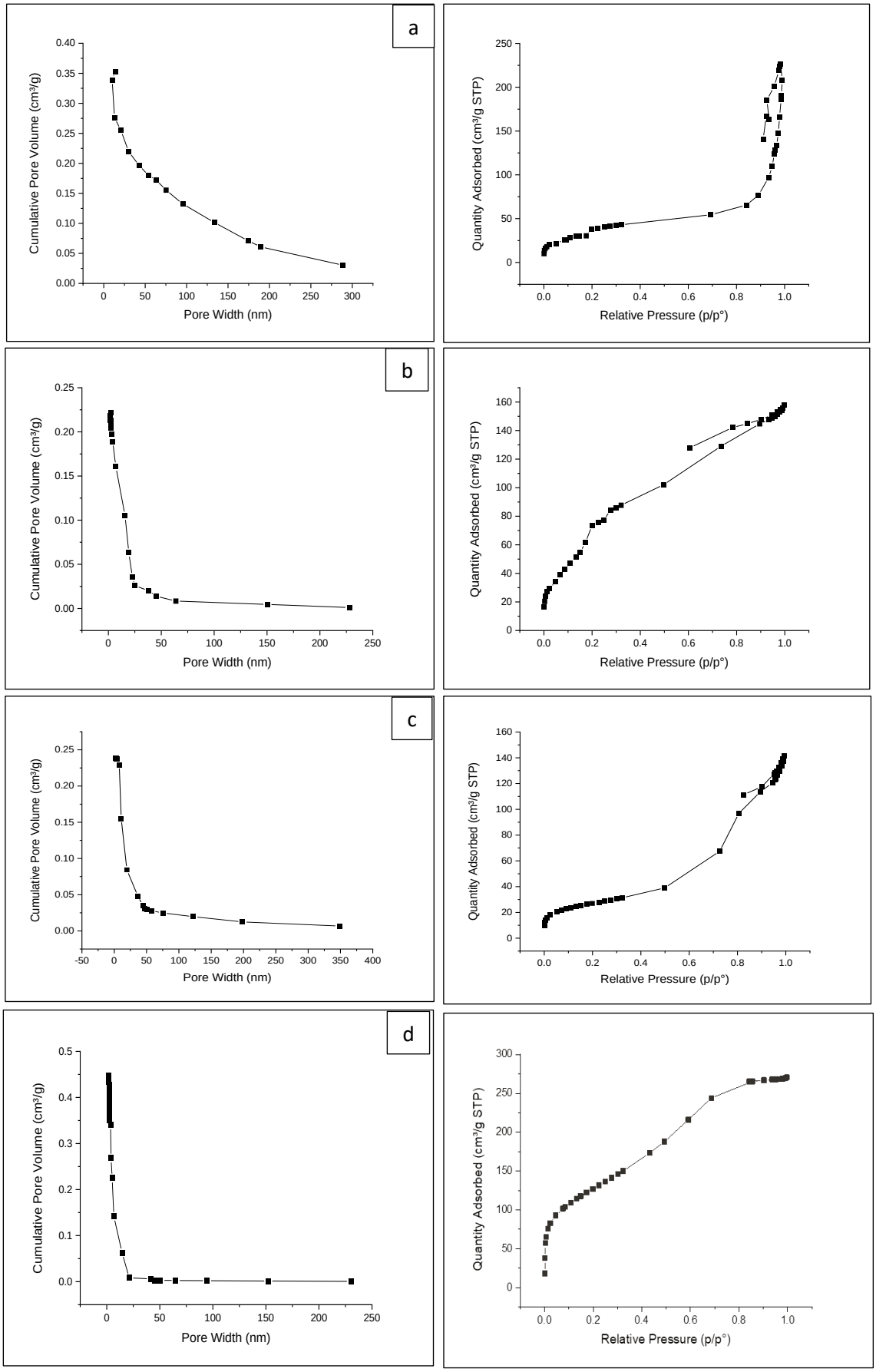

Figure 3-28. Nitrogen adsorption isotherms and pore size distribution for MgO/SiO_2 a.(E2-MG-25), b.(E1-MG-75),c .(E3-MG-90) and d. (E4-MG-50).

Table 3-11. Surface area BET(m^2/g) of nano binary oxide MgO /SiO_2 at a different percentage.

Antibiotic MgO/SiO_2 300 ˚C	Surface area BET(m^2/g)	Average Pore Volume(cm^3/g)	Average Pore Diameter (nm)	Average size crystal (nm)
Antibiotic 2 (E1-MG-75)	100.967	0.185575	6.0725	49.51826
Antibiotic 1 (E2-MG-25)	183.1429	0.265510	4.9774	33.3581
Antibiotic 3 (E3-MG-90)	97.5276	0.129338	6.4211	58.10052
Antibiotic4 (E4-MG-50)	457.3802w	0.415274	3.63193	13.1182

3-3-4. Brunauer-Emmett-Teller (BET) Surface Area and Pore-Size Distribution of nano binary oxide MgO/SiO_2 E4-MG-50

Nano binary oxide MgO/SiO_2 E4-MG-50 degassing for 3 hours at a different range of calcination temperatures from (300 to 700) ˚C, the surface areas of nano binary oxide MgO/SiO_2 are measured using nitrogen adsorption. The areas of the BET surfaces of the difference calcination temperatures of nano binary oxide E4-MG-50 are determined to be (457.380 m^2/g) at 300 ˚C. BET decreased with increased calcination temperatures because the particle size increased with increasing calcination temperatures. as shown in table (3-12). The surface area of mixed oxide is larger than silica oxide at the same calcination temperatures, figures (3-29) are classified as type IV isotherms by the International Union of Pure and Applied Chemistry. The average diameter of the BJH pores is between (4-7) nm, indicating that they are mesoporous.

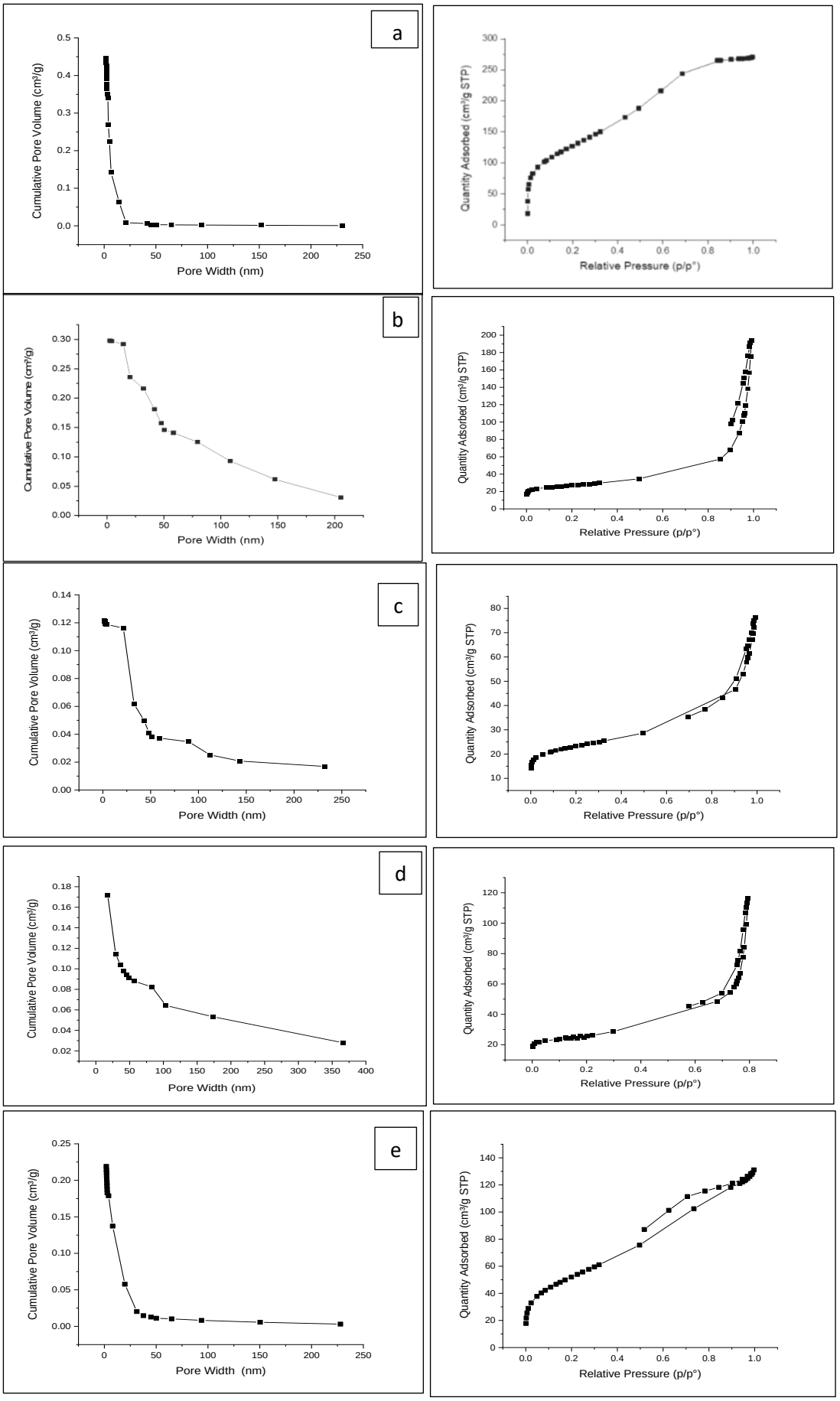

Figure3-29. Nitrogen adsorption isotherms and pore size distribution for MgO/SiO_2 a.(E4-MG-50),b.(D4-MG-50),c.(C4-MG-50),d. (B4-MG-50) and e.(A4-MG-50).

Table 3-12. Effect calcination temperatures on Surface area BET(m^2/g) of nano binary oxide MgO/ SiO_2.

MgO/ SiO_2 0.5:0.5	Calcination temperature ˚C	Surface area (m^2/g)	Average Pore Volume (cm^3/g)	Average Pore Diameter (nm)	Average size crystal (nm)
E4-MG-50		457.3802	0.415274	3.63193	13.1182
D4-MG-50		258.9010	0.374175	6.37950	20.477
C4-MG-50		247.3168	0.336095	6.1267	22.953
B4-MG-50		239.1648	0.330185	7.40347	25.409
A4-MG-50		200.147	0.288012	4.40347	29.0323

3-3-5 Brunauer-Emmett-Teller (BET) Surface Area and Pore-Size Distribution of nano binary oxide Fe_xO_y/SiO_2

After degassing for 3 hours at (300 to 700) ˚C, the surface areas of nano binary oxide Fe_xO_y/SiO_2 are measured using the Horiba SA-9600 by nitrogen adsorption. It is determined that the surface area BET of nanomagnetic oxides was 221.7817 m^2/g at a calcination temperature of 400 ˚C. The magnitude of the surface area of nano binary oxide Fe_xO_y/SiO_2 is comparable to that reported [205] for Fe/silicon mixed oxide generated by the sol-gel method. The modest variance in surface area can be attributed to the manner of preparation, as composition oxides are prepared in a variety of ways. Additionally, the surface areas of nano binary oxide Fe_xO_y/SiO_2 burning at 400 ˚C, be greater than other calcination temperatures as shown in table (3-13). With a rise in the calcination temperature, both the pore volume and surface area decrease in the table (3-13). Indeed, the microscopic holes present on the surface of nano binary oxide Fe_xO_y/SiO_2 clogged up during the sintering process, resulting in a reduction in surface area. This decline is particularly pronounced between (500 and 700) ˚C, this is because nano binary oxide Fe_xO_y/SiO_2 crystallizes

between (500 and 700) ˚C [206]. All figures (3-30) are classified as type VI isotherms by the International Union of Pure and Applied Chemistry. The average diameter of the BJH pores is between (8 -10 nm), indicating that they are mesoporous.

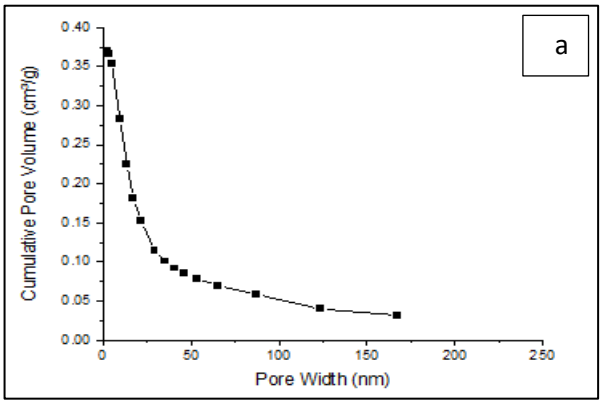

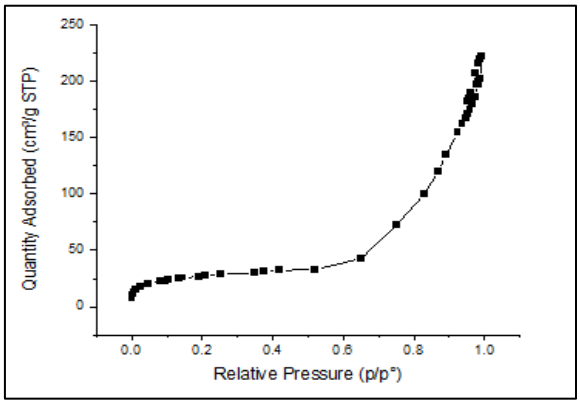

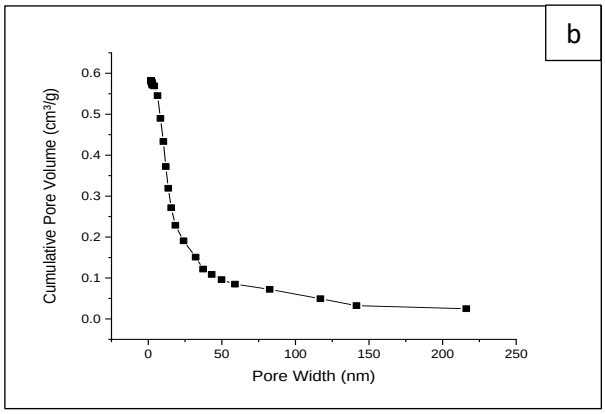

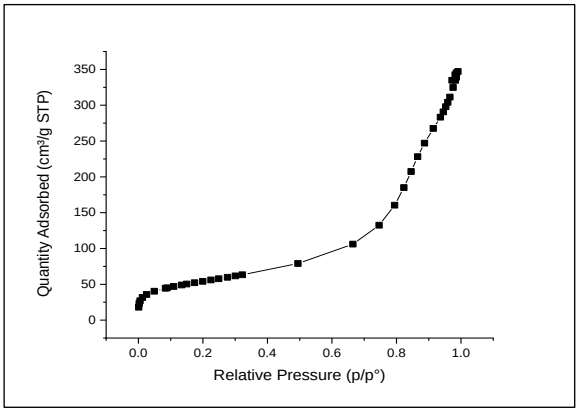

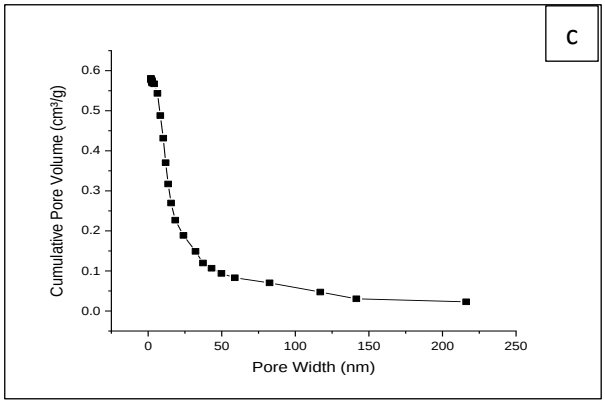

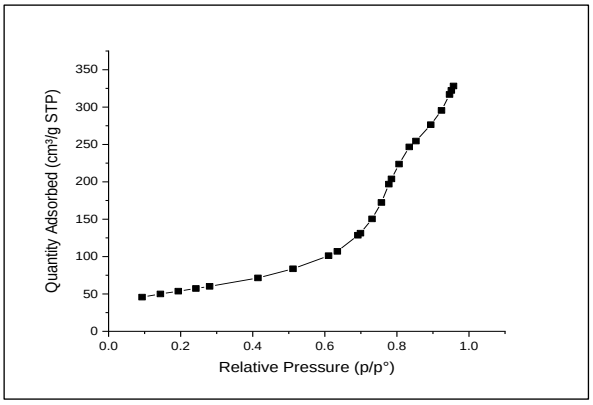

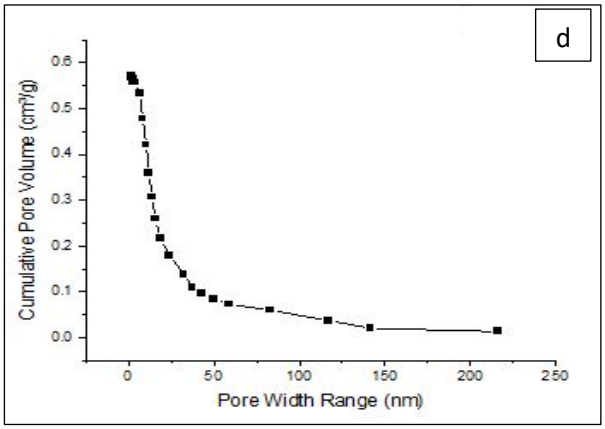

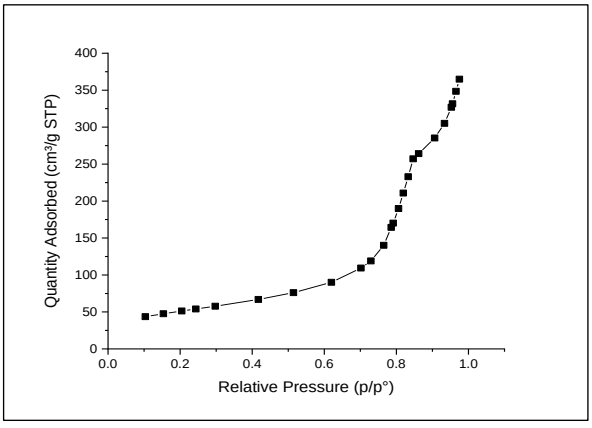

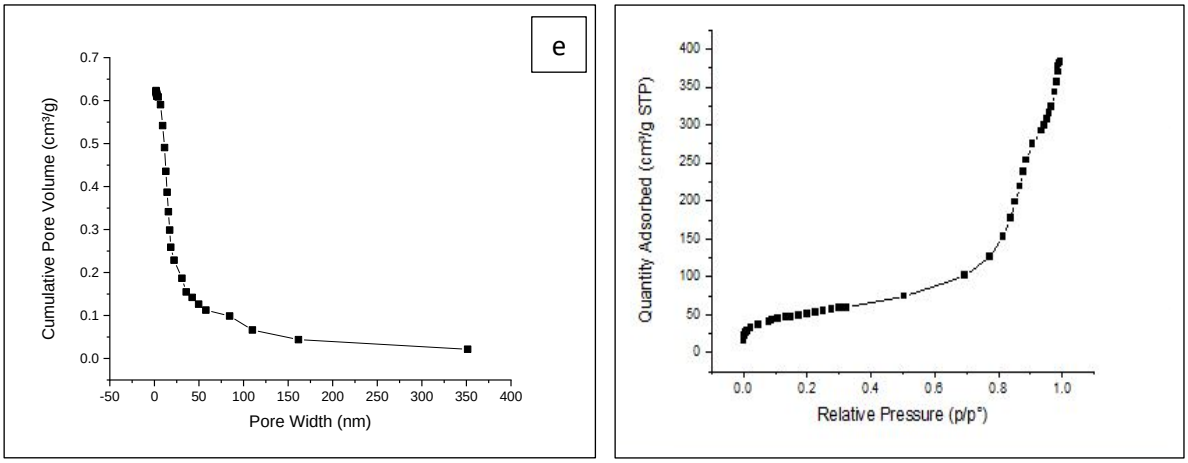

Figure3-30.Nitrogen adsorption isotherms and pore size distribution for Fe_xO_y/SiO_2 at (a. 300,b. 400, c. 500 d. 600, and e.700) ˚C.

Table 3-13. Surface area BET(m^2/g)for nano binary oxide Fe_xO_y/SiO_2 at different calcination temperatures ˚C.

Fe_xO_y/SiO_2	Calcination temperature ˚C	Surface area (m^2/g)	Average Pore Volume (cm^3/g)	Average Pore Diameter (nm)	Average size crystal (nm)
	300	101.1230	0.280343	10.337	46.337
	400	221.7817	0.515293	10.152	28.479
	500	190.5198	0.455831	8.786	30.381
	600	190.1759	0.455015	9.576	31.549
	700	182.6296	0.411045	10.376	32.853

3-4Energy-Dispersive X-ray Spectroscopy (EDX)

3-4-1 Energy-Dispersive X-ray Spectroscopy (EDX) for silica oxide

EDX (energy-dispersive X-ray spectroscopy) is a widely used technique for determining the elemental composition of specimens. This technique may be used to measure the relative or absolute concentrations of all components. Additionally, the purity of a specimen's nanoparticles can be determined [207]. Figures (3-31[a,b, c,d and e]) show the percentage of elements that present with a nano-silica oxide that indicated the impurity of samples at digestion temperatures (300,400, 500, 600 and 700)˚C respectively.

The energy-dispersive X-ray spectroscopy (EDX) result for nano silica oxide in figure (e.3-31) at the reflexing process and digestion temperature of 700˚C agree with the stoichiometry of the results that show the concentration of elements at 700^0C, indicating that silicon exists in oxide form, silicon and oxygen have the largest peaks (208,209). Nano-silica generated from rice husk has silicon peaks with high purity at 700 ◦C when compared to other samples with smaller calcination temperatures. The elemental analysis data graphs confirm the presence of silica.

From results of EDX can explain why the surface area of nano silica oxide at 700 ˚C, less than at calcination temperature of 500˚C, may be due to the sample of silica oxide at 500 ˚C containing many other elements with it such as shown in the results of energy-dispersive X-ray spectroscopy (EDX), but when comparing the results of EDX for silica oxide sample at calcination 700 ˚C, noted the sample content just carbon, oxygen and silica oxide contains. The sample with temperature calcination of 300 ℃ (Figure 3-31a) is found by the presence of elements with different percentage weight and distribution peaks along

chart, the major element of carbon (C) oxygen (O), silicon (Si), together with a minor element of sulphur (S) and sodium (Na). The presence of carbon due to the effects of simultaneous heating followed by carbon formation began to form and distributed to cover silica on the surface of the sample, with a significant amount of carbon 26.35% (C) and 32.20% (Si). According to the leading particles are most likely the carbon present as larger particles, indicating that the sample is dominated by carbon. The EDX data in figures (3-31) demonstrated the considerable effect of increasing the calcination temperature on the composition of the samples. As can be observed in the figures, the sample included a significant amount of carbon and the proportion of this element was reduced to 2.41% as the calcination temperature was increased to 700 ˚C, also noted the concentration of silica (Si) increased with digestion temperature increase [210].

3-4-2. Energy-Dispersive X-ray Spectroscopy (EDX) for nano binary oxide SiO_2/V_2O_5.

EDX solid catalyst sample is crushed to a very fine powder and a small amount is applied to a stub of carbon tape (sample holder). The samples are then examined for non-conductive and conductive materials under accelerating voltages of 0.0–10 kV. Additionally, the EDX detector is utilized to investigate the surface composition of each sample, providing qualitative and quantitative data via surface scanning, point mapping, and line mapping investigations, for nano binary oxide and silica investigated at a different range of calcination temperatures, figures (3-32[a,b,c,d, ande]), energy dispersive X-rays are able to provide qualitative information about the nano binary oxide V_2O_5/SiO_2 surface. noted carbon contains decrease with increased calcination temperatures, while vanadium decrease with increased calcination temperature, and the EDX spectrum figure (3-32 a), reveals that the nano binary oxide contains 16.55%, 20.20%, weight percent vanadium and silica,

respectively with digestion temperature 300 ˚C. Figure (e.3-32) show nano binary oxide contains 8.92%, 27.04%, weight percent vanadium and silica, respectively with digestion temperature 700˚C [211].

3-4-3. Energy-Dispersive X-ray Spectroscopy (EDX) for nano binary oxide SiO_2/MgO

To assess the chemical composition of nano binary oxide MgO/SiO_2 elemental analysis is performed as depicted in figures (3-33[a,b, c,d, and e]). As demonstrated by the observed result, the nano binary oxide, contained significant amounts of major components such as magnesium, oxygen, carbon, and silica with different weight percentages as shown in the tables attached to figures (3-33[a,b, c,d, and e]). It is self-evident from the elemental analysis that carbon decrease with increased calcination temperatures, oxygen is the most abundant element, followed by silicon. Noted the weight percentages of magnesium decrease with increase calcination temperatures. The study demonstrated that the process of heat treatment of the MgO/SiO_2 powder, implemented via calcination, is a very effective method to change their physicochemical and structural properties. The dispersive characteristics of obtained calcinates depend mainly on the calcination temperature. MgO/SiO_2 powder is characterized by EDX with a percentage weight of 25.301% (Mg) at 300 ˚C smaller when compared to the percentage weight of 20.69% (Mg) at 700 ˚C calcinated sample.

3-4-3. Energy-Dispersive X-ray Spectroscopy (EDX) for nano binary oxide Fe_xO_y /SiO_2.

The FESEM image demonstrates that the surface of nanomagnetic binary oxides Fe_xO_y/SiO_2 is porous. Composition oxide particles are uneven in shape and lack a distinct morphology. The FESEM image of nanomagnetic binary oxides Fe_xO_y /SiO_2 at difference calcination demonstrates that the particles become coarser during the calcination process calcination temperature increases, indicating particle agglomeration caused by the sintering process at elevated temperatures (more than 400 °C). The EDX studies revealed that all nanomagnetic binary oxides Fe_xO_y/SiO_2 at different calcination samples such as shown in figures (3-34) have a significant silica concentration more than Iron concentration at their surfaces. Silica particles are negatively charged and bigger in size particles, in comparison to iron oxide particles that are positively charged. The presence of a high concentration of bigger silica on the surface of compotation oxide obscure Iron particles [212].

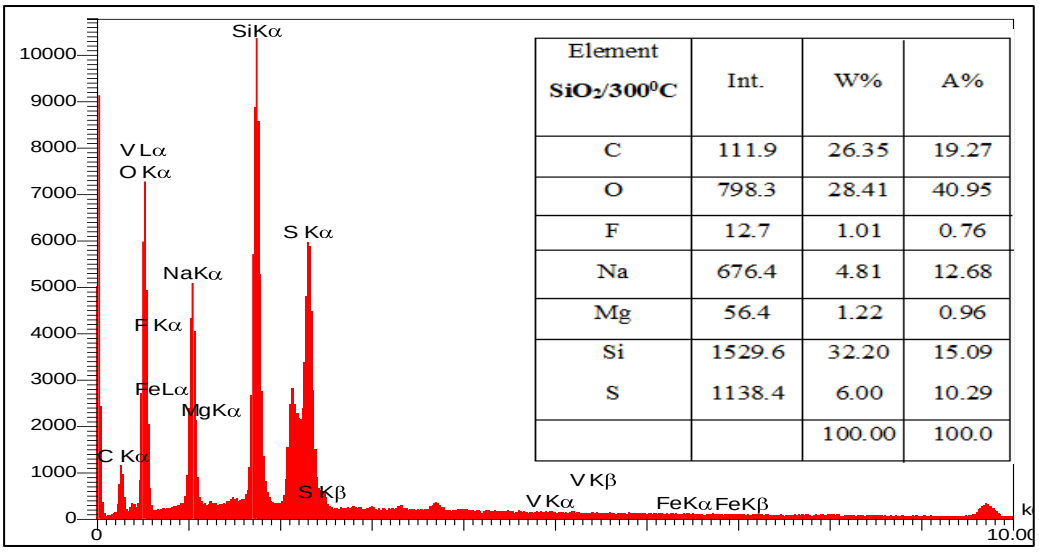

Element SiO_2/300^{0}C	Int.	W%	A%
C	111.9	26.35	19.27
O	798.3	28.41	40.95
F	12.7	1.01	0.76
Na	676.4	4.81	12.68
Mg	56.4	1.22	0.96
Si	1529.6	32.20	15.09
S	1138.4	6.00	10.29
		100.00	100.0

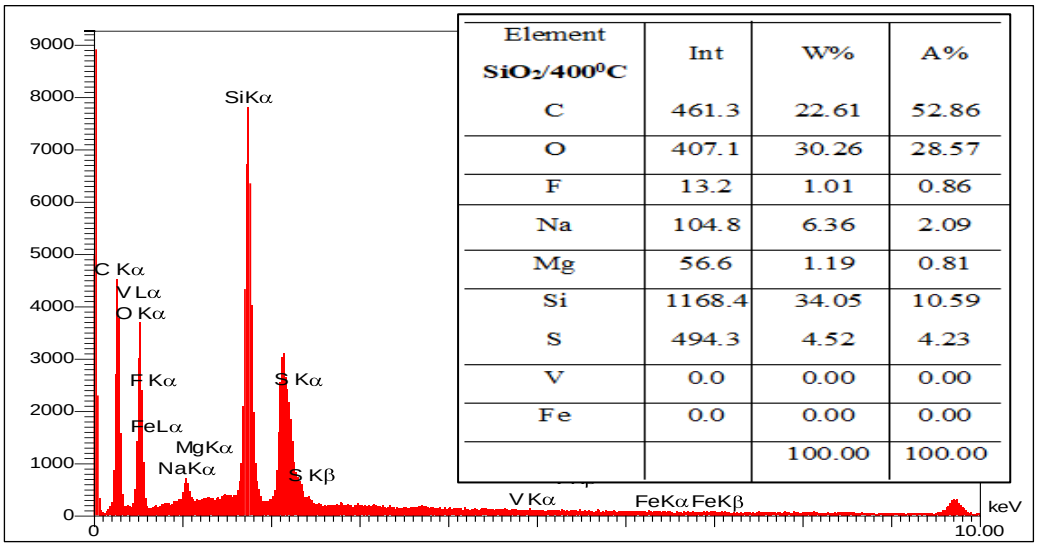

Element SiO_2/400^{0}C	Int	W%	A%
C	461.3	22.61	52.86
O	407.1	30.26	28.57
F	13.2	1.01	0.86
Na	104.8	6.36	2.09
Mg	56.6	1.19	0.81
Si	1168.4	34.05	10.59
S	494.3	4.52	4.23
V	0.0	0.00	0.00
Fe	0.0	0.00	0.00
		100.00	100.00

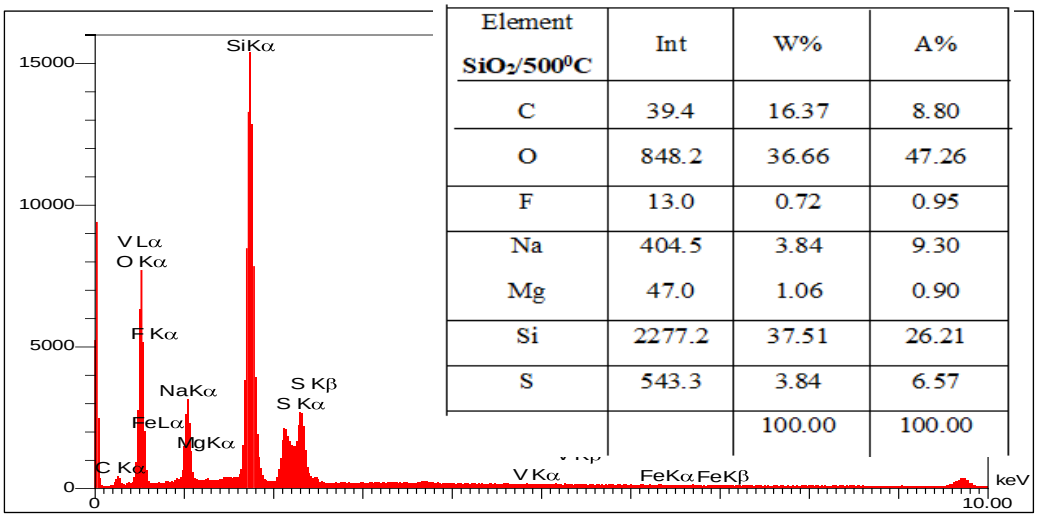

Element SiO_2/500^{0}C	Int	W%	A%
C	39.4	16.37	8.80
O	848.2	36.66	47.26
F	13.0	0.72	0.95
Na	404.5	3.84	9.30
Mg	47.0	1.06	0.90
Si	2277.2	37.51	26.21
S	543.3	3.84	6.57
		100.00	100.00

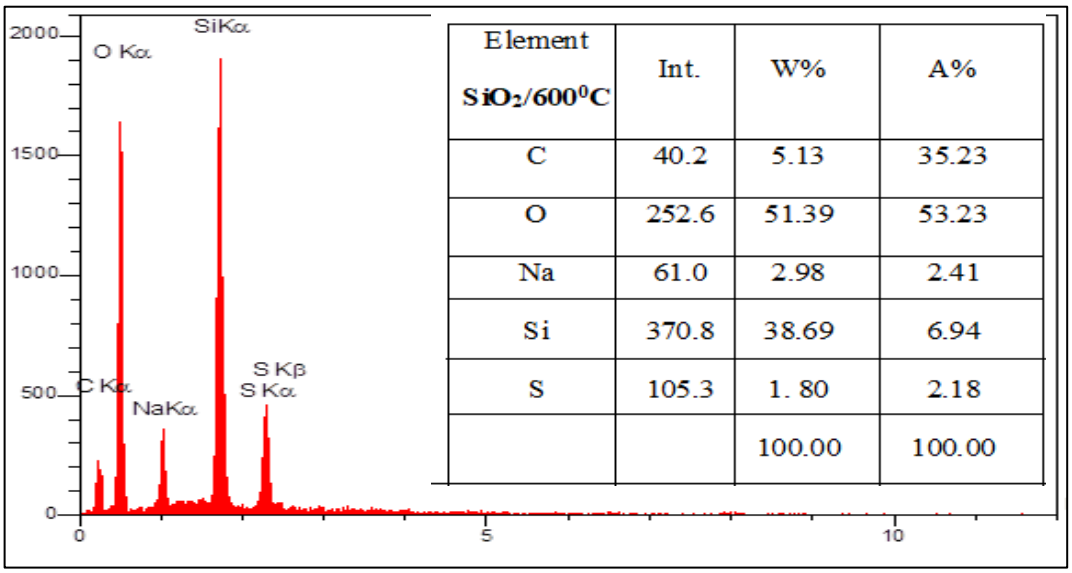

Element SiO_2/600^{0}C	Int.	W%	A%
C	40.2	5.13	35.23
O	252.6	51.39	53.23
Na	61.0	2.98	2.41
Si	370.8	38.69	6.94
S	105.3	1. 80	2.18
		100.00	100.00

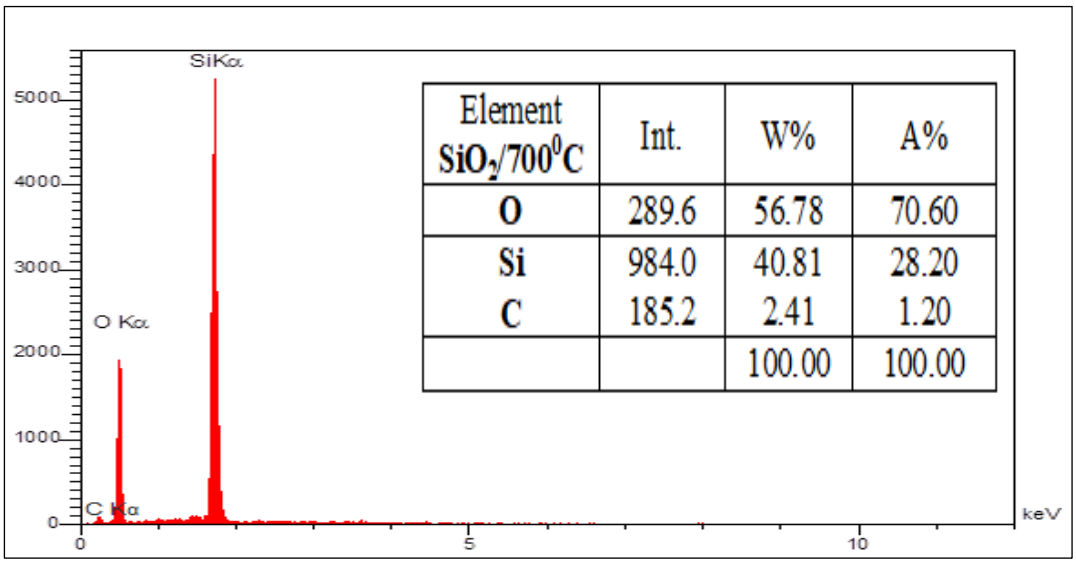

Element SiO_2/700^{0}C	Int.	W%	A%
O	289.6	56.78	70.60
Si	984.0	40.81	28.20
C	185.2	2.41	1.20
		100.00	100.00

Figure 3-31.EDX spectrum of nano Silica oxide at calcination temperatures. a.300 ˚C ,b. 400 ˚Cand c.500 ˚C. d.600 ˚C and e.700 ˚C.

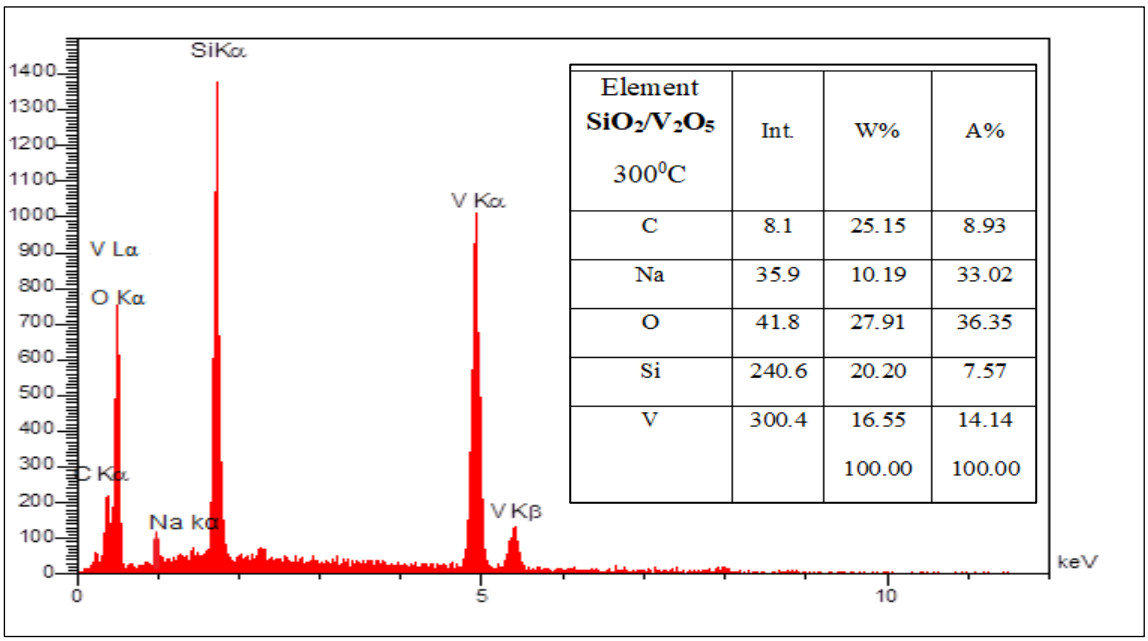

Element SiO_2/V_2O_5 300^{0}C	Int.	W%	A%
C	8.1	25.15	8.93
Na	35.9	10.19	33.02
O	41.8	27.91	36.35
Si	240.6	20.20	7.57
V	300.4	16.55	14.14
		100.00	100.00

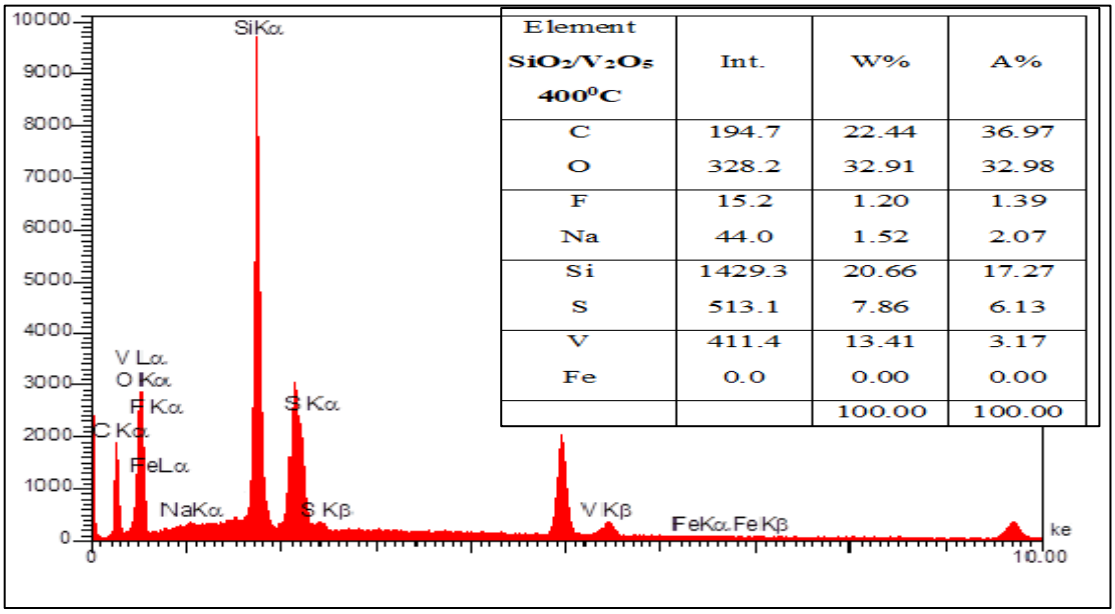

Element SiO_2/V_2O_5 400°C	Int.	W%	A%
C	194.7	22.44	36.97
O	328.2	32.91	32.98
F	15.2	1.20	1.39
Na	44.0	1.52	2.07
Si	1429.3	20.66	17.27
S	513.1	7.86	6.13
V	411.4	13.41	3.17
Fe	0.0	0.00	0.00
		100.00	100.00

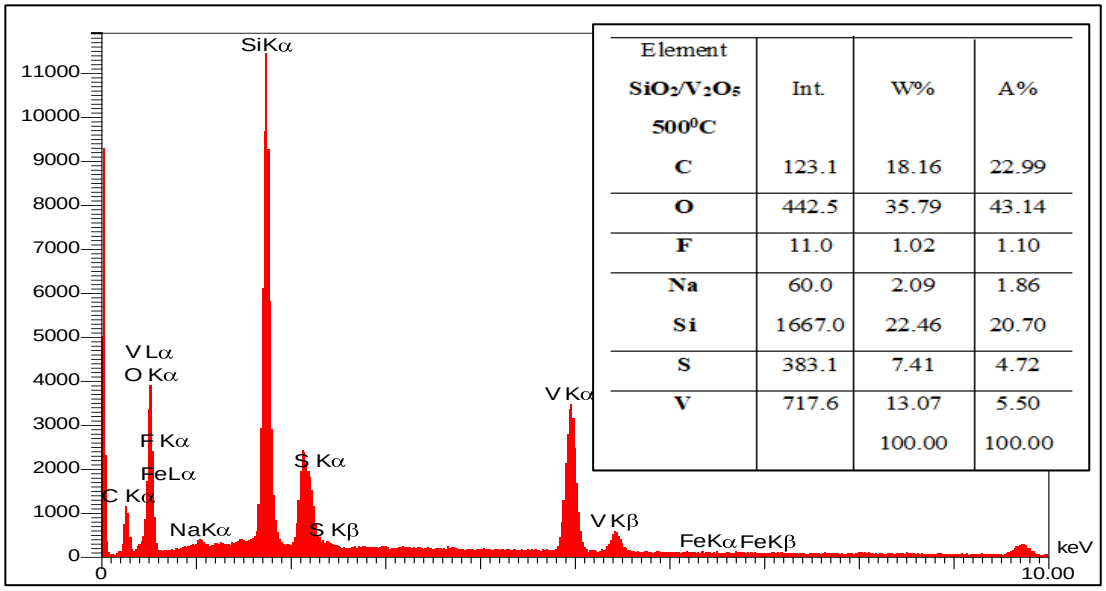

Element SiO_2/V_2O_5 500°C	Int.	W%	A%
C	123.1	18.16	22.99
O	442.5	35.79	43.14
F	11.0	1.02	1.10
Na	60.0	2.09	1.86
Si	1667.0	22.46	20.70
S	383.1	7.41	4.72
V	717.6	13.07	5.50
		100.00	100.00

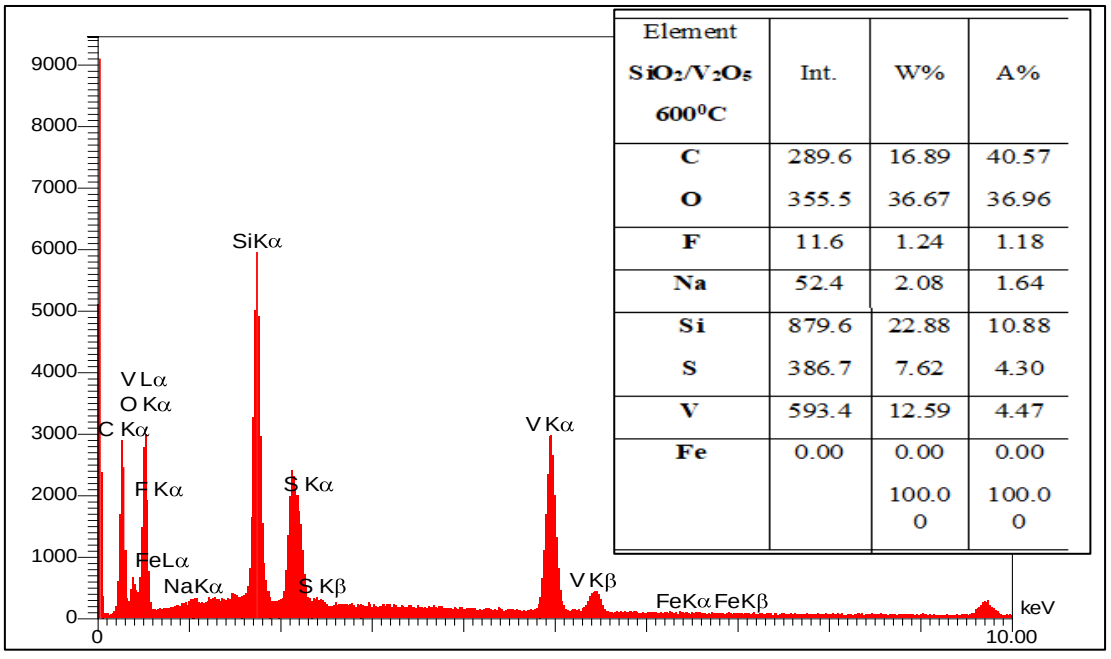

Element SiO_2/V_2O_5 600°C	Int.	W%	A%
C	289.6	16.89	40.57
O	355.5	36.67	36.96
F	11.6	1.24	1.18
Na	52.4	2.08	1.64
Si	879.6	22.88	10.88
S	386.7	7.62	4.30
V	593.4	12.59	4.47
Fe	0.00	0.00	0.00
		100.00	100.00

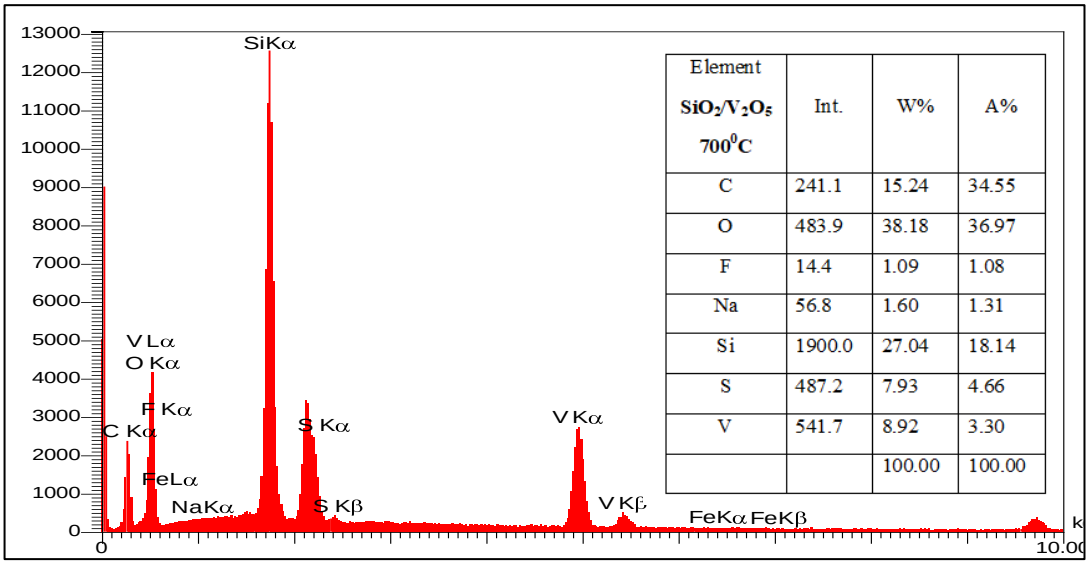

Element SiO_2/V_2O_5 700^{0}C	Int.	W%	A%
C	241.1	15.24	34.55
O	483.9	38.18	36.97
F	14.4	1.09	1.08
Na	56.8	1.60	1.31
Si	1900.0	27.04	18.14
S	487.2	7.93	4.66
V	541.7	8.92	3.30
		100.00	100.00

Figure 3-32.EDX spectrum of nano binary oxide SiO_2/V_2O_5 at calcination temperatures. a.300 ^{0}C b.400 ^{0}C and C.500 ˚C.d.600 ˚C and e.700 ˚C.

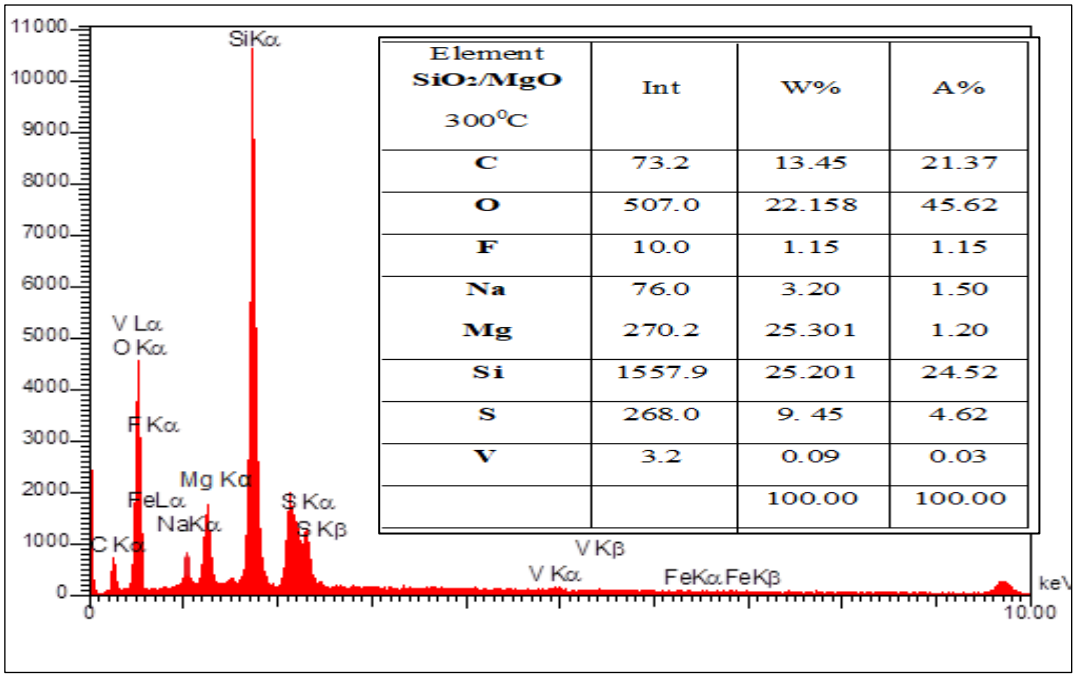

Element SiO_2/MgO 300^{0}C	Int	W%	A%
C	73.2	13.45	21.37
O	507.0	22.158	45.62
F	10.0	1.15	1.15
Na	76.0	3.20	1.50
Mg	270.2	25.301	1.20
Si	1557.9	25.201	24.52
S	268.0	9. 45	4.62
V	3.2	0.09	0.03
		100.00	100.00

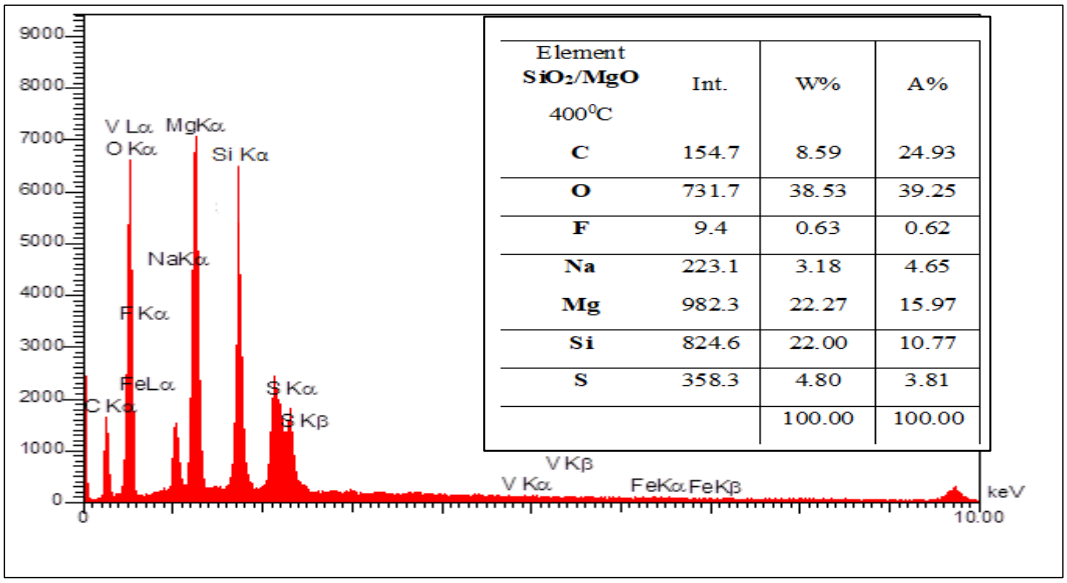

Element SiO_2/MgO 400^{0}C	Int.	W%	A%
C	154.7	8.59	24.93
O	731.7	38.53	39.25
F	9.4	0.63	0.62
Na	223.1	3.18	4.65
Mg	982.3	22.27	15.97
Si	824.6	22.00	10.77
S	358.3	4.80	3.81
		100.00	100.00

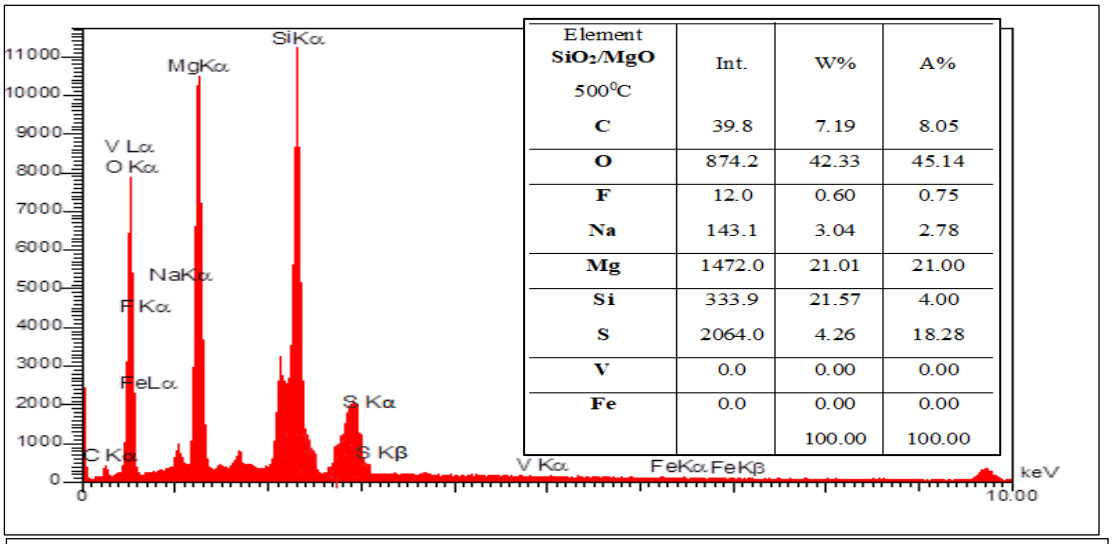

Element SiO_2/MgO 500°C	Int.	W%	A%
C	39.8	7.19	8.05
O	874.2	42.33	45.14
F	12.0	0.60	0.75
Na	143.1	3.04	2.78
Mg	1472.0	21.01	21.00
Si	333.9	21.57	4.00
S	2064.0	4.26	18.28
V	0.0	0.00	0.00
Fe	0.0	0.00	0.00
		100.00	100.00

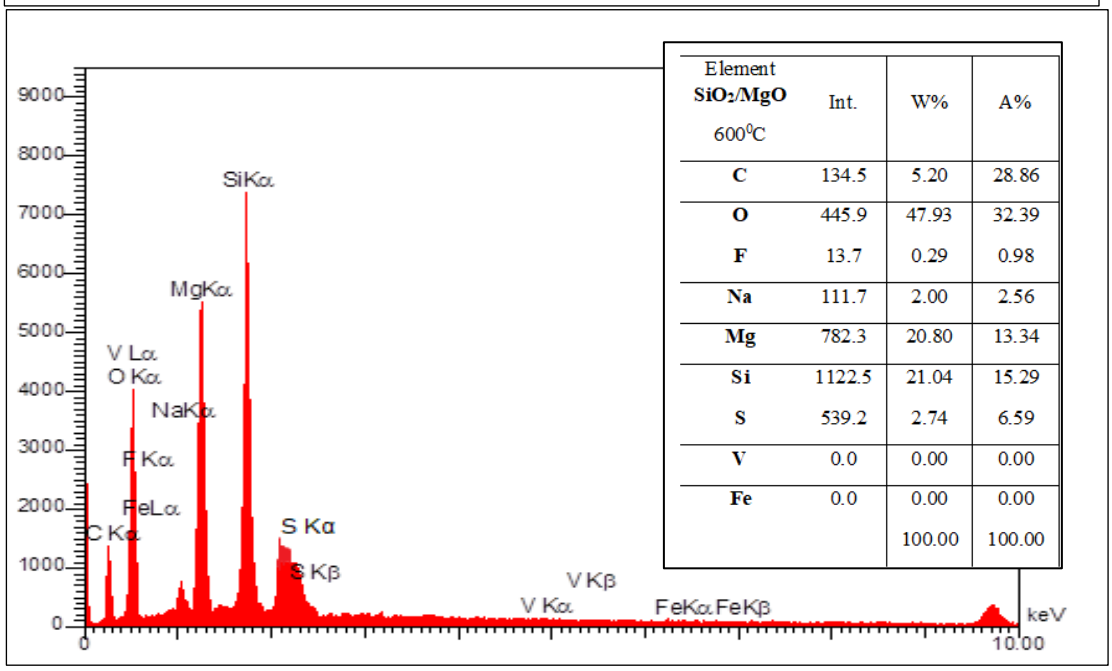

Element SiO_2/MgO 600°C	Int.	W%	A%
C	134.5	5.20	28.86
O	445.9	47.93	32.39
F	13.7	0.29	0.98
Na	111.7	2.00	2.56
Mg	782.3	20.80	13.34
Si	1122.5	21.04	15.29
S	539.2	2.74	6.59
V	0.0	0.00	0.00
Fe	0.0	0.00	0.00
		100.00	100.00

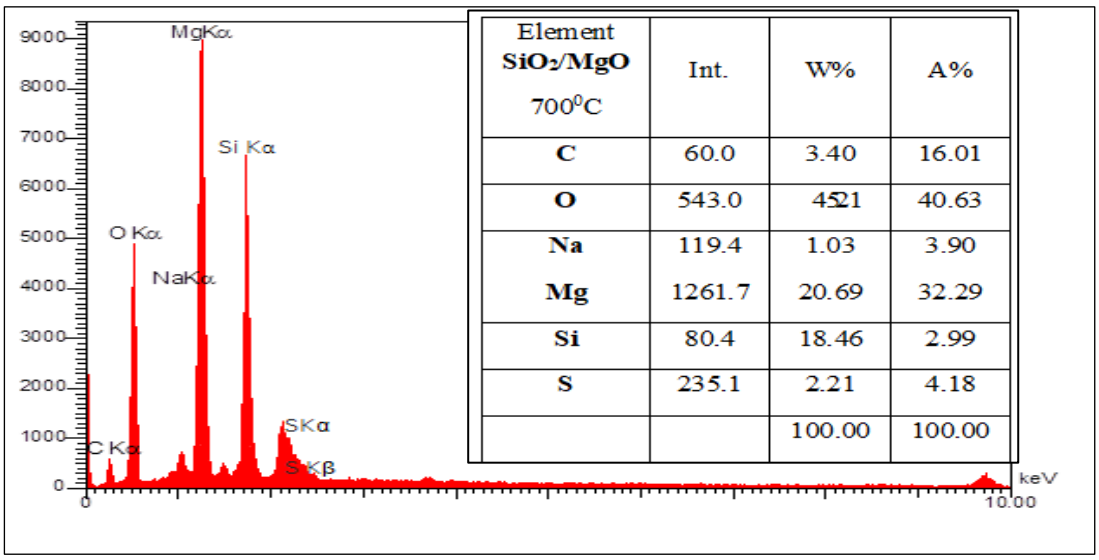

Element SiO_2/MgO 700°C	Int.	W%	A%
C	60.0	3.40	16.01
O	543.0	45.21	40.63
Na	119.4	1.03	3.90
Mg	1261.7	20.69	32.29
Si	80.4	18.46	2.99
S	235.1	2.21	4.18
		100.00	100.00

Figure 3-33.EDX spectrum of nano binary oxide MgO /SiO_2. at calcination temperatures . a.300 ˚C b.400 ˚C and ˚C.500˚C.d.600 ˚C and e.700 ˚C.

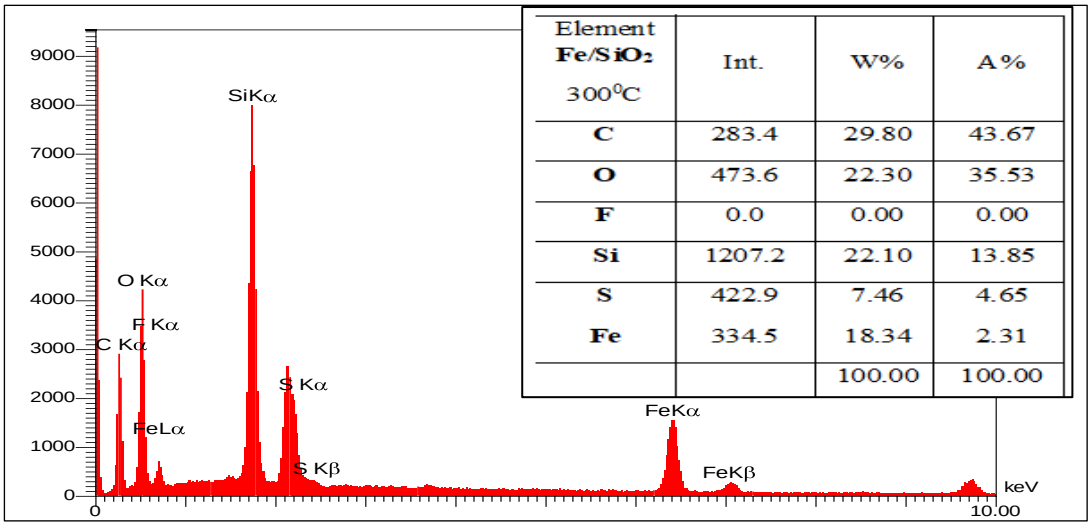

Element Fe/SiO_2 300°C	Int.	W%	A%
C	283.4	29.80	43.67
O	473.6	22.30	35.53
F	0.0	0.00	0.00
Si	1207.2	22.10	13.85
S	422.9	7.46	4.65
Fe	334.5	18.34	2.31
		100.00	100.00

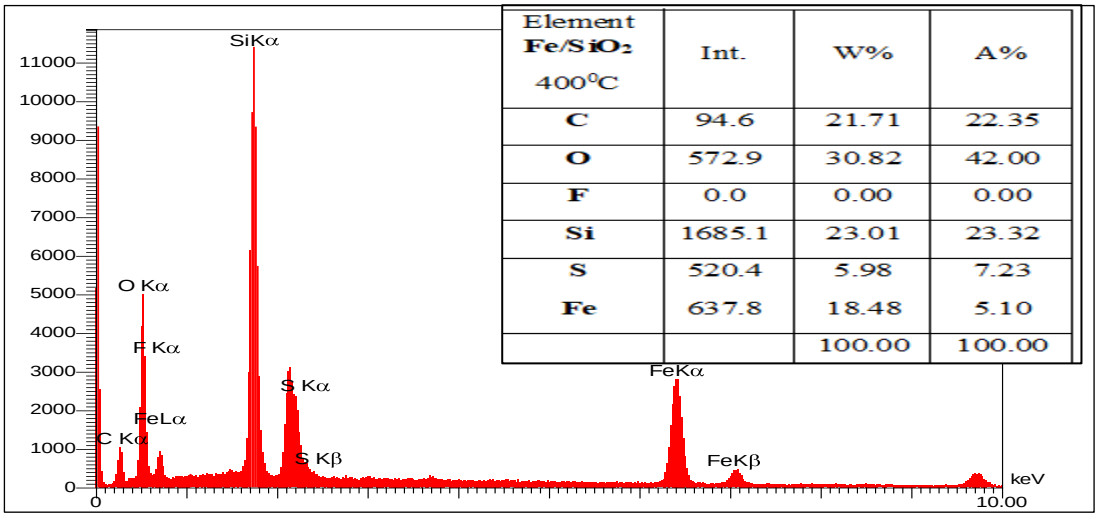

Element Fe/SiO_2 400°C	Int.	W%	A%
C	94.6	21.71	22.35
O	572.9	30.82	42.00
F	0.0	0.00	0.00
Si	1685.1	23.01	23.32
S	520.4	5.98	7.23
Fe	637.8	18.48	5.10
		100.00	100.00

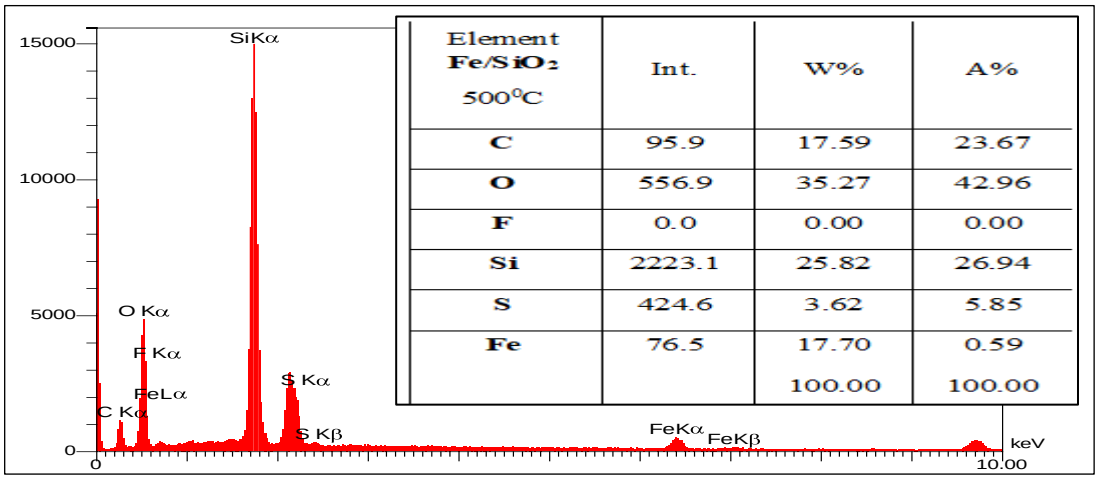

Element Fe/SiO_2 500°C	Int.	W%	A%
C	95.9	17.59	23.67
O	556.9	35.27	42.96
F	0.0	0.00	0.00
Si	2223.1	25.82	26.94
S	424.6	3.62	5.85
Fe	76.5	17.70	0.59
		100.00	100.00

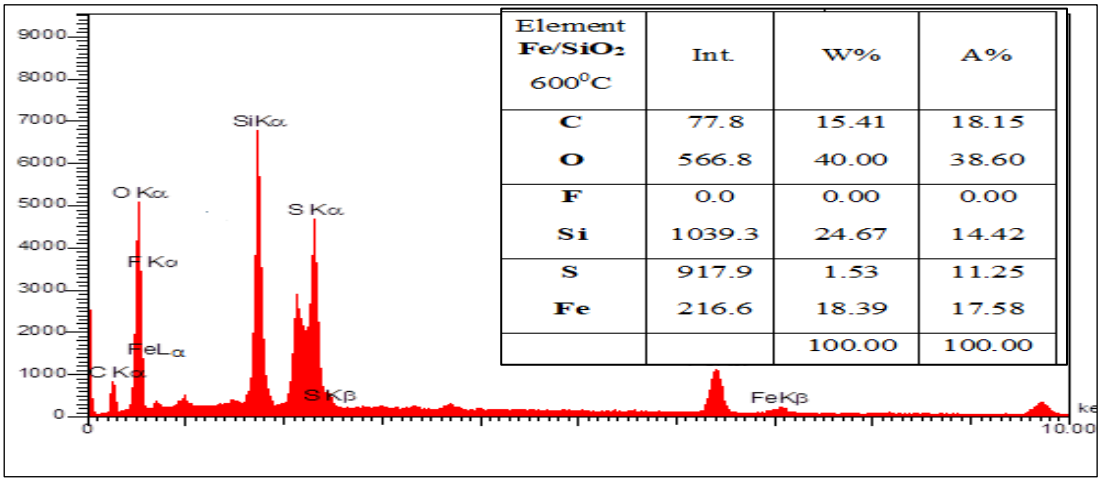

Element Fe/SiO_2 600°C	Int.	W%	A%
C	77.8	15.41	18.15
O	566.8	40.00	38.60
F	0.0	0.00	0.00
Si	1039.3	24.67	14.42
S	917.9	1.53	11.25
Fe	216.6	18.39	17.58
		100.00	100.00

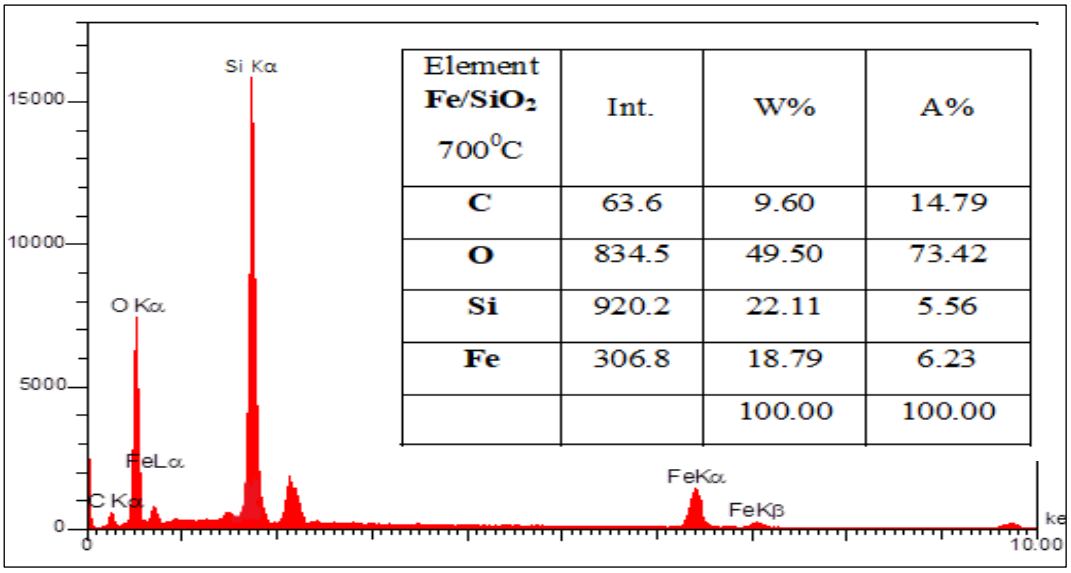

Element Fe/SiO_2 700°C	Int.	W%	A%
C	63.6	9.60	14.79
O	834.5	49.50	73.42
Si	920.2	22.11	5.56
Fe	306.8	18.79	6.23
		100.00	100.00

Figure 3-34.EDX spectrum of magnetic nano binary oxide Fe_xO_y /SiO_2. at calcination temperatures . a.300 ˚C b.400 ˚C and c.500 ˚C .d.600 ˚C and e.700 ˚C .

3-5. Fourier Transform Infrared spectra (FTIR)

FT-IR spectra of silica oxide and nano binary oxide (SiO_2/ V_2O_5, Fe_xO_y /SiO_2 and SiO_2/MgO) nanoparticles were measured in the range of 4000–400 cm. $^{-1}$

3-5.1Fourier Transform Infrared spectra: silica oxide

FT-IR spectra of nano-silica powder are represented in figure (3-35a.). Since appearing absorbance band at wavelength 1072.46 cm^{-1} due to asymmetric vibration Si-O-Si (siloxane group), symmetric vibration at 883.43 cm^{-1} by bond Si-O-Si and 484.14cm^{-1} attributed to the bending vibration of Si-O at 300˚C. FT-IR measurements are used to determine the chemical functionality of silica nanoparticles with difference calcination temperatures, FT-IR spectra are presented in figures(3-35 a,b.c,d,and e), exhibits bending vibration of Si-O bond for silica (464.86, 484.15,461.00, 430.14,and 476.34) cm^{-1} at 300˚C,400 ˚C, 500˚C, 600˚C,and 700 ˚C respectively. The absorption bands at 1072, 808.20 cm^{-1}, asymmetric stretching of Si–O–Si, and symmetric stretching of Si–O–Si, respectively as shown in figure(3-35b) at 400˚C [213,214].

Bending vibrations of Si–O–Si at 484.15 cm^{-1}. Figure(3-35.c) at 500 ˚C, noted asymmetric stretching of Si–O–Si and symmetric stretching of Si–O–Si shifted to the wavelength at 1091.75,806.22 cm^{-1}- respectively at a burning temperature of 500 ˚C. But in figure (3-35.d) at 600˚C asymmetric stretching of Si–O–Si for mesoporous silica doesn't occur shift at a burning temperature of 600˚C [215].

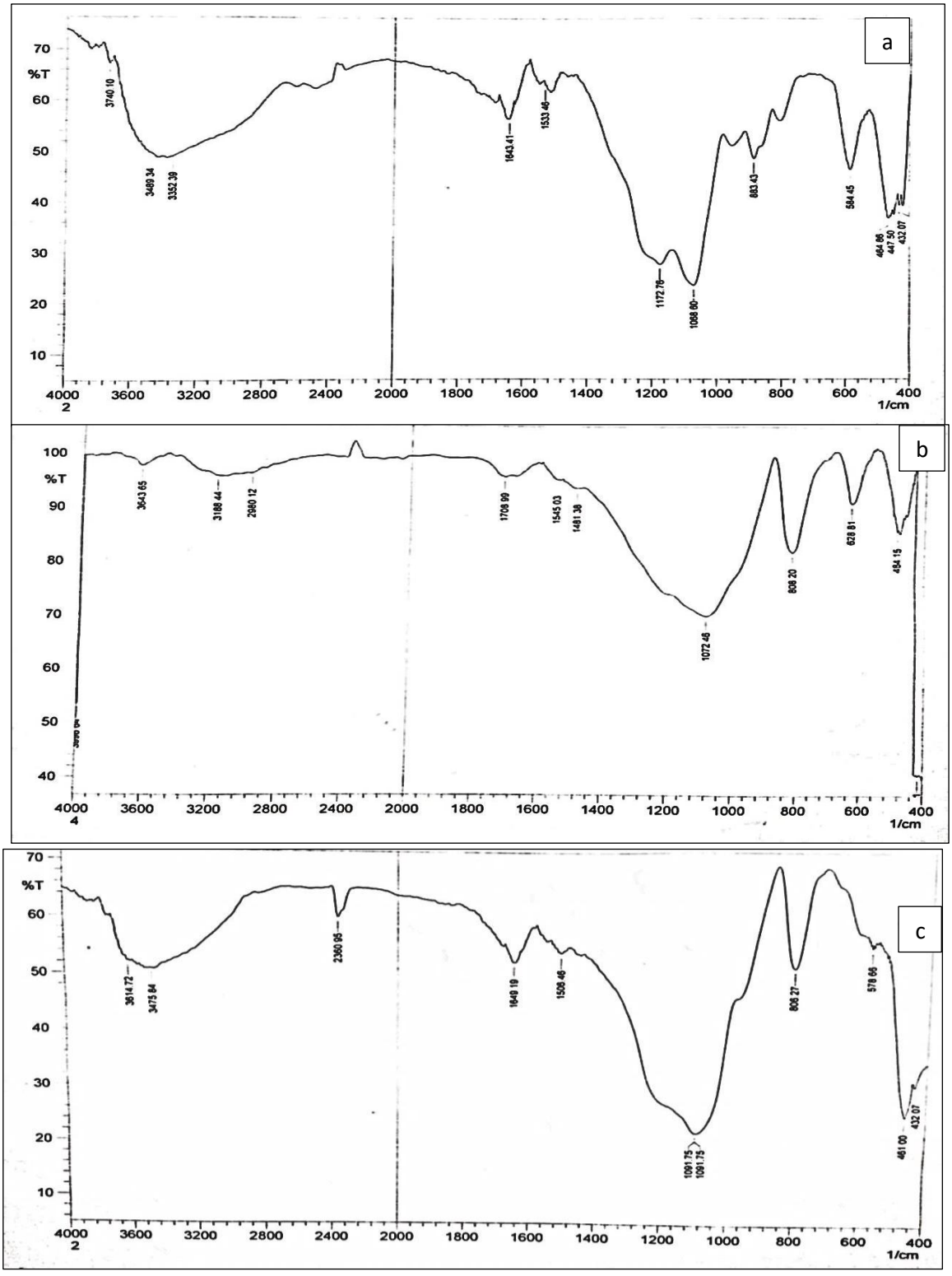

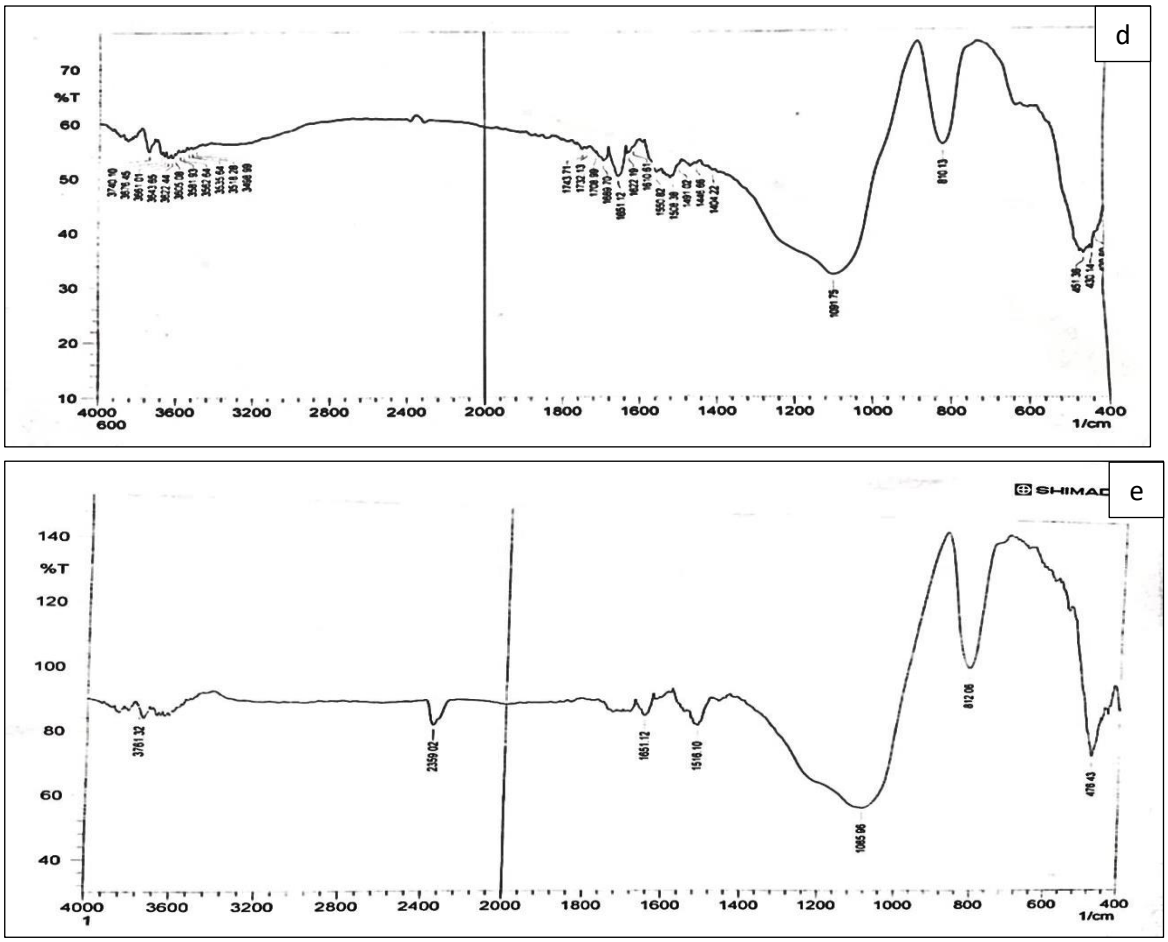

Figure 3-35.FT-IR of nano silica oxide at a. 300˚C,b.400 ˚C,c.500 ˚C, d.600˚C, and e.700˚C.

3-5-2. Fourier Transform Infrared spectra (FTIR): SiO_2/V_2O_5

FTIR spectra analysis of pure vanadium oxide V_2O_5 involves in region 400 – 4000 cm^{-1} (216). Figure (3-36. a) shows pure vanadium oxide the absorbance bands at 1012.66 cm^{-1}corresponding bending vibrations of indicating to V=O, the absorbance band at 817.85 cm^{-1} assigned to V-O-V symmetric bond and asymmetric of V-O bond vibration at absorbance bands range 600 to 400 cm^{-1}. The peaks at 922.00, 844.85 and 484.15 cm^{-1} represent Si-O-V and Si-O-Si bending vibrations [216,217]. FT-IR spectrum of pure vanadium oxide V_2O_5 and **SiO_2/V_2O_5** Nanoparticles can be detected in the presence of typical bands of this oxide V=O 1012.66 cm^{-1}. Symmetric bond V−O−V at 542.02 cm^{-1}, in the spectrum of nano binary oxide SiO_2/V_2O_5 nanoparticles. Absorbance bands at 1091-900 cm^{-1} are indicated on the

presented Si–O–Si vibration bond as shown in figure (3-36b) [218]. This indicated on formation interaction between the surface negative charge of silica oxide and the surface of vanadium oxide, such as shown in the EDX technique that appears the content elements in samples.

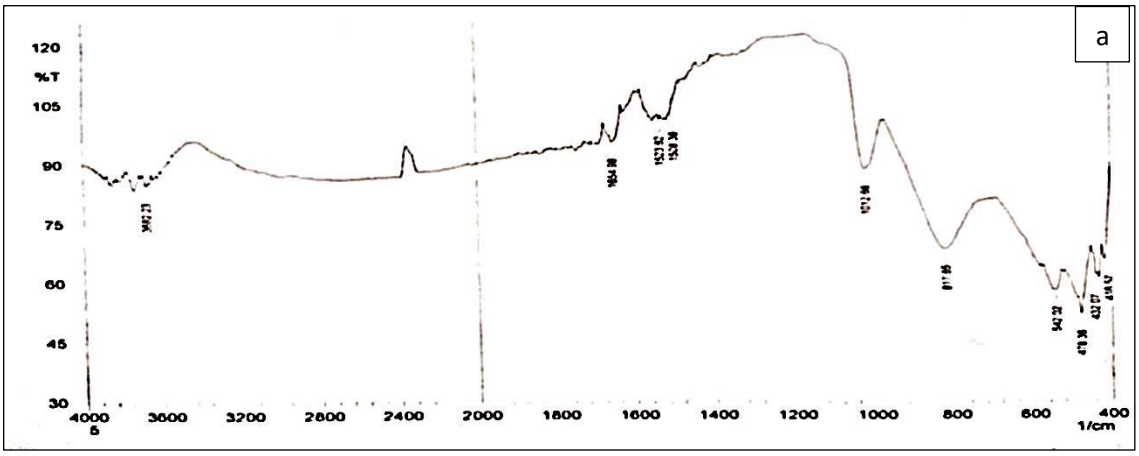

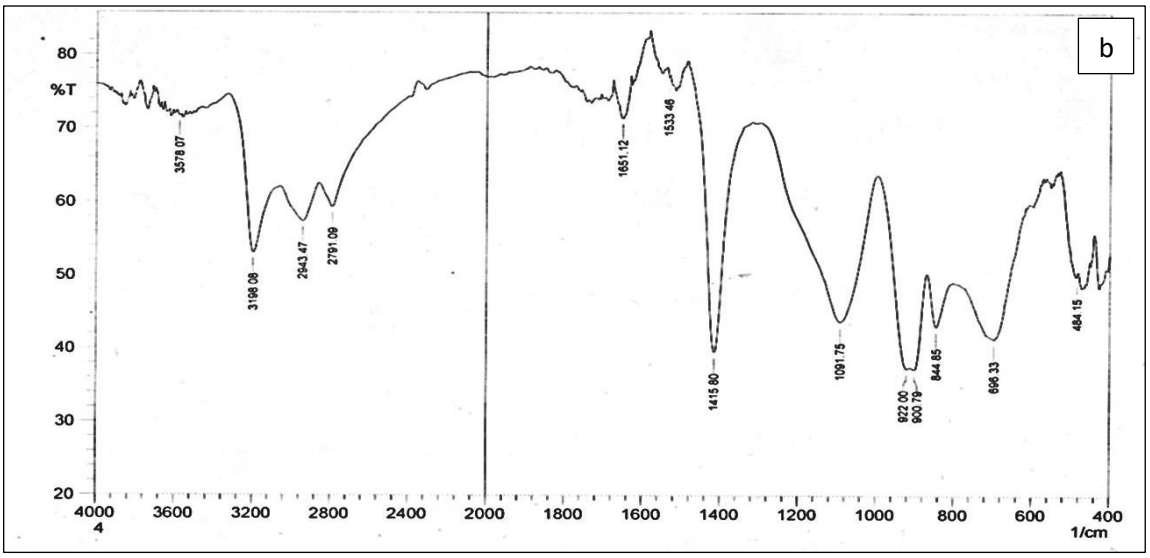

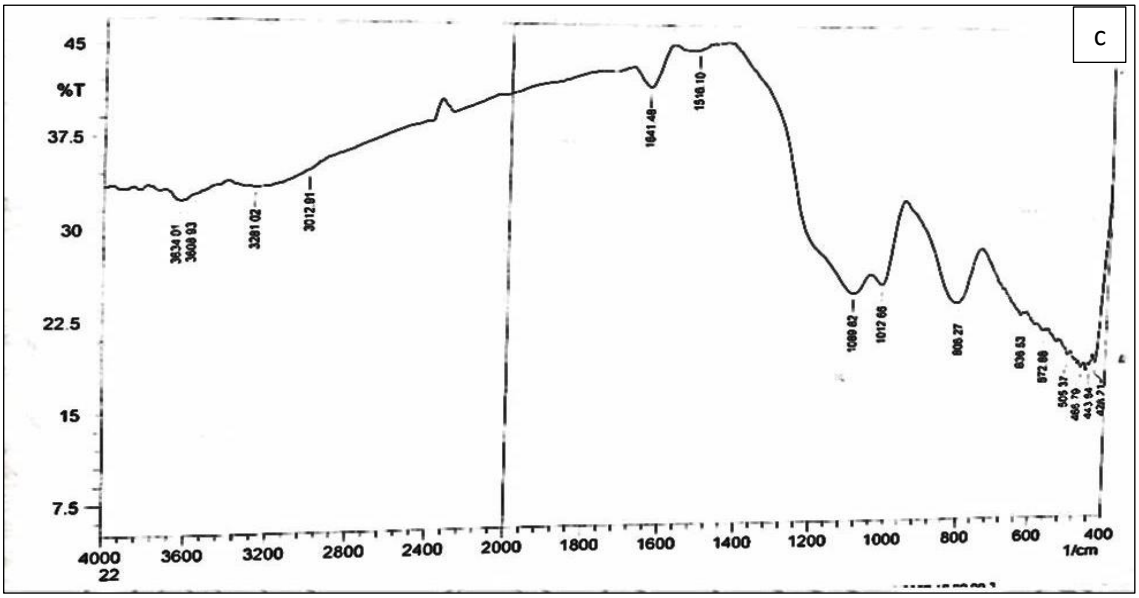

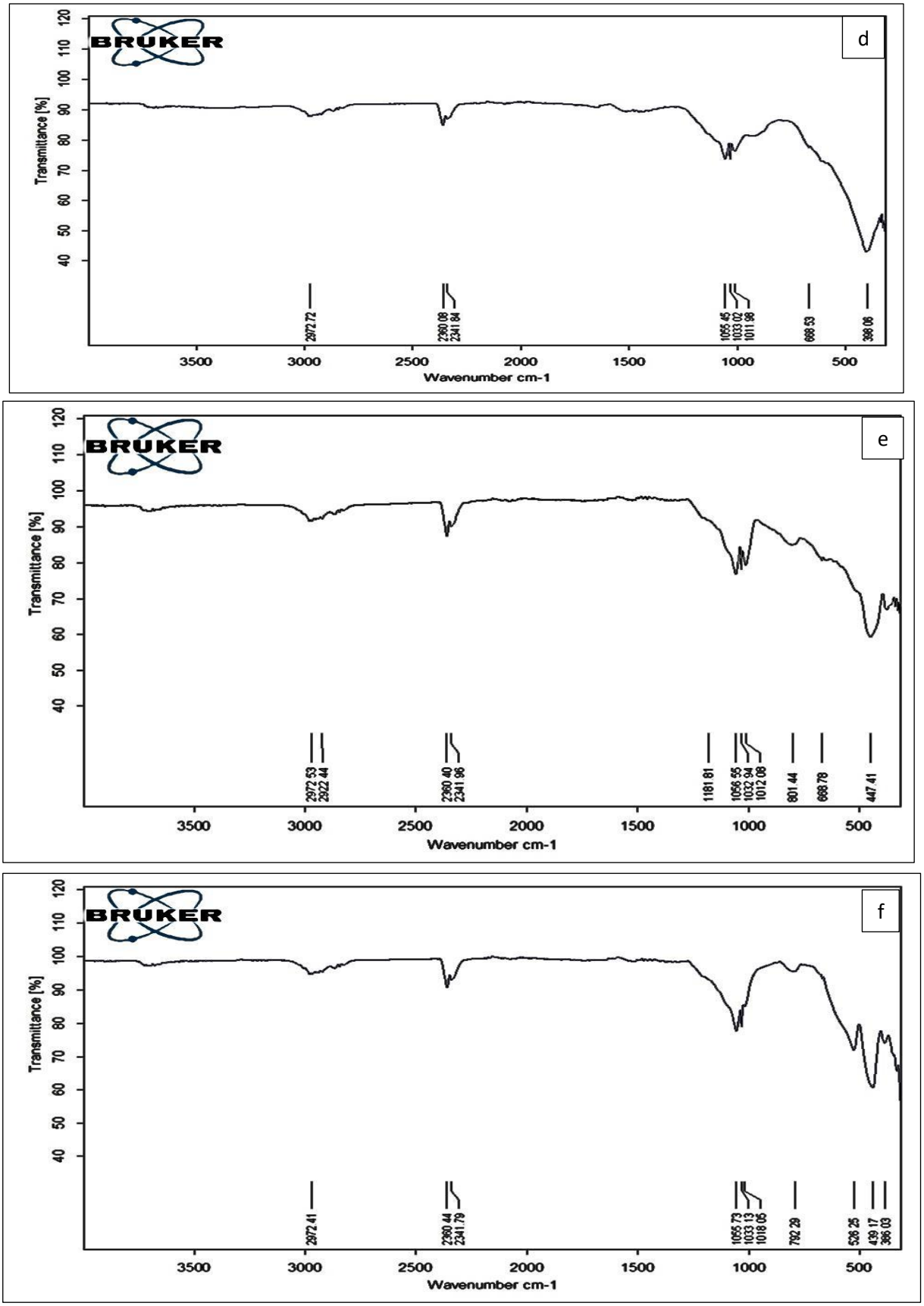

Figure3-36.FT-IR of a. pure vanadium oxide V_2O_5 at a.300^{0}C,b. nano binary oxide SiO_2/V_2O_5 at 300˚ C, c.at 400˚C,d.500˚C,e. 600˚C and f.700˚C.

3-5-3. Fourier Transform Infrared spectra (FTIR): MgO/SiO_2

The FT-IR technique is used to determine the composition of the individual samples. The transmission spectra are analyzed to collect information on the structural properties of the nano binary oxide magnesia-silica samples and to characterize silica oxide interaction with magnesium oxide. Figure (3-37a) illustrates the FT-IR spectrum of pure magnesium oxide particles on the spectrum. There are peaks at 3502 cm^{-1} corresponding to the O–H stretching mode of hydroxyl groups indicted on the moisture surface. The band at 1636 cm^{-1} could be attributed to the bending vibrations of water molecules [219]. Vibrating in the bending mode 426 cm^{-1}were the primary peaks confirming Mg-O vibrations [220,221], figure (3-37a) spectrum of pure MgO does not have an absorbance band at 800 cm^{-1}. FT-IR spectrum of nano binary oxide MgO/SiO_2 noted appearance absorbance peaks at 800 cm^{-1} represented symmetric stretching of Si–O– Si [218].

Three separate strong absorption bands at 1072.46 cm^{-1} relate to the asymmetric Si-O-Si stretching mode, symmetric Si-O-Si bond vibration at 808.20 cm^{-1}, 484.14 cm^{-1} ascribed to the Si-O bending vibration such as shown above. 696 cm^{-1} attributed to the Mg-O stretching vibration. Notable is the absorption band at 468 cm^{-1}, which is characteristic of the Si-O-Mg stretching vibration [222].

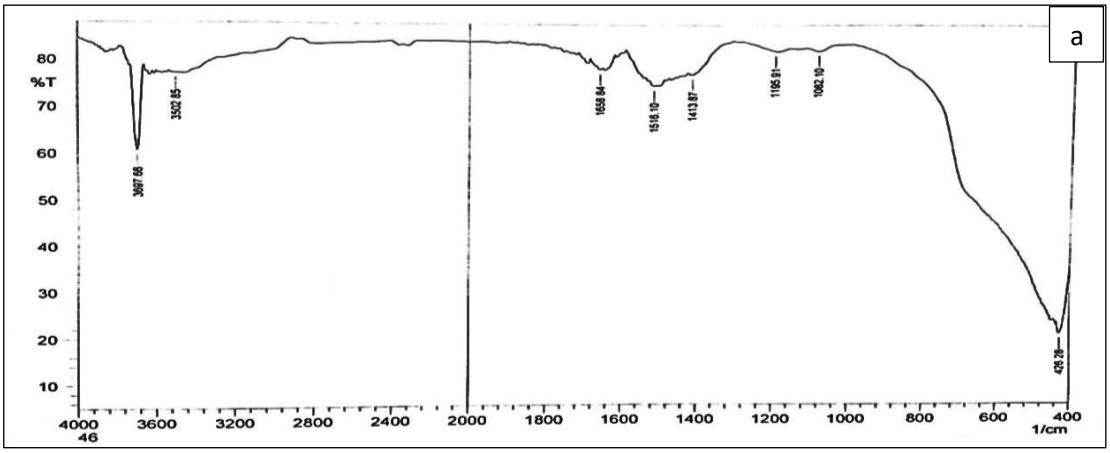
a
%T
1/cm

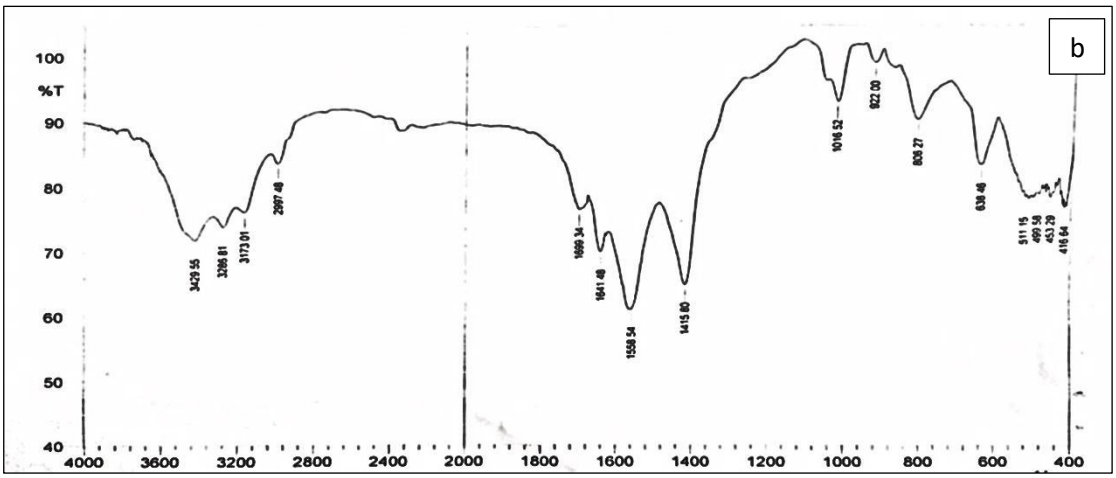
b
%T

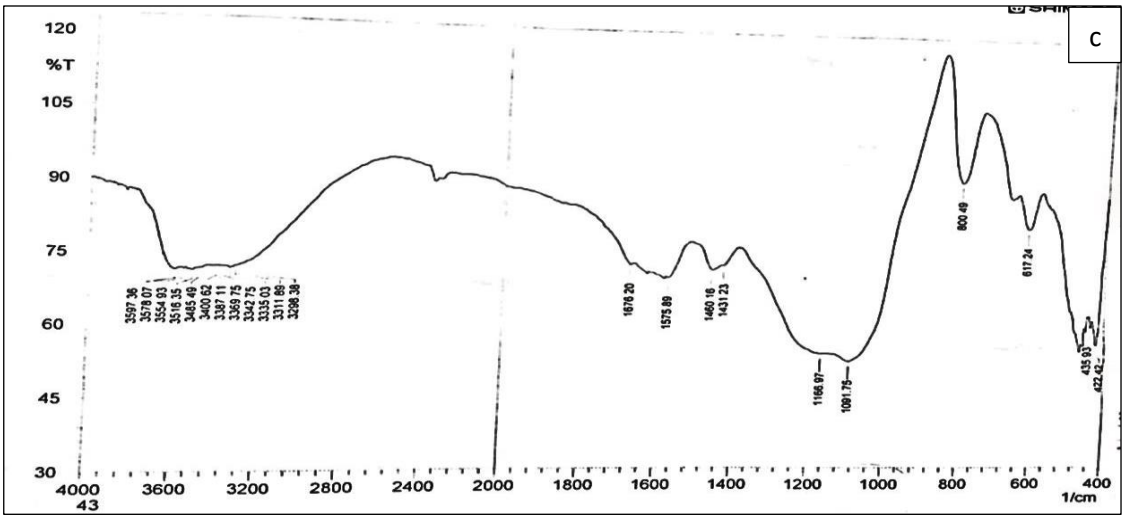
c
%T
1/cm

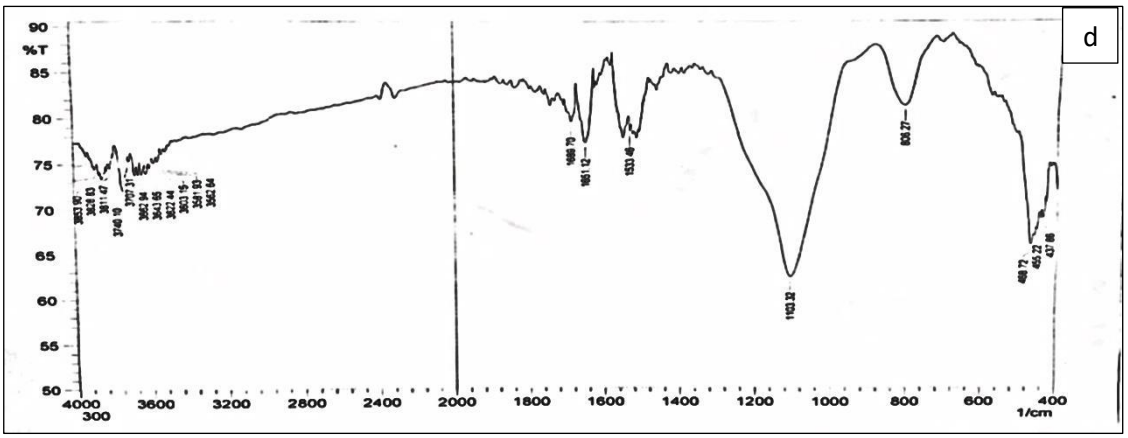
d
%T
1/cm

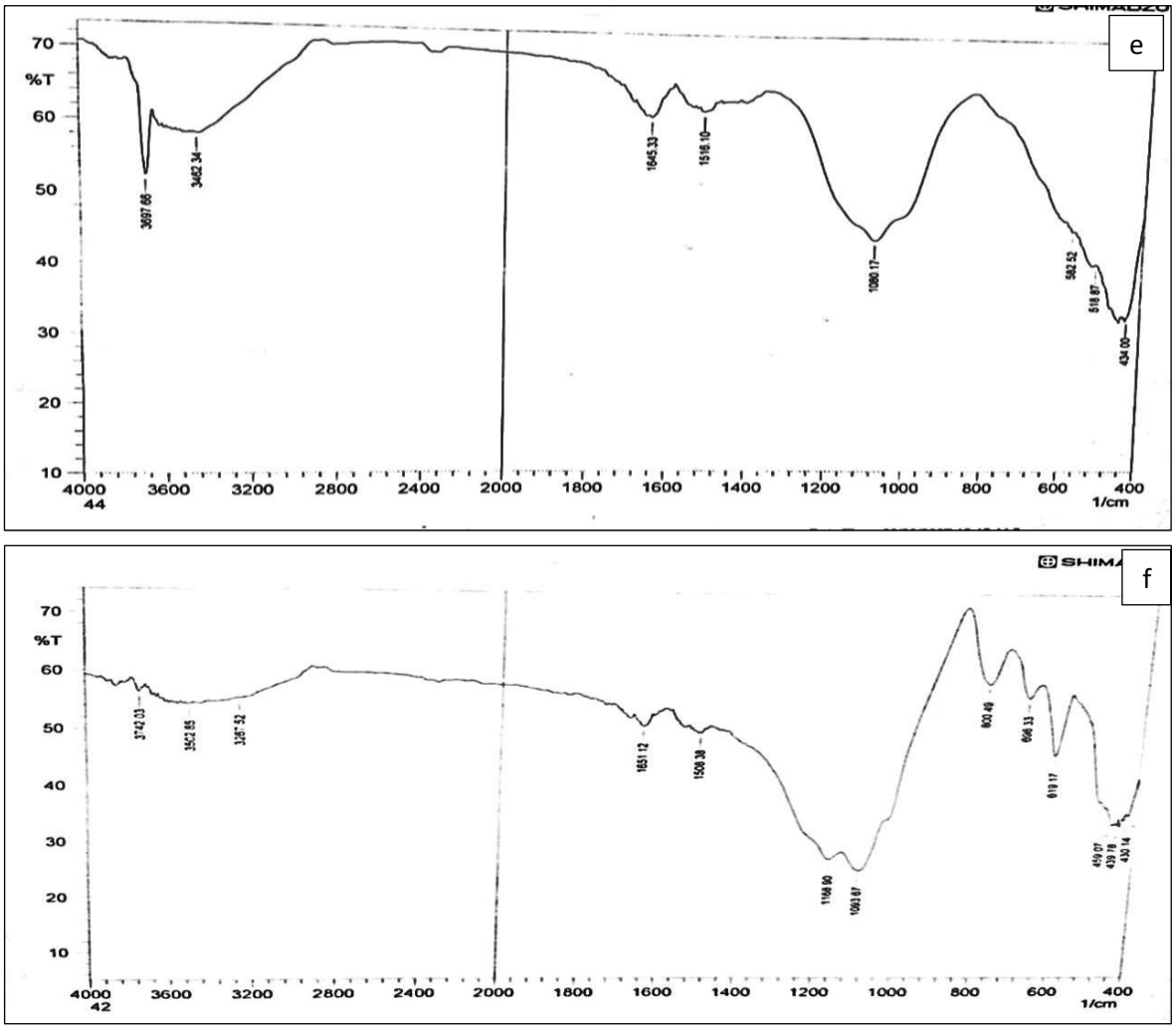

Figure 3-37. FT-IR of a. pure magnesium oxide MgO at 300˚C, b. of nano binary oxide MgO/SiO_2 at (E4-MG-50),c. (D4-MG-50),d. (C4-MG-50) ,e. (B4-MG-50), and f. (A4-MG-50).

3-5-4. Fourier Transform Infrared spectra (FTIR): Fe_xO_y/SiO_2

Figure (3-38) illustrates the infrared spectra of magnetic binary oxides **Fe_xO_y/SiO_2**. Absorption peaks are found at (800 and 1099) cm^{-1} at 300^0C, (808 and 1103) cm^{-1} at 400 ˚C (813 and 1097) cm^{-1} at 500^0C,(802 and 1101) cm^{-1} at 600˚C,(808 and 1089) cm^{-1} at 700˚Care indicted to present absorption peak to symmetric and asymmetric stretching modes of Si-O-Si, structures in silica oxide such as shown in figure (3-35.a) at 300°C. Absorption bands are visible indifference calcination samples close to 553,540,586,555, and 623 cm^{-1}, which is ascribed to the distinctive Fe-O at calcination temperatures (300,400,500,600, and 700)˚C respectively [223]. The bands near 1396 cm^{-1} are caused by organic impurities and are attributed to C- H bending, resulting from the presence of tetraethyl orthosilicate. Results of FT-IR show interaction between iron oxides and silica.

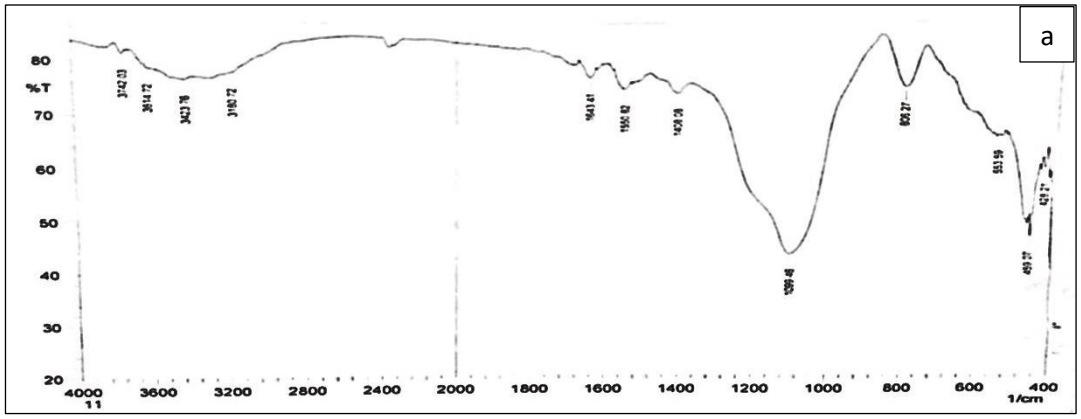

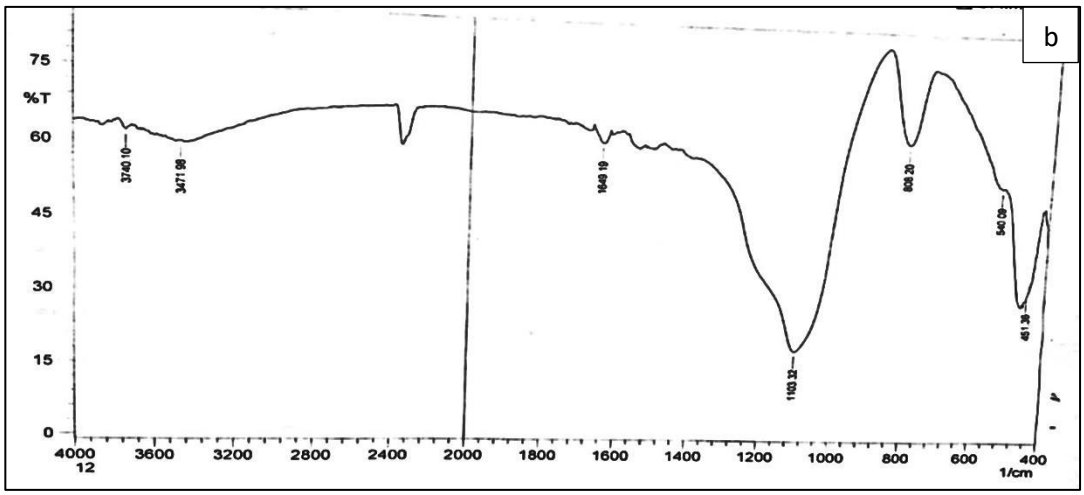

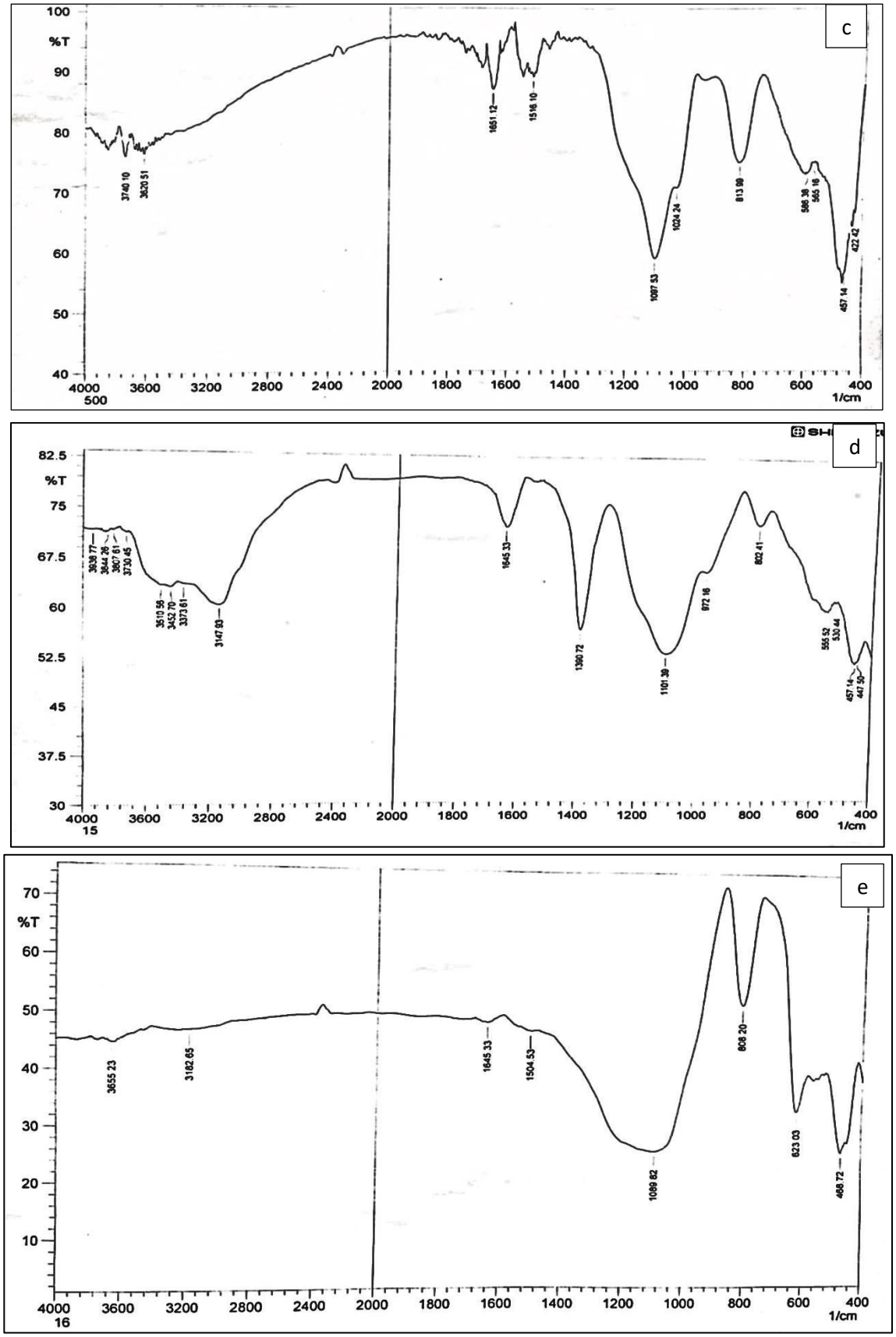

Figure 3-38. FT-IR of nano binary oxide Fe_xO_y/SiO_2 a. at 300 ˚C, b.at 400˚C, c.at 500˚C d. at 600 ˚C, and e.at 700˚C.

4-1. Antibiotic activity of nano Silica oxide

The microbial activity of silica nanoparticles depends on particle size, the physicochemical properties of silica nanoparticles, such as their size, shape, and porosity, are crucial for payload delivery to the target site [224]. Silica nanoparticles (SiNPs) that extraction from RHA has a size range (35-46) nm as shown in table 3-5 at different calcination temperatures. SiNPs are non-toxic materials [225]. SiNPs have been demonstrated to be a viable option for a variety of medicinal applications, particularly cancer and antibacterial therapies [226]. Given the growing threat of antimicrobial resistance, the adaptability of SiNPs is particularly helpful for antimicrobial therapies, including biofilm treatment. Because these nanoparticles can attack pathogens via a variety of mechanisms, including physical damage to cell membranes. ROS production, in addition to the antimicrobial activity induced by the cargo, the window for the development of antimicrobial resistance is quite narrow. So this present work focused on the study activity of nano-silica oxide against some microbial wounded such as *Escherichia Coli*, *S.aureas* and *Pseudomonas* . The result shows excellent antibiotic activity agents *Escherichia Coli* and *S.aureas*, but has resistance against *Pseudomonas*. The inhibition percentage study at a different range of calcination temperatures. The inhibition percentage of SiNPs sample at calcination temperature 500˚C, for *E.Coli*, *S.aureas*, and *Pseudomonas* was (77.646, 68.630, and 65.545)% at concentration 625 µg/ml respectively such as shown in tables (4-1,4-2, and 4-3). The antibiotic activity is best when sample calcination temperatures are at 500˚C, due to nano-silica oxide having a high surface area at this temperature and a small particle size of 34.525nm. The results of antibiotics at 500 ˚C show MIC(minimum inhibition concentration) is 1250 µg/ml and MBC(minimum bacterial

concentration) was 1500 µg/ml as shown in figure (4-19). All figures (4-1,4-2, and 4-3,) show inhibition growth percentages with a different range of calcination temperature.

Table 4-1. The percentage of inhibition growth of bacterial (*E. Coli*) with different doses of Silica nanoparticles at different calcination temperatures.

Concentration µg/ml	Calcination temperatures /˚C				
	700	600	500	400	300
	Inhibition Growth %				
0	0	0	0	0	0
1500 (4.8 ml)	80.529	96.629	100	94.382	90.912
1250 (4 ml)	75.832	89.827	98.961	88.951	85.591
625 (2 ml)	68.432	74.146	77.646	71.512	71.965
312.5 (1ml)	58.451	65.017	67.966	63.385	61.831
156.2 (0.5 ml)	21.578	28.843	31.837	27.197	23.357
31.25 (100µl)	3.582	11.642	28.933	8.853	5.928

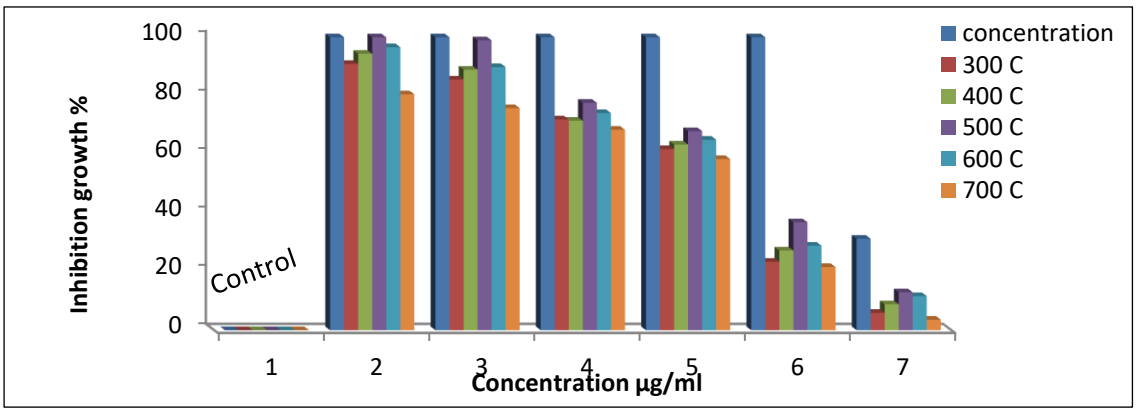

Figure 4-1. Effect of concentration of Silica nanoparticle's on inhibition growth of bacterial (*E. Coli*) with different calcination temperatures.

Table 4-2. The percentage inhibition growth of bacterial (*S.aurease*) with different doses of Silica nanoparticles at different calcination temperatures.

Concentration µg/ml	Calcination temperatures /˚C				
	700	600	500	400	300
	Inhibition Growth %				
0	0	0	0	0	0
1500 (4.8 ml)	77.866	95.841	100	93.871	90.412
1250 (4 ml)	68.931	88.951	98.549	86.863	82.956
625 (2 ml)	50.432	61.831	68.630	65.934	61.321
312.5 (1ml)	42.727	57.981	62.264	50.853	54.351
156.2 (0.5 ml)	16.324	26.643	30.255	22.692	18.932
31.25 (100µl)	2.326	6.552	8.454	4.683	2.663

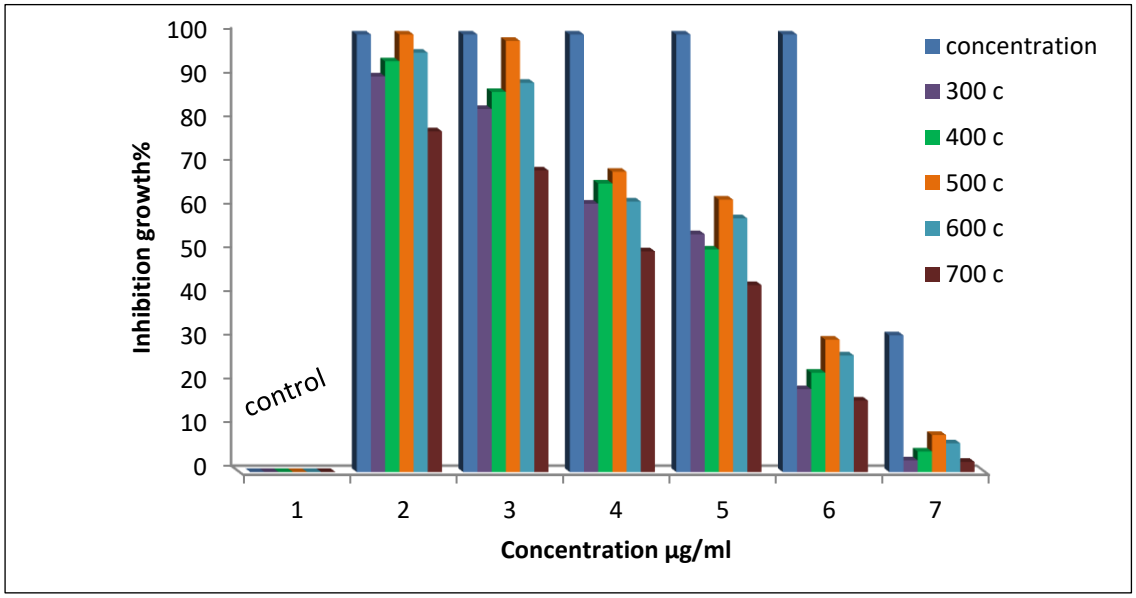

Figure 4-2. Effect of concentration of Silica nanoparticles on inhibition growth of bacterial (*S.aureas*) with different calcination temperatures.

Table 4-3. The percentage inhibition growth of bacteria (*Pseudomonas*) with different doses of Silica nanoparticles at different calcination temperatures.

Concentration µg/ml	Calcination temperatures/°C				
	700	600	500	400	300
	Inhibition Growth%				
0	0	0	0	0	0
1500 (4.8 ml)	75.035	87.003	100	85.011	82.831
1250 (4 ml)	61.924	80.713	98.510	77.844	73.33
625 (2 ml)	55.325	63.823	65.545	59.864	53.972
312.5 (1ml)	47.643	55.312	25.321	23.467	21.931
156.2 (0.5 ml)	10.723	12.649	19.478	21.546	15.619
31.25 (100µl)	1.932	4.513	6.764	2.666	2.038

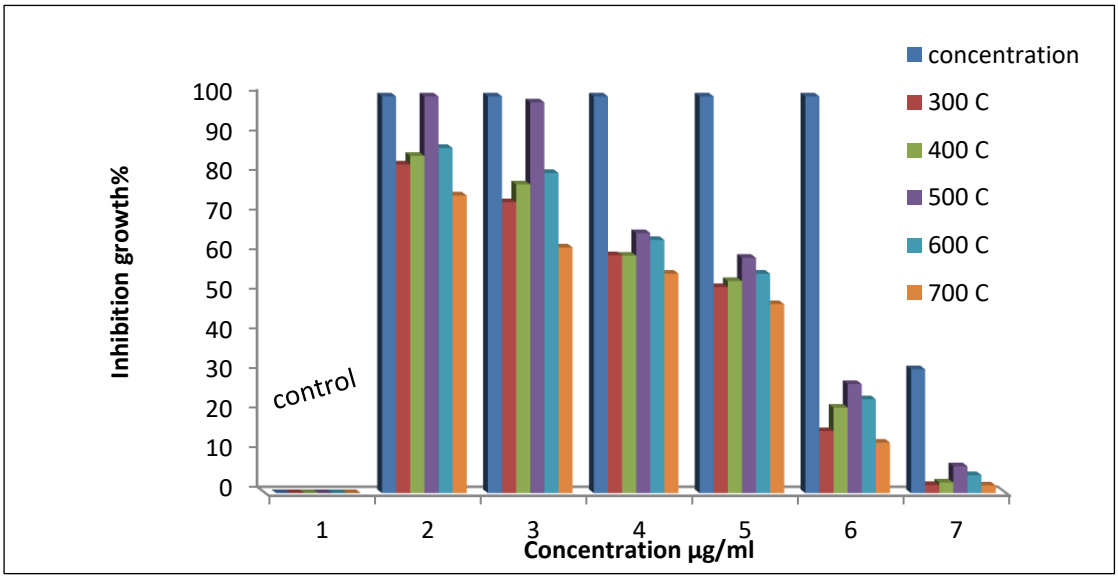

Figure 4-3. Effect of concentration of Silica nanoparticle's on inhibition growth of bacterial (*Pseudomonas*) with different calcination temperatures.

4-2.Antibiotic activity of nano binary oxide SiO_2/V_2O_5

The results show that minimum inhibition concentration (MIC) of nano binary oxide SiO_2/V_2O_5 required to be more than 50% of bacterial growth is determined to be (312.5 µg/ml) and MBC (minimum bacterial concentration) is 625 µg/ml in the case of E. coli such as shown in figure (4-20). Nano binary oxide SiO_2/V_2O_5 exhibited antibiotic activity more than silica oxide at the same concentration agents *E.Coli, S.aureas* and *Pseudomonas* (100, 95, and 80)% respectively, this due to nano binary oxide SiO_2/V_2O_5 having surface area more than nano-silica oxide (195 m^2/g) at calcination temperature 300 ˚C such as shown in table (3-11). Figures (4-4,4-5, and 4-6) shows percentages inhibition for nano binary oxide silica oxide /V_2O_5 against difference microbial (*E.Coli, S.aureas* and *Pseudomonas*)with various doses of antibiotic prepared at different calcination temperatures.

Nano binary oxide SiO_2/V_2O_5 can be disrupted the bacterial cell by releasing Si^{+4}, V^{+5} and O^{-2} ions, that's interact with bacterial membranes. This type of interaction involves generation ROS, and the results shows nano binary oxide exhibited activity agents *E. Coli* higher than *S.aureas* because a thin layer of the peptidoglycan thickness consists primarily of polymers, amino acids, and sugars, forming an outer layer of the plasma membrane (cell wall) that provides stability to the structure responding to the cytoplasm's osmotic pressure. Its thickness ranges 50% more in Gram-positive bacteria and 8% greater in Gram-negative Gram-positive bacteria are composed of numerous layers of peptidoglycan [227].

Table 4-4. The percentage of inhibition growth of bacterial (*E.Coli)* with different doses of nano binary Silica oxide /V_2O_5 nanoparticles at different calcination temperatures.

Concentration µg/ml	Calcination temperature / ˚C				
	700	600	500	400	300
	Inhibition Growth%				
0	0	0	0	0	0
625 (2 ml)	80.472	72.332	85.841	88.942	100
312.5 (1ml)	71.827	66.374	78.932	80.652	97.391
156.2 (0.5 ml)	60.941	55.832	76.531	78.872	95.936
31.25 (100µl)	52.637	54.659	70.326	75.542	78.452

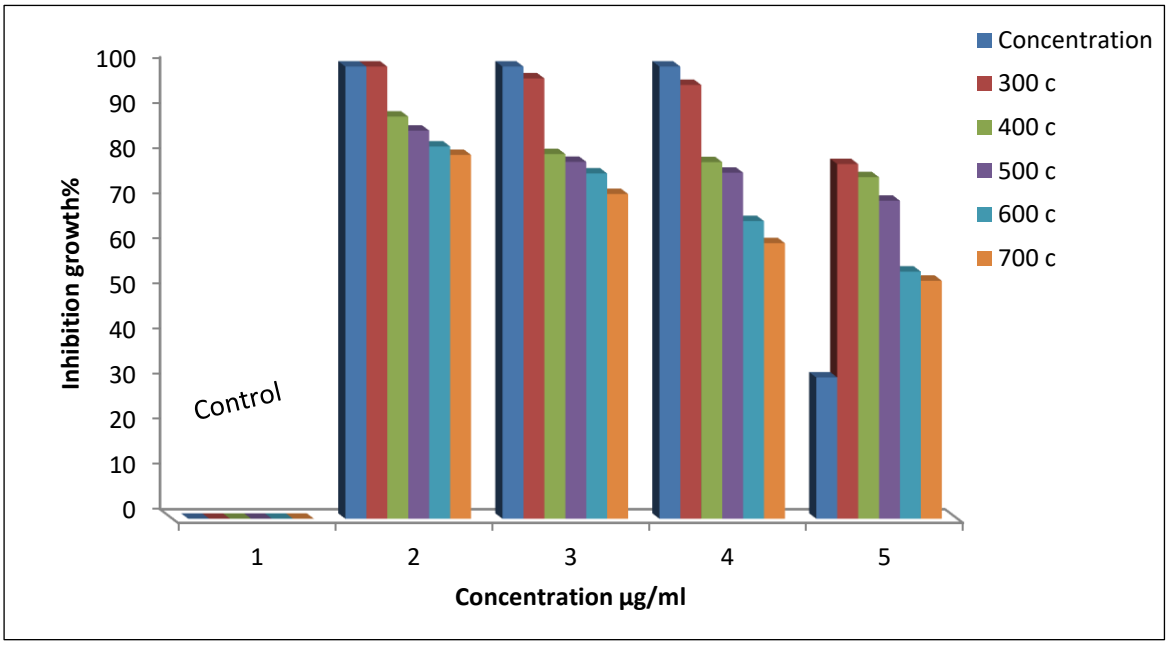

Figure 4-4. Effect of different doses of antibiotic nano binary silica oxide /V_2O_5 on inhibition growth for microbial *E.coli* at different calcination temperatures.

Table 4-5. The percentage of inhibition growth of bacterial (*S.aureas*) with different doses of nano binary oxide Silica /V_2O_5 nanoparticles at different calcination temperatures.

Concentration µg/ml	Calcination temperature /°C				
	700	600	500	400	300
Inhibition Growth %					
0	0	0	0	0	0
625 (2 ml)	76.375	78.931	79.713	83.763	95.263
312.5 (1ml)	68.684	73.981	75.981	77.391	91.463
156.2 (0.5 ml)	57.837	64.542	66.632	73.835	83.431
31.25 (100µl)	45.781	48.312	57.833	71.555	76.933

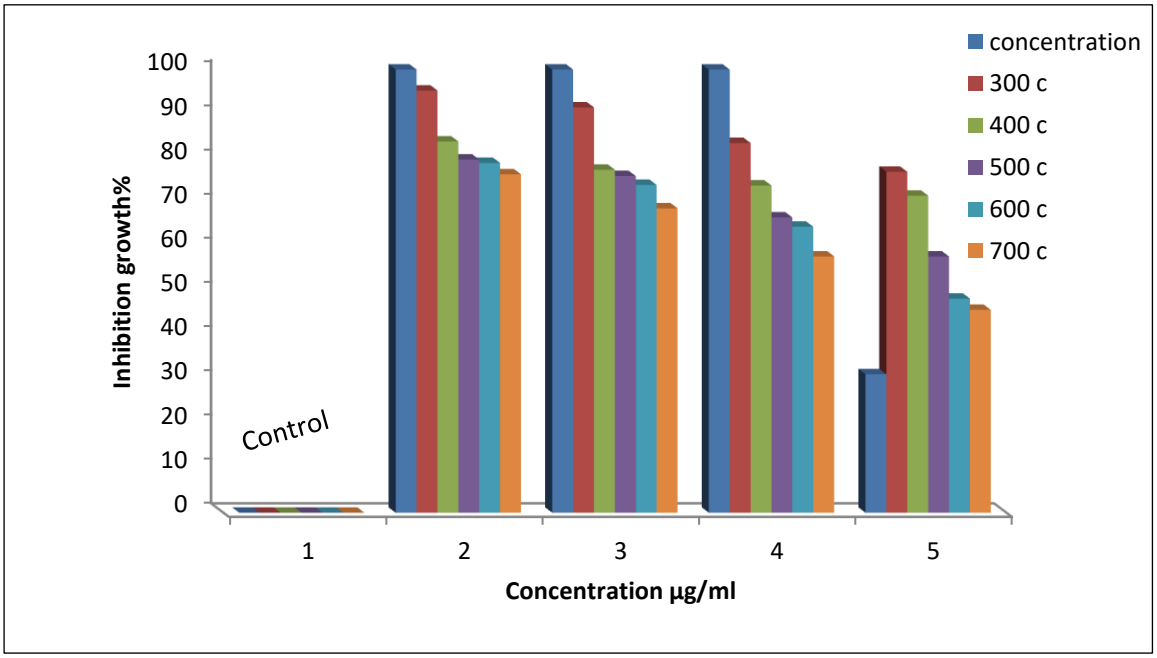

Figure 4-5. Effect of different doses of antibiotic nano binary Silica oxide /V_2O_5 nanoparticles on growth inhibition for microbial *S.aureas* at different calcination temperatures.

Table 4-6. The percentage of inhibition growth of bacteria (*Pseudomonas*) with different doses of nano binary Silica oxide /V_2O_5 nanoparticles at different calcination temperatures.

Concentration µg/ml	Calcination temperature /˚C				
	700	600	500	400	300
	Inhibition Growth%				
0	0	0	0	0	0
625 (2 ml)	58.953	65.158	68.352	71.461	80.106
312.5 (1ml)	50.463	58.103	64.587	67.621	73.447
156.2 (0.5 ml)	48.945	55.642	61.632	64.097	68.631
31.25 (100µl)	33.655	37.513	45.854	50.358	55.413

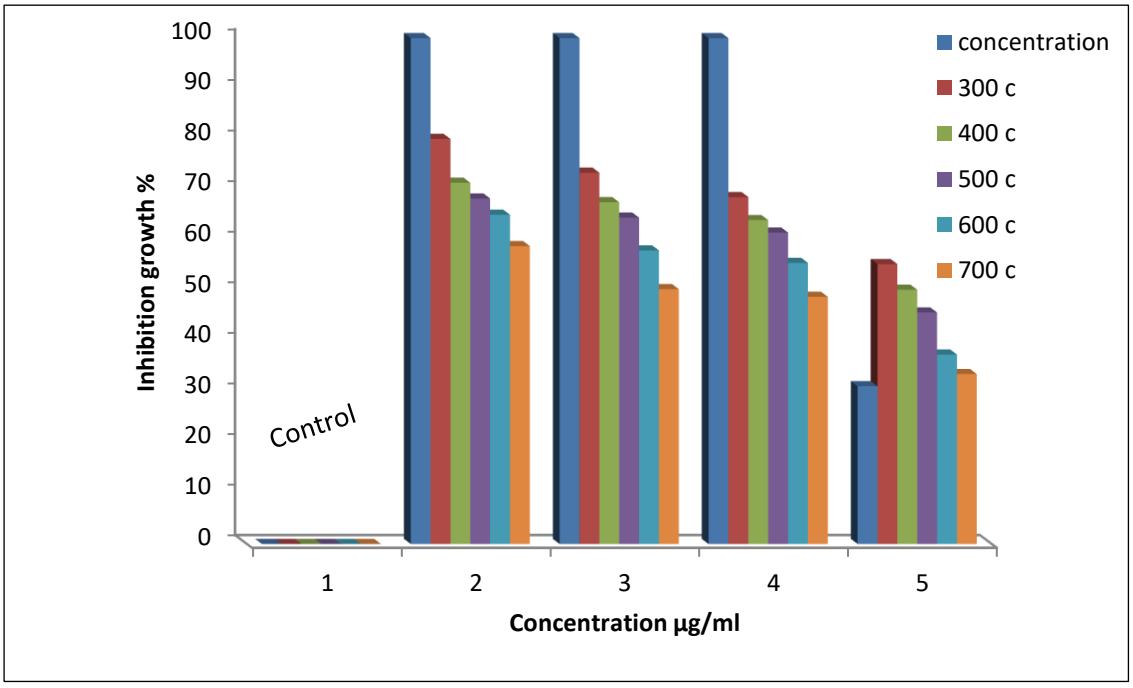

Figure 4-6. Effect of different doses of antibiotic nano binary oxide silica oxide/V_2O_5 nanoparticles on growth inhibition for microbial *Pseudomonas* at different calcination temperatures.

4-3. Antibiotic activity of nano binary oxide MgO/SiO_2 nanoparticles

Numerous analytical techniques have been utilized to determine the antibacterial activity of MgO/SiO_2 nanoparticles, the antibiotic activity of MgO/SiO_2 nanoparticles observe an increase with antibiotic E4-MG-50 more than in other antibiotics (E2-MG-25, E1-MG-75, and E3-MG-90). This is due to antibacterial activity depending on particle size when the particle size of MgO/SiO_2 increased the activity decreased, the results show particle size at antibiotic A4-MG-50 equal to 29.0323 nm larger than another antibiotic such as shown in table (3-12). Previous study , revealed that magnesium oxide nanoparticles with particle size (45-70) nm are effective against Escherichia coli and *S.aureus* [228]. Also, the results show the antibiotic activity of E2-MG-25 against Escherichia Coli more than A2-MG-25 as shown in table (4-7). This is due to the effect of calcination temperature on partials size that increased with increased calcination temperature, therefore, noted antibiotic activity decrease, this due smaller-sized particles can effectively interact with bacterial membranes due to their large surface area, thus enhancing their antibacterial efficiency and vice versa.

The results demonstrated a distinct size effect, with the number of bacteria destroyed being highly dependent on particle size. Previous study examined the effect of the size of magnesium oxide nanoparticles on their antibacterial activity, and they are founded MgO NPs has antibiotic activity with MIC 1000 µg/ml and 500 µg/ml agents pseudomonas and E.Coli reversely [229]. The results of our study indicated that nano binary oxide MgO/SiO_2 nanoparticles (E4-MG-50) with a smaller size exhibited superior antibacterial activity against both gram-positive (*S. aureus*) and

gram-negative (*E. Coli* and *Pseudomonas*) bacteria such as shown in table (4-11) and figure (4-11). Designation of the minimum inhibition concentration (MIC) and minimum bacterial concentration MBC values of E4-MG-50 antibiotics are equal to (156.2) and (312.5) µg/ml respectively as shown in figures (4-21). Also exhibited high antibacterial activity against pseudomonas that show resistance with other nano binary oxide. Additionally, MgO/SiO_2 nanoparticles are more active against gram-negative bacteria than gram-positive bacteria. Gram-positive and Gram-negative bacteria are structurally different, the cell wall of Gram-positive bacteria has thick a peptidoglycan layer bound to teichoic acids that are unique to these bacteria. In contrast, Gram-negative bacteria the cell wall consists of a thin layer of peptidoglycan located in the middle of two membranes, the outer and inner membrane. The outer membrane contains lipopolysaccharides and proteins called porins, where the transport of nutrients and ions that are essential for the structural. These structural differences influence Gram- negative bacteria to be generally more sensitive to NPs than Gram- positive bacteria because they do not have thick a peptidoglycan layer barrier.

In general, the specific surface area of nano binary oxide nanoparticles increases as the size of the nanoparticles decreases. Increased surface area increases the number of reactive groups on the particle surface, which are expected to exhibit significant antibacterial activity. Nano binary oxide MgO/SiO_2 exhibited various antibiotic activity with different ratios of magnesium oxide and silica oxide each ratio has special antibiotic activity with bacterial *E.Coli* as shown in figures and tables (4-7,4-8,4-9,and4-11).

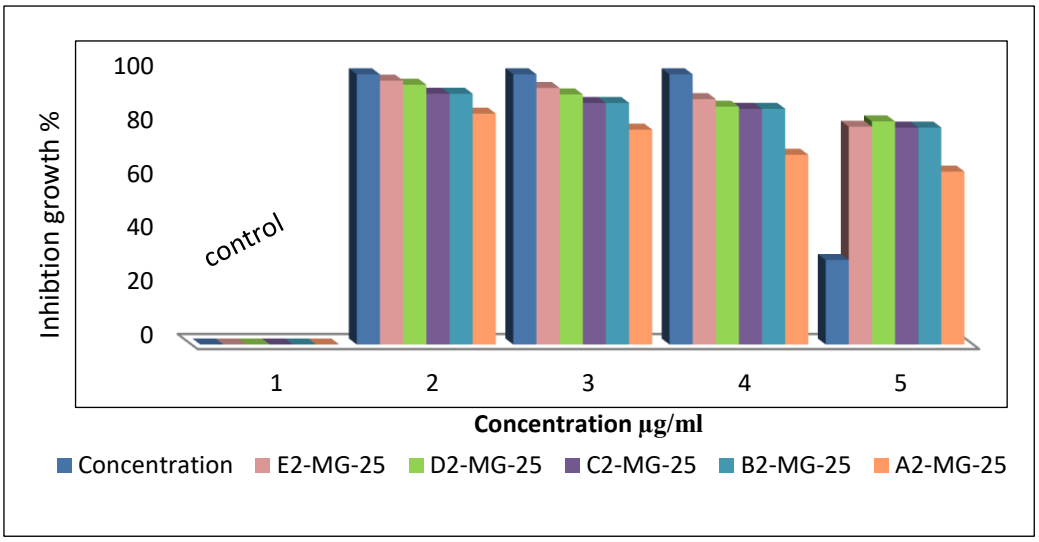

Figure 4-7. Inhibition growth of G-negative (*E.Coli*) at a different dose of antibiotic of MgO/SiO_2 (0.25/0.75) at various calcination temperatures.

Table.4-7. Antibiotic activity for nano binary oxide MgO/SiO_2 at a percentage (0.25/0.75) against (*E.Coli*) at different calcination temperatures.

Concentration µg/ml	A2-MG-25	B2-MG-25	C2-MG-25	D2-MG-25	E2-MG-25
	Inhibition Growth%				
0	0	0	0	0	0
625 (2 ml)	85.417	88.110	92.815	96.142	97.647
312.5 (1ml)	79.511	86.525	89.405	92.548	94.932
156.2 (0.5 ml)	70.229	80.229	87.207	88.031	90.819
31.25 (100µl)	63.982	77.732	80.296	80.591	82.571

Table 4- 8. Antibiotic activity of nano binary oxide MgO/SiO_2 at the percentage (0.75/0.25) against G-negative (*E.Coli*) at different calcination temperatures.

Concentration µg/ml	A1-MG-75	B1-MG-75	C1-MG-75	D1-MG-75	E1-MG-75
	Inhibition Growth%				
0	0	0	0	0	0
625 (2 ml)	80.961	84.741	87.7655	90.629	93.168
312.5 (1ml)	73.871	75.941	77.193	80.537	86.51
156.2 (0.5 ml)	66.531	67.644	69.642	72.831	78.628
31.25 (100µl)	58.319	63.106	67.912	69.992	73.548

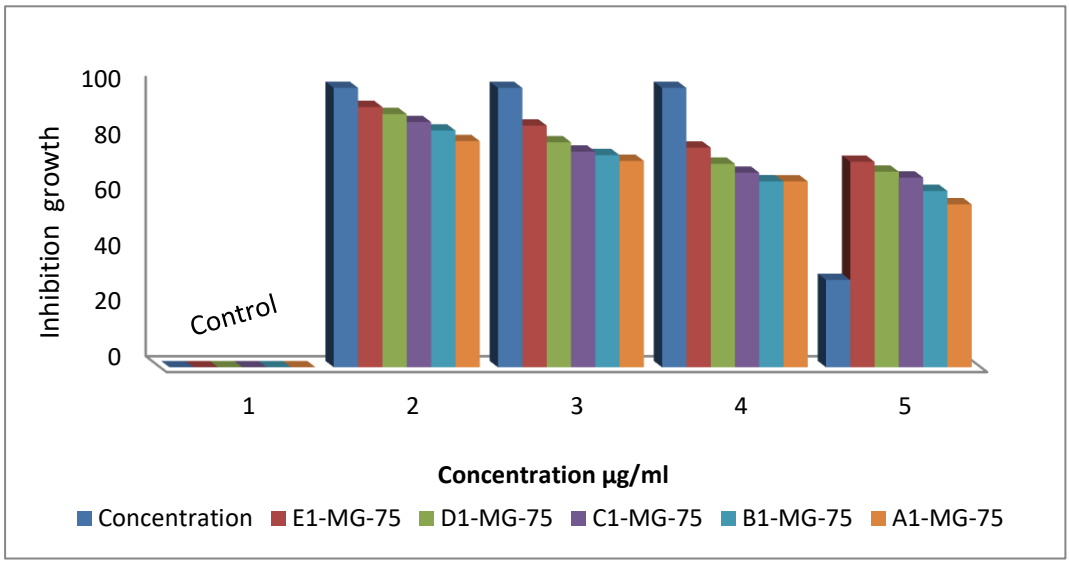

Figure 4-8. Inhibition growth of G-negative (*E.Coli*) at a different dose of antibiotic of MgO/SiO_2 (0.75/0.25) at various calcination temperatures.

Table 4-9. Antibiotic activity for nano binary oxide MgO/SiO_2 at a percentage (0.9/0.1) against G-negative (*E.Coli*) at different calcination temperatures.

Concentration µg/ml	A3-MG-90 700˚C	B3-MG-90 600˚C	C3-MG-90 500˚C	D3-MG-90 400˚C	E3-MG-90 300˚C
	Inhibition Growth %				
0	0	0	0	0	0
625 (2 ml)	78.104	78.617	82.512	87.421	88.751
312.5 (1ml)	69.381	72.542	75.913	83.311	84.319
156.2 (0.5 ml)	59.958	61.314	66.966	70.632	76.612
31.25 (100µl)	57.602	58.413	63.443	67.941	69.810

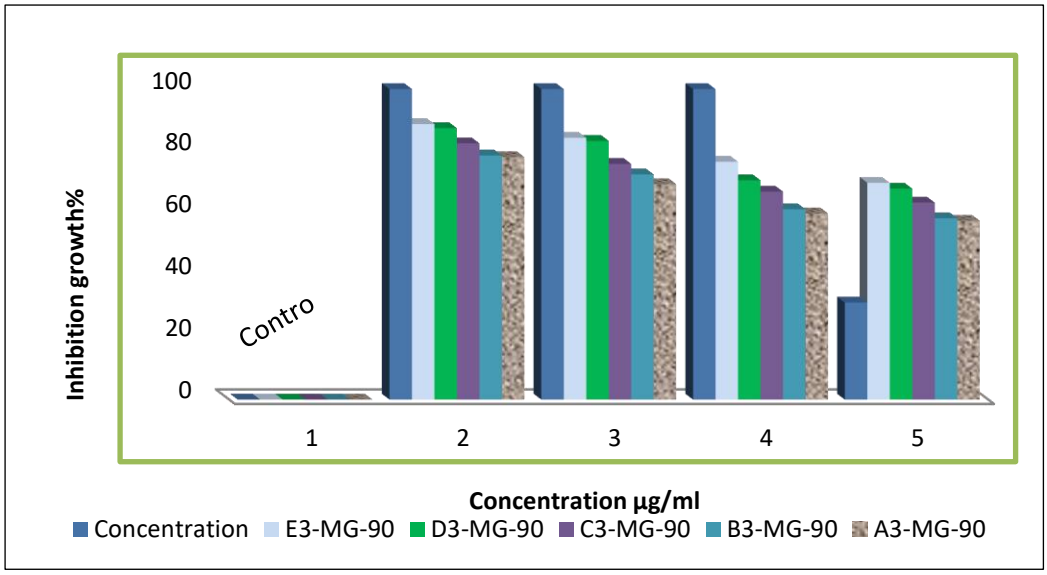

Figure 4-9. Inhibition growth of G-negative (*E.Coli*) at the different doses of antibiotic of MgO/SiO_2 (0.9/0.1) at various calcination temperatures.

Table 4-10. Antibiotic activity of nano binary oxide MgO/SiO_2 at a percentage (0.5/0.5) against G-negative (*E.Coli*) at different calcination temperatures.

Concentration µg/ml	A4-MG-50	B4-MG-50	C4-MG-50	D4-MG-50	E4-MG-50
	Inhibition Growth%				
0	0	0	0	0	0
625 (2 ml)	100	100	100	100	100
312.5 (1ml)	99.517	99.981	100	100	100
156.2 (0.5 ml)	90.437	92.915	93.063	95.673	97.947
31.25 (100µl)	72.946	75.321	78.643	80.631	95.634
15.625(50 µl)	69.979	70.31	73.667	76.541	78.538

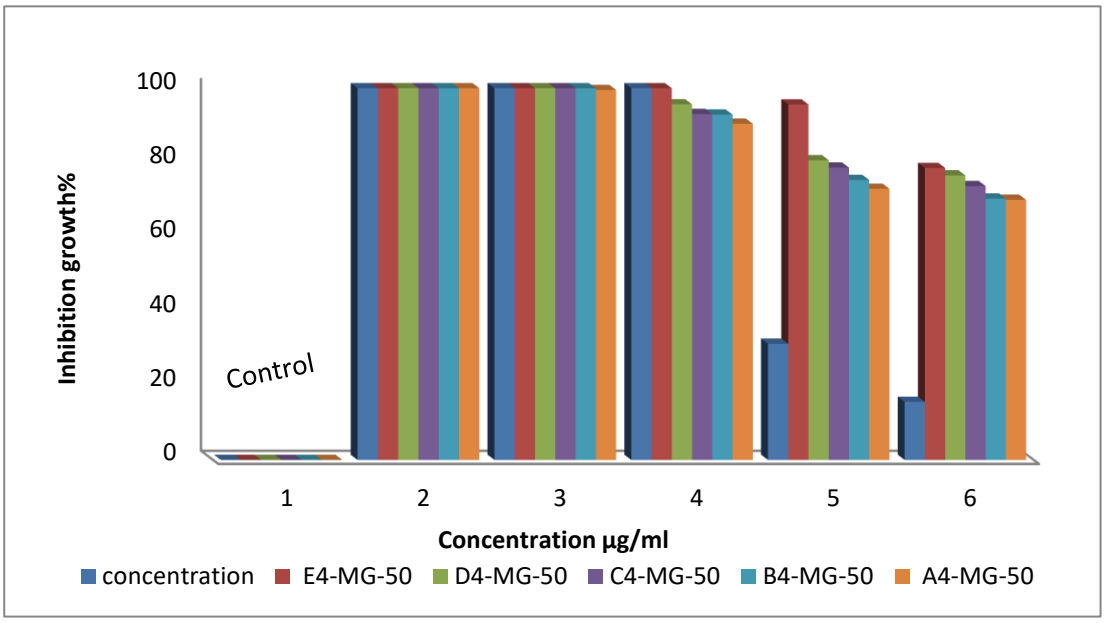

Figure 4-10. Effect of concentration of antibiotic of MgO/SiO_2 (0.5/0.5) at various calcination temperatures on inhibition growth of G-negative (*E.Coli*).

Table 4- 11. The percentage of antibiotic activity of nano binary oxide E4-MG-50against G-negative (E.coli, pseudomonas) and G-positive (*S.aureas*).

Concentration µg/ml	Pseudomonas	S.aureas	E.coli
	Inhibition Growth%		
0	0	0	0
625 (2 ml)	100	100	100
312.5 (1ml)	100	100	100
156.2 (0.5 ml)	91.713	95.853	97.947
31.25 (100µl)	83.547	88.163	95.634
15.625(50 µl)	70.631	72.147	78.538

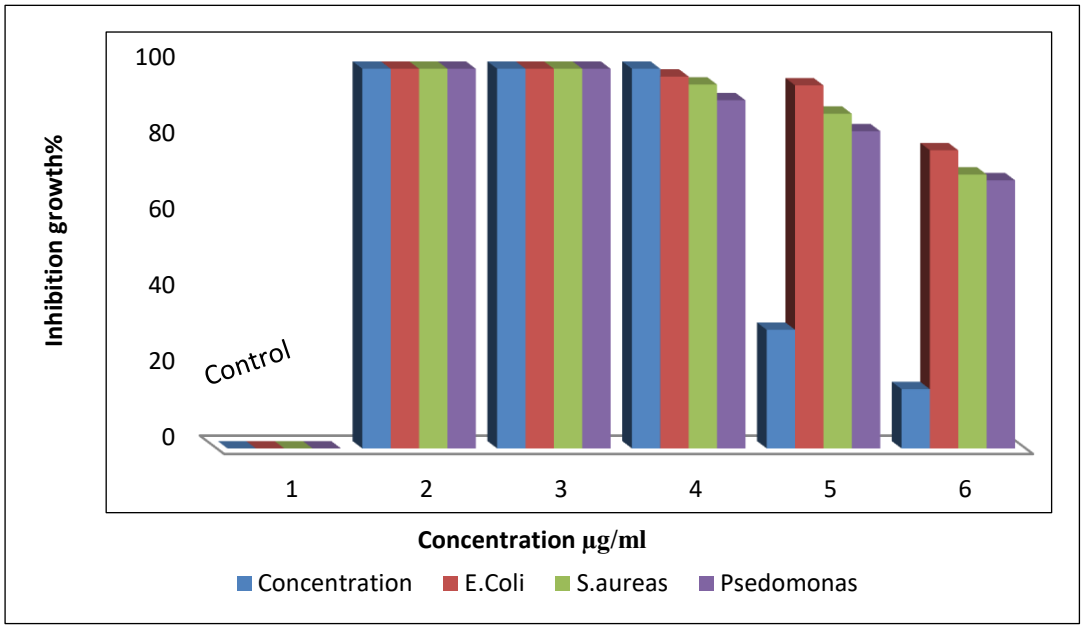

Figure 4-11. Effect of different doses of antibiotic E4-MG-50 on inhibition growth of G-negative (*E.Coli* and *Pseudomonas*) and G-Positive (*S.aureas*).

4-4. Antibiotic activity of magnetic nano binary oxide Fe_xO_y/SiO_2

this work evaluated the sterilizing magnetic nano binary oxide Fe_xO_y/SiO_2 on gram-negative and gram-positive bacterial such as *E.Coli*, *Pseudomonas* and *S.aureas* respectively, to investigate the antibacterial properties, figures (4-12 -4-14) plotted bacterial inhibitory growth curves for gram-negative and gram-positive with a various dose of magnetic nano binary oxide Fe_xO_y/SiO_2, high dose (1000)µg/ml give excellent inhibition growth such as shown results in tables (4-12-4-14). The antibacterial activity for magnetic nano binary oxide Fe_xO_y/SiO_2 at calcination temperature's 400^0C more than other samples with more calcination temperatures. Antibacterial activity increases as particle size decreases. larger nanoparticles have a limited number of active sites for oxygen absorption on the surface because of the low surface area to volume ratio, while small size nanoparticles may easily pass through the cell membranes. Generally, a high surface to volume ratio of the nanoparticles results in better penetration and fusion with the bacterial cell membranes. Therefore, the antibacterial activity of these nanoparticles may involve the production of reactive oxygen species and accumulation of nanoparticles in the cytoplasm or on the outer membranes [230]. The MIC and MBC are investigated against *E.Coli,* the values are calculated (937 and 1000) µg/ml respectively as shown in figures (4-22).

Table 4- 12. The percentage of antibiotic activity for magnetic nano binary oxide Fe_xO_y/SiO_2 against G-negative (*E.Coli*) at different calcination temperatures.

Concentration µg/ml	Calcination temperatures °C				
	700	600	500	400	300
	Inhibition Growth%				
0	0	0	0	0	0
1000	80.347	84.415	84.793	100	79.831
937	60.514	73.542	76.465	98.125	58.125
625	58.632	60.384	62.391	82.372	53.372
312.5	46.625	48.519	51.431	76.421	42.421
156.2	35.9221	37.579	42.469	51.942	33.831
31.25	28.719	31.474	35.741	45.927	26.452

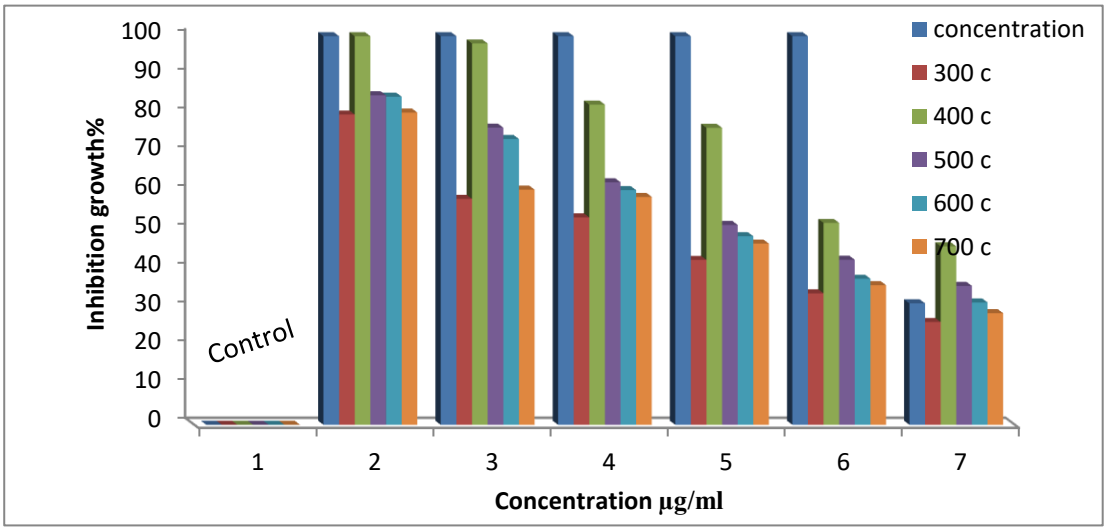

Figure 4-12. Effect of different doses of magnetic nano binary oxide Fe_xO_y/SiO_2 on inhibition growth against G-negative (*E.Coli*) at different calcination temperatures.

Table 4-13. The percentage antibiotic activity for magnetic nano binary oxide Fe_xO_y/SiO_2 against G-positive (*S.aureas*) at different calcination temperatures.

Concentration µg/ml	Calcination temperatures				
	700	600	500	400	300
	Inhibition Growth%				
0	0	0	0	0	0
1000	73.311	76.389	78.348	88.503	64.503
937	61.451	65.481	71.59	80.362	55.362
625	52.216	58.974	60.863	74.528	48.528
312.5	41.548	46.511	50.392	73.631	40.631
156.2	28.453	30.721	38.944	48.966	25.357
31.25	20.794	22.923	27.991	40.1	19.772

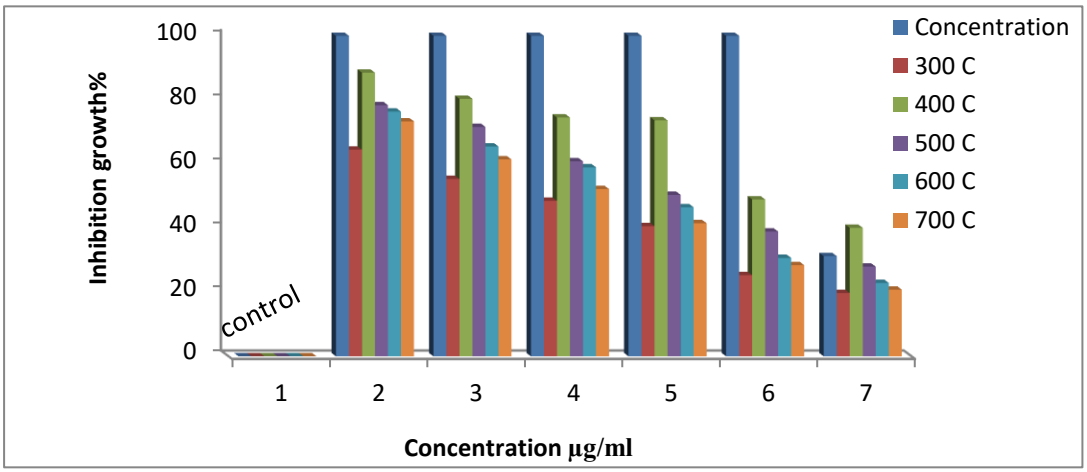

Figure 4-13. Effect of different concentrations of magnetic nano binary oxide Fe_xO_y/SiO_2 on inhibition growth against G-positive (*S.aureas*) at different calcination temperatures.

Table 4-14. The percentage of inhibition growth of magnetic nano binary oxide Fe_xO_y/SiO_2 against G-negative (*Pseudomonas*) at different calcination temperatures.

Concentration µg/ml	Calcination temperatures ˚C				
	700	600	500	400	300
	Inhibition Growth%				
0	0	0	0	0	0
1000	63.483	68.642	73.524	79.354	60.354
937	56.417	62.124	65.631	70.936	51.936
625	47.681	53.315	58.985	61.291	45.291
312.5	40.532	43.324	45.214	50.507	37.507
156.2	21.845	25.811	30.921	42.571	22.726
31.25	15.912	16.719	19.988	23.833	13.491

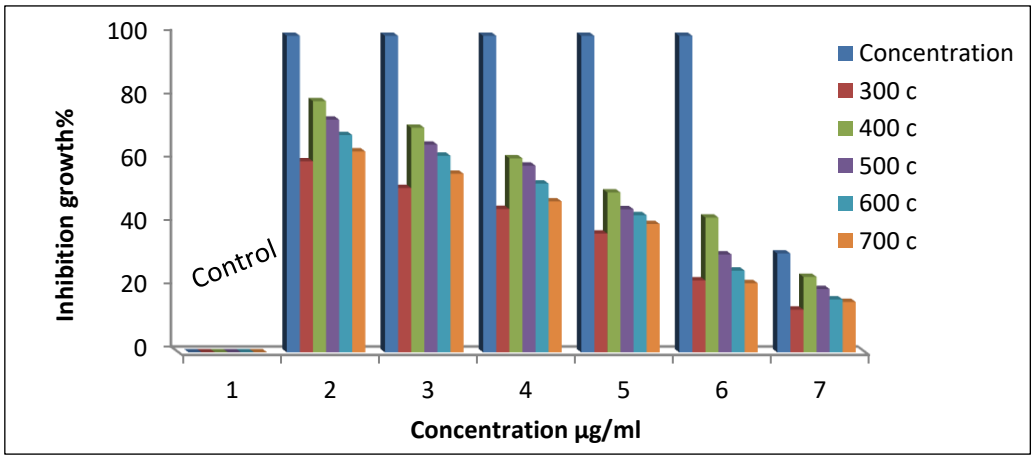

Figure 4-14. Effect of different concentrations of magnetic nano binary oxide Fe_xO_y/SiO_2 on inhibition growth against G-negative (*Pseudomonas*) at different calcination temperatures.

4-5. Antibiotic assay of nano-silica oxide and nano binary oxide by using a wound dressing

Wounds that are infected by bacteria can impede healing and even endanger human life. Wound dressings that can detect and cure bacterial infections are urgently needed. Because of their unique qualities, nanoparticles have been used in wound dressings. Nanoparticle-based wound dressings for bacterial detection and treatment have made considerable advances, as demonstrated in this study. One of the most common complications in diabetic patients is a chronic ulcer with deep tissue damage. Which is associated with abnormal fibroblast and keratinocyte proliferation, decreased cell migration, and decreased angiogenesis, all of which can result in impaired vascularization, delayed wound contraction, and the formation of non-healing diabetic wounds [231]. Not only diabetic wounds, but also leg ulcers, vascular insufficiency, and burns all result in significant morbidity and mortality, impairing quality of life and imposing a significant economic burden [232]. In general, wounds are classified as acute or chronic [233]. As a result of the diversity of bacteria found in wounds, there is a widely recognized need for novel antibacterial medicines to combat the global rise in resistance. The increasing prevalence of antibiotic resistance among pathogenic bacteria is one of the most serious health problems confronting humanity today [234]. Thus, this work uses strategies for overcoming bacterial resistance including the use of raw natural material (RHA) and extracted nanoparticles from it then used on wound dressing as antibiotics materials. Particularly nanomaterials that are applied on wound dressing after sterling appear promising results for the treatment of G-positive and G-negative microbial that infect wounds as shown in figures (4-15,4-16,4-17 and 4-18).

Zone inhibition for the antibiotic of nano-silica oxide and nano binary oxide SiO_2/ V_2O_5, Fe_xO_y/SiO_2 and E4-MG-50) are shown in tables (4-15,4-16,4-17 and 4-18). respectively after applying it to the wound dressing.

Table 4-15. Zone inhibition for various microbial at different doses of nano-silica oxide.

Concentration µg/ml SiO_2	Zone inhibition mm E.Coli	Zone inhibition mm S.aureas	Zone inhibition mm Pseudomonas
625 H.D	22	19	5.5
312.5 M.D	16.5	15	No
31.25 L.D	5.2	3	No

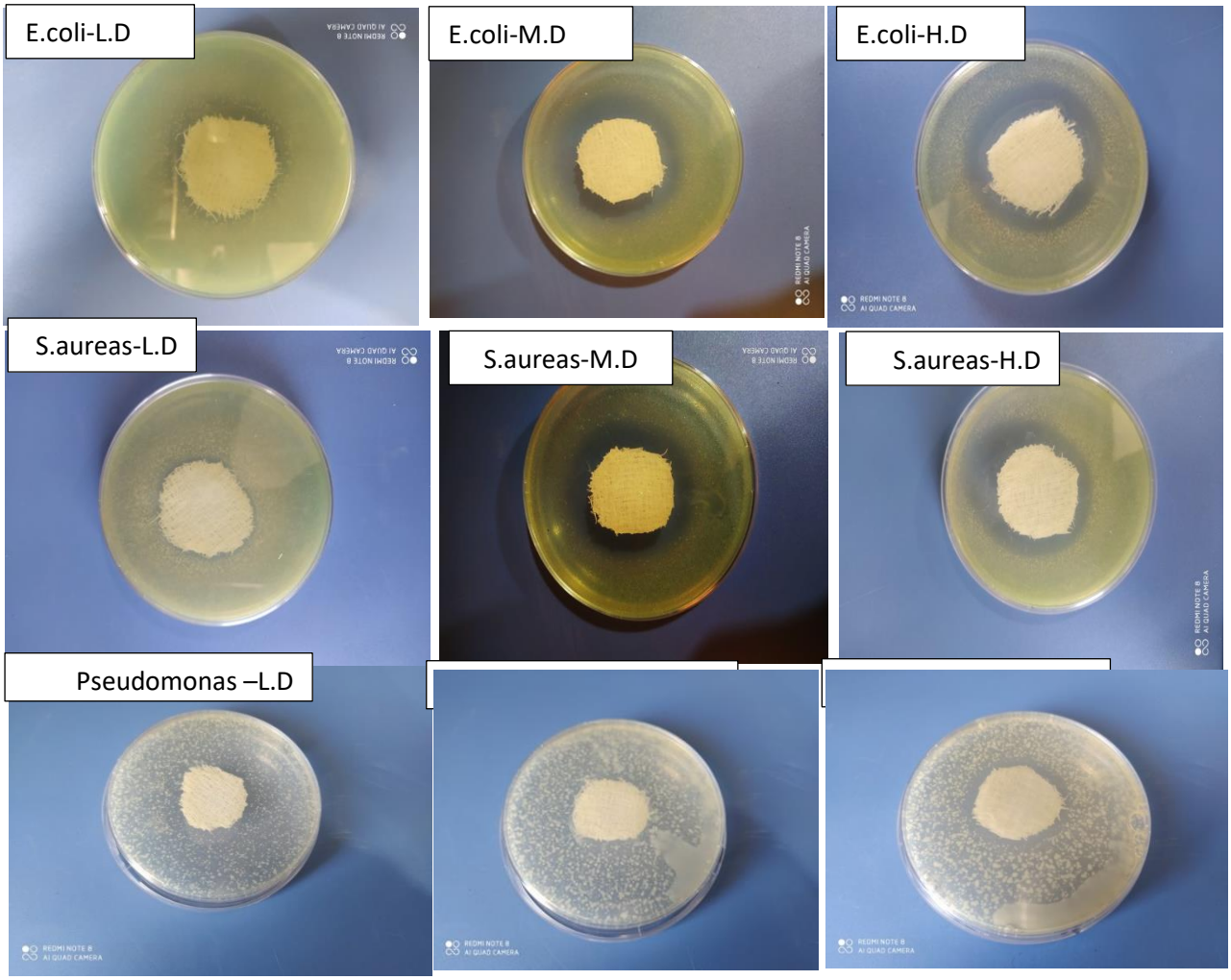

Figure 4- 15. Zone inhibition for antibiotic silica oxide with various doses after applying it on wound dress against a. *E.Coli*, b. *S.aureas*, and c.*Pseudomonas* at(high, medium and low dose).

Table 4-16. Zone inhibition for various microbial at different doses of nano binary oxide SiO_2/V_2O_5.

Concentration SiO_2/V_2O_5 µg/ml	Zone inhibition mm *E.Coli*	Zone inhibition mm *S.aureas*	Zone inhibition mm *Pseudomonas*
625	Non	27	23
312.5	26	25	18.2
31.25	22	20	10.1

Table 4-17. Zone inhibition for various microbial at different doses of nano binary oxide Fe_xO_y/SiO_2.

Concentration Fe_xO_y /SiO_2 µg/ml	Zone inhibition mm *E.Coli*	Zone inhibition mm *S.aureas*	Zone inhibition mm *Pseudomonas*
625 (H.D)	25	15	13
156.2 (M.D)	17	12.1	10
31.25 (L.D)	8.5	8	5

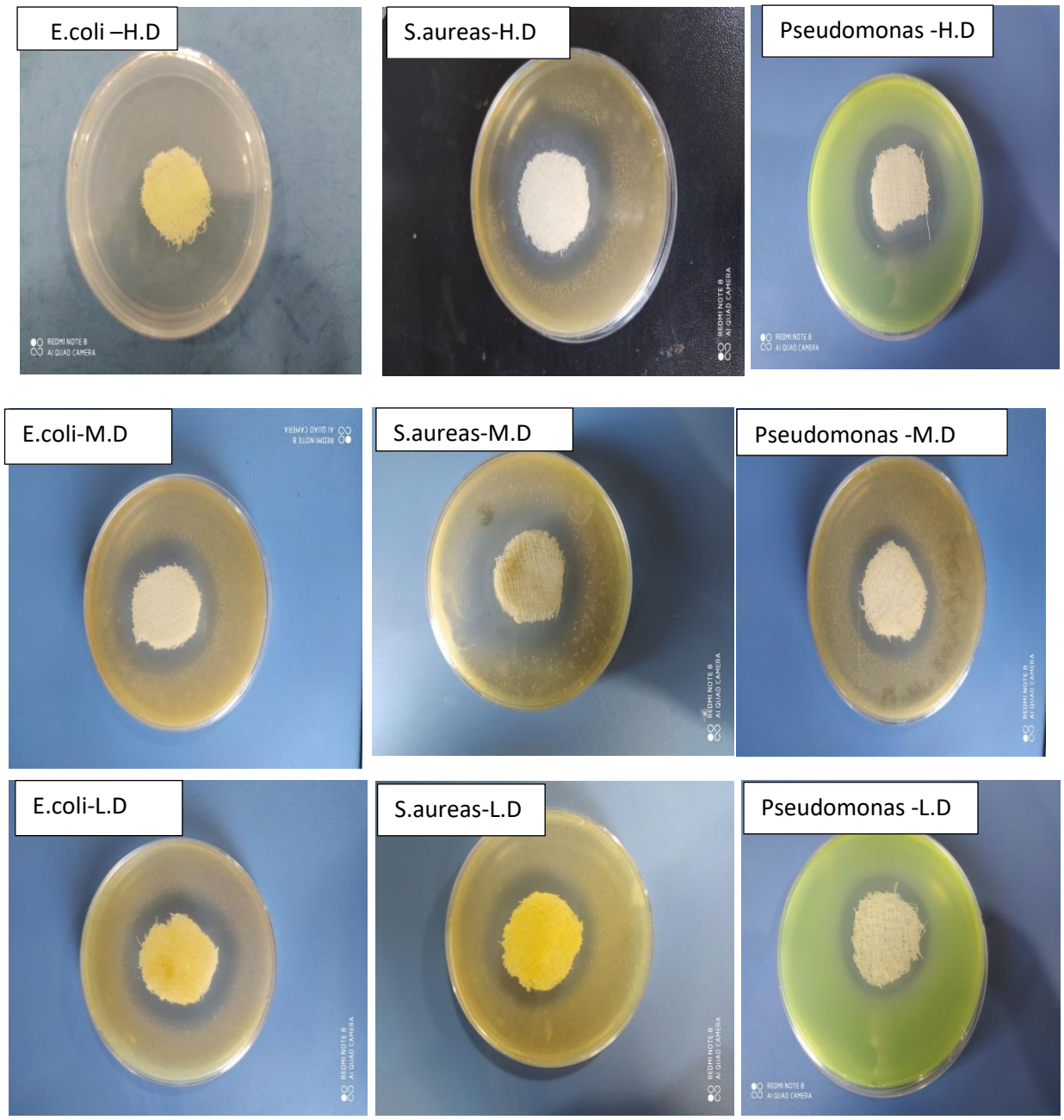

Figure 4- 16. Zone inhibition for antibiotic silica oxide/ V_2O_5 after applying it on wound dress against a. *E.Coli*, b. *S.aureas*, and c.*Pseudomonas* at(high, medium and low dose).

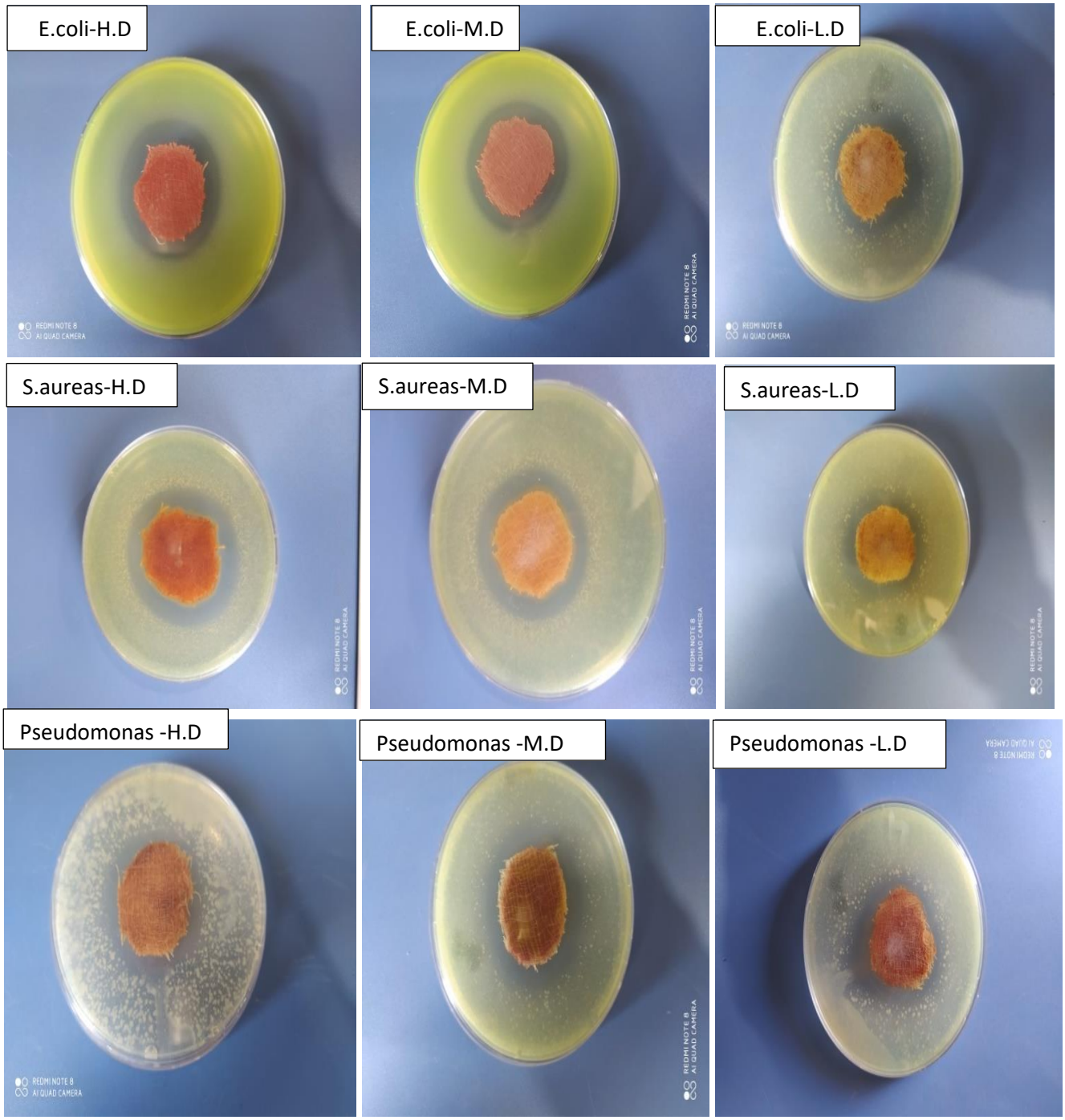

Figure 4-17. Zone inhibition for nano binary oxide Fe_xO_y/SiO_2 after applying it on wound dress against a. *E.Coli*, b. *S.aureas*, and c. *Pseudomonas* at(high, medium and low dose).

Table 4-18. Zone inhibition for various microbial at different doses of nano binary oxide E4-MG-50.

Concentration MgO/SiO_2 µg/ml	Zone inhibition *E.Coli* /mm	Zone inhibition *S.aureas* /mm	Zone inhibition *Pseudomonas*
312.5	Non	non	non
156.2	74	70	60
31.25	65	50	45

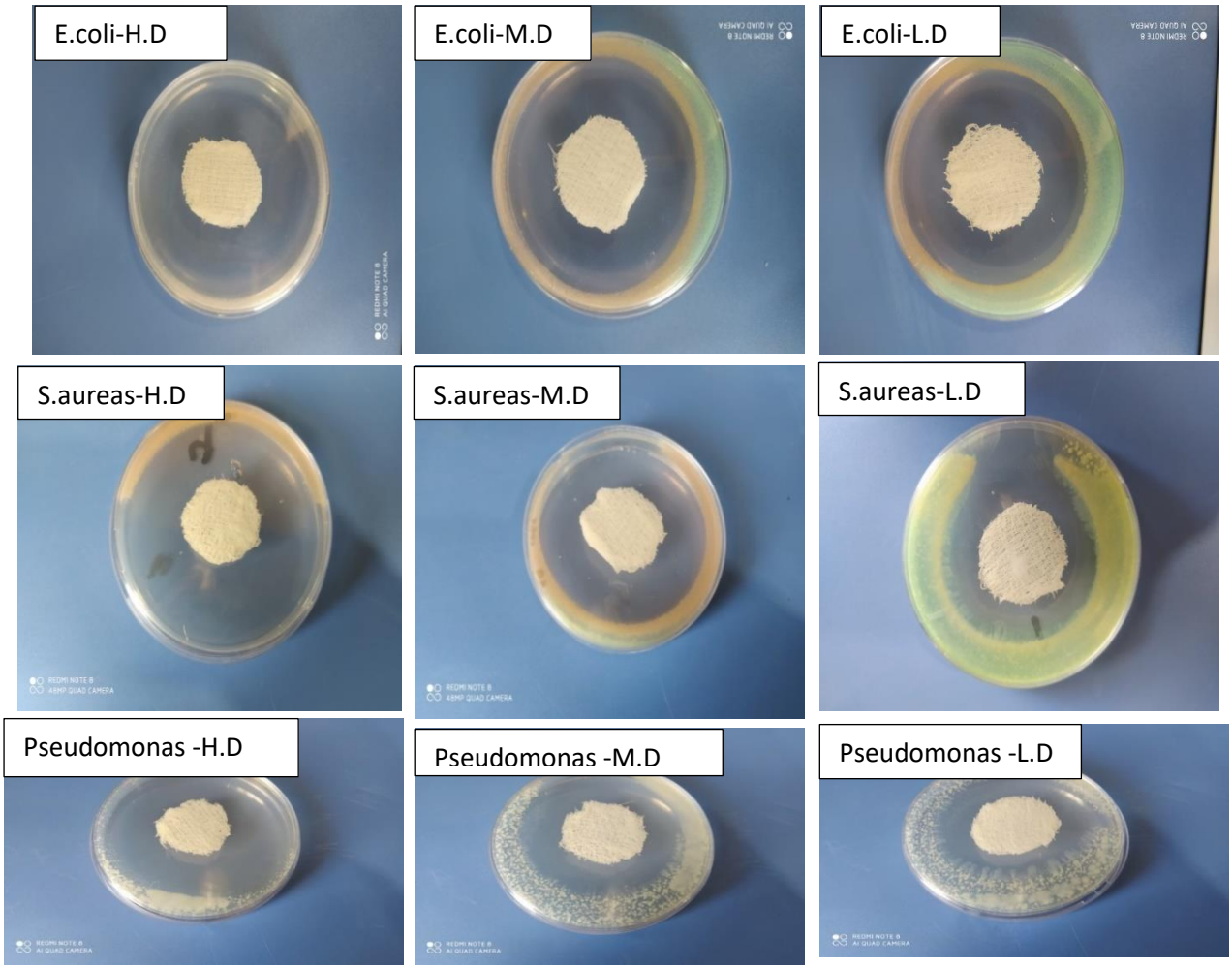

Figure 4-18. Zone inhibition of nano binary oxide E4-MG-50 after applying it on wound dress against a. *E.Coli*, b. *S.aureas*, and c.*Pseudomonas* at(high, medium and low dose).

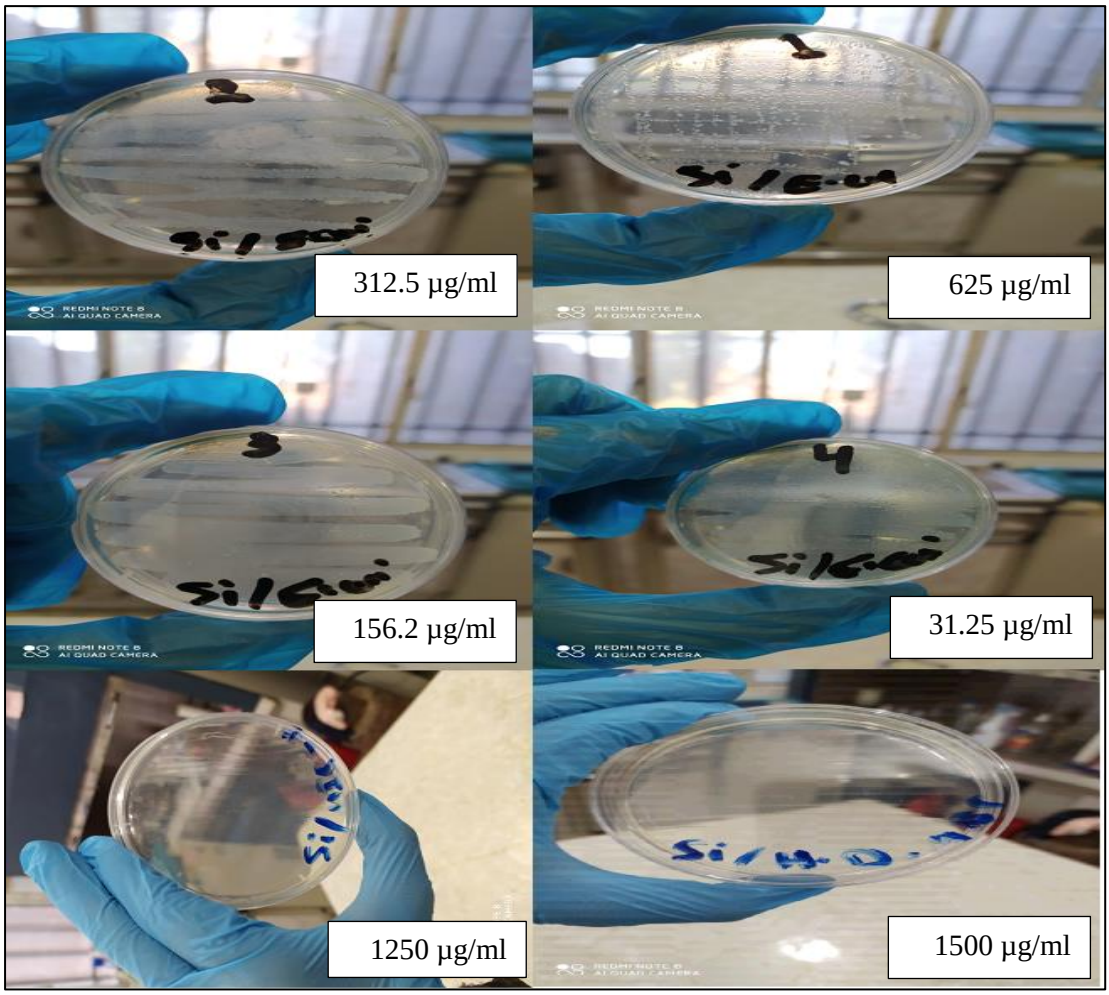

Figure 4-19. Inhibition growth of *E.Coli* for nano silica oxide to designation MIC and MBC at different concentrations after incubation for 24 hours (1500, 1250,625, 312.5, 156.2, and 31.25) µg/ml.

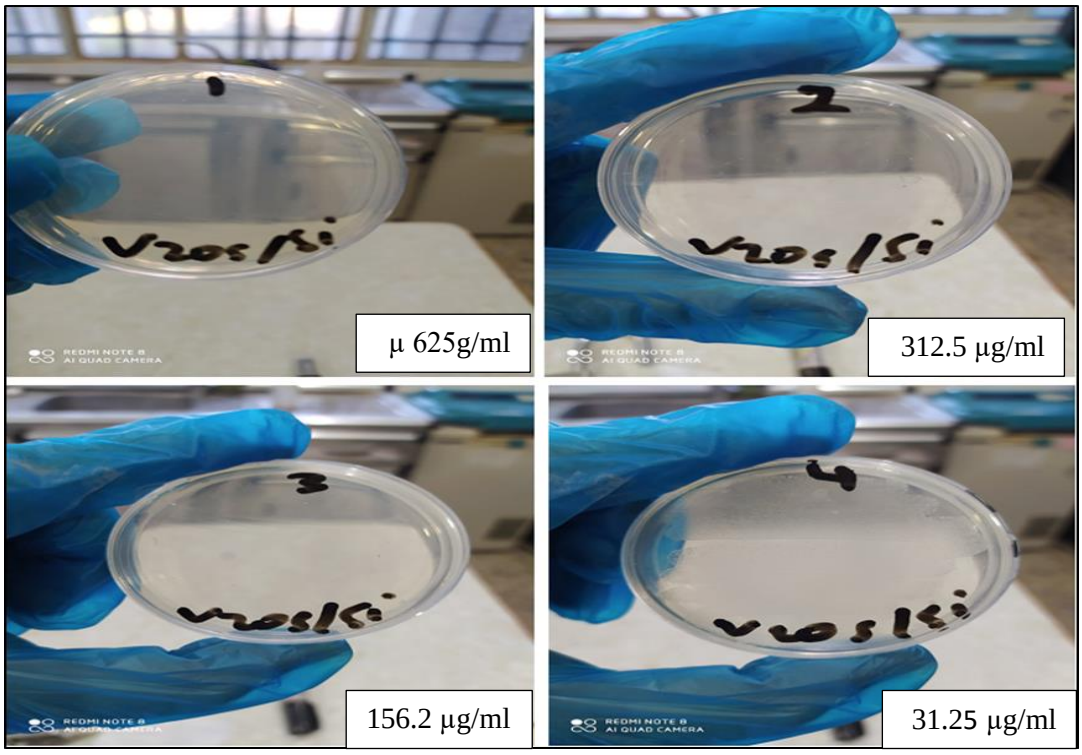

Figure4-20. Inhibition growth of *E.Coli* for silica oxide /V_2O_5 to designation MIC and MBC at different concentrations after incubation for 24 hours (625, 312.5, 156.2, and 31.25,) µg/ml.

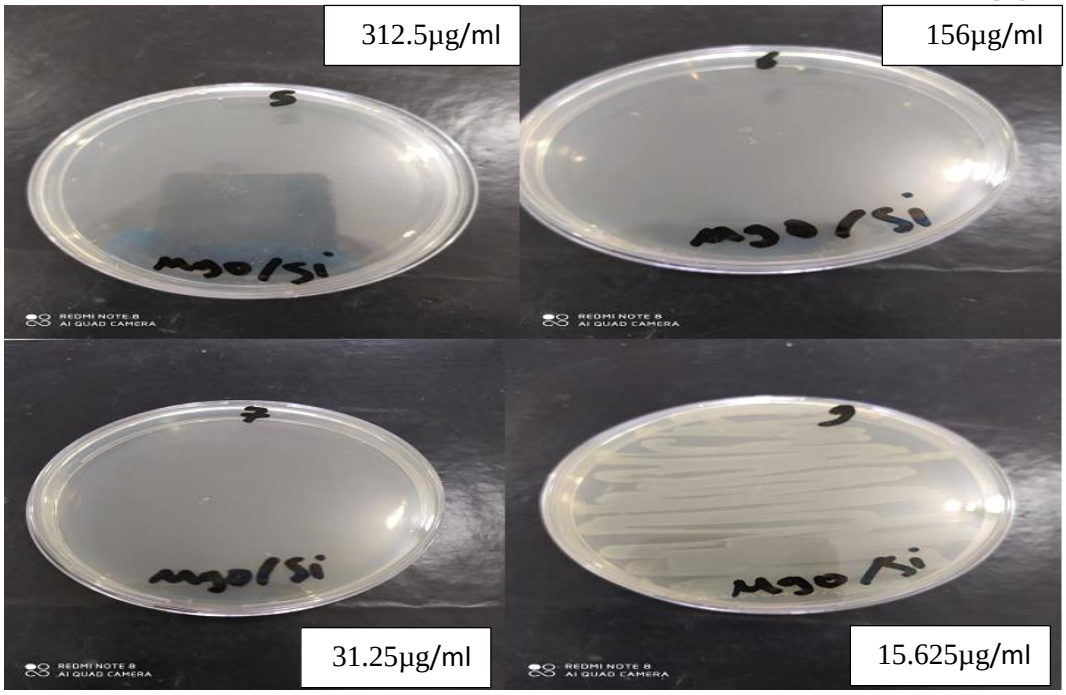

Figure4-21. Inhibition growth of *E.Coli* for E4-MG-50 to designation MIC and MBC at difference concentration after incubate for 24 hour (312.5, 156.2,31.25,and 15.625) µg/ml.

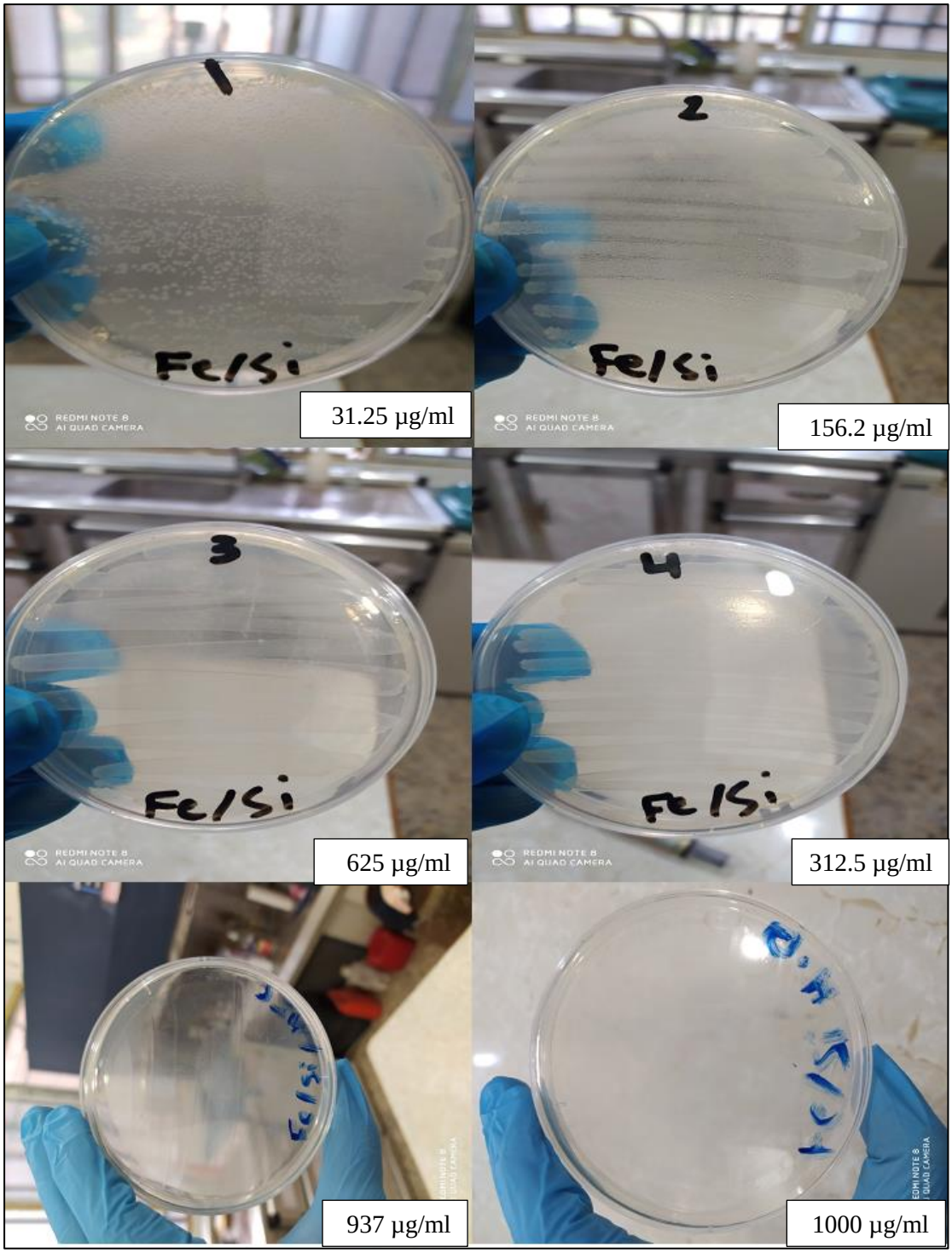

Figure 4-22. Inhibition growth of *E.Coli* for silica oxide /Fe_xO_y at difference concentration after incubate for 24 h (1000, 937,625, 312.5, 156.2, and 31.25)µg/ml.

4-6. Activity estimation of suggested medical ointment on *S.aureas*

The suggested antibacterial activity of nano binary oxide SiO_2/V_2O_5 and E4-MG-50 NPs as medical ointment was evaluated against Gram-positive bacteria *S.aureas.* The results of the assay show the diameter of the inhibition zones increased with increasing nano ointment dose. The percentage weight range from (4- 10) % as shown in table 4-19. Nano binary oxide silica oxide/V_2O_5 and E4-MG-50 NPs because of their small size and applicability, nanoparticles have prompted a lot of interest. Play a role in providing a healthy environment, and assist in wound healing by inhibiting microbial growth [235]. The results of medical ointment for nano binary oxide silica oxide/V_2O_5 and E4-MG-50NPs that show 10% give high zone inhibition as shown in figures 4-23. So the nano ointment can be used for antimicrobial and wound healing. Especially since the nano binary oxide silica oxide/V_2O_5 and E4-MG-50 NPs showed low toxicity assay.

Table 4-19. Table 4-19. The activity of nano binary oxide (silica oxide/V_2O_5 and E4-MG-50) ointment with different percentage weights.

Wight%	Zone inhibition /mm SiO_2/ V_2O_5	Zone inhibition /mm E4-MG-50
10%	19	22
8%	12	17
6%	9	12
4%	7	7.5

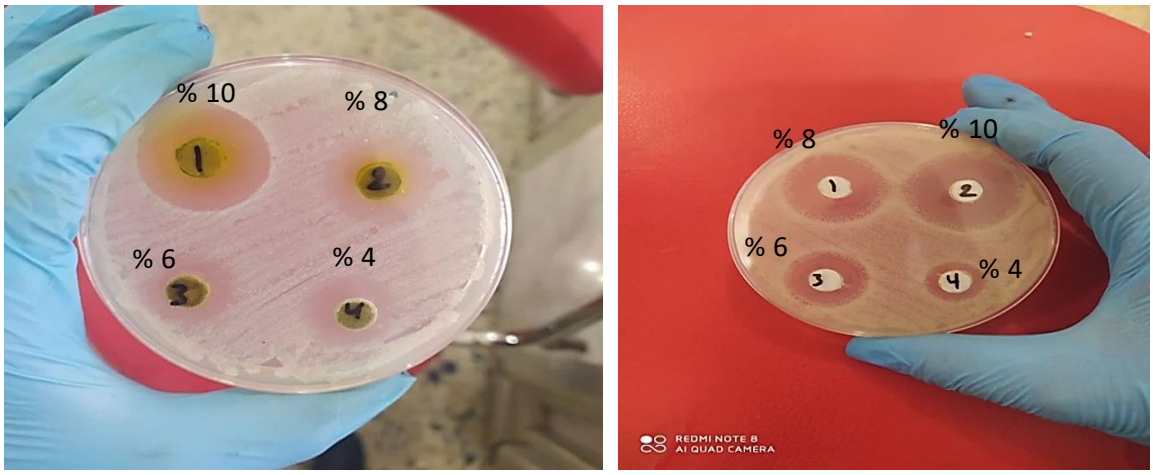

Figure 4-23. Image of zone inhibition of nano binary oxide (silica oxide/V_2O_5 and E4-MG-50) medical ointment.

4-7. Cytotoxicity evaluation of silica oxide, Nano binary oxide (SiO_2/V_2O_5, Fe_xO_y /SiO_2, and SiO_2/MgO[E4-MG-50]) NPs agents skin cancer-A431cells and Vero cells-101.

The results of silica oxide extracted from RHA and nano binary oxide (SiO_2/MgO, SiO_2/ V_2O_5, and Fe_xO_y /SiO_2) nanoparticles showed significant change in viability for skin cancer-A431cells and Vero cells-101 line.

Nano binary oxide SiO_2/MgO(E4-MG-50) show a decrease in viability of skin cancer-A431cells at different range concentrations (2000,1000,500, 250,125,62.5,31.25,15.62, and 7.81) µg/ml for nano binary oxide E4-MG-50, Which is characterized by showing effective toxicity against skin cancer-A431cells at low concentrations7.81 µg/ml when compared with the control group, such as shown in the figure. (4-24).

A previous study showed that MgO NPs can exhibit specific cytotoxicity against the K562 cell line and can be considered a new anticancer agent. Also shown that ROS production in cancer cells initiates apoptosis-mediated MgO NPs. More research on other cancer types and normal cells

is needed to determine whether MgO NPs' anticancer activity is equally applicable and productive against other cancer cell lines [236].

The current study demonstrates that nano binary oxide E4-MG-50 exhibited selective cytotoxicity against skin cancer-A431cells and Vero cells-101 as shown in figures 4-24 and table 4-20. The results appear that nano binary oxide SiO_2/MgO has high cytotoxicity on skin cancer-A431cells and low cytotoxicity effect on Vero cells-101. The results confirmed the cytotoxicity effect increase with increased concentration, the inhibition of nano binary oxide E4-MG-50 be 77.614 % with a concentration of 250 µgl/ml on skin cancer-A431cells and inhibition of nano binary oxide E4-MG-50 be 24.285 % on Vero cells-101at the same concentration. Results exhibited that nano binary oxide E4-MG-50 can be considered a novel anticancer agent. It is recently found that nano-MgO outperforms copper, silver, TiO_2, and other bactericides, anti-cancer, sporicidal, and antiviral activity. [237]

The concentration required for a 50% inhibition of viability (IC50) is determined by using an excel sheet and fitted by blotting graphically of relative cell inhibition percentage on the Y-axis versus the concentration of each compound used on the X-axis. Calculation of cell viability is done by dividing absorbance measured for each concentration by the absorbance of the control multiplied by 100 [238].

The concentration of nano binary oxide E4-MG-50 required for a 50% inhibition of viability (IC50) was 214.122 and 968.859 µgl/ml for skin cancer-A431cells and Vero cells-101line respectively as shown in figure (4-25).

Table 4-20. The cytotoxicity effect of nano binary oxide E4-MG-50 on skin cancer A431 line cells and Vero cells-101line cells data is presented as mean ± SD of four independent experiments.

	Vero cells-101line cells			Skin cancer A431 line cells		
Concentrations µg/ml	Inhibition	Stander deviation %SD	Average %	Inhibition	Stander deviation %SD	Average %
2000	80.413	10.780	19.587	99.043	4.823	0.957
1000	71.282	7.449	28.718	97.693	1.056	2.306
500	39.411	7.148	60.589	85.592	2.706	14.407
250	24.286	9.898	75.714	77.614	6.380	22.385
125	19.283	9.299	80.717	47.154	2.6205	52.845
62.5	13.042	6.404	86.958	44.001	2.786	55.998
31.25	2.359	8.712	97.641	30.248	4.415	69.751
15.62	1.169	7.925	98.831	26.095	3.918	73.904
7.81	0.188	7.542	99.812	20.270	7.900	79.729
Control	-	8.913	100	-	1.103	100

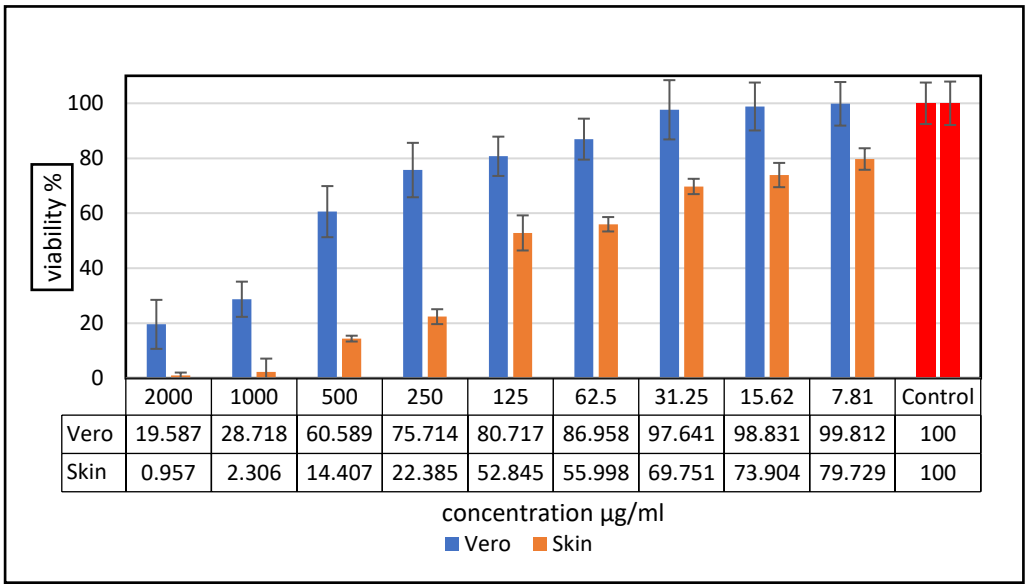

Figure 4-24. Effects of nano binary oxide E4-MG-50 on the viability of Skin cancer A431 line cell line and Vero cells-101using MTT assay.

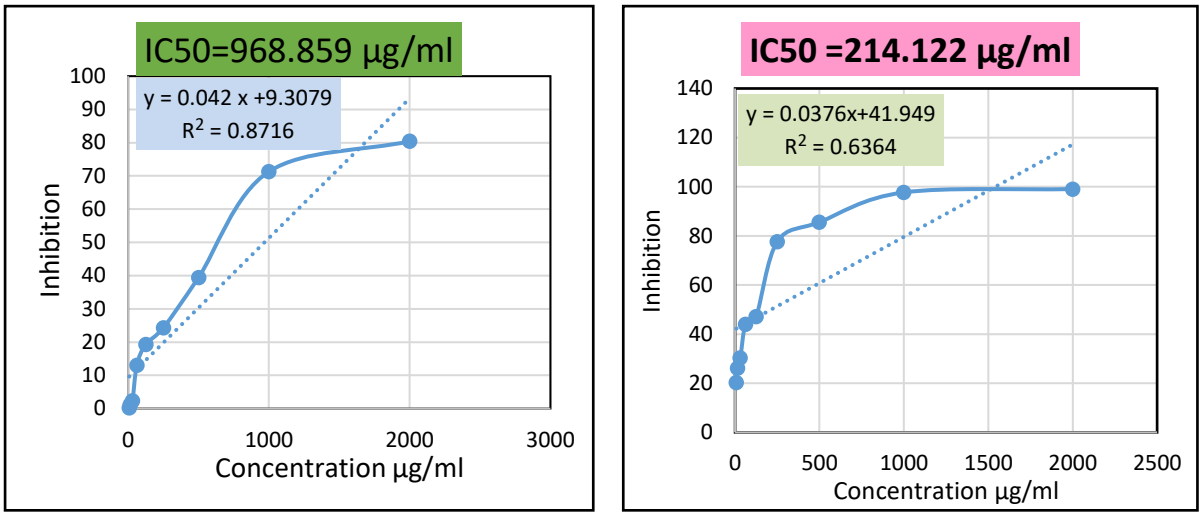

Figure 4-25. IC50 measurements of nano binary oxide E4-MG-50 on skin cancer line A431 cells (right) and Vero cells-101line (left).

Nano binary oxide SiO_2/V_2O_5 shows promising selectivity against skin cancer line A431cells, this is due to ROS that could be produced by the addition of nano binary oxide SiO_2/V_2O_5 nanoparticles with crystal size 29.845 nm. Alternatively, aside from the generation of ROS, another mechanism could be involved in nano binary oxide silica oxide/V_2O_5 cytotoxicity. It's fine it is well known that vanadium compounds inhibit a variety of enzymes specifically, protein tyrosine phosphatases (PTP). PTP allows glucose uptake into cells to be stimulated a high concentration of glucose within the cells should affect cellular metabolism.

Furthermore, if the supply of oxygen to cells is insufficient, the sequence of reactions (glycolytic pathway) will convert glucose into as a final result, pyruvate converted to lactate. Lactate accumulation lowers intracellular pH, which results in. This, in turn, has a negative impact on the activity of several enzymes the net electric charge of membranes and other cellular metabolic activities is altered. In general, these two possible processes, the production of ROS, and the reduction in. The previous study found the accumulation of lactate in the cell could have resulted in a decrease in cellular pH an increase in the cytotoxicity of nanoparticles

V_2O_5 to FsaR and L929 cells furthermore, because of the high cytotoxicity. The effect observed on FsaR cells suggested that nano size V_2O_5 was used particles in the environment could be considered poisonous FsaR fibrosarcoma cell therapy. Nano cytotoxicity agents like nano V_2O_5 are characterized by the ability to treat cancerous tumours by stimulating the production of ROS, and higher levels of antioxidative enzymes in tumour cells that work on ingestion of ROS [339]. In this work using nano binary oxide silica oxide /V_2O_5 that preparation by using rice husk as raw material instead of chemicals to study cytotoxicity on skin cancer line A431cells and Vero cells-101line, the result shows the half-maximal inhibitory concentration values for its IC50 is 411.296 µg/ml and 792.660 µg/ml for skin cancer line A431cells and Vero cells-101line respectively such as shown in figure 4-27, that make it has selective cytotoxicity. At a high concentration of 2000 µg/ml, no selective toxicity was observed on skin cancer line A431cells and Vero cells-101line such as shown in table 4-21 and figure 4-26 that show affect the viability of cells at concentrations (2000,1000, 500, 250, 125, 62.5,31.25,15.62 and 7.81) µg/ml of nano binary SiO_2/V_2O_5.In previously studied, many search study effects of V_2O_5 on several cell lines including MDA-MB-231 (human breast cancer cell line), V79 (hamster lung fibroblast cell line), SCCVII (squamous carcinoma cells), FsaR (fibrosarcoma cells), L929 (murine fibroblast cell line) cells and also in B16F10 cells, showing cytotoxicity in all of the examined cell [240,241]. Overall, demonstrated in this study that nano binary oxide SiO_2 /V_2O_5 NPs could give a new route for alternative treatment options for anti-bacterial and anti-cancer.

Table 4-21. Cytotoxicity effect of nano binary SiO_2/V_2O_5 NPs on skin cancer A431 line cells and Vero cells-101 line and data are presented as mean ± SD of four independent experiments.

Vero cells-101 line				Skin cancer cells -A431line		
Concentration SiO_2/V_2O_5	Inhibition	Stander deviation %SD	Average %	Inhibition	Stander deviation %SD	Average %
2000	94.864	4.081	5.136	97.989	7.943	2.011
1000	70.302	4.347	29.698	83.652	1.3776	16.348
500	41.177	4.743	58.823	68.73	5.453	31.270
250	35.131	6.724	46.869	48.428	4.728	51.572
125	23.852	4.510	76.148	43.059	3.549	56.941
62.5	19.530	5.644	80.470	40.179	3.764	59.821
31.25	14.086	5.020	85.920	33.099	6.062	66.901
15.62	9.935	7.041	90.065	25.74	1.496	74.260
7.81	4.137	4.731	95.863	19.641	8.954	80.359
Control	-	6.459	100	-	4.939	100

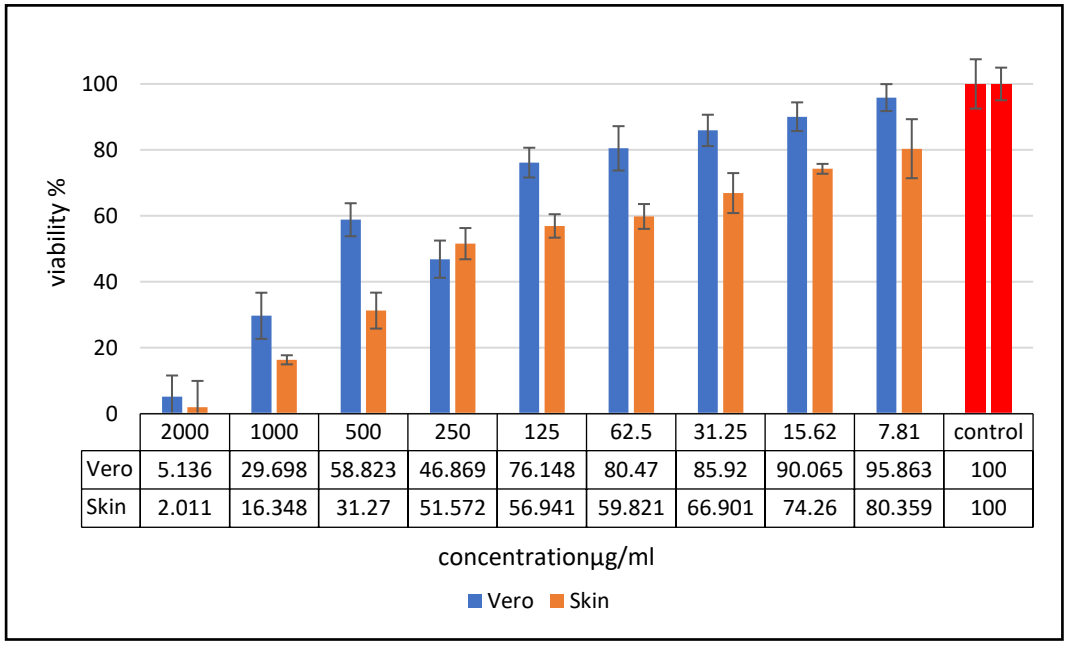

Figure 4-26. Effects of nano binary oxide SiO_2/V_2O_5 on the viability of Skin cancer A431 cells line and Vero cells-101 cells line using MTT assay.

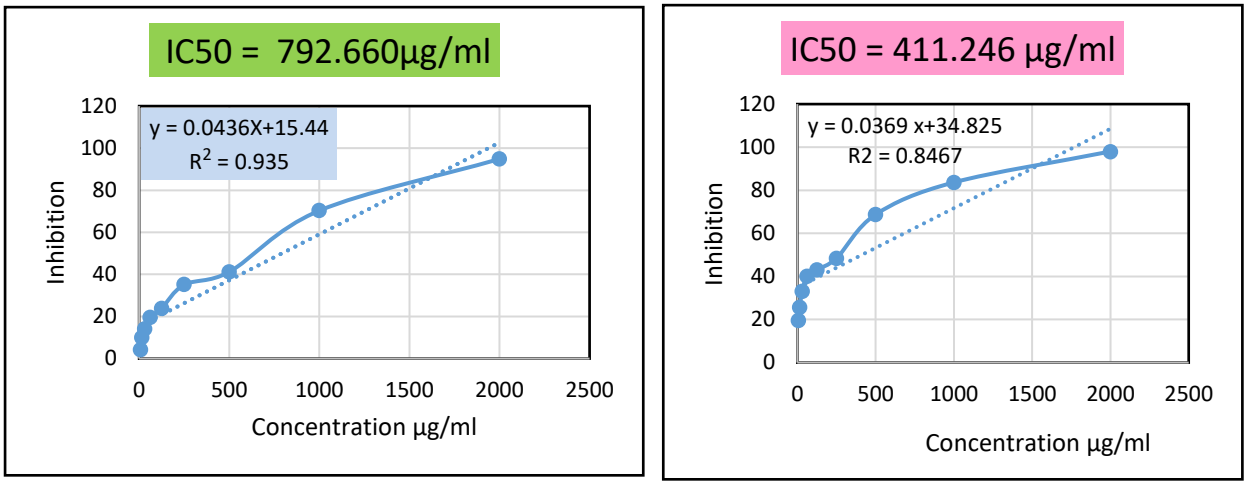

Figure 4-27.IC50 measurements of nano binary silica oxide/V_2O_5 on skin cancer line A431cells(right) and Vero cells-101line (left).

Metallic nanoparticles have recently garnered interest due to their biological, biomedical, environmental, and commercial relevance [242]. Iron oxide nanoparticles are now being studied due to their potential use in a variety of sectors, including medication and gene delivery, biosensors, and cancer treatment. Magnetic nanoparticles (MNPs) with sizes ranging from 10 to 100 nm that respond to a magnetic field are used as multimodal drug delivery systems due to their superparamagnetic characteristics. This means that we can manage the concentration of nanoparticles, reducing the cytotoxic effects on normal tissue [243].

This study involved treatment of skin cancer A-431 cells line and Vero cell line for 24 hours, by magnetic nano binary oxide Fe_xO_y/silica oxide (MNPs) maximal cell viability is found at a concentration of 62.5 µg/ml which means this concentration is not suitable for the treatment of skin cancer cells, also observe the same viability for skin cancer A-431 cells line and Vero cell line at concentration 2000 µg/ml as shown in table 4-22 and figure 4-28 the perfect concentration noted at 1000 µg/ml in this concentration the percentage inhibition was 80.820 % and 75.582 %for skin cancer cells and Vero cell line respectively. When used at

concentrations low than 1000 µg/ml noted the ratio inhibition of Vero cell 101 line (normal cells) to cancerous cells makes it unsuitable for use as an anti-cancer, but its effect can be studied by other researchers on other types of cancer cells and find out the effectiveness. IC50 the half-maximal inhibitory concentration values of magnetic nano binary oxide Fe_xO_y/SiO_2 NPs on skin cancer A-431 cells line and Vero cell line (537.075 and 671.145) µg/ml respectively, as shown in figure (4-29). In a previous study. In a recent work on cells treated by, FeO NPs cell viability depends on the type of cells. The vitality of Vero cells is affected by concentration and exposure time. In the case of PK 15 cells, increasing the concentration of FeO NPs and the exposure period resulted in enhanced cell viability. There was no significant difference between concentration and exposure period in MDBK cells [244].

Table 4-22. Cytotoxicity effect of magnetic nano binary oxide Fe_xO_y/SiO_2 NPs on skin cancer A431 line cells and Vero cells-101line cells and data are presented as mean ± SD of four independent experiments.

Concentration µg/ml	Vero Cells-101 line			Skin cancer cells-A143line		
	Inhibition	Stander deviation %SD	Average %	Inhibition	Stander deviation %SD	Average %
control	-	4.061	100	-	2.8195	100
62.5	20.792	8.809	79.208	23.353	4.789	76.647
125	28.788	6.647	71.212	34.003	5.8118	65.997
250	34.995	7.983	65.005	43.839	8.430	56.161
500	41.249	4.878	58.751	48.326	8.440	51.673
1000	75.582	5.631	24.418	80.820	6.966	19.180
2000	95.148	6.322	4.852	95.444	5.790	4.556

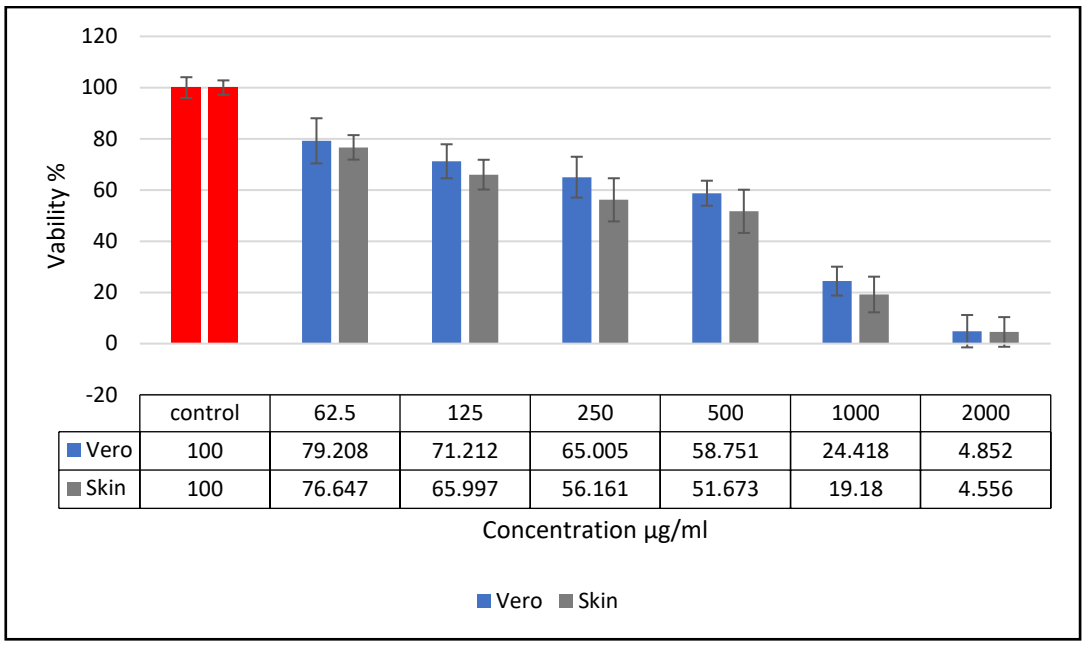

Figure 4-28. Effects of magnetic nano binary oxide Fe_xO_y/SiO_2 on the viability of Skin cancer A431cells line and Vero cells-101line MTT assay.

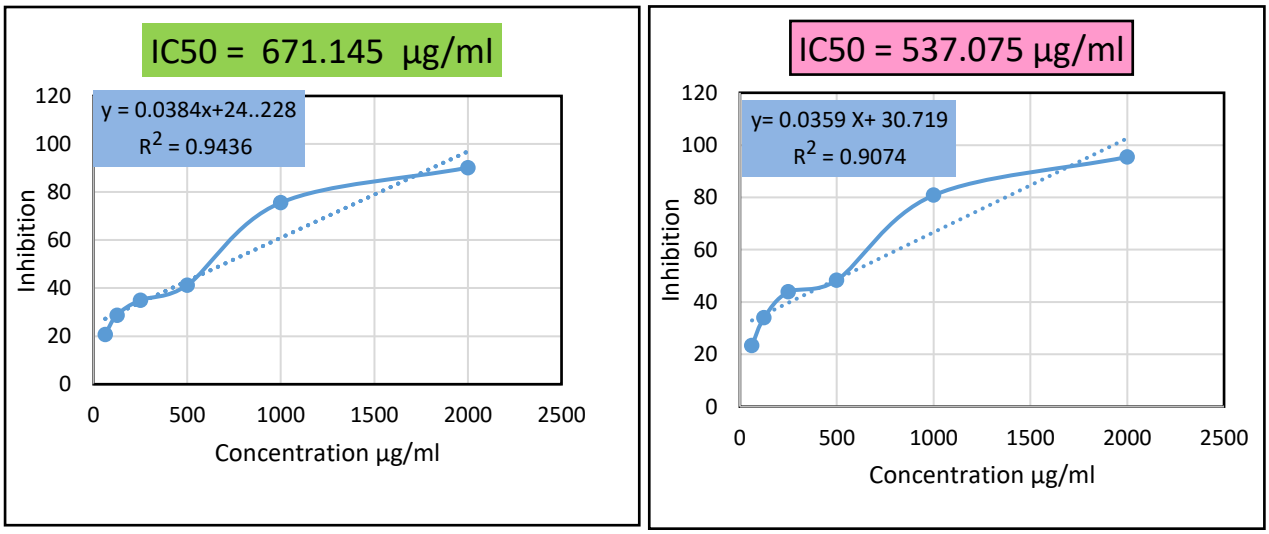

Figure4-29. IC50 measurements of magnetic nano binary oxide Fe_xO_y/SiO_2 on skin cancer line A431cells (right) and Vero cells-101line (left).

The MTT cell viability assay results of silica oxide prepared from rice husk ash to evaluate the cytotoxicity of it on skin cancer line A431cells and Vero cells-101line as shown in table 4-23 and figure (4-30)

The use of silica nanoparticles (SiO_2 NPs) in medicine opens up new possibilities in biosensors, medication delivery, and cancer therapy [245]. However, concerns have been expressed about the potentially toxic and detrimental consequences of SiO_2 NPs. The purpose of this study is to look at the phenomenon of cytotoxicity Silica oxide NPs size 35 nm at calcination temperature 500 ˚C produced dose-dependent cytotoxicity on both types of cells in human skin cancer cells -line(A431) and Vero cell line 101 concentration range (2000,1000,500,250,125, and 62.5) µg/ml as evidenced by the MTT cell viability assay. This assay is based on the ability of mitochondrial succinate dehydrogenase enzyme to convert yellow tetrazolium dye into formazan crystal. The tetrazolium ring of MTT is cleaved and it is reduced to a purple formazan, which is then solubilized by DMSO. That provided rapid and complete solubilization of formazan crystal. The rate of formazan crystal formation is directly proportional to cell viability (ig reflects the enzymatic activity of the living cells [244] which is measured in terms of optical density. Results showed a statistically significant increase in cell viability at low a concentration of 62.5 µg/ml and a decrease in cell viability at concentrations of (2000 and 1000) µg/ml when compared to the control group. The half-maximal inhibitory concentration (IC50) of Silica oxide NPs size 35 nm are (919.371 and 1220.641) µg/ml for skin cancer line A431cells and Vero cells-101line respectively. According to the mechanics of previous studies to deal with nano-oxides with cancer cells is suggested that silica oxide NPs cause cytotoxicity and apoptosis in skin cancer line A431cells and Vero cells-101line at high concentration, which is most likely mediated by ROS production and oxidative stress [245].

Table 4-23. Cytotoxicity effect of nano-silica oxide NPs on skin cancer A431 cells line and Vero cells-101line and data are presented as mean ± SD of four independent experiments.

Vero cells-101line				Skin cancer A431cells line		
Concentration µg/ml	**Inhibition**	**Stander Deviation %SD**	**Average %**	**Inhibition**	**Stander Deviation %SD**	**Average %**
control	-	7.564	100	-	6.310	100
62.5	2.855	6.741	97.145	2.456	4.024	97.544
125	5.813	7.688	94.186	5.300	5.040	92.700
250	9.842	8.942	90.157	13.788	4.406	86.212
500	28.55	7.831	71.450	39.294	6.832	60.706
1000	43.509	7.935	56.491	76.084	6.952	23.916
2000	78.145	10.743	20.855	88.88	5.954	11.120

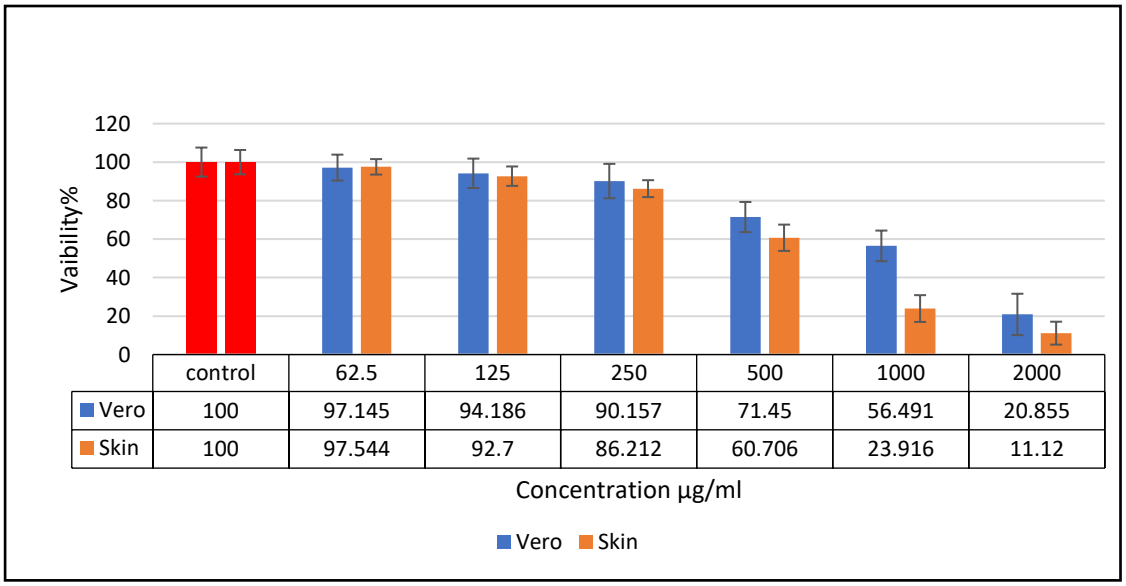

Figure 4-30. Effects of nano-silica oxide extracted from rice husk ash on the viability of Skin cancer A431 line cell line and Vero cells-101line using MTT assay.

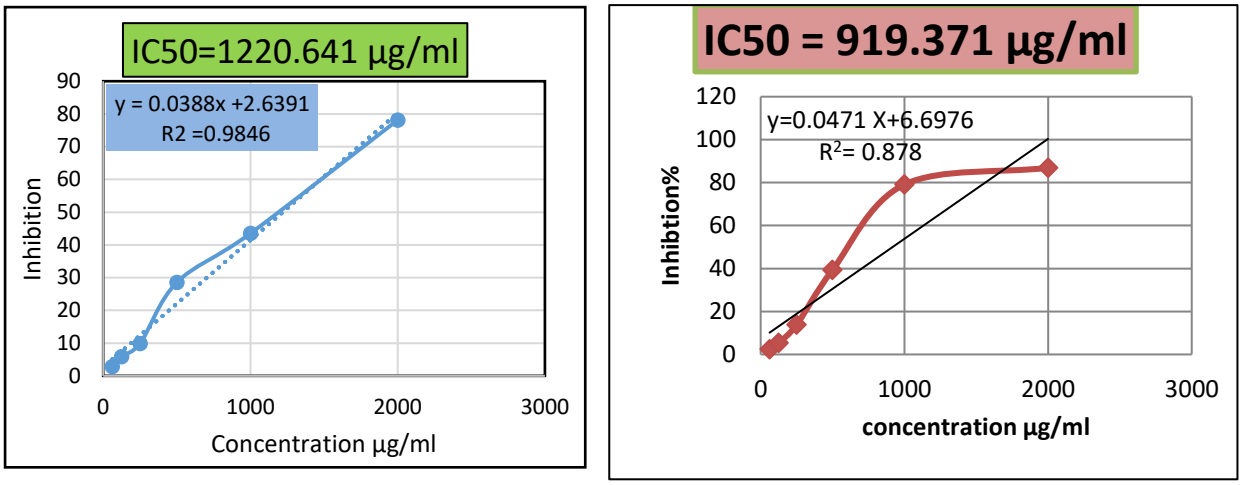

Figure 4-31. IC50 measurements of nano-silica oxide extracted from rice husk ash on skin cancer line A431cells (right) and Vero cells-101line (left).

It is concluded from the current study when comparing the results of half-half-maximal inhibitory concentration (IC50) for four preparation nanoparticle oxides. It is found that the toxicity of the prepared oxides on the Vero cells 101 line is as follows:

Fe_xO_y /SiO_2 > SiO_2/V_2O_5 >E4-MG-50>Silica oxide.

Nano silica oxide prepared from RHA is less toxic as it needs the highest concentration of IC50 1220 µg/ml when compared with other oxides to inhibit the growth of 50% of Vero cells- 101 line (normal cells). While the magnetic nano binary oxide Fe_xO_y/SiO_2 is considered the highest toxicity as it needs the lowest concentration of IC50 671.145 µg/ml to inhibit the growth of Vero cells- 101 line to 50%. While other oxides (SiO_2/V_2O_5 and E4-MG-50) showed promising and selective results towards the toxicity of natural and cancerous cells, as well as the high effectiveness against microbes as shown in the previous paragraphs.

The study showed promising results for the production of medical treatments that have high selective efficacy, as the prepared oxides

showed toxicity against human skin cancer cells –line (A431). When comparing the results of the half-half-maximal inhibitory concentration (IC50) was founded that MgO/ Silica oxide (E4-MG-50) has perfect activity against human skin cancer cells -line(A431) with IC50 214.122 µg/ml.

5-1 Conclusions

1. Each 10 g of RHA can produce 1 gram from high-quality amorphous nano silica oxide (SiO_2NPs) powder. Then, the process could be used for production on an industrial scale.

2. Particle grain size of Silica oxide and nano binary oxide of SiO_2/V_2O_5, MgO/SiO_2, and Fe_xO_y/SiO_2 affected by calcination temperatures.

3. The antibacterial activity is more activity against Gram-negative bacterium (*E.Coli*) than Gram-positive ones (*S.aureas*). The fabricated nanoparticles are spherical having various size ranges in nanometer.

4. Silica oxide and nano binary oxide of SiO_2/V_2O_5, MgO/SiO_2, and Fe_xO_y/SiO_2 nanoparticles show potential performance as an antimicrobial against Gram-negative bacterium *Pseudomonas* Which is characterized by its high resistance to many antibiotics.

5. The present study demonstrates that the MIC and MBC for nano binary oxide of SiO_2/V_2O_5, MgO/SiO_2, and Fe_xO_y/SiO_2 are much lower than of nano-silica oxide that calculation of inhibition growth by turbidity method.

6. Antibiotic activity of nano binary oxide MgO/SiO_2 > SiO_2/V_2O_5> Fe_xO_y/SiO_2> and Silica oxide nanoparticles show zone inhibition when applying them to the medical wound dressing.

7. Medical ointment creams preparation for best antibiotics activity of nano binary oxide MgO/SiO_2 and SiO_2/V_2O_5 nanoparticles. It gave promising results to use it as an antibacterial against (*S.aureas*) for the treatment of bacterial burns and wounds.

8. Silica nanoparticles show very low toxicity against Vero cell line 101.

9. Silica oxide and nano binary oxide MgO/SiO_2, SiO_2/V_2O_5, and Fe_xO_y/SiO_2 antibiotic nanoparticles have selective cytotoxicity on Vero cell line-101 and skin cancer cell line 431. So can be very useful to use as an anticancer drug.

5-2 Recommendations

1. Application of wound dresses and medical ointment on laboratory animals to use on humans.
2. Study the effect of prepared nanomaterials on another cancer line.
3. Investigation of the effect of prepared nanomaterials on anti-fungal instead of bacteria.
4. Silica oxide NPs composited with another type of inorganic or organic oxide nanomaterials.

5-3 Reference

1. Sengupta, J., Ghosh, S., Datta, P., Gomes, A., and Gomes, A. "Physiologically important metal nanoparticles and their toxicity." Journal of nanoscience and nanotechnology.Vol. 14(1) (2014): 990-1006.

2. Mahmoud ,N.S., Mohammad ,S. S. and Zahra, I . Book: An Introduction to Green Nanotechnology."Applications of nanotechnology in daily life." Interface Science and Technology. Chapter 4.Vol. 28 (2019): 113-143.

3. Suttee, A, and Neeraj, C. "Nanotechnology Applications in Medicine " .Nanotechnology. Book 1st Edition, (2020): 45-60.

4. Cai, P., Zhang, X., Wang, M., Wu, Y. L., and Chen, X. "Combinatorial nano–bio interfaces." ACS nano. Vol.12(6) (2018): 5078-5084.

5. Stanicki, D., Vangijzegem, T., Ternad, I., and Laurent, S. "An update on the applications and characteristics of magnetic iron oxide nanoparticles for drug delivery." Expert Opinion on Drug Delivery. Vol. 19(3) (2022): 321-335.

6. Al-Fartusie, Falah S., and Saja N. Mohssan. "Essential trace elements and their vital roles in human body." Indian J Adv Chem Sci .Vol.5 (3)(2017): 127-136.

7. Singh, J., Dutta, T., Kim, K. H., Rawat, M., Samddar, P., and Kumar, P. "Green synthesis of metals and their oxide nanoparticles: applications for environmental remediation." Journal of nanobiotechnology .Vol. 16(1) (2018): 1-24.

8. Usman, K. A. S., Maina, J. W., Seyedin, S., Conato, M. T., Payawan, L. M., Dumée, L. F., and Razal, J. M."Downsizing metal–organic frameworks by bottom-up and top-down methods." NPG Asia Materials .Vol.12(1) (2020): 1-18.

9. Yadav, Thakur Prasad, R. Manohar Yadav, and D. Pratap Singh. "Mechanical milling: a top down approach for the synthesis of nanomaterials and nanocomposites." Nanoscience and Nanotechnology .Vol. 2 (3)(2012): 22-48.

10. Lopez-Serrano, A., Olivas, R. M., Landaluze, J. S., and Camara, C. "Nanoparticles: a global vision. Characterization, separation, and quantification methods. Potential environmental and health impact." Analytical Methods .Vol.6 (1)(2014): 38-56.

11. Zottel, Alja, Alja Videtic Paska, and Ivana Jovcevska. "Nanotechnology meets oncology: nanomaterials in brain cancer research, diagnosis and therapy." Materials.Vol. 12(10) (2019): 1-28.

12. Kaul, S., Gulati, N., Verma, D., Mukherjee, S., and Nagaich, U.. Role of nanotechnology in cosmeceuticals: a review of recent advances. Journal of pharmaceutics. Vol.2018 (2018):1-19.

13. Jeyaraj, M., Gurunathan, S., Qasim, M., Kang, M. H., and Kim, J. "A comprehensive review on the synthesis, characterization, and biomedical application of platinum nanoparticles." Nanomaterials .Vol.9 (12)(2019): 1-41.

14. Pokropivny, V.V. and Skorokhod, V.V. "Classification of nanostructures by dimensionality and concept of surface forms engineering in nanomaterial science". Mater. Sci. Eng. Vol.27(5-8) (2007) :990–993.

15. Tiwari, J.N., Tiwari, R.N.and Kim, K.S. "Zero-dimensional, one-dimensional, two-dimensional and three-dimensional nanostructured materials for advanced electrochemical energy devices". Prog. Mater. Sci.Vol.57(4) (2012) :724–803.

16. Abobatta,and Waleed Fouad. "Nanotechnology application in agriculture." Acta Scientific Agriculture.Vol. 2(6) (2018): 99-102.

17. Marslin, G., Siram, K.; Maqbool, Q., Selvakesavan, R.K., Kruszka, D.; Kachlicki, P., Franklin, G." Secondary Metabolites in the Green Synthesis of Metallic" Nanoparticles. Materials.Vol.11(6)(2018): 1-25.

18. Hu, X., Zhang, Y., Ding, T., Liu, J., and Zhao, H.. "Multifunctional gold nanoparticles: a novel nanomaterial for various medical applications and biological activities." *Frontiers in* Bioengineering and Biotechnology .Vol (8) (2020): 1-17.

19. Mukherjee, B., Dey, N. S., Maji, R., Bhowmik, P., Das, P. J., and Paul, P. "Current status and future scope for nanomaterials in drug delivery." *Application of nanotechnology in drug delivery*. IntechOpen.Chapter.16(2014):1-20.

20. Yang, Bowen, Yu Chen, and Jianlin Shi. "Nanocatalytic medicine." Advanced Materials.Vol 31(39) (2019): 1-45.

21. Shankar, P. D., Shobana, S., Karuppusamy, I., Pugazhendhi, A., Ramkumar, V. S., Arvindnarayan, S., and Kumar, G. "A review on the biosynthesis of metallic nanoparticles (gold and silver) using bio-components of microalgae: Formation mechanism and applications." Enzyme and Microbial Technology .Vol.95 (2016): 28-44.

22. Kalantari, K., Mostafavi, E., Afifi, A. M., Izadiyan, Z., Jahangirian, H., Rafiee-Moghaddam, R., and Webster, T. J.. "Wound dressings functionalized with silver nanoparticles: promises and pitfalls." Nanoscale.Vol. 12 (4)(2020): 2268-2291.

23.Reshma, S. C., and P. V. Mohanan. "Graphene: a multifaceted nanomaterial for cutting edge biomedical application." Int J Med Nano Res .Vol.1.003 (2014):1-16.

24. Ediyilyam, S., Lalitha, M. M., George, B., Shankar, S. S., Wacławek, S., Cerník, M., and Padil, V. V. T. "Synthesis, Characterization and Physicochemical Properties of Biogenic Silver Nanoparticle-Encapsulated Chitosan Bionanocomposites." Polymers .Vol.14(3) (2022): 1-15.

25. Kwiatkowska, A., Drabik, M., Lipko, A., Grzeczkowicz, A., Stachowiak, R., Marszalik, A., and Granicka, L. H. "Composite Membrane Dressings System with Metallic Nanoparticles as an Antibacterial Factor in Wound Healing." Membranes.Vol. 12(2) (2022): 1-25.

26. Jiang, Z., Zhao, L., He, F., Tan, H., Li, Y., Tang, Y., and Li, Y. "Palmatine-loaded electrospun poly (ε-caprolactone)/gelatin nanofibrous scaffolds accelerate wound healing and inhibit hypertrophic scar formation in a rabbit ear model." Journal of Biomaterials Applications .Vol.35 (2021): 869-886.

27.Jeyaraj, Muniyandi, "A comprehensive review on the synthesis, characterization, and biomedical application of platinum nanoparticles." Nanomaterials .Vol.9 (12)(2019): 1-41.

28. Zhou, F., Zhu, Y., Yang, L., Yang, D. Q., and Sacher, E.. "Ag NP catalysis of Cu ions in the preparation of AgCu NPs and the mechanism of their enhanced antibacterial efficacy." Colloids and Surfaces A: Physicochemical and Engineering Aspects .Vol.632 (2022): 127831.

29. Trace, Djalal, Vijay Kumar Thakur, and Rabah Boukherroub. "Cellulose nanocrystals/graphene hybrids-a promising new class of materials for advanced applications." Nanomaterials.Vol. 10(8) (2020): 1-34.

30. Agi, Augustine,. "Synthesis and application of rice husk silica nanoparticles for chemical enhanced oil recovery." Journal of Materials Research and Technology .Vol.9 (2020): 13054-13066.

31. Khan, Ibrahim, Khalid Saeed, and Idrees Khan. "Nanoparticles: Properties, applications and toxicities." Arabian journal of chemistry .Vol.12(7) (2019): 908-931.

32. Naika, H. Raja,. "Green synthesis of CuO nanoparticles using Gloriosa superba L. extract and their antibacterial activity." Journal of Taibah University for Science.Vol. 9(1) (2015): 7-12.

33. Gross, Erin M. "Green chemistry and sustainability: An undergraduate course for science and nonscience majors." Journal of Chemical Education .Vol.90 (4) (2013): 429-431.

34. Sasidharan, S., Raj, S., Sonawane, S., Sonawane, S., Pinjari, D., Pandit, A. B., and Saudagar, P. "Nanomaterial synthesis: chemical and biological route and applications. " Nanomaterials Synthesis. Elsevier, Chapter 2 (2019): 27-51.

35. Zimmerman, Julie B., Paul T. Anastas, and Hanno C. Erythrope." Designing for a green chemistry future". Science. Vol.367(6476) (2020): 397-400.

36.Dunn, Peter J. The importance of green chemistry in process research and development. Chemical Society Reviews.Vol.41(4)(2012): 1452-1461

37. Pirtarighat, S, Ghannadnia, Maryam,and Baghshahi, S. "Green synthesis of silver nanoparticles using the plant extract of Salvia spinosa grown in vitro and their antibacterial activity assessment". Journal of Nanostructure in Chemistry. Vol.9(1) (2019): 1-9.

38.Nambela, Lutamyo, Haule, Liberato Venant,and Mgani, Q." A review on source, chemistry, green synthesis and application of textile colorants". Journal of Cleaner Production. Vol. 246(10)(2020): 119036.

39.Lee, Xin Jiat,. "Review on graphene and its derivatives: Synthesis methods and potential industrial implementation". Journal of the Taiwan Institute of Chemical Engineers. Vol.98 (2019): 163-180.

40.Dabrowska, Sylwia,." Current trends in the development of microwave reactors for the synthesis of nanomaterials in laboratories and industries: a review". Crystals. Vol.8(10) (2018): 1-26.

41.Mehwish, and Hafiza Mahreen, . "Green synthesis of a silver nanoparticle using Moringa oleifera seed and its applications for antimicrobial and sun-light mediated photocatalytic water detoxification". Journal of Environmental Chemical Engineering.Vol. 9(4)(2021): 1-13.

42.Bian, Huiyang . "Producing wood-based nanomaterials by rapid fractionation of wood at 8° C using a recyclable acid hydrotrope". Green Chemistry. Vol.19(14)(2017): 3370-3379.

43. Zhu, Kai, . Magnetic nanomaterials: Chemical design, synthesis, and potential applications. Accounts of chemical research. Vol. 51(2)(2018): 404-413.

44. Gul, S., Yousuf, M. A., Anwar, A., Warsi, M. F., Agboola, P. O., Shakir, I., and Shahid, M. "Al-substituted zinc spinel ferrite nanoparticles: Preparation and evaluation of structural, electrical, magnetic and photocatalytic properties." Ceramics International .Vol. 46(9) (2020): 14195-14205.

45. Irshad, M. A., Nawaz, R., ur Rehman, M. Z., Adrees, M., Rizwan M., Ali, S., and Tasleem, S. "Synthesis, characterization and advanced sustainable applications of titanium dioxide nanoparticles: A review." Ecotoxicology and environmental safety.Vol. 212 (2021): 1-14.

46. Kumar, S., Jain, S., Nehra, M., Dilbaghi, N., Marrazza, G., and Kim, K. H."Green synthesis of metal–organic frameworks: A state-of-the-art review of potential environmental and medical applications." Coordination Chemistry Reviews .Vol.420 (2020): 1-27.

47. Srivastava, R. K., Shetti, N. P., Reddy, K. R., Kwon, E. E., Nadagouda, M. N., and Aminabhavi, T. M. "Biomass utilization and production of biofuels from carbon neutral materials." Environmental Pollution.Vol. 276 (2021): 1-25.

48. Naidu, R., Biswas, B., Willett, I. R., Cribb, J., Singh, B. K., Nathanail, C. P., and Aitken, R. J. "Chemical pollution: A growing peril and potential catastrophic risk to humanity." Environment International.Vol. 156 (2021): 1-12.

49. Ivankovic, A., Dronjić, A., Bevanda, A. M., and Talic, S. . "Review of 12 principles of green chemistry in practice." International Journal of Sustainable and Green Energy.Vol. 6(3) (2017): 39-48.

50. Habeeb, Ghassan Abood, and Hilmi Bin Mahmud. "Study on properties of rice husk ash and its use as cement replacement material." Materials research.Vol. 13(2)(2010): 185-190.

51.Gheorghita Puscaselu, R., Lobiuc, A., Dimian, M., and Covasa, M.. "Alginate: From food industry to biomedical applications and management of metabolic disorders." Polymers.Vol. 12(10) (2020): 1-28.

52. Sharma, D., Rajput, J., Kaith, B. S., Kaur, M., and Sharma, S." Synthesis of ZnO nanoparticles and study of their antibacterial and antifungal properties". Thin solid films.Vol. 519(3) (2010): 1224-1229.

53. Singh, A., Singh, N. B., Hussain, I., Singh, H., and Singh, S. C." Plant-nanoparticle interaction: an approach to improve agricultural practices and plant productivity. Int J Pharm Sci Invent.Vol. 4(8) (2015): 25-40.

54. Parihar, V., Raja, M., and Paulose, R.. A brief review of structural, electrical and electrochemical properties of zinc oxide nanoparticles. Reviews on Advanced Materials Science.Vol. 53(2) (2018):119-130.

55. Bernholc, J., Roland, C., and Yakobson, B. I." Nanotubes". Current Opinion in Solid State and Materials Science, 2(6), (1997): 706-715.

56. Amen, R., Mukhtar, A., Saqib, S., Ullah, S., Al-Sehemi, A. G. Mehdi, S. E. H., and Bustam, M. A.,. "History and development of nanomaterials." Nanomaterials: Synthesis, Characterization, Hazards and Safety. Elsevier, chapter 1 (2021): 1-14.

57. Singh, Veer, Priyanka Yadav, and Vishal Mishra. "Recent advances on classification, properties, synthesis, and characterization of nanomaterials." Green Synthesis of Nanomaterials for Bioenergy Applications .chapter 3(2020): 83-97.

58. Silver, Simon, Le T. Phung, and Gregg Silver. "Silver as biocides in burn and wound dressings and bacterial resistance to silver compounds." Journal of Industrial Microbiology and Biotechnology .Vol.33(7)(2006): 627-634.

59. Zheng, K., Setyawati, M. I., Leong, D. T., and Xie, J.. "Antimicrobial silver nanomaterials." Coordination Chemistry Reviews .Vol.357 (2018): 1-17.

60.Fox Jr, Charles L., and Shanta M. Modak. "Mechanism of silver sulfadiazine action on burn wound infections." Antimicrobial agents and chemotherapy .Vol.5(6)(1974): 582-588.

61. Modak, Shanta M., Lester Sampath, and C. L. Fox Jr. "Combined topical use of silver sulfadiazine and antibiotics as a possible solution to bacterial resistance in burn wounds." The Journal of burn care and rehabilitation.Vol. 9(4) (1988): 359-363.

62. Colino, Clara I., Jose M. Lanao, and Carmen Gutiérrez-Millan. "Recent advances in functionalized nanomaterials for the diagnosis and treatment of bacterial infections." Materials Science and Engineering.Vol.121(2021): 1-22.

63. Wang, Y., Malkmes, M. J., Jiang, C., Wang, P., Zhu, L., Zhang, H., and Jiang, L.. "Antibacterial mechanism and transcriptome analysis of ultra-small gold nanoclusters as an alternative of harmful antibiotics against Gram-negative bacteria." Journal of Hazardous Materials.Vol.416 (2021): 1-13.

64. Shahzadi, Shamaila, Nosheen Zafar, and Rehana Sharif. "Antibacterial activity of metallic nanoparticles." Bacterial pathogenesis and antibacterial control.Chapter3.Vol. 51 (2018):51-70.

65. Dizaj SM, Lotfipour F, Barzegar-Jalali M, Zarrintan MH, and Adibkia K. "Antimicrobial activity of the metals and metal oxide nanoparticles. Materials Science and Engineering .Vol.44(2014):278-284.

66. Raffi M, Hussain F, Bhatti TM, Akhter JI, Hameed A,and Hasan MM. "Antibacterial characterization of silver nanoparticles against E. coli ATCC-15224". Journal of Material Science and Technology. Vol.24(2) (2008):192-196.

67. Baek YW, An YJ. Microbial toxicity of metal oxide nanoparticles (CuO, NiO, ZnO, and Sb_2O_3) to Escherichia coli, Bacillus subtilis, and Streptococcus aureus. Science of the Total Environment. Vol. 409 (8)(2011):1603-160 .

68. Prabhu, Sukumaran, and Eldho K. Poulose. "Silver nanoparticles: mechanism of antimicrobial action, synthesis, medical applications, and toxicity effects." International nano letters.Vol. 2(1) (2012): 1-10.

69. Dutta RK, Nenavathu BP, Gangishetty MK, and Reddy AVR." Studies on antibacterial activity of ZnO nanoparticles by ROS induced lipid peroxidation". Colloids Surfaces B Bio interfaces.Vol.94(2012):143-150.

70. Jung WK, Koo HC, Kim KW, Shin S, Kim SH, and Park YH. Antibacterial activity and mechanism of action of the silver ion in Staphylococcus aureus and Escherichia coli. Applied of Environmental Microbiology. Vol. 74(7) (2008):1-9.

71. Haase, H., Jordan, L., Keitel, L., Keil, C., and Mahltig, B.. "Comparison of methods for determining the effectiveness of antibacterial functionalized textiles." PLoS One .Vol.12(11) (2017): 1-16.

72. Kyrosi L, Rodio M, Domotor D, Kovács T, Papp S,and Diaspro A, "Intartaglia R, Beke S. Ultrasmall, ligand-free Ag nanoparticles with high antibacterial activity prepared by pulsed laser ablation in liquid". Hindawi Publishing Corporation Journal of Chemistry.Vol.2016 (2016): 1-9.

73. da Silva Junior, A. G., Frias, I. A., Lima-Neto, R. G., Sa, S. R., Oliveira, M. D., and Andrade, C. A"Concanavalin A differentiates gram-positive bacteria through hierarchized nanostructured transducer." Microbiological Research.Vol. 251 (2021): 1-9.

74. Tavares, T. D., Antunes, J. C., Padrao, J., Ribeiro, A. I., Zille, A., Amorim, M. T. P., and Felgueiras, H. P. "Activity of specialized biomolecules against gram-positive and gram-negative bacteria." Antibiotics .Vol.9(6) (2020): 1-16.

75. Suresh Kumar Kailasa, Tae-Jung Park ,J igneshkumar V. Rohit and Janardhan Reddy Koduru. "Antimicrobial activity of silver nanoparticles." Nanoparticles in pharmacotherapy. William Andrew Publishing Chapter14. (2019): 461-484.

76. Diganta Hatiboruah, Damayanti Y. Devi , Nima D. Namsa, and Pabitra Nath . Turbidimetric analysis of growth kinetics of bacteria in the laboratory environment using smartphon. n Journal of Biophotonics.13(8) (2021):1-8.

77. Zafar N, Shamaila S, Nazir J, Sharif R, Rafique MS, Hasan J, Ammara S, Khalid H. "Antibacterial action of chemically synthesized and laser generated silver nanoparticles against human pathogenic bacteria". Journal of Material Science and Technology.Vol. 32(8) (2016):721-728.

78. Zhen-Xing T and Bin-Feng L. "MgO Nanoparticles as antibacterial agent: preparation and activity and ". Brazilian Journal of Chemical Engineering. Vol. 31(3) (2014):591-601.

79. Grace AN, Pandian K. Antibacterial efficacy of amino glycosidic antibiotics protected gold nanoparticles—A brief study. Colloids and Surfaces A: Physicochemical and Engineering Aspects.Vol.297(1-3) (2007):63-70.

80. Nagoba, B. S., Gandhi, R. C., Hartalkar, A. R., Wadher, B. J., and Selkar, S. P. "Simple, effective and affordable approach for the treatment of burns infections." Burns .Vol.36(8)(2010): 1242-1247.

81. Lu, J., Yang, M., Zhan, M., Xu, X., Yue, J., and Xu, T.. "Antibiotics for treating infected burn wounds." The Cochrane database of systematic reviews .Vol.2017(7) (2017):1-11.

82. Amira A Bhalodi, Tjitske S R van Engelen, Harjeet S Virk, and W Joost Wiersinga. "Impact of antimicrobial therapy on the gut microbiome." Journal of Antimicrobial Chemotherapy .Vol.74 (2019): 1-10.

83 . Church, D., Elsayed, S., Reid, O., Winston, B., and Lindsay, R. "Burn wound infections." Clinical microbiology reviews .Vol.19(2) (2006): 403-434.

84. Roberts, Derek J., and Richard I. Hall. "Drug absorption, distribution, metabolism and excretion considerations in critically ill adults." Expert opinion on drug metabolism & toxicology .Vol.9(9) (2013): 1067-1084.

85. Laurie C. D'Avignon, MD, Jeffrey R. Saffle, MD, Kevin K. Chung, MD, and Leopoldo C. Cancio, MD. "Prevention and management of infections associated with burns in the combat casualty." Journal of Trauma and Acute Care Surgery.Vol. 64(3) (2008): 5277-5286.

86. Harper, Daniel, Alistair Young, and Clare-Ellen McNaught. "The physiology of wound healing." Surgery (Oxford) .Vol.32(9) (2014): 445-450.

87. Kucharzewski, M., Rojczyk, E., Wilemska-Kucharzewska, K., Wilk, R., Hudecki, J., and Los, M. J.. "Novel trends in application of stem cells in skin wound healing." European journal of pharmacology.Vol. 843 (2019): 307-315.

88. Han, George, and Roger Ceilley. "Chronic wound healing: a review of current management and treatments." Advances in therapy .Vol.34(3) (2017): 599-610.

89. Bryant, Ruth, and Denise Nix. Acute and chronic wounds: current management concepts. Elsevier Health Sciences. 5 edition Chapter 32(2015):487.

90. Verdolino, D. V., Thomason, H. A., Fotticchia, A., and Cartmell, S. "Wound dressings: curbing inflammation in chronic wound healing." Emerging Topics in Life Sciences .Vol.5(4) (2021): 523-537.

91. Nqakala, Z. B., Sibuyi, N. R., Fadaka, A. O., Meyer, M., Onani, M. O., and Madiehe, A. M. "Advances in Nanotechnology towards Development of Silver Nanoparticle-Based Wound-Healing Agents." International journal of molecular sciences.Vol. 22(20) (2021): 1-26.

92. Stoica, Alexandra Elena, Cristina Chircov, and Alexandru Mihai Grumezescu. "Nanomaterials for wound dressings: an up-to-date overview." Molecules .Vol.25(11) (2020): 1-25.

93. Naskar, Atanu, and Kwang-sun Kim. "Recent advances in nanomaterial-basedwound-healing therapeutics." Pharmaceutics .Vol.12(6)(2020): 1-20.

94. Basavegowda, Nagaraj, and Kwang-Hyun Baek. "Multimetallic Nanoparticles as Alternative Antimicrobial Agents: Challenges and Perspectives." Molecules.Vol. 26(4) (2021): 1-21.

95. Zwietering, M. H., Jongenburger, I., Rombouts, F. M., and Van't Riet, K. J. A. E. M "Modeling of the bacterial growth curve." Applied and environmental microbiology .Vol.56(6) (1990): 1875-1881.

96 .Todkar, Bajirao S., Onkar A. Deorukhkar, and Satyajeet M. Deshmukh. "Extraction of silica from rice husk." International Journal of Engineering Research and Development .Vol.12(3) (2016): 69-74.

97. Japhet, J. A., A. Tokan, and M. H. Muhammad. "Production and characterization of rice husk pellet." American Journal of Engineering Research (AJER) .Vol.4(12) (2015): 112-119.

98. Dizaji, H. B., Zeng, T., Holzig, H., Bauer, J., Kloß, G., and Enke, D.. "Ash transformation mechanism during combustion of rice husk and rice straw." Fuel .Vol.307 (2022): 1-18.

99. Subbukrishna, D. N., Suresh, K. C., Paul, P. J., Dasappa, S., and Rajan, N. K. S. "Precipitated silica from rice husk ash by IPSIT process." 15th European Biomass Conference & Exhibition.Vol.7(11)(2007):1-4.

100. Thuc, Chi Nhan Ha, and Huy Ha Thuc. "Synthesis of silica nanoparticles from Vietnamese rice husk by sol–gel method." Nanoscale research letters .Vol.8(1) (2013): 1-10.

101. Amutha, K., R. Ravibaskar, and G. Sivakumar. "Extraction, synthesis and characterization of nanosilica from rice husk ash." International Journal of Nanotechnology and applications.Vol. 4(1) (2010): 61-66.

102. Laad, Meena, Rinku Datkhile, and S. Shanmugan. "Synthesis and Characterization of Powder Silica: A Judicious Recycling of the Natural Ceramic Rice Husk Ash." Silicon .Vol.14(3)(2021): 1123–1132.

103. Usgodaarachchi, L., Thambiliyagodage, C., Wijesekera, R., and Bakker, M. G. "Synthesis of mesoporous silica nanoparticles derived from rice husk and surface-controlled amine functionalization for efficient adsorption of methylene blue from aqueous solution." Current Research in Green and Sustainable Chemistry .Vol.4 (2021): 1-11.

104. Huang, C. H., Chang, K. P., Ou, H. D., Chiang, Y. C., and Wang, C.F "Adsorption of cationic dyes onto mesoporous silica." Microporous and Mesoporous Materials .Vol 141(1-3) (2011): 102-109.

105. Nelson Martinez, B.S. Wettability of silicon, silicon dioxide, and organosilicate glass, Thesis Prepared for the Degree of master of science ,university of north Texas December Department of Materials Science and Engineering 2009.

106. Fernandes, I. J., Calheiro, D., Sanchez, F. A., Camacho, A. L. D. Rocha, T. L. A. D. C., Moraes, C. A. M., and Sousa, V. C. D.,. "Characterization of silica produced from rice husk ash: comparison of purification and processing methods." Materials Research.Vol. 20 (2)(2017): 512-518.

107. Kalapathy U, Proctor A, Shultz J. A simple method for production of pure silica from rice hull ash . Bioresource Technology Vol.73(3) (2000):257-262.

108 . Yao, Jun, Mei Yang, and Yixiang Duan. "Chemistry, biology, and medicine of fluorescent nanomaterials and related systems: new insights into biosensing, bioimaging, genomics, diagnostics, and therapy." Chemical reviews.Vil. 114(12)(2014): 6130-6178.

109. Il'Ves, Vladislav G., Michael G. Zuev, and Sergey Yu Sokovnin. "Properties of silicon dioxide amorphous nanopowder produced by pulsed electron beam evaporation." Journal of Nanotechnology .Vol.2015 (2015):1-9.

110. Huan, Chang, and Sun Shu-Qing. "Silicon nanoparticles: Preparation, properties, and applications." Chinese Physics B.Vol. 23(8) (2014): 1-14.

111. Farahmandjou, M., and N. Abaeiyan. "Chemical synthesis of vanadium oxide (V_2O_5) nanoparticles prepared by sodium metavanadate." Journal of Nanomedicine Research.Vol. 5(1) (2017): 1-4.

112. Chen, R. S., Wang, W. C., Chan, C. H., Hsu, H. P., Tien, L. C., and Chen, Y. J. "Photoconductivities in monocrystalline layered V_2O_5 nanowires grown by physical vapor deposition." Nanoscale research letters Vol. 8(1) (2013): 1-8.

113. Letifi, H., Litaiem, Y., Dridi, D., Ammar, S., and Chtourou, R. "Enhanced photocatalytic activity of vanadium-doped SnO_2 nanoparticles in rhodamine B degradation." Advances in Condensed Matter Physics.Vol. 2019 (2019):1-12.

114 .Sun, H., Yang, Z., Pu, Y., Dou, W., Wang, C., Wang, W., and Guo, Z . "Zinc oxide/vanadium pentoxide heterostructures with enhanced day-night antibacterial activities." Journal of colloid and interface science.Vol. 547 (2019): 40-49.

115. Suma, P. R. P., Nair, R. V., Paul, W., and Jayasree, R. S. "Vanadium pentoxide nanoplates: Synthesis, characterization and unveiling the intrinsic anti-bacterial activity." Materials Letters .Vol.269 (2020): 1-13.

116. Murgia, V., Torres, E. M. F., Gottifredi, J. C., and Sham, E. L. "Sol–gel synthesis of V_2O_5–SiO_2 catalyst in the oxidative dehydrogenation of n-butane." Applied Catalysis A: General .Vol.312 (2006): 134-143.

117.Liu, M., Su, B., Tang, Y., Jiang, X., & Yu, A. "Recent advances in nanostructured vanadium oxides and composites for energy conversion." Advanced Energy Materials.Vol. 7(23) (2017): 1-34.

118 .Mousavi, M., M. Nadafan, and Sh Tabatabai Yazdi. "Third-order optical nonlinear properties of Co-doped V_2O_5 nanoparticles ." Optik .Vol.226 (2021): 1-26.

119. Moghaddam, Mohammad, Leila Mehdizadeh, and Zahra Sharifi. "Macro-and microelement content and health risk assessment of heavy

metals in various herbs of Iran." Environmental Science and Pollution Research.Vol 27(11) (2020): 12320-12331.

120.Soetan, K. O., C. O. Olaiya, and O. E. Oyewole. "The importance of mineral elements for humans, domestic animals and plants-A review." African journal of food science .Vol.4(5) (2010): 200-222.

121. Tang, Zhen-Xing, and Bin-Feng Lv. "MgO nanoparticles as antibacterial agent: preparation and activity." Brazilian Journal of Chemical Engineering.Vol. 31 (2014): 591-601.

122 Al-Gaashani, R., Radiman, S., Al-Douri, Y., Tabet, N. and Daud, A. R., Investigation of the optical properties of $Mg(OH)_2$ and MgO nanostructures obtained by microwave-assisted methods. Journal of Alloys and Compounds.Vol. 52(2012): 71-76.

123. Mirzaei, H. and Davoodnia, A., Microwave assisted sol-gel synthesis of MgO nanoparticles and their catalytic activity in the synthesis of hantzsch 1, 4-dihydropyridines. Chinese Journal of Catalysis.Vol. 33(2012):1502-1507.

124. Quaid M, Kenneth R. "Drugs used in the treatment of gastrointestinal diseases." Basic and clinical pharmacology .Chapter 62.Vol.12 (2018): 1087-1114.

125.Di, D. R., He, Z. Z., Sun, Z. Q. and Liu, J., A new nano-cryosurgical modality for tumor treatment using biodegradable MgO nanoparticles. Nanomedicine.Vol.8(2012): 1233-1241.

126. Bindhu, M., RUmadevi, M., Micheal, M. K., Arasu, M. V., and Al-Dhabi, N.. "Structural, morphological and optical properties of MgO nanoparticles for antibacterial applications." Materials Letters.Vol. 166 (2016): 19-22.

127. Yang, J., Cao, X., Zhao, Y., Wang, L., Liu, B., Jia, J., and Chen,M "Enhanced pH stability, cell viability and reduced degradation rate of poly (L-lactide)-based composite in vitro: Effect of modified magnesium oxide nanoparticles." Journal of Biomaterials science, Polymer edition .Vol.28(5)(2017): 486-503.

128. Sengupta, J., Ghosh, S., Datta, P., Gomes, A., and Gomes, A"Physiologically important metal nanoparticles and their toxicity." Journal of nanoscience and nanotechnology .Vol.14(1) (2014): 990-1006.

129. Ankita Sahay. Magnesium Oxide Formula: Structure, Properties, Reactions(2021): 9-16.

130. Ganapathe, L. S., Mohamed, M. A., Mohamad Yunus, R., and Berhanuddin, D. D "Magnetite (Fe_3O_4) nanoparticles in biomedical application: from synthesis to surface functionalisation." Magnetochemistry.Vol. 6(4)(2020): 1-35.

131 .Alahmer, A., Al-Amayreh, M., Mostafa, A. O., Al-Dabbas, M., and Rezk, H. "Magnetic Refrigeration Design Technologies: State of the Art and General Perspectives." Energies .Vol.14(15) (2021): 1-26.

132. Sharma, R. K., Dutta, S., Sharma, S., Zboril, R., Varma, R. S., and Gawande, M. B. . "Fe $_3$ O $_4$ (iron oxide)-supported nanocatalysts: synthesis, characterization and applications in coupling reactions." Green Chemistry .Vol.18(11) (2016): 3184-3209.

133. Marengo-Rowe, Alain J. "Structure-function relations of human hemoglobins." Baylor University Medical Center Proceedings. Vol. 19. (3) (2006) : 239-245.

134. Govan, Joseph, and Yurii K. Gun'ko. "Recent advances in the application of magnetic nanoparticles as a support for homogeneous catalysts." Nanomaterials .Vol.4(2)(2014): 222-241.

135. Poumirol, J. M., Paradisanos, I., Shree, S., Agez, G., Marie, X., Robert, C., ... and Urbaszek, B.. "Unveiling the optical emission channels of monolayer semiconductors coupled to silicon nanoantennas." ACS photonics.Vol. 7(11) (2020): 3106-3115.

136. Amaterz, E., Tara, A., Bouddouch, A., Taoufyq, A., Bakiz, B., Benlhachemi, A., and Jbara, O. "Photo-electrochemical degradation of wastewaters containing organics catalysed by phosphate-based materials: a review." Reviews in Environmental Science and Bio/Technology .Vol. 19 (4)(2020): 843-872.

137. Marchelek, M., Grabowska, E., Klimczuk, T., Lisowski, W., and. Zaleska-Medynska, A "Various types of semiconductor photocatalysts modified by CdTe QDs and Pt NPs for toluene photooxidation in the gas phase under visible light." Applied Surface Science .Vol.393 (2017): 262-275.

138 Mainil, Jacques. "Escherichia coli virulence factors." Veterinary immunology and immunopathology .Vol.152(1-2) (2013): 2-12.

139. Wanger, A., Chavez, V., Huang, R. S. P., Wahed, A., Actor, J. K. and Dasgupta, A. Microbiology and Molecular Diagnosis in Pathology. Elsevier Inc. All Rights Reserved. (2017).

140. Lai, Y. M.; Zaw, M. T.; Aung, T. S. and Lin, Z.. Detection of Sequence Type 131 in Multi-Drug Resistant Uropathogenic Escherichia coli Isolates from Two Hospitals of Sabah. AJP.Vol. 10 (3) (2016): 421-424.

141.Zahraa Hamid Alwan Al-Saadi Phenotypic and molecular detection of Escherichia coli efflux pumps from UTI patients Thesis." Biochem. Cell. Arch.Vol.19 (2019): 2371-2376.

142 . Allocati, N., Masulli, M., Alexeyev, M. F., and Di Ilio, C.. "Escherichia coli in Europe: an overview." International journal of environmental research and public health .Vol.10(12)(2013): 6235-6254.

143. Taylor, Tracey A., and Chandrashekhar G. Unakal. "Staphylococcus aureus." StatPearls (2021).

144. Fair RJ, Tor Y. Antibiotics and bacterial resistance in the 21st century. Perspect Medicin Chem. Vol.6(2014):25-64.

145.Coates M, Lee MJ, Norton D, and MacLeod AS. "The Skin and Intestinal Microbiota and Their Specific Innate Immune Systems". Frontiers in Immunology. Vol. 10(2019): 1-11.

146.Marks, James G., and Jeffrey J. Miller. Lookingbill and Marks' Principles of Dermatology E-Book. Elsevier Health Sciences, chapter 1(2017):1-29.

147. Quintieri, Laura, Francesca Fanelli, and Leonardo Caputo. "Antibiotic resistant Pseudomonas spp. spoilers in fresh dairy products: an underestimated risk and the control strategies." Foods .Vol.8(9)(2019): 1-32 .

148. Zhang, Li, Y., Zeng, J., Chang, Y., Han, S., Zhao, J., and Cao, B. "Risk factors for mortality of inpatients with Pseudomonas aeruginosa bacteremia in China: impact of resistance profile in the mortality." Infection and Drug Resistance.Vol. 13 (2020): 4115–4123.

149. Iglewski BH. Pseudomonas. In: Baron S, editor. Medical Microbiology. 4th edition. Galveston (TX): University of Texas Medical Branch at Galveston,. Chapter 27. (1996).

150. Lynn, Dwight E. "Cell culture." Encyclopedia of Insects. Academic Press, Chapter 39. (2009):144-145.

151.Segeritz, Charis-P., and Ludovic Vallier. "Cell culture: growing cells as model systems in vitro." Basic Science Methods for Clinical Researchers. Academic Press.Chapter9(2017): 151-172.

152. Aslanturk, Ozlem Sultan. Chapter1"In vitro cytotoxicity and cell viability assays: principles, advantages, and disadvantages." Genotoxicity-A predictable risk to our actual world.Vol. 2 (2018): 64-80.

153 . Ammerman, Nicole C., Magda Beier-Sexton, and Abdu F. Azad. "Growth and maintenance of Vero cell lines." Current protocols in microbiology .Vol.11(1) (2008): 1-7.

154. Krishnan, Vinu, and Samir Mitragotri. "Nanoparticles for topical drug delivery: Potential for skin cancer treatment." Advanced Drug Delivery Reviews.Vol 153 (2020): 87-108.

155. Simoes, MC Filipe, JJ Simoes Sousa, and AAC Canelas Pais. "Skin cancer and new treatment perspectives: A review." Cancer letters.Vol 357(1) (2015): 8-42.

156. Kleesz, P., R. Darlenski, and J. W. Fluhr. "Full-body skin mapping for six biophysical parameters: baseline values at 16 anatomical sites in 125 human subjects." Skin pharmacology and physiology .Vol.25(1) (2012): 25-33.

157 .Gordon, Randy. "Skin cancer: an overview of epidemiology and risk factors." Seminars in oncology nursing. Vol. 29 (3) (2013): 160-169.

158.Huaxu G, Na L and Yitai Q." Synthesis of SiO_2/C Nanocomposites and Their Electrochemical Properties". Int. J. Electrochem. Sci.Vol 8(2013): 9811 – 9817.

159. Zhou Mao, Q. W, Min W, Yushi Y, Jia L and Xiaohui C." Tunable synthesis of SiO_2-encapsulated zero-valent iron nanoparticles for degradation of organic dyes" *Nanoscale Research Letters*.Vol. 9(501)(2014):1-9.

160. Bharti, C., Nagaich, U., Pal, A. K., and Gulati, N. . "Mesoporous silica nanoparticles in target drug delivery system: A review." International journal of pharmaceutical investigation 5(3) (2015): 124–133.

161. Liu, X., Yang, Z., Li, X., Zhang, Z., Zhao, M., and Su, C "Preparation of silica-supported nanoFe/Ni alloy and its application in viscosity reduction of heavy oil." Micro and Nano Letters .Vol.10(3)(2015): 167-171.

162 .Ho, V. T. "Preparation and Characterization of Fe/SiO_2 Nanoparticles Composite via Sol-Gel and Chemical Reduction Method." International Journal of Advanced Engineering Research and Science.Vol. 3(7) (2016): 45-49.

163. Zulfiqar, Usama, Tayyab Subhani, and S. Wilayat Husain. "Synthesis of silica nanoparticles from sodium silicate under alkaline conditions." Journal of Sol-Gel Science and Technology .Vol.77(3) (2016): 753-758.

164. Lazareva, S. V., Shikina, N. V., Tatarova, L. E., and Ismagilov, Z. R.. "Synthesis of high-purity silica nanoparticles by Sol-gel method." Eurasian Chemico-Technological Journal .Vol.19(4)(2017): 295-302.

165. Jahanbakhsh, Ali, Sajad Pirsa, and Morteza Bahram. "Synthesis and characterization of magnetic nanocomposites based on Hydrogel-Fe_3O_4 and application to remove of organic dye from waste water." Main Group Chemistry.Vol. 16(2) (2017): 85-94.

166. Yang, E., Lee, J. G., Kim, D. H., Jung, Y. S., Kwak, J. H., Park, E. D., and An, K. . "SiO_2@ V_2O_5@ Al_2O_3 core–shell catalysts with high activity and stability for methane oxidation to formaldehyde." Journal of Catalysis .Vol.368 (2018): 134-144.

167. Taifan, William W. E., Li, Y., Baltrus, J. P., Zhang, L., Frenkel, A. I., and Baltrusaitis, J.. "Operando structure determination of Cu and Zn on supported MgO/SiO_2 catalysts during ethanol conversion to 1, 3-butadiene." ACS Catalysis. Vol9(1)(2018): 269-285.

168. Lee, Dae-Won, Hira Fatima, and Kyo-Seon Kim. "Preparation of silica coated magnetic nanoparticles for bioseparation." Journal of nanoscience and nanotechnology .Vol.18(2) (2018): 1414-1418.

169 .Yadav, Virendra Kumar, and M. H. Fulekar. "Green synthesis and characterization of amorphous silica nanoparticles from fly ash." Materials Today: Proceedings .Vol.18 (2019): 4351-4359.

170. Nemeth, K., Varro, N., Reti, B., Berki, P., Adam, B., Belina, K., andHernadi, K.. "Synthesis and investigation of SiO 2-MgO coated MWCNTs and their potential application." Scientific reports.Vol. 9(1) (2019): 1-11.

171. Abdulrazzaq, H. T., Rahmani Chokanlu, A., Frederick, B. G., and Schwartz, T. J.. "Reaction Kinetics Analysis of Ethanol Dehydrogenation Catalyzed by MgO–SiO_2." ACS Catalysis .Vol.10(11) (2020): 6318-6331.

172.Sastre-Hernández, J., Aguilar-Hernandez, J. R., Santoyo-Salazar, J., Alfaro, H. M., Hoyos-García, J. E., Tufiño-VelázquezM., and Contreras-Puente, G.. "Influence of sodium peroxide during the synthesis of SiO_2 obtained from rice husk." Materials Science in Semiconductor Processing .Vol.114 (2020): 1-5.

173.UsgodaarachchiL., Thambiliyagodage, C., Wijesekera, R., and Bakker, M. G.. "Synthesis of mesoporous silica nanoparticles derived from rice husk and surface-controlled amine functionalization for efficient adsorption of methylene blue from aqueous solution." Current Research in Green and Sustainable Chemistry.Vol.4 (2021): 1-11.

174. Yang, E., Lee, J. G., Park, E. D., and An, K.. "Methane oxidation to formaldehyde over vanadium oxide supported on various mesoporous silicas." Korean Journal of Chemical Engineering .Vol. 38(6)(2021): 1-7.

175. Mohammadi, Somaye, and Hossein Naeimi. "Preparation and Characterization of Hollow MgO/SiO_2 Nanocomposites and using as Reusable Catalyst for Synthesis of 1H-Isochromenes".Springer Silicon " Vol.(14)(8)(2021):1-18.

176. Shi, Shi, J., Ci, Y., Zheng, Y., Chen, W., and Chen, X.. "Submicron silica particles have cytotoxicities on hepatocellular carcinoma, non-small cell lung cancer and breast cancer by unified regulating the XLOC_001659/miR-98-5p/MAP3K2-mediated pathway." Toxicology Research.Vol. 10(4) (2021): 824-834.

177. Pratibha, S J.and Prakash,R,K. "An insight into the green synthesis of SiO_2 nanostructures as a novel adsorbent for removal of toxic water pollutants" Environmental Research.Vol.212(2022): 113328.

178. Uda, M. N. A., Gopinath, S. C., Hashim, U., Halim, N. H., Parmin,"Production and characterization of silica nanoparticles from fly ash: conversion of agro-waste into resource." Preparative biochemistry & biotechnology .Vol.51(1) (2021): 86-95.

179. Sharifnasab, Hooman, and Mohammad Younesi Alamooti. "Preparation of silica powder from rice husk." Agricultural Engineering International: CIGR Journal .Vol.19(1) (2017): 158-161.

180. A Ajeel, Sami, Khalid A Sukkar, and Naser K Zedin. "Chemical Extraction Process for Producing High Purity Nanosilica from Iraqi Rice Husk." Engineering and Technology Journal .Vol.39(1) (2021): 56-63.

181. Isberto, C. D., Labra, K. L., Landicho, J. M. B., and De Jesus, R. "Optimized preparation of rice husk ash (RHA) as a supplementary cementitious material." International Journal of Geomate.Vol.16 (57)(2019): 56-61.

182. Ramasamy, , M., Das, M., An, S. S. A., and Yi, D. K. "Role of surface modification in zinc oxide nanoparticles and its toxicity assessment toward human dermal fibroblast cells." International journal of nanomedicine.Vol. 9 (2014): 3707–3718.

183. Rafiee, H. R., Feyzi, M., Jafari, F., and Safari, B "Preparation and characterization of promoted Fe-V/SiO_2 nanocatalysts for oxidation of alcohols." Journal of Chemistry .Vol.2013 (2013):1-11.

184. Chinenye. N. Ugwu1, Ezinwanne. N. Ezeibe1 , Chinekwu. S. Nwagwu , and Chinelo. C. "Preparation and evaluation of burns wound healing ointment base of leaves and stem bark of Anthocleista djalonensis (L) extract using animal model". International Journal of Pharmaceutical Education and Research.Vol.1(2)(2019):1-8. .

185. Wenhui Gaoa, Cristina Legido-Quigley. Fast and sensitive high performance liquid chromatography analysis of cosmetic creams for hydroquinone, phenol and six preservativesJournal of Chromatography A

Vol.1218(28) (2011): 4307-4311.

186. Phelan, K., and May, K. M.,. "Mammalian cell tissue culture techniques. Current Protocols in Molecular Biology.Vol.2017(2017) 1–23.

187. Meleady, P., and O,Connor, R.,. General procedures for cell culture. Cell Biology.Vol.4(1) (2006):13–20.

188. Freshney, R. I., ."Cell line provenance". Cytotechnology.Vol. 39(2) (2002): 55–67.

189. Viazzi, S., Lambrechts, T., Schrooten, J., Papantoniou, I., and Aerts, J. M.. "Real-time characterisation of the harvesting process for adherent mesenchymal stem cell cultures based on on-line imaging and model-based monitoring". Biosystems Engineering.Vol.138 (2015): 104-113.

190.Nikbakht, Mohammad, Babak Pakbin, and Gholamreza Nikbakht Brujeni. "Evaluation of a new lymphocyte proliferation assay based on cyclic voltammetry; an alternative method." Scientific Reports .Vol.9(1) (2019): 1-7.

191. Bunaciu, Andrei A., Elena Gabriela UdriŞTioiu, and Hassan Y. Aboul-Enein. "X-ray diffraction: instrumentation and applications " Critical reviews in analytical chemistry .Vol.45(4)(2015): 289-299.

192. Wang, Gongda, Kai Wang, and Tingxiang Ren. "Improved analytic methods for coal surface area and pore size distribution determination using 77 K nitrogen adsorption experiment." International Journal of Mining Science and Technology.Vol. 24(3) (2014): 329-334.

193. Thangarasu, R., Babu, B., Kumar, N. S., Ho, M. S.,. Balasundaram, O. N., and Elangovan, T. "Impact of Cu doping on the structural,

morphological and optical activity of V_2O_5 nanorods for photodiode fabrication and their characteristics." RSC advances .Vol.9(29) (2019): 16541-16553.

194.Xiong, Xiaobo, and Jiangchun Li. "Luminescence Properties of Si^{4+}-doped $LiZnPO_4$: Eu^{3+} and Application in the Development of Latent Fingermarks." Transactions on Electrical and Electronic Materials.Vol. 22(1) (2021): 67-72.

195. Lin, Q., Lin, J., Yang, X., He, Y., Wang, L., and Dong, J. "The effects of Mg^{2+} and Ba^{2+} dopants on the microstructure and magnetic properties of doubly-doped LaFeO3 perovskite catalytic nanocrystals." Ceramics International .Vol.45 (3) (2019): 3333-3340.

196. Michael I. Y. Synthesis of zinc oxide nanoparticles with different morphologies by wet chemistry routes, PhD thesis. Loughborough University, London(2016).

197.Alshoaibi, Adil, and Shumaila Islam. "Synthesis and characterization of bromophenol blue encapsulated silica and silica-titania nanocomposites for detection of volatile organic vapors." Physica B: Condensed Matter.Vol. 614 (2021): 1-10.

198. Shimpi, N. G., Khan, M., Shirole, S., and Sonawane, S. "Process Optimization for the Synthesis of Silver (AgNPs), Iron Oxide (α-FeONPs) and Core-Shell (Ag-FeOCNPs) Nanoparticles Using the Aqueous Extract of: A Greener Approach." The Open Materials Science Journal .Vol.12(1) (2018):29-39.

199. Kishore, P. N. R., and P. Jeevanandam. "A novel thermal decomposition approach for the synthesis of silica-iron oxide core–shell nanoparticles." Journal of alloys and compounds.Vol. 522 (2012): 51-62.

200. Zhang, X., Lin, R. B., Wang, J., Wang, B., Liang, B., Yildirim, T. and Chen, B., "Optimization of the pore structures of MOFs for record high hydrogen volumetric working capacity." Advanced Materials .Vol.32(17) (2020): 1-6.

201. Utku, S., Topal, M., Döğen, A., and Serin, M. S. "Synthesis, characterization, antibacterial and antifungal evaluation of some new platinum (II) complexes of 2-phenylbenzimidazole ligands." Turkish Journal of Chemistry .Vol.34(3) (2010): 427-436.

202. Sellick, David R., David J. Morgan, and Stuart H. Taylor. "Silica supported platinum catalysts for total oxidation of the polyaromatic hydrocarbon naphthalene: An investigation of metal loading and calcination temperature." Catalysts.Vol. 5(2) (2015): 690-702.

203. Bet. Marberger, A., Elsener, M., Ferri, D., and Krocher, O.. "VOx surface coverage optimization of V_2O_5/WO_3-TiO_2 SCR catalysts by variation of the V loading and by aging." Catalysts .Vol.5(4) (2015): 1704-1720.

204.Betmgo. Reschetilowski, W., Hauser, M., Alscher, F., Klauck, M., and Kalies,G. "Studies on the Binary MgO/SiO_2 Mixed Oxide Catalysts for the Conversion of Ethanol to 1, 3-Butadiene." Catalysts .Vol.10(8) (2020): 1-17.

205. Bet, FE. Mahmood, T., Din, S. U., Naeem, A., Mustafa, S., Waseem, M., and Hamayun, M. "Adsorption of arsenate from aqueous solution on binary mixed oxide of iron and silicon." Chemical Engineering Journal .Vol.192 (2012): 90-98.

206. Zhou, J., Zhou, X., Yang, K., Cao, Z., Wang, Z., Zhou, C., and Xu, X. "Adsorption behavior and mechanism of arsenic on mesoporous silica modified by iron-manganese binary oxide (FeMnOx/SBA-15) from aqueous systems." Journal of hazardous materials .Vol.384 (2020): 1-47.

207.Edx . Shamhari, N. M., Wee, B. S., Chin, S. F., and Kok, K. Y. . "Synthesis and characterization of zinc oxide nanoparticles with small particle size distribution." Acta Chimica Slovenica .Vol.65(3) (2018): 578-585.

208. Kavaz, Doga, and Ashok Vaseashta. "Synthesizing Nano Silica Nanoparticles from Barley Grain Waste: Effect of Temperature on Mechanical Properties." Polish Journal of Environmental Studies.Vol. 28(4) (2019):2514-2521.

209. Vaseashta, Ashok, and Doga Kavaz. "Novel Magnetic Nano Silica Synthesis Using Barley Husk Waste for Removing Petroleum from Polluted Water for Environmental Sustainability." Vol.12(24) (2020): 1-16.

210. Sembiring, S., Riyanto, A., Firdaus, I., and Situmeang, R. "Effect of calcination temperature on silica-asphalt composite properties using amorphous rice husk silica." Journal of Physics: Conference Series. Vol. 1751(1)(2021):1-14.

211.Ncanana, Zamani Siphephelo. Catalytic oxidation of cresols using molecular ozone. Diss. AThesis Department of Chemistry at the University of Zululand (2017).

212. Sanderson, P., Su, S. S., Chang, I. T. H., Saborit, J. D Kepaptsoglou, D. M., Weber, R. J. M., and Harrison, R. M. "Characterisation of iron-rich atmospheric submicrometre particles in the roadside environment." Atmospheric environment Vol.140 (2016): 167-175.

213. Hu, Q., Suzuki, H., Gao, H., Araki, H., Yang, W., and Noda, T. "High-frequency FTIR absorption of SiO2/Si nanowires." Chemical physics letters .Vol.378(3-4) (2003): 299-304.

214. Murashkevich, A., Lavitskaya, A., Barannikova, T., & Zharskii, I. "Infrared absorption spectra and structure of TiO 2-SiO $_2$ composites." Journal of Applied Spectroscopy.Vol. 75(5) (2008): 730-734.

215. Battegazzore, D., Bocchini, S., Alongi, J., & Frache, A. "Rice husk as bio-source of silica: preparation and characterization of PLA–silica bio-composites." RSC Advances Vol.4(97) (2014): 54703-54712.

216 .Kumari SR. Study of structural and optical properties of V_2O_5/SiO_2 nanocomposites. Int. J. Sci. Res. Vol. 4(10)(2015): 168-170.

217 .Karthik K. Ultrasound-assisted synthesis of V_2O_5 nanoparticles for photocatalytic and antibacterial studies. Mater. Res . Vol. 24(4) (2020): 229-234.

218.Yang, E., Lee, J. G., Kim, D. H., Jung, Y. S., Kwak, J. H., Park, E. D., and An, K.. "SiO_2@ V_2O_5@ Al_2O_3 core–shell catalysts with high activity and stability for methane oxidation to formaldehyde." Journal of Catalysis .Vol.368 (2018): 134-144.

219. Li, D., Teoh, W. Y., Selomulya, C., Woodward, R. C., Munroe, P., and Amal, R. "Insight into microstructural and magnetic properties of flame-made γ-Fe $_2$ O $_3$ nanoparticles." Journal of Materials Chemistry .Vol.17(46) (2007): 4876-4884.

220. Tamilselvi, P., Yelilarasi, A., Hema, M., and Anbarasan, R. "Synthesis of hierarchical structured MgO by sol-gel method." Nano Bulletin Vol.2(1) (2013): 1-6.

221. Rezaei, Mehran, Majid Khajenoori, and Behzad Nematollahi. "Synthesis of high surface area nanocrystalline MgO by pluronic P123 triblock copolymer surfactant." Powder technology .Vol.205(1-3)(2011): 112-116.

222. Dhaouadi, Hassouna, Hedia Chaabane, and Fathi Touati. "Mg (OH) $_2$ nanorods synthesized by a facile hydrothermal method in the presence of CTAB." Nano-Micro Letters Vol.3(3) (2011): 153-159.

223. Stefov, V., Najdoski, M., Engelen, B., Ilievski, Z., and Cahil, A. "Very low H–O–H Bending Frequncies.VI. Vibrational Spectra of $CdCl_2 \cdot H_2O$." Contributions, Section of Natural, Mathematical and Biotechnical Sciences Vol.38(1) (2017): 91-99.

224.Al-Khafaji, M. A., Gaál, A., Wacha, A., Bóta, A., & Varga, Z.. "Particle Size Distribution of Bimodal Silica Nanoparticles: A Comparison of Different Measurement Techniques." Materials Vol.13(14) (2020): 1-14.

225. Croissant, J. G., Butler, K. S., Zink, J. I., & Brinker, C. J. "Synthetic amorphous silica nanoparticles: toxicity, biomedical and environmental implications." Nature Reviews Materials Vol.5(12) (2020): 886-909.

226. Selvarajan, Vanitha, Sybil Obuobi, and Pui Lai Rachel Ee. "Silica Nanoparticles—A Versatile Tool for the Treatment of Bacterial Infections." Frontiers in chemistry Vol.8 (2020): 1-16.

227. Suma, P. R. P., Nair, R. V., Paul, W., and Jayasree, R. S. "Vanadium pentoxide nanoplates: Synthesis, characterization and unveiling the intrinsic anti-bacterial activity." Materials Letters Vol. 269 (2020): 1-13.

228. Tang, Zhen-Xing, and Bin-Feng Lv. "MgO nanoparticles as antibacterial agent: preparation and activity." Brazilian Journal of Chemical Engineering Vol.31 (2014): 591-601.

229. Krishnamoorthy, K., Manivannan, G., Kim, S. J., Jeyasubramanian, K., and Premanathan, M. "Antibacterial activity of MgO nanoparticles based on lipid peroxidation by oxygen vacancy." Journal of Nanoparticle Research Vol. 14(9) (2012): 1-10.

230. K. Kombaiaha , J. Judith Vijayaa, L. John Kennedyb ,and M. Bououdina." Okra extract-assisted green synthesis of CoFe2O4 nanoparticles and their optical, magnetic, and antimicrobial properties ." Materials Chemistry and Physics Vol.204(15)(2018): 410-419.

231. Xu, C., Akakuru, O. U., Ma, X., Zheng, J., Zheng, J., andWu, A. "Nanoparticle-based wound dressing: recent progress in the detection and therapy of bacterial infections." Bioconjugate Chemistry Vol.31(7) (2020): 1708-1723.

232. Mihai, M. M., Dima, M. B., Dima, B., and Holban, A. M.. "Nanomaterials for wound healing and infection control." Materials Vol.12(13) (2019): 1-16.

233. Rezvani Ghomi, Erfan, et al. "Wound dressings: Current advances and future directions." Journal of Applied Polymer Science Vol. 136(27) (2019): 1-12.

234.Natan, Michal, and Ehud Banin. "From Nano to Micro: using nanotechnology to combat microorganisms and their multidrug resistance." FEMS microbiology reviews Vol.41(3) (2017): 302-322.

235. Batool, M., Khurshid, S., Qureshi, Z., and Daoush, W. M.. "Adsorption, antimicrobial and wound healing activities of biosynthesised zinc oxide nanoparticles." Chemical Papers Vol.75(3) (2021): 893-907.

236. Behzadi, E., Sarsharzadeh, R., Nouri, M., Attar, F., Akhtari, K., Shahpas and, K., and Falahati, M. "Albumin binding and anticancer effect of magnesium oxide nanoparticles." International journal of nanomedicine Vol.14 (2019): 257-270.

237. Akram, M. W., Fakhar-e-Alam, M., Atif, M., Butt, A. R., Asghar A., Jamil, Y., and Wang, Z. M.. "In vitro evaluation of the toxic effects of MgO nanostructure in Hela cell line." Scientific reports Vol. 8(1) (2018): 1-11.

238.Chiang, L. C., Chiang, W., Chang, M. Y., and Lin, C. C.,. In vitro cytotoxic, antiviral and immunomodulatory effects of Plantago major and Plantago asiatica. American Journal of Chinese Medicine Vol. 31(2) (2003): 225–234.

239. vankovic, S., Music, S., Gotic, M., and Ljubesic, N.. "Cytotoxicity of nanosize V_2O_5 particles to selected fibroblast and tumor cells." Toxicology in vitro Vol.20(3) (2006): 286-294.

240. Amante, C., Sousa-Coelho, D., Luísa, A., and Aureliano, M.. "Vanadium and melanoma: A systematic review." Metals Vol.11(5) (2021): 1-24.

241. Das, S., Roy, A., Barui, A. K., Alabbasi, M. M. A., and Kuncha, M "Anti-angiogenic vanadium pentoxide nanoparticles for the treatment of melanoma and their in vivo toxicity study." Nanoscale Vol.12(14) (2020): 7604-7621.

242. Madkour, Loutfy H. "Biogenic–biosynthesis metallic nanoparticles (MNPs) for pharmacological, biomedical and environmental nanobiotechnological applications." Chron. Pharm. Sci. J Vol.2(1) (2018): 384-444.

243. Orthaber, K., Pristovnik, M., Skok, K., Perić, B., and Maver, U. "Skin cancer and its treatment: novel treatment approaches with emphasis on nanotechnology." Journal of nanomaterials.Vol. 2017 (2017):1-21.

244. Saranya, S., Vijayaranai, K., Pavithra, S., Raihana, N., and Kumanan, K . "In vitro cytotoxicity of zinc oxide, iron oxide and copper nanopowders prepared by green synthesis." Toxicology Reports Vol. 4 (2017): 427-430.

245. Ahamed, Maqusood. "Silica nanoparticles-induced cytotoxicity, oxidative stress and apoptosis in cultured A431 and A549 cells." Human & experimental toxicology Vol.32(2) (2013): 186-195.